Alma Mater Studiorum – Università di Bologna

DOTTORATO DI RICERCA IN

CHIMICA

Ciclo 35

**Settore Concorsuale:** 03/C1 – CHIMICA ORGANICA

**Settore Scientifico Disciplinare:** CHIM/06 – CHIMICA ORGANICA

# LOW-MOLECULAR-WEIGHT GELS: FROM THE RATIONAL DESIGN TO THE APPLICATION OF VERSATILE SOFT MATERIALS

**Presentata da:** Paolo Ravarino

**Coordinatore Dottorato** Luca Prodi

**Supervisore** Claudia Tomasini

**Esame finale anno 2022**

# *Abstract*

Low-molecular-weight (LMW) gels are a versatile class of soft materials that gained increasing interest over the last few decades. They are made of a small percentage, often lower than 1.0 %, of organic molecules called gelators, dispersed in a liquid medium. Such molecules have a molecular weight usually lower than 1 kDa.

The gelator molecules start to interact after the addition of a trigger, which alters their solubility in that medium. They form small repeating units called fibrils, which in turn interact with each other to form fibres, whose entanglement is able to trap the solvent molecules through capillary forces, causing the gelation.

A plethora of LMW gelators have been designed, including conjugated aromatic molecules, sugars, and short peptides. This last class is probably the most studied, as they present several advantages: (i) the synthesis is easy and can be performed on a multigram scale; (ii) they are usually biocompatible and biodegradable; (iii) it is possible to make small variations on the peptide scaffolds to rationalise the gelation phenomenon; (iv) they find potential application in several fields.

In this thesis, an overview of several peptide based LMW gels is presented. In each study, the gelation conditions were carefully studied, then a thorough investigation of the final material was carried out. First, the gelation ability of a fluorinated phenylalanine was assessed, to understand how the presence of a rigid moiety as an oxazolidinone and the presence of fluorine may influence the gelation ability. In this context, a method for the dissolution of sensitive gelators was studied. Then, the control over the gel formation was studied both over time and space, taking advantage of either the pH-annealing of the gel or the reaction-diffusion of a hydrolysing reagent.

Some gels were then probed for their potential application in various fields. Due to their ability of trapping water and organic solvents, we used gels for trapping pollutants dissolved in water, as well as a medium for the controlled release of either fragrances or bioactive compounds. Finally, the interaction of the gel matrix with a light-responsive

molecule was assessed to understand wether the gel properties or the interaction of the additive with light were somehow affected by the medium.

*A tutta la mia famiglia*

# *Index*

# *List of abbreviations*

1D = one-dimensional

2Cl-Z = carbonyl (2-chloro)benzyloxy

3D = three-dimensional

ACN = acetonitrile

Aib = 2-amino isobutyric acid

Ala = alanine

API = atmospheric pressure ionization

ATR = attenuated total reflectance

Bn = benzyl

Boc = *tert*-butyloxycarbonyl

BTC = bis-trichlorocarbonate

CD = circular dichroism

CDI = N,N'-carbonyl diimidazole

CGC = critical gelation concentration

cHex = cyclohexane

DAP = 1,3-diaminopropane

DCM = dichloromethane

Dec. = decomposition

DIEA = N,N-diisopropyl ethylamina

DMSO = dimethylsulphoxide

Dopa = 3,4-dihydroxyphenylalanine

DPBS = Dulbecco's phosphate buffered saline

EDA = 1,2-ethylendiamine

Eq. = equivalents

ESI = electron spray ionization

FBS = fetal bovine serum

Fmoc = fluorenyl methoxycarbonyl

FT = Fourier transform

GdL = glucono-δ-lactone

Gln = glutamine

HaCaT = keratinocyte cell line from adult human skin

HBTU = hexafluorophosphate benzotriazolyl uronium

HOMO = highest occupied molecular orbital

HP = liquid chromatography

HR = high resolution

IR = infrared

LC = liquid chromatography

LUMO = lowest unoccupied molecular orbital

LVER = linear viscoelastic range

Lys = lysine

MAS = magic angle spinning

MEM = minimum essential medium

MeOH = methanol

m.p. = melting point

MS = mass spectrometry

MTT = 3-(4,5-dimethylthiazol-2-yl)-2,5-diphenyltetrazolium

NEAA = non-essential amino acid

NIH-3T3 = cell line from mouse embryonic fibroblasts

NMR = nuclear magnetic resonance

OD = optical density

Oxd = oxazolidin-2-one

Pal = palmitic

Phe = phenylalanine

Phe(F) = 4-fluorophenylalanine

Phe($F_2$) = 3,4-difluorophenylalanine

PB = phosphate buffer

PBS = phosphate buffered saline

PMMA = polymethylmetacrylate

POM = polarized optical microscopy

PrS = 1,3-propanesultone

r.t. = room temperature

SIM = single ion monitoring

TBME = *tert*-butyl methyl ether

TIC = total ion current

tBu = *tert*-butyl

TFA = trifluoroacetic acid

TFAc = trifluoroacetyl

$T_{gel}$ = melting temperature of the gel

Tyr = tyrosine

Val = valine

# *Chapter 1. Introduction*

Gels are soft materials that behave as solids and liquids simultaneously. This peculiarity arises from the presence of solid ordered structures, i.e., fibres, from which the solid-like properties derive, dispersed in a liquid medium responsible for the liquid-like properties. The entanglement of these fibres is strong enough to hold the liquid phase through surface tension and form a self-supporting material.[1,2] From a rheological point of view, these materials have a viscoelastic behaviour, with the solid-like properties overcoming the liquid-like ones, and do not flow when subjected to gravity.

Among all the gels it is possible to distinguish two macro classes, based on the kind of bond between the fibres: chemical and physical gels. In the first case, the gels fibres are held together by covalent bonds, therefore these are though, hard to break and usually not reversible. This means that once the gel is broken, it is not able to regain its original shape through self-healing. An example is represented by contact lenses, which are hydrogels historically prepared by the chemical crosslink of polymethyl methacrylate (PMMA).[3] Physical gels, on the other hand, are held by weak supramolecular interactions, such as electrostatic interactions, π-π stacking, and H-bonds, and for this reason such gels are often called supramolecular gels. These gels are generally weaker than the previous ones, quite easy to break and usually easy to reform. Considering another polymer as an example, alginate forms physical gels through electrostatic crosslinking with calcium ions.[4]

Apart from the distinction according to the nature of the bonds, gels can also be divided according to the nature of the molecules composing the fibres, also called "gelators". In this context, we can find polymeric gels, as discussed so far, and low-molecular-weight (LMW) gels. The last one is an intriguing class of soft materials usually prepared exploiting physical interactions between the gelator molecules, therefore most of the gels prepared with such molecules are physical. As the name suggests, such molecules are small, with a molecular weight (MW) usually below 1 kDa.

As in my PhD I focussed my attention primarily on this category, I will discuss the details around LMW gelators and gels, shelving the polymeric ones.

## *1.1. Low-molecular-weight gels*

When a physical gel is formed, a large number of supramolecular interactions take place, such as H-bonds, hydrophobic interactions, π-π, cation-π, and halogen bonds to name some. For this reason, most of the LMW gelators possess features able to create such interactions. Good candidates are conjugated aromatic molecules,[5,6] sugars,[7,8] and short peptides.[9,10] As during my PhD I worked with peptide- and pseudopeptide-based LMW gelators, I will discuss more in detail such molecules. These offer a plethora of weak interactions and, being chiral, are able to create chiral supramolecular structures, so they represent very good candidates as gelators.

When preparing a LMW gel, a small amount of the gelator is dissolved in a suitable solvent. The solubilisation of the gelator can be carried out through numerous techniques, such as simple swirling, vigorous stirring, ultrasound sonication, heating, and so on. Depending on the nature of the solvent and of the gelator, in this step the gelator molecules can be either dissolved as free molecules or form micellar aggregates (Figure 1.1). For example, the dipeptide 2Nap-$^{L}$Phe-$^{L}$Phe-OH, thoroughly investigated by Adams et al.,[11,12] can be readily dissolved as free molecules in dimethyl sulfoxide (DMSO), while in water at basic pH (pH > 9) it behaves as a surfactant, forming worm-like micelles, due to the high hydrophobicity of the aromatic features, that in aqueous environment start to interact and aggregate.[13]

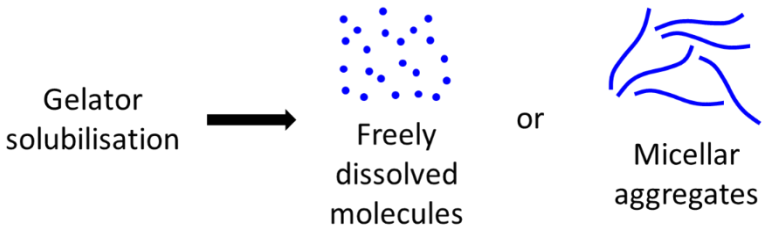


**Figure 1.1**. Cartoon showing how the gelator molecules behave in solution, being freely dispersed or interacting to form micellar aggregates.

After the solubilisation step, the gelation is triggered through the application of an external stimulus, or trigger. This induces a variation in the solubility of the gelator molecules, that start the self-assembly process. Then, the viscosity of the material gradually increases, due to the formation of fibrils, ordered structures that represent the smallest repeat unit, whose entanglement generates fibres, until the complete formation of the gel (Figure 1.2).[14,15] When the gel is formed, a self-supporting material is obtained, and it can be visualised by the inversion test. However, the inversion of the vial should be considered as a mere preliminary test, as also highly viscous solutions are often reluctant to flow, therefore the material should be characterised through rheology.[16]

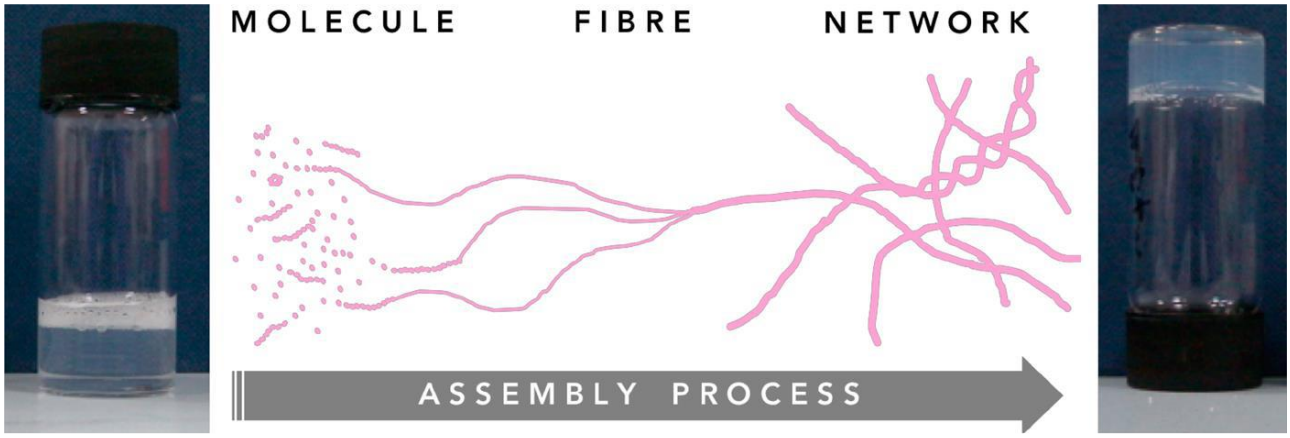


**Figure 1.2**. Schematic representation of the self-assembly process. Figure adapted from ref.[15]

It is also possible to form gels using more than one gelator.[17,18] Gels containing two or more gelators are commonly referred to as multicomponent gels and can offer the possibility of combining the properties of all the gelators composing the gels, thus resulting more intriguing than the single-component ones.[19,20] When the various gelators concur to the formation of the fibril, co-assembly takes place. When each gelator forms its own network instead the gel is referred to as self-sorted (Figure 1.3). In the first case, the properties of the single-components are usually dramatically different from the final material, while in the second case, they appear as coupled.

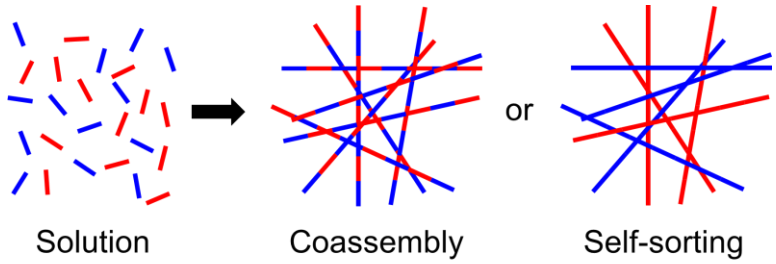


**Figure 1.3**. Schematic representation of possible outcomes in the self-assembly process involving a bicomponent system.

LMW gels gained increasing interest over the years due to the their easy preparation, their general reversibility,[21,22] and the wide range of applications, such as in electronic devices,[23,24] controlled drug release,[25,26] cell culture and release,[27,28] and water remediation.[29,30] Mixing two or more gelators opens up the possibility of coupling more properties, widening the application spectrum.

Before digging into the triggers that can be used, it is important to distinguish between two more gels categories. This distinction is made according to the solvent composing the gel. If the solvent, or even part of it, is water, the gel will be indicated as a hydrogel. On the other hand, if the gel is composed of only organic solvents, it will be indicated as organogel. As fibres are held together by surface tension and capillary forces,[31,32] hydrogels will generally result stiffer than organogels.

## *1.2. Triggers*

Gels can be triggered in a plethora of ways. The choice of the trigger is often crucial as the final gel may have different properties according to the trigger chosen. They basically consist in an energy input that allows the gelator molecules to overcome an energy barrier, form fibres and reach a relative minimum in energy (Figure 1.4). The gel state, being a relative minimum in energy, is a kinetically trapped state. This means that most of the times, it is stable enough to not evolve to more thermodynamically stable states, even though some examples report the formation of crystals from the gel matrix[33,34] or the gel disruption to have a solution again.[35,36]

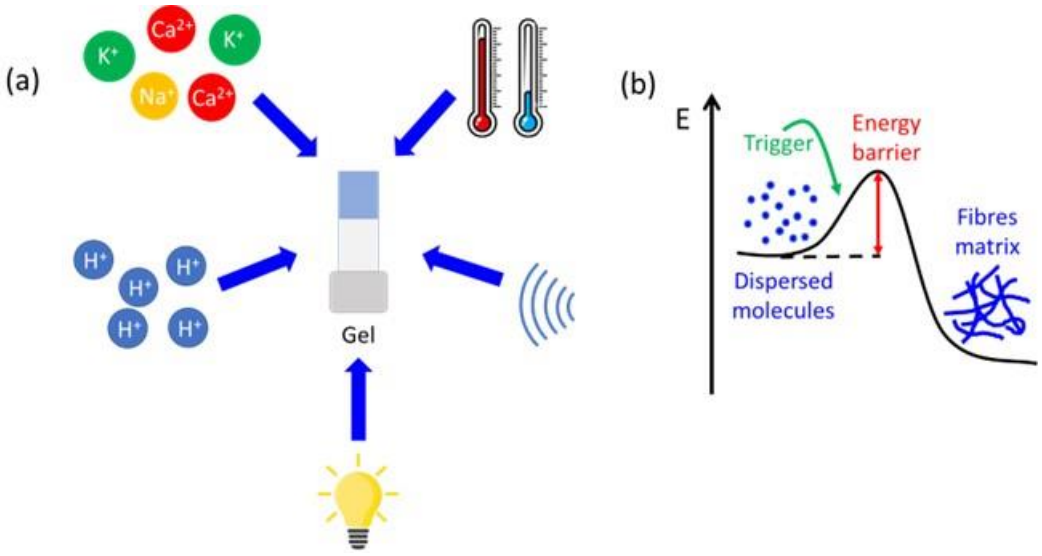


**Figure 1.4**. Cartoon showing (a) some triggers used to carry out gelation and (b) the energy path on going from dispersed molecules (either freely dissolved or in micellar aggregates) to the formation of the fibrous matrix.

### 1.2.1. Solvent switch

In gels triggered via solvent switch, the gelator is primarily dissolved in a proper solvent, typically in a polar organic solvent,[37,38] such as hexafluoro isopropyl alcohol (HFIP) or DMSO, then a second solvent in which the gelator is not soluble is added. The unbalance in the solubility causes a phase separation, ending up in gelation. In this case the gelation

is pretty fast and usually happens within few minutes from the addition of the non-solubilising solvent.

Most of the times, the non-solubilising solvent consists in water. In this way hydrogels are prepared. However, few examples report also the formation of organogels upon addition of a second organic solvent.[39] The properties of gels triggered via solvent switch mainly rely on the ratio between the solubilising and the non-solubilising solvent. Considering a fixed concentration of gelator, the use of more solubilising solvents will result in a weaker gel, until a limit is reached over which only solutions can be formed; on the other hand, the use of more non-solubilising solvent will result in stiffer gel, until a limit is reached over which the gelation does not take place anymore, and other phenomena related to the poor solubility, such as crystallisation or precipitation, occur.

### 1.2.2. pH change

This methodology is only used for hydrogels and takes advantage of acidic or basic functionalities of the gelator. In this case, the hydrophobic gelator is initially dissolved in water by ionizing such groups. This happens at basic pH for acidic gelators and at acidic pH for basic gelators. In this environment the gelator is more hydrophilic and gets more easily dissolved. However, most of the times the hydrophobicity of the hydrogelator is so prominent that it already forms ordered anisotropic structures such as worm-like micelles in this environment.[11,13,40]

After this, the trigger is added and causes a pH variation that makes the gelator insoluble again. It consists in the addition of an acid for acidic gelators or a base for basic gelators. In this case, the pH variation is generally fast and so is the gelation. This leads to the formation of inhomogeneous and poorly reproducible gels. Other methods that allow a slow pH change have been developed and they consist it the addition of species that slowly undergo a chemical reaction releasing an acid (or base). In this case the rate of pH change is governed by the kinetics of the chemical reaction that leads to the formation of the specimen that changes the pH. Adams *et al.* investigated the use of glucono-δ-lactone

(GdL) as hydrolysing reagent to produce gluconic acid and slowly reduce the pH. This allowed a controlled change in pH and the formation of homogeneous and reproducible gels (Figure 1.5a).[41] In the same context, Panzarasa *et al.* employed instead the use of 1,3-propanesultone, that in aqueous environment got hydrolysed to produce 3-hydroxypropane-1-sulfonic acid (Figure 1.5b).[42] This reaction is even slower than the one of GdL, especially at high pH, where the hydrolysis of GdL is in the order of minutes, while the of 1,3-propanesultone is in the order of hours.[43] In this case, the hydrolysis reaction is acid autocatalyzed, meaning that the reaction at high pH proceeds slowly until it reaches a pH after which the acidic environment catalyses the production of further acid. This methodology allows to reach lower values in pH compared to the use of GdL, as the p$K_a$ of 3-hydroxypropane-1-sulfonic acid is 1.53, while gluconic acid is 3.86.

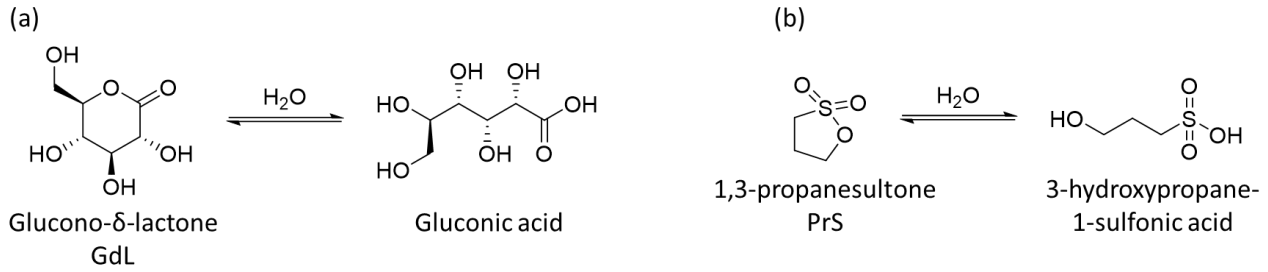


**Figure 1.5**. Hydrolysis reaction of (a) GdL to produce gluconic acid employed by Adams *et al.*, and (b) PrS to produce 3-hydroxypropane-1-sulfonic acid exploited by Panzarasa *et al.*.

Both these methods allow the controlled formation of acidic hydrogels, while no methodology employing a hydrolysing reagent in the aqueous solution has been employed to enhance the pH and form basic gels. To prepare such gels in a controlled way there have been devised methods exploiting enzymes[44,45] or reaction-diffusion,[46,47] which will be clarified later on.

## 1.2.3. Addition of ions

This methodology is employed mainly in the formation of hydrogels, although a few examples report the addition of ions in organogels.[48] The basic principle relying on this methodology is the same seen for the pH change, in the sense that the variation in pH might be regarded as an addition of ions, $H^+$ in the case of acidic gels, $HO^-$ in the case of basic gels. Therefore, the addition of cations for acidic gelators may lead to gelation, as well as the addition of anions for basic gelators, although only little in this latter case has been explored.[49,50] Generally, the addition of monovalent cations such as sodium or potassium has been poorly investigated,[51] as these rarely lead to gelation. The use of divalent cations, on the other hand, proved to be more efficient and calcium is the cation most widely studied. Usually added in molar ratio gelator:calcium 2:1, it is able to electrostatically crosslink two gelator molecules and create other interactions in its coordination sphere, such as cation-π bonds, that further strengthen the gel matrix.

The use of other cations such as copper and iron with different oxidation state has been also explored. For example, Fortunato *et al.* devised a gel for food freshness monitoring containing copper.[52] This gel, possessing a light blue colour at the beginning, in presence of amine vapours it became darker. In particular, in presence of the products of degradation of rotten meat, it became dark brown, and was able to regain its initial colour after exposure to fresh air for several hours.

The possibility of forming gels with only some ions may be attributed (at least partially) to the hard and soft acids and bases (HSAB) theory. Gelators with hard functionalities interact better with hard ions, therefore a gel will more likely be formed when the hard/soft properties of both gelator and ion match.

## 1.2.4. Temperature variation

With this methodology both hydrogels and organogels can be formed. It simply consists in pouring solvent on the solid gelator, varying the temperature to better solubilise it and return to the initial temperature where the gelator was insoluble. Upon the second

temperature change, the gelator molecules start to aggregate again, leading to the formation of fibres and eventually of the gel.

Most of the examples reported in literature show gelation upon a heat-cool cycle, i.e., heating the gel solution and leaving it to cool down.[53–55] This is basically the same principle used for recrystallisation, and in fact, other phenomena may occur in this scenario, such as crystallisation or precipitation. Nonetheless, peptide based gelators are usually sensitive to high temperatures, therefore care should be taken when forming gels with this method. However, few examples report the formation of the gel at high temperature, while at low temperature the gel falls apart.[56] Even though this behaviour is quite unusual, it is important to keep in mind that the gel state is a kinetically trapped state,[57] that can be reached giving energy to the system. When the energy input is switched off, most of the times the system does not receive enough energy to change state, but it is also possible that a thermodynamically preferred minimum can be reached even without the energy input.

### 1.2.5. Ultrasound sonication

Ultrasound sonication is often used to break aggregates and clusters of molecules. Nonetheless, it also provides energy to the system. These phenomena both concur to the disaggregation and reaggregation of gelator molecules, that eventually form fibres and gels.[58,59] In this sense, the use of ultrasound sonication is very close to the temperature variation method showed above. This methodology can be used both for organogels and for hydrogels and takes advantage of the partial solubility of the gelator molecules in the solvent. Apparently insoluble at the beginning, the gelator aggregates get dissolved after the application of ultrasound sonication and as soon as it gets enough energy, it forms fibres.

## 1.2.6. Light

Some gelators display photosensitive features, that allow the interconversion between two (or more) species by applying different wavelengths of light. Usually, one specimen is soluble in the solvent chosen, while the other is not. At the beginning the soluble form is used, then after irradiation with light the gelator undergoes a change in its structure and the gel is formed. Photosensitive units commonly used are azobenzenes,[60,61] stilbenes,[62,63] spiropyrans,[64,65] or diarylethenes,[66,67] therefore, a good strategy to prepare photosensitive gels is incorporating these units in the gelator features. All these molecules possess a conjugated double bond that can undergo a *cis-trans* isomerisation with light irradiation. While the *trans*-form is generally planar and rigid, important properties for gelators (as will be discussed thoroughly in the following sections), the *cis*-form tend to bend due to steric interactions. In some cases, the *cis*-form spontaneously cyclize to form a molecule with a twisted geometry, often unsuitable for gelation.

## 1.2.7. *In situ* chemical reactions

Some gelators can be formed *in situ* after a chemical reaction. For example, Zhao *et al.* reported a gelator unable to form gels via pH or temperature variation. This instead, was able to form gels when its precursor was hydrolysed *in situ* in an aqueous basic environment or in presence of an enzyme (Figure 1.6).

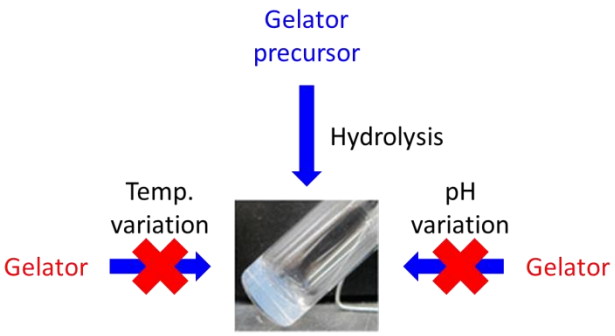


**Figure 1.6**. Schematic representation of the formation of a gel via *in situ* hydrolysis of the gelator precursor. When the gelator is triggered via either pH or temperature change the gel does not form. Figure adapted from reference[68].

The gel formed in this way was stable over a wide range of pH and temperature.[68] It is also possible to form a LMW gel, use it as a reaction vessel and convert the gelator to a second gelator through chemical crosslinking with other species present in the gel, maintaining the gel phase.[69]

## 1.2.8. Mixed triggers

It is often useful to be able to obtain a gel using various triggers as well as to disrupt it when needed using an orthogonal stimulus, i.e., not the opposite stimulus applied to obtain the gelation. Literature reports some elegant systems where gels are formed with one trigger and disrupted using an orthogonal trigger. For example, Qiu *et al.* studied a spiropyran-containing hydrogelator that could be triggered via a pH change, then by irradiating the gel with white light, the spiropyran was interconverted and caused the gel to fall apart (Figure 1.7).[70] Other examples report a gel-to-gel transition, i.e., a change in the structure and morphology of the gel rather than observing a gel-to-sol transition.[65,71] The possibility of using more triggers can be exploited also in multicomponent systems. For example, a chiral additive may induce its chirality for the formation of fibres from an achiral gelator.[72]

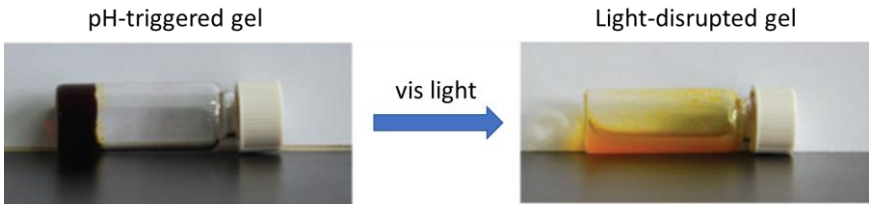


**Figure 1.7**. Pictures of a pH-triggered gel containing a spiropyran moiety. The gel is disrupted by applying an orthogonal trigger, i.e., white light. Figure adapted from ref. [70]

Whether the trigger is, once the LMW gel has been prepared, it is usually left to rest some time for the fibres to be completely formed and entangled, then it is analysed.

## *1.3. LMW gels characterisation*

As previously said, LMW gels are composed by a hierarchical assembly: the gelator molecules form fibrils that in turn form fibres and their entanglement lead to the gelation. Therefore, gels can be characterised through several techniques, from the molecular to the bulk level.

### 1.3.1. Table-top rheology

The so called "table-top" rheology is a useful tool for a preliminary study of gels. It consists in quick and simple ways to assess the macroscopic behaviour of a gel and can be performed without any specific equipment. This kind of rheology is used to determine two main parameters for a particular gel: the critical gelation concentration (CGC) and the gel-sol transition temperature ($T_{gel}$). The first parameter is usually assessed through the "inversion test". Different concentrations of gelator are probed and gelled using the same methodology. The lowest concentration at which the sample forms a self-supporting gel is considered the CGC. The $T_{gel}$ is usually measured with the dropping ball method. On the top of the gel a small glass (or metal) sphere is posed, then the gel is heated until the glass ball drops, as ideally the gel matrix should sustain the weight of the ball, while in a solution it should drop.

### 1.3.2. Nuclear magnetic resonance (NMR)

This technique gives information about specific nuclei composing the molecule ($^{1}$H- $^{13}$C- $^{19}$F-NMR and so on) therefore can be used for the molecular recognition of the molecule in solution. When the gel is formed, however, the signals of the gelator should disappear, as fibres are NMR-invisible, being not in solution anymore.[73,74] Such techniques are useful for example when the assembly kinetics is low or when analysing multicomponent systems. When no signal apart from the one of the solvent is present it means that all the gelators or additives in the gel matrix concur to the formation of fibres, while when the

signal of other gelators are still detectable it means that these did not form the fibres and are still dispersed in solution.

In this field, it is also worth citing solid state NMR techniques. These techniques are usually referred to as magic angle spinning (MAS) NMR because of the orientation dependence of the nuclear spin interactions in the solid state.[75,76] High resolution (HR) MAS NMR is commonly used to analyse soft materials, as it allows the detection of NMR resonances between a conformationally mobile moiety and an immobile phase,[77] therefore it can be used to distinguish between features of the gelling molecule involved in the formation of fibres and those conformationally free.

### 1.3.3. Infrared spectroscopy

Fourier-Transform infrared (FTIR) spectroscopy allows the molecular recognition of functional groups in the gelator molecules. It also gives information about the H-bonds formed in the aggregates, shifting some signals relative to the N-H and C=O bonds.[78,79] Therefore, it is informative of the molecular packing in the fibres. For example, it allows the determination of a β-sheet structure,[80,81] typical of most gel fibres, when this is formed. In multicomponent systems it also allows the distinction between a co-assembled network of fibres and a self-sorted one.[82,83] Normally, in the first case the peaks belonging to the same functional groups of each gelator should merge, creating a broad peak located half-way between the signals of the components separated. In the latter case instead, the peak of each gelator should be visible and not merged with others.

### 1.3.4. UV-vis absorption and fluorescence emission spectroscopy

Molecules containing π-electrons or non-bonding electrons (n-electrons) can absorb the energy in the form of ultraviolet or visible light to excite these electrons to higher anti-bonding molecular orbitals. These electrons can be excited easily due to a low energy gap between the highest occupied molecular orbital, HOMO, and the lowest unoccupied

molecular orbital, LUMO. As organic gelators usually contain aromatic features that enhance their gelation ability, they can often be characterised with this technique. The wavelength of absorbance of the free molecules and of the fibres is slightly different and usually undergo a red-shift due to a lower energy gap between the HOMO and the LUMO in stacked structures than in free molecules (Figure 1.8a).[84]

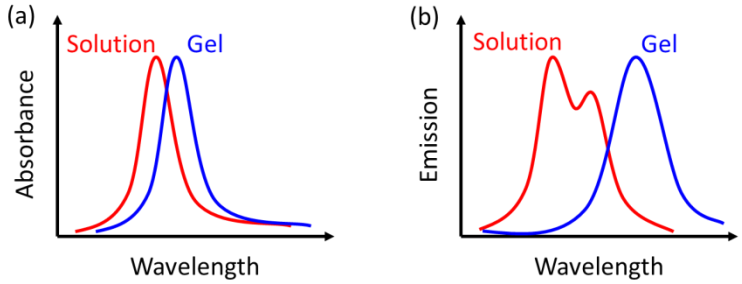


**Figure 1.8**. Cartoons representing the red-shifts happening in gel compared to the solution in (a) a general UV-vis absorption spectrum and (b) a Fmoc-containing gelator fluorescence emission spectrum.

This technique is also exploited to probe the transparency of the gel, usually expressed as means of transmittance in the visible region. This property is important when the gel is needed for optical application.

Some organic molecules are able to emit light when excited and can be analysed through fluorescence emission spectroscopy. This analysis usually requires a study of UV-vis absorption to find the adequate wavelength to use to excite the molecule. Most conjugated and aromatic molecules are able to emit light, such as the ones containing a fluorenylmethyloxy carbonyl (Fmoc) protecting group in their features, widely used on peptides. Unlike the UV-vis absorption, the difference in emission between the molecules in solution and in fibres can be very remarkably red-shifted (Figure 1.8b). This happens mainly because in the gel the various gelator molecules form stacked structures, while in solution they do not.[85,86]

### 1.3.5. Circular dichroism (CD)

This technique is used to determine how the medium interacts with circularly polarized light and can be done both when the gelator is in solution and in gelled state. As only chiral entities are able to interact with light, through this technique achiral molecules will not be detectable. Chiral molecules on the other hand will have CD signals in the same region of their UV-vis absorption signals. However, when solvated, chiral molecules have a relatively low CD signal intensity.[14] When assembled into chiral nanostructures, the interaction with polarized light will be remarkably improved, therefore exhibiting larger CD bands. After comparing the CD signals of the gelator both in solution and in gel, the presence of a CD signal more prominent in gel than in solution can be then taken as a proof of the formation of chiral assembly. This analysis helps also to elucidate whether a multicomponent system is formed or co-assembled fibres or self-sorted ones.[87–89]

### 1.3.6. Small-angle neutron scattering (SANS) and X-ray scattering (SAXS)

Gels tend to scatter X-rays and neutrons broadly rather than giving well defined diffraction patterns, as crystals do. This is due to the irregular packing of fibres in the gel matrix.[90,91] However, at low angles, the scattering data can be fitted to an appropriate model. The scattering data for gels are usually modelled as a group of cylinders or tapes and the output of this fitting provides information about the nanoscale dimension, such as the tape width. In this way, the small-angle scattering data provide information about the size of the fibrils, the smallest repeating unit, and thus about the morphologies that lead to gelation.[14,92] However, the access to such techniques is quite limited as, given the high level of disorder in these media, it is necessary to use a synchrotron source. X-ray can also be used on dried gels, which present a higher level of order compared to the wet gel and a standard small-angle X-ray diffractometer can be employed.

### 1.3.7. Scanning electron microscopy (SEM) and other electron microscopies

This technique is used to identify the fibres of a gel, unlike the scattering techniques which instead analyse the fibrils. It allows to acquire high-quality images of the morphology of the gel and is often very informative. To prepare the sample, a small amount of the gel is first dried to form either a xerogel or an aerogel. At this point, the dried gel is coated with a metallic layer and finally imaged.

Both the methods for drying the gel present advantages and disadvantages. In xerogels, the solvent is left to dry in ambient conditions. As the evaporation proceeds, the gel fibres slowly collapse on the others to obtain a thin layer of collapsed fibres. In aerogels, the solvent is frozen then sublimated under reduced pressure. In this case the fibres are not collapsed, and the original gel shape is unaltered. However, hydrogels swell during freezing due to the expansion of water. This can break the gel fibres or alter their shape. Even though this technique results very informative, drying the gel sample is disregarded, as the gelator in this case is desolvated and the gel network may undergo a reorganisation.[1,93] Nonetheless, it can lead to artifacts changing the nanostructure of the fibres.[92] For this reason, other techniques that image the wet gel are commonly preferred.

Other electron microscopies are employed with gels, such as transmission electron microscopy (TEM), although in this case it is usually needed a heavy metal staining agent to enhance image contrast.[94]

Cryo-electron microscopy techniques are used to minimise the disruption of the self-assembled network due to drying.[95,96] To do so, the gel is rapidly frozen to limit thermal motion, usually at liquid nitrogen temperatures. Sometimes, the solvent is sublimated by freeze drying and the low temperatures usually limit the network reorganisation due to desolvation.

### 1.3.8. Optical and confocal microscopy

Both these microscopies can be performed on the wet samples, thus leaving unaltered the fibres environment. Besides being advantageous from the point of view of the reliability of the images taken, these techniques have a lower degree of resolution compared to the electron microscopies. Opaque gels, being made of microscopic aggregates are easily visualised with optical microscopy. On the other hand, transparent gels, being made of nanometric-sized aggregates, need a higher resolution or the creation of a layer. This can be carried out by leaving a piece of the gel to slowly dry, creating a xerogel, and incurring in the drawbacks mentioned before. Confocal microscopy allows to "create a layer" by selecting a focus plane, remarkably improving the resolution thus, even transparent gels are easily imaged. Most of the times a dye is needed to visualise the fibres, such as Nile blue.

Birifrangent fibrous structures can be visualised with polarized optical microscopy (POM). Although not all LMW gels fibres display this feature,[97–99] this technique can be also used to investigate crystalline structures in the gel matrix.

## *1.4. Rheology*

Rheology is the main tool to study the bulk properties of gels in response to applied stress. A deformation is applied to the material, i.e., the displacement of points of a body, and it can be divided into two: flow and elasticity. Flow represents the irreversible deformation, therefore when the stress is removed, the material does not regain its original form. Flow properties are defined as means of viscosity (indicated as $\eta$ and measured in [Pa s] or [cP]), i.e., the resistance to flow when a fluid is sheared between two surfaces. Elasticity instead is reversible deformation, thus after removing the stress the material recovers its shape. The elastic properties of a solid may be studied by applying a stress and measuring the strain. Fluids exhibiting both flow and elastic behaviour, such as gels, are called viscoelastic.

A rheometer is the instrument generally implied to probe the viscoelastic behaviour of gels. This instrument is composed by two plates: one fixed at the bottom to hold the sample, and one mobile at the top, possessing a shaft that probes the resistance opposed by the material (Figure 1.9a, b). It is useful defining some parameters that can be obtained from the rheological analyses, before outlining each of those.

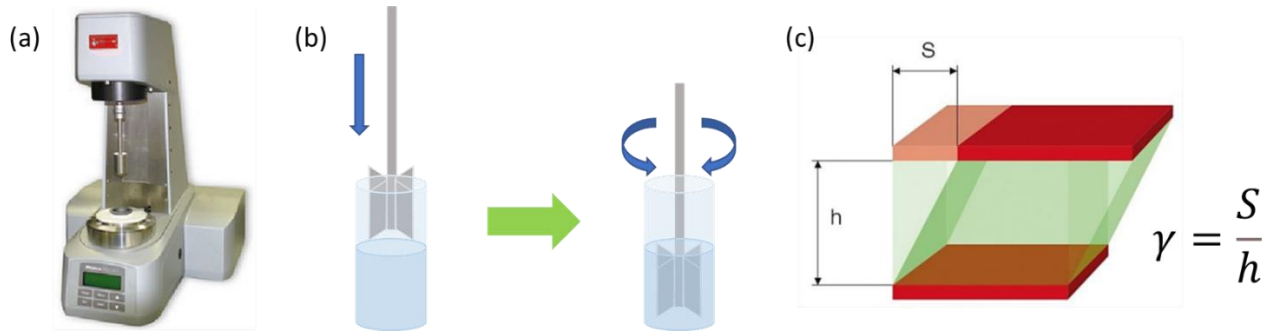


**Figure 1.9**. (a) photograph of a rheometer, (b) cartoon representing how a general analysis with the rheometer moves the shaft in the gel matrix, and (c) cartoon defining the shear stress $\gamma$ as the deflection path S divided by the shear gap width h.

When a stress is applied to the material, the parallel plate model is used to define the shear strain. It is indicated as $\gamma$, is dimensionless or expressed as percentage, and is defined as

the deflection path (S) of the upper movable plate, divided by the shear gap width (h), i.e., the distance between the plates (Figure 1.9c).

When a stress is applied to an elastic material, it stores energy, while a liquid dissipates it as heat. A sinusoidal stress applied to an ideal elastic material produces a sinusoidal stress proportional to the stress and in phase with it. For ideal viscous materials the stress and strain are out of phase by 90°. In real viscoelastic materials, the strain is proportional to the stress, but it is lagged by a certain angle δ whose value spans from 0° to 90°. Therefore, the complex dynamic modulus, indicated as G*, of a viscoelastic material can be resolved in two components: G' = G*cosδ and G" = G*sinδ. The storage modulus, indicated as G' and measured in [Pa], is a measure of the elastic behaviour of the material and can pictorially be translated as the "solid-like" behaviour of the gel. The loss modulus, indicated as G" and measured in [Pa], is instead the quantification of the flow properties of a gel, therefore the "liquid-like" demeanour of the gel. The ratio between these two parameters (G"/G') is the tangent of the phase angle, or tan δ, and represents the ratio between energy dissipated and energy stored.[14] It can have values between 0, representing a fully elastic material, and infinite, representing a fully viscous material, so helps to draw a line to distinguish between solid- and liquid-like materials.

### 1.4.1. Amplitude sweep or strain sweep

With this analysis, the gel is posed under increasing the shear strain γ over time keeping constant the angular frequency ω (Figure 1.10a). The outcome is represented as a diagram representing on the *x*-axis the shear strain on a logarithmic scale, and on the *y*-axis the storage and loss moduli G' and G", both on a logarithmic scale. The strain sweep experiment reveals some important features of the gel, such as the linear viscoelastic range (LVER), i.e., the region where both G' and G" follow a linear trend. At a certain point, indicated by the linearity limit or gel strength ($\gamma_L$), both the moduli will undergo a decrease, usually more prominent for G' than G", after which the gel network is starting to break. As the moduli decrease, they will cross over at a certain point. This is called yield value $\gamma_F$

and represents the shear strain after which the material structure is destroyed, and the material can flow (Figure 1.10b).

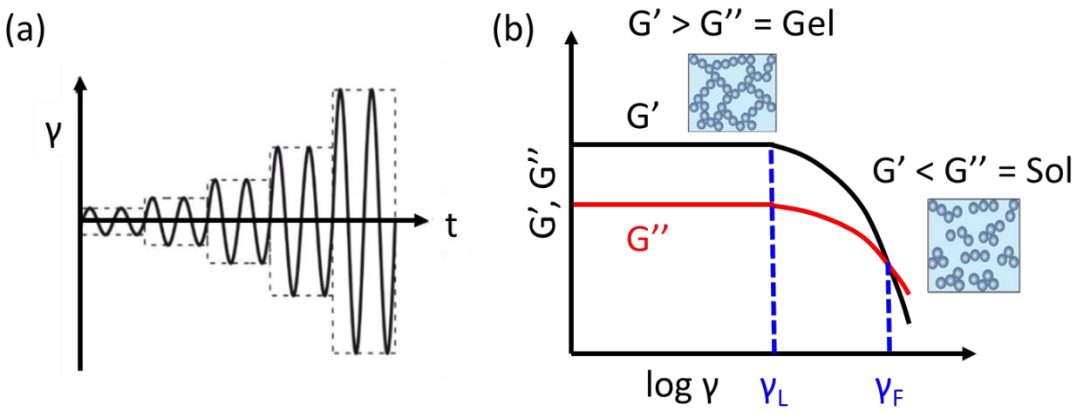


**Figure 1.10**. (a) Set of an amplitude sweep experiment, with increasing strain (γ) over time at a fixed angular frequency, (b) representation of an amplitude sweep test on a gel sample, with G' > G" before the crossover point.

Amplitude sweep experiments are usually the first rheological characterisation, since all the other oscillatory tests require that the measure is performed at a strain within the linear viscoelastic range.

## 1.4.2. Frequency sweep

This analysis, unlike the amplitude sweep, varies the angular frequency ω of the applied stress, keeping constant the shear strain γ in a non-destructive deformation range, i.e., in the linear viscoelastic range (Figure 1.11a). High frequencies are used to simulate fast motion on short timescales, whereas low frequencies simulate slow motion on long timescales or at rest. Basically, with the frequency sweep analysis it is possible to gain information about the inner structure of the material. The frequency sweep graphs have on the x-axis the angular frequency ω in a logarithmic scale and on the y-axis G' and G" on a logarithmic scale, as for the amplitude sweep. This analysis allows a distinction between viscoelastic materials such as gels and viscous solutions. Sometimes, also viscous

solutions are reluctant to flow, and with the inversion test a viscous solution could appear as a gel. However, viscous solutions have a frequency-dependent network, therefore, on increasing the angular frequency, a crossover of the moduli should appear. Gels instead have a frequency-independent behaviour, since the relaxation time of the material is shorter than the frequency change, so in this case the moduli do not change on variation of ω (Figure 1.11b).

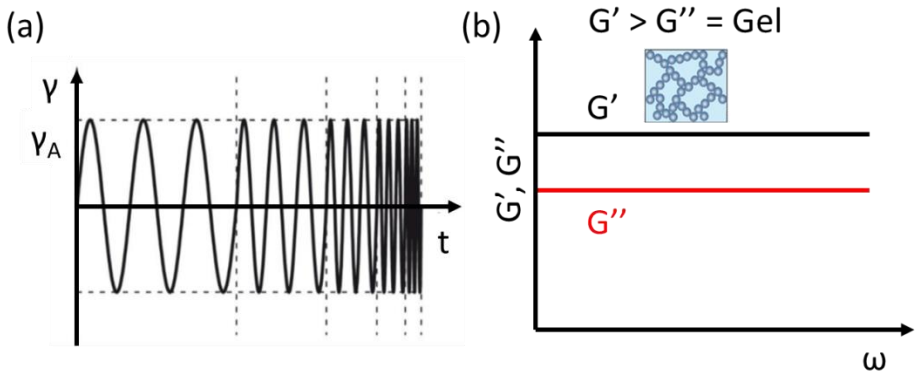


**Figure 1.11**. (a) Set of a frequency sweep experiment, with increasing frequency (ω) over time at a fixed shear strain, (b) representation of a frequency sweep test on a gel sample. G' and G" do not cross over.

## 1.4.3. Thixotropy or step-strain

With this analysis it is possible to probe the ability of the material to recover its viscoelastic properties after the repeated disruption of the gel matrix. To do so, the gel is analysed at a constant shear strain γ, in the linear viscoelastic range of the gel, for few minutes (here, G' > G"). Then the shear strain is increased to a value out of the LVER and ideally beyond its yield value $\gamma_F$, to be sure of breaking the gel network (here, G' < G"). The shear strain is left for other few minutes at this value, then it is decreased again to its initial value in the LVER. At this point, if the gel is not able to regain its original shape, the gel is broken and the G" remains higher than G'. Otherwise, if the gel is thixotropic, it can regain its viscoelastic properties, the moduli rapidly increase again to their initial values (G' > G") (Figure 1.12). In thixotropic gels, this cycle can be repeated multiple times, and these gels

will not lose their thixotropic ability. During the whole analysis, the angular frequency ω is kept constant.

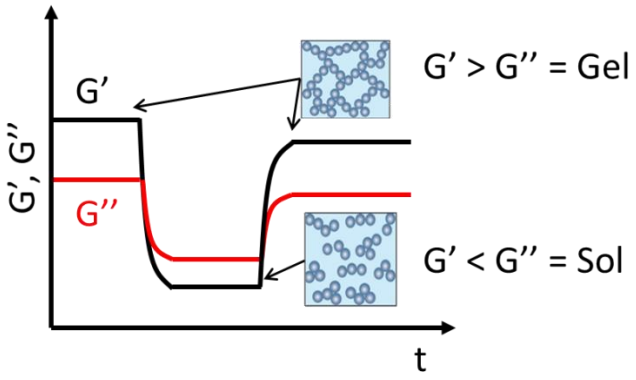


**Figure 1.12**. Representation of a step-strain test on a thixotropic gel sample. G' and G'' cross over at high strain and the gel matrix is recovered at low strain.

## 1.4.4. Time sweep

This analysis is used where the gelation takes some time to reach completion. For example, it is used in systems where gelation is triggered with slow hydrolysis reactions such as the ones involving GdL, rather than the ones triggered via solvent change. It is used to understand the time required for a system to be gelled, therefore its gelation kinetics. In this case both the shear strain and the angular frequency are kept constant at a value that do not interfere with the gelation process, i.e., in the LVER. At the beginning, the G'' usually dominates over G', as gelation has not occurred yet, then when the gelation starts a crossover of the moduli is observed and they continue to increase until a plateau is reached. At this point, the gel fibres are completely formed (Figure 1.13). This analysis, however, is also useful to study other system that undergo changes over time, for example gel-to-gel transitions where even though no crossover is observed, the fibres change during the process and so the mechanical properties.

The rheological analyses described so far are the ones I performed for the studies in my thesis, however, the rheometer offers the possibility to analyse gels under many other points of view. For example, it is possible to study the gel formation as the temperature

varies through a temperature sweep, or adhesive gels can be studied with the tack test, as well as their viscosity can be analysed with the viscosity test. However, for the purpose of this thesis, I will not discuss any further about such techniques.

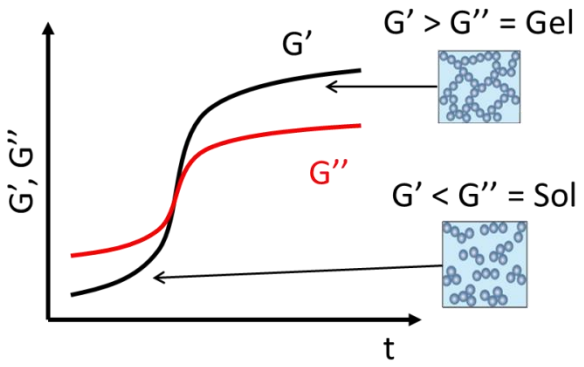


**Figure 1.13**. Representation of a time sweep test on a gel sample. G' and G'' cross over as the gelation starts.

## *1.5. Aim of the thesis*

The purpose of this thesis is to present peptide-based LMW gels. All the gels will be characterised from the molecular to the bulk level using several techniques to properly correlate the gel properties with the gelator structure, and the different conditions to obtain the material, such as solvent and trigger.

New gelators will be rationally synthesised, including atoms or moieties that affect the gelation ability of the resulting molecule. Then, the best gelation conditions will be investigated, paying particular attention to sensitive groups on the gelator.

The gel formation will be controlled over time and space, to obtain either a change in the morphology of the fibres or the formation of a gradient gel. These results will be achieved by annealing the gel matrix or exploiting the reaction-diffusion of a hydrolysing reagent through the gel matrix.

The final materials will be thoroughly studied for possible applications as media for the controlled release of fragrances a well as bioactive compounds. Other gels will instead be investigated for their ability of trapping dyes and pharmaceutical pollutants from waste water. Finally, the interaction of the gel matrix with a light-responsive molecule will be probed to outline how the gel matrix and the additive affect each other.

In the following paragraphs I will indicate the gelators synthesised with numbers, while the materials will be indicated by numbers followed by letters, referring respectively to the gelator and the conditions used for the gel formation (e.g., **3c**). Moreover, multicomponent systems will be indicated with numbers in brackets, followed by a letter (e.g., **(7+8)a**). When gel layers will be formed by preparing one gel on the other, they will be indicated by their own codes (number + letter, e.g. **7a** and **8b**) separated by a slash. The code before the slash will indicate the gel on the top, the one after the slash will indicate the gel at the bottom, e.g., **7a/8b**.

All the details concerning the synthesis and characterisation of molecules, as well as the specifics for the preparation and analysis of the gels prepared will be shown at the end of the manuscript, in chapter 6.

# *Chapter 2. Design of LMW gelators and control over delicate steps in gelation*

When designing a new LMW gelator it is possible to follow few guidelines. As they form fibres through weak interactions, inserting more sites that can create such bonds is highly desirable. Peptides have amide bonds, therefore can create H-bonds. One of the most important interaction that controls the formation of fibres is π-π stacking.[100–104] For this reason, a lot of peptide based gelators include either aromatic amino acids or an aromatic protecting group in their feature. The presence of rigid moieties also enhances the gelation ability of a molecule. For example, the presence of an oxazolidinone (Oxd) derived from threonine (Thr)[105] introduces a constraint that may favour the formation of intermolecular interactions (Figure 2.1a).[39,106,107] For example, the dipeptide Boc-$^{L}$Phe-$^{D}$Oxd-OBn forms a fibre-like material due to the spontaneous formation of 1D infinite chains, where the parallel dipeptide units are connected by single hydrogen bonds. This effect is explained by the imide (pseudo-peptide) bond between the Oxd ring and the Phe. The nitrogen atom connects an exo- to an endocyclic carbonyl, so that, on formation of the imide bond, the two carbonyl groups lie *anti* to each another, thus adopting a rigid *trans* conformation.[108] Such moieties are often called "privileged scaffolds".[109,110]

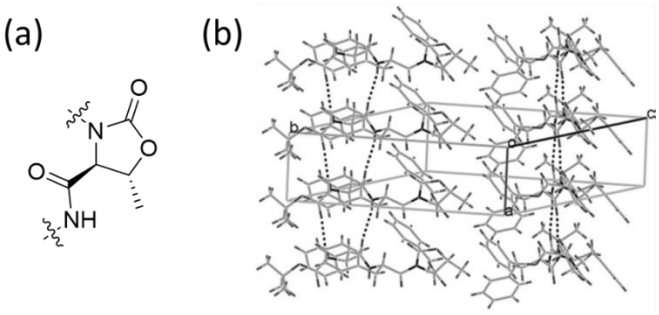


**Figure 2.1**. (a) Molecular structure of the Oxd moiety forming peptide bonds, (b) β-sheet crystal packing of the gelator Boc-$^{L}$Phe-$^{L}$Phe-$^{D}$Oxd-OBn. Figure (b) is adapted from reference[106].

In another example, two very similar molecules were compared. Both composed by the Boc-protected diphenylalanine (Boc-$^{L}$Phe-$^{L}$Phe), they were coupled with D-proline ($^{D}$Pro) and $^{D}$Oxd, to obtain respectively the tripeptides Boc-$^{L}$Phe-$^{L}$Phe-$^{D}$Pro-OH and Boc-$^{L}$Phe-$^{L}$Phe-$^{D}$Oxd-OH. These were compared to outline differences in their ability to form fibres. Being more flexible, the tripeptide Boc-$^{L}$Phe-$^{L}$Phe-$^{D}$Pro-OH in solution appeared as a mixture of conformers, as the peptide bond is in a *trans-cis* mixture. On the other hand, the second tripeptide Boc-$^{L}$Phe-$^{L}$Phe-$^{D}$Oxd-OH in solution existed as the single *trans*-conformer and formed an infinite parallel β-sheet structure, reveraled through single crystal X-ray diffraction (Figure 2.1b). From these differences arose different macroscopic behaviour, i.e., the incapacity of Boc-$^{L}$Phe-$^{L}$Phe-$^{D}$Pro-OH to form fibre-like materials and the ability of Boc-$^{L}$Phe-$^{L}$Phe-$^{D}$Oxd-OH to form gels.[39,106,111]

## *2.1. Rational design of a LMW gelator*

During my PhD thesis, we used a Boc-protected difluorinated phenylalanine (Boc-$^{D}$Phe($F_2$)-OH, **1**) to prepare hydrogels. This amino acid contains an aromatic ring linked to two fluorine atoms, that may create additional interactions, such as C-F···H-C bonds. Being the most electronegative atom on the periodic table, fluorine is able to polarise the C-H covalent bonds and create such weak hydrogen bonds, with a halogen-bond character, i.e., halogen-hydrogen bonds. The strength of these bonds, however, is pretty weak and spans from 0.5 to 1.6 kcal/mol.[112]

The gelator was dissolved in water with containing NaOH, then GdL was added to the solution, to obtain materials **1a**, **1b**, and **1c**, with a concentration of 0.5 %, 1.0 %, and 2.0 % w/V respectively. GdL gets hydrolysed in aqueous media, releasing gluconic acid and decreasing the pH in a controlled manner.[41] A complete self-supporting material was obtained only in concentrations of gelator equal or higher than 1.0% w/V (Figure 2.2, Table 2.1).

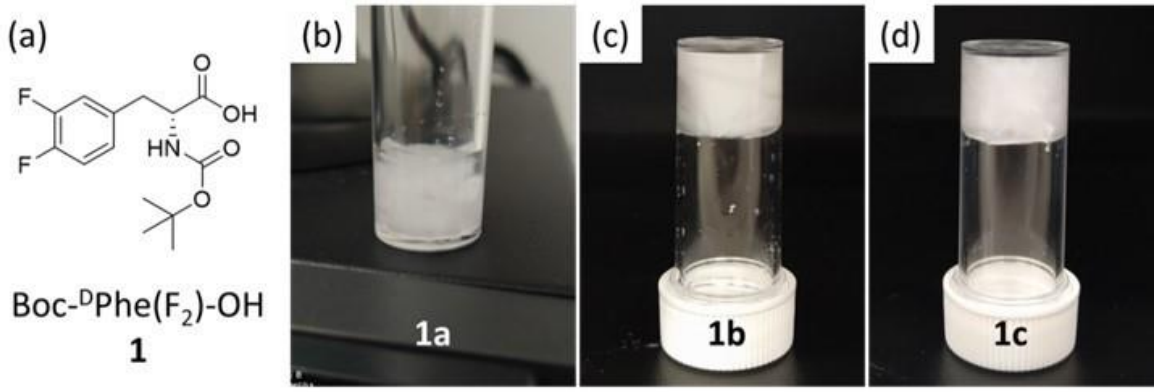


**Figure 2.2**. (a) Molecular structure of the gelator **1**; (b-d) photographs of the gels (b) **1a**, (c) **1b**, and (d) **1c**, in concentrations of (b) 0.5%, (c) 1.0%, and (d) 2.0% w/V of **1** respectively. For (b-d) gels are obtained after dissolution of **1** in water containing NaOH and addition of GdL.

We analysed the morphological appearance of gels **1b** and **1c** both with optical microscopy and scanning electron microscopy (SEM). Sample **1b** with a concentration of 1.0 % w/V

of gelator was taken as model sample, as it formed a stable gel in the lowest concentration tested. Gel **1b** revealed a network composed of a bundle of long thick fibres (Figure 2.3).

**Table 2.1**. Summary of the gels of **1** prepared.

| Gel | Conc. (%) | Solvent | Trigger | Result | G' (kPa) | G" (kPa) |
|---|---|---|---|---|---|---|
| **1a** | 0.5 | $H_2O$ (NaOH) | GdL | PG | N.D. | N.D. |
| **1b** | 1.0 | $H_2O$ (NaOH) | GdL | Gel | 93 ± 42 | 6.2 ± 3.6 |
| **1c** | 2.0 | $H_2O$ (NaOH) | GdL | Gel | 470 ± 61 | 30 ± 6.4 |

PG = partial gel; N.D. = not determined; G' and G" are referred to $\gamma$ = 0.046 %.

We also studied the rheological behaviour of the samples where a stable gel was formed, both over the time required for their formation and after their complete gelation. Gelation of **1b** starts after 2 h, and after the complete formation of the gel its stiffness reaches 90 kPa. On the other hand, gel **1c** starts the self-assembly after 30 minutes and after 16 hours it appears five times stiffer than gel **1b**. These results agree with the different gelator concentration in the two trials (Table 2.1, Figure 2.4).

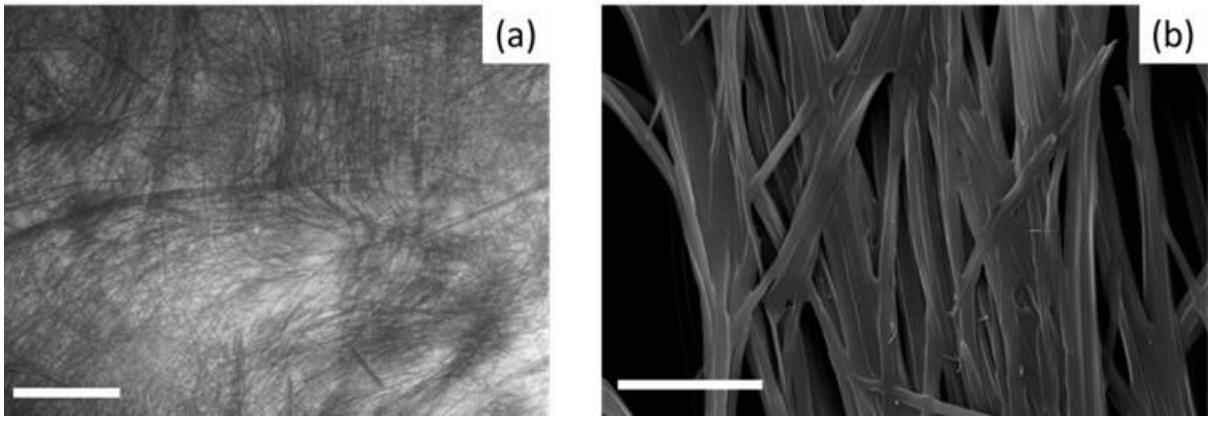


**Figure 2.3**. (a) Optical microscope and (b) scanning electron microscope (SEM) images of the dried gel **1b**. The scalebars are 200 μm for (a) and 15 μm for (b). In all cases, the gels are obtained after dissolution of **1** in water with 1.2 eq. of NaOH and addition of 1.4 eq. of GdL.

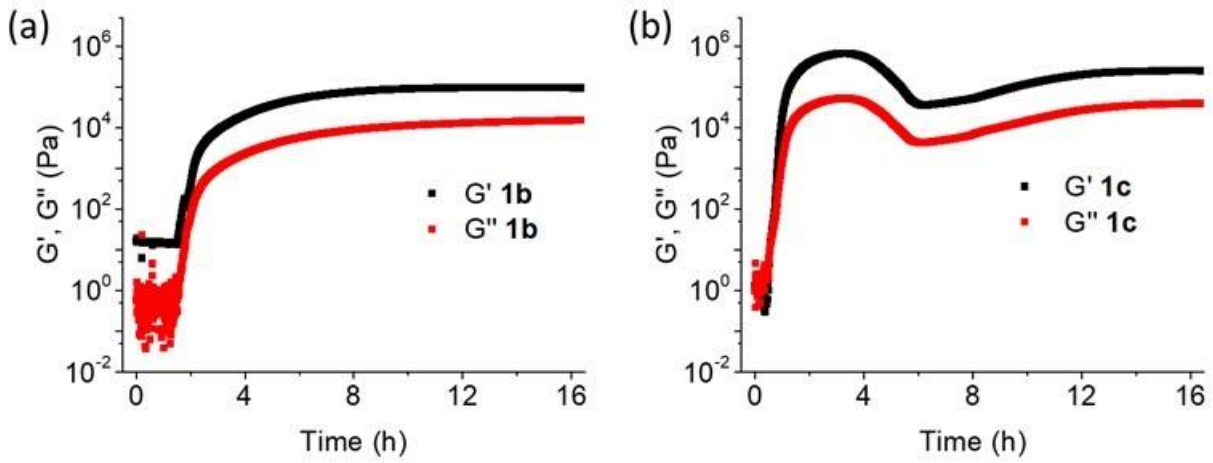


**Figure 2.4**. Time sweeps of the gels **1b** (a) and **1c** (b), at the concentration of 1.0% and 2.0% w/V of **1** respectively.

This amino acid was coupled with the oxazolidinone (Oxd) derived from the cyclization of either D- or L-threonine to obtain respectively molecules Boc-$^{D}$Phe($F_2$)-$^{D}$Oxd-OH, **2** and Boc-$^{D}$Phe($F_2$)-$^{L}$Oxd-OH, **3** (Figure 2.5), to understand how it would affect the gelation ability of the resulting molecule. This moiety is very rigid and may enhance the gelation ability of the scaffold, allowing the resulting molecule to gel at concentrations lower than 1.0% w/V, using the same methodology adopted for Boc-$^{D}$Phe($F_2$)-OH, **1**.

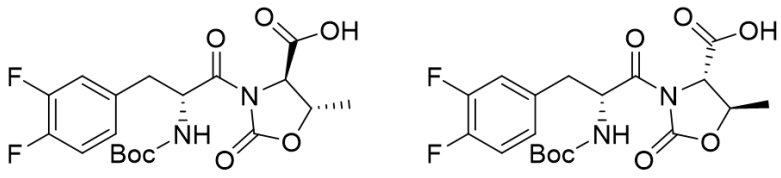


**Figure 2.5**. Molecular structures of the gelators **2** and **3**.

However, the chirality of the Oxd moiety has a pivotal role in the gelling ability of the molecule, as shown by the behaviour of **2** coupled with $^{D}$Oxd against **3** coupled with $^{L}$Oxd. Only turbid solutions can be obtained from **2**, where nanometric-sized aggregates revealed through dynamic light scattering (DLS) are formed in a homogeneous dispersion (data not

shown). On the other hand, **3** can form gels in the concentrations tested for molecule **1** (Table 2.2, Figure 2.6). Taking sample **3a** as example, we revealed a network of thin condensed fibres both through optical microscopy and SEM (Figure 2.7).

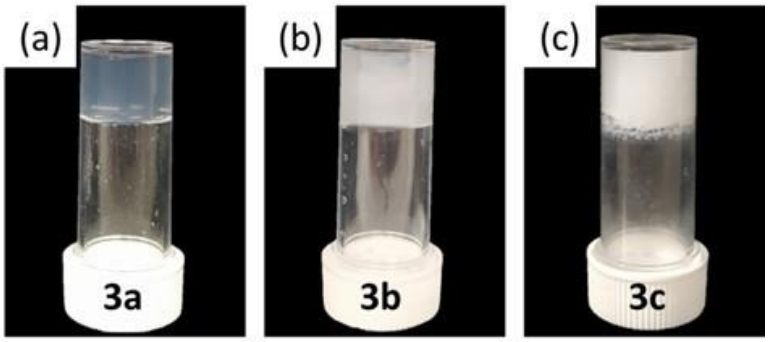


**Figure 2.6**. Photographs of the gels (a) **3a**, (b) **3b**, and (c) **3c** in concentrations of 0.5 %, 1.0 %, and 2.0 % w/V of **3** respectively. In all cases, gels are obtained after dissolution of **3** in water containing NaOH and addition of GdL.

**Table 2.2**. Summary of the gels of **3** prepared.

| Gel | Conc. (%) | Solvent | Trigger | Result | G' (kPa) | G" (kPa) |
|---|---|---|---|---|---|---|
| **3a** | 0.5 | $H_2O$ (NaOH) | GdL | Gel | 16 ± 3.1 | 3.0 ± 0.8 |
| **3b** | 1.0 | $H_2O$ (NaOH) | GdL | Gel | N.D. | N.D. |
| **3c** | 2.0 | $H_2O$ (NaOH) | GdL | Gel | N.D. | N.D. |
| **3d** | 0.5 | PB pH 7.4 | GdL | Gel | 23 ± 1.4 | 3.7 ± 0.6 |

N.D. = not determined; G' and G" are referred to $\gamma$ = 0.046 %.

These gels were characterised from a rheological point of view with time sweep (Figure 2.8). We could notice that the formation of these gels was poorly reproducible and as noticed from their rheology in different concentrations. Although the kinetics of the gels' formation increase with the concentration, the final moduli G' and G" do not, as one would expect.

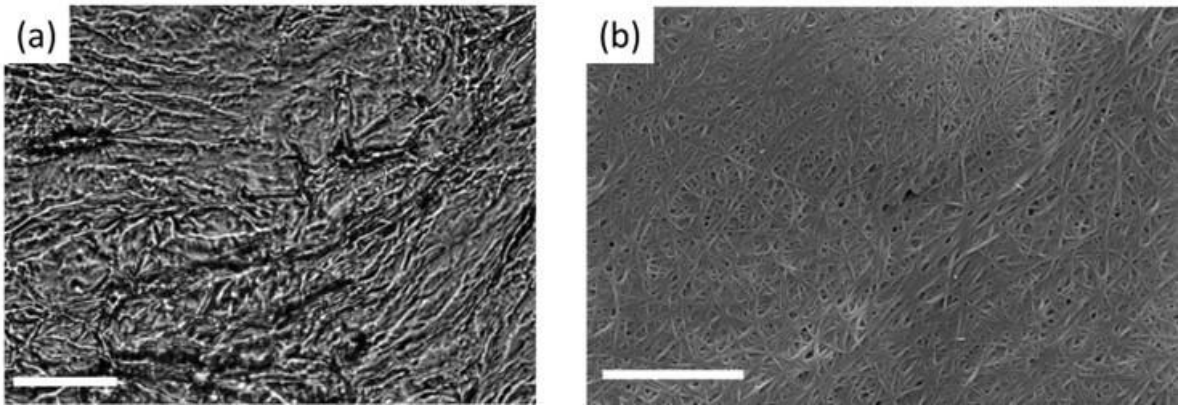


**Figure 2.7**. (a) Optical microscope and (b) scanning electron microscope (SEM) image of the dried gel **3a**. The scalebars are 50 μm for (a) and 15 μm for (b). In all cases, the gels are obtained after dissolution of **3** in water containing NaOH and addition of GdL.

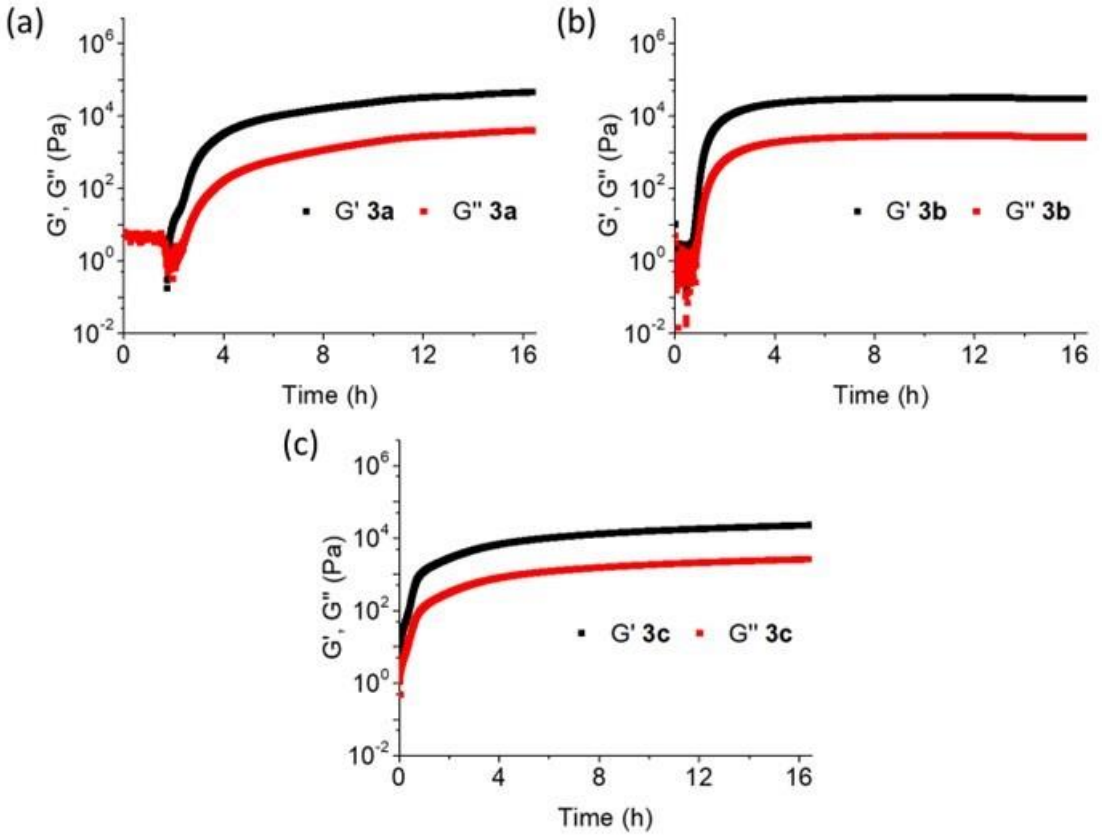


**Figure 2.8**. Time sweeps of the gels (a) **3a**, (b) **3b**, and (c) **3c** at the concentration of 0.5 %, 1.0 % and 2.0 % w/V of **3** respectively.

We investigated whether the reason was by performing HPLC-MS analyses. These revealed that during the dissolution step some gelator got hydrolysed to produce **1** and the free Oxd molecule (Figure 2.9), and this effect was more prominent with the increase of the concentration, going from the 30 % of hydrolysis for the gel with 0.5 % w/V to the 60 % for the gel with 2.0 % w/V concentration.

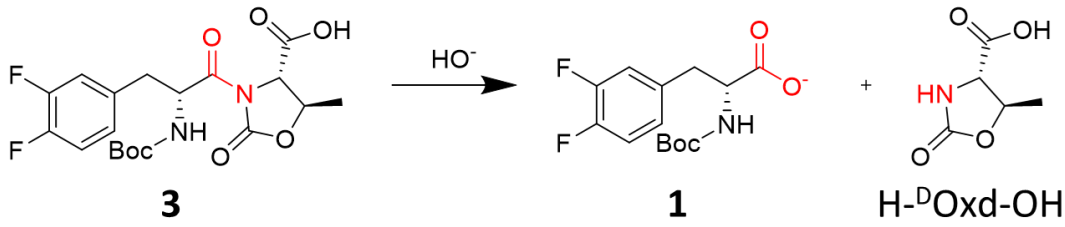


**Figure 2.9**. Hydrolysis reaction of gelator **3** in basic environment to produce **1** and H-$^{D}$Oxd-OH.

For this reason, we limited the hydrolysis by focussing our attention on the gel with the lowest concentration and replacing the NaOH with a milder 30 mM phosphate buffer solution at pH 7.4.

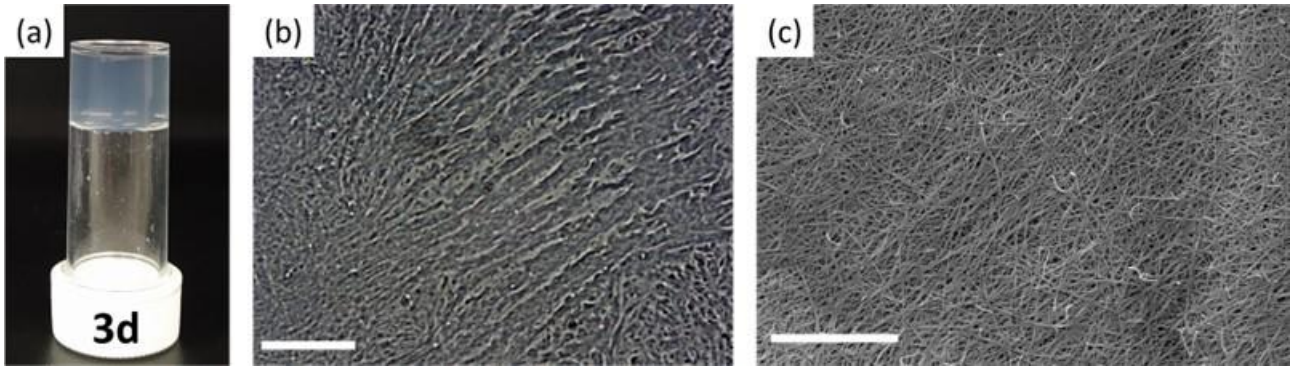


**Figure 2.10**. (a) Photograph of the gel **3d** in concentration 0.5 % w/V of **3**; (b) optical microscope and (c) scanning electron microscope (SEM) image of the dried gel **3d**. The scalebars are 50 μm for (a) and 15 μm for (b). In all cases, the gels are obtained after dissolution of **3** in 30 mM PB and addition of GdL.

After the gelator dissolution, the pH was slightly lower than 7, as the gelator and the phosphate buffer had comparable concentrations. In this way, the phosphate ions are not used to buffer the solution but rather to control the pH to remain at a value high enough to allow the complete dissolution of the gelator. This allowed also to obtain a final pH of the gel close to the one obtained with the dissolution in NaOH. In this methodology the hydrolysis of the gelator was negligible and the gel formation more reproducible. In this way we obtained gel **3d** (Figure 2.10), which presented a morphology very similar to gel **3a**, composted of a network of thin fibres. These gels were characterised from a rheological point of view with time sweep, strain sweep, and thixotropy. This allows to understand whether a gel network can be restored after being broken. The stiffness of the gel is slightly improved compared to the one obtained with dissolution with NaOH, and displays a thixotropic behaviour, as the moduli have the same order of magnitude before and after breaking (Figure 2.11).

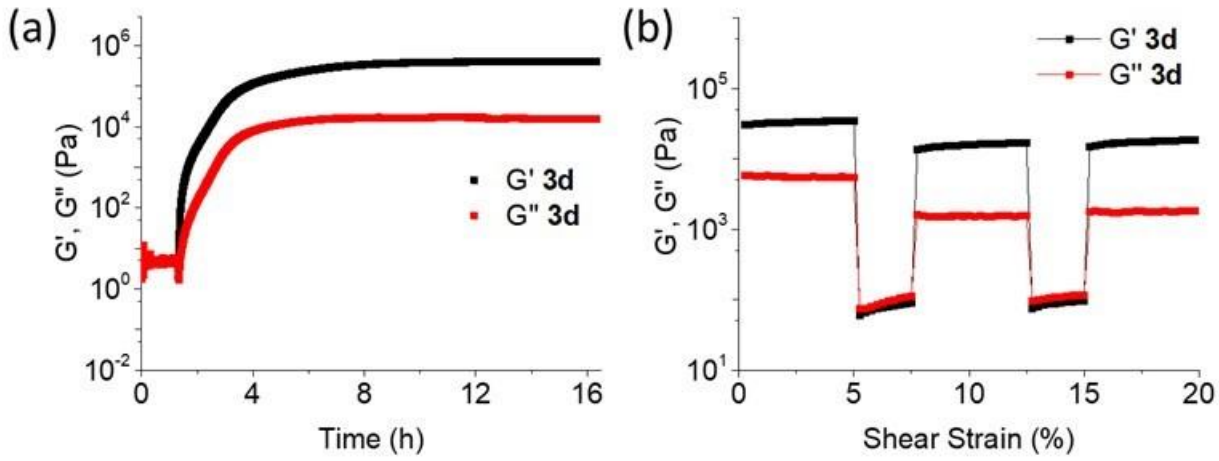


**Figure 2.11**. (a) Time sweep and (b) thixotropy of the gel **3d** at the concentration of 0.5 % w/V of **3**. In all cases, G' is represented in black, G" in red.

As fluorine may be involved in halogen-hydrogen bonds that further strengthen the gel matrix, it may play a role in the gelation ability of a molecule.

## *2.2. Fluorine role in the gelation ability of a shared scaffold*

As the replacement of hydrogen with halogen atoms have an impact on the gelation ability of a molecule,[36,113,114] another strategy to improve the gelation ability could be the insertion of halogen atoms. They change the polarity and the size of the molecule, may create new physical interactions, like halogen bonds, therefore altering the solubility of the molecule in the medium.[112] However, fluorine efficacy is still controversial, as not always it improves the gelation ability.[115,116]

Having considered the involvement of fluorine atoms in the gelation ability, we decided to compare the behaviour of Boc-$^{D}$Phe($F_2$)-$^{L}$Oxd-OH **3** against molecules Boc-$^{D}$Phe(F)-$^{L}$Oxd-OH **4** and Boc-$^{D}$Phe-$^{L}$Oxd-OH **5**, sharing the same scaffold and containing respectively one and no fluorine atoms on the aromatic ring (Figure 2.12).[117]

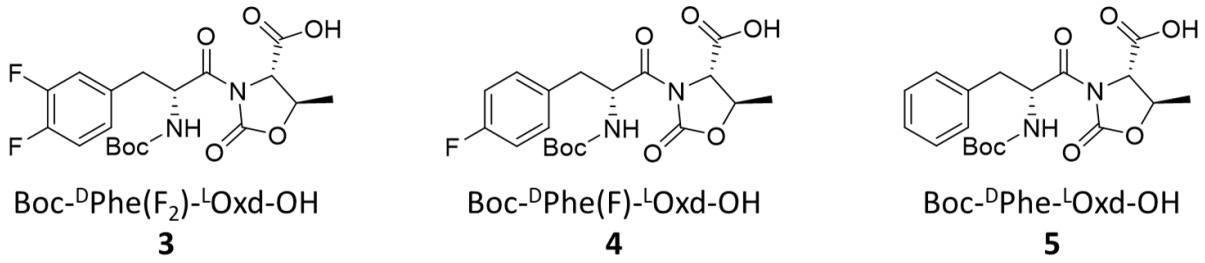


**Figure 2.12**. Molecular structures of the gelators **3**, **4**, and **5**.

We tested the gelation of these three molecules in different conditions and using different triggers. Using the same methodology adopted for the previous study, we dissolved these molecules, in concentration either 0.5 % or 1.0 % w/V in 30 mM or 60 mM PB solutions at pH 7.4 respectively. Then, we triggered the gelation by adding either GdL, to form gels **3d**, **3e**, **4a**, **4b**, **5a**, and **5b**, or calcium chloride to form gels **3f**, **3g**, **4c**, **4d**, **5c**, and **5d**, obtained from gelators **3**, **4**, and **5** respectively (Figure 2.13). Calcium cations are divalent ions and can be chelated by two gelator molecules containing a carboxyl anion. Moreover, further weak bonds such as cation-π interactions concur to stabilise the fibres and form a gel.

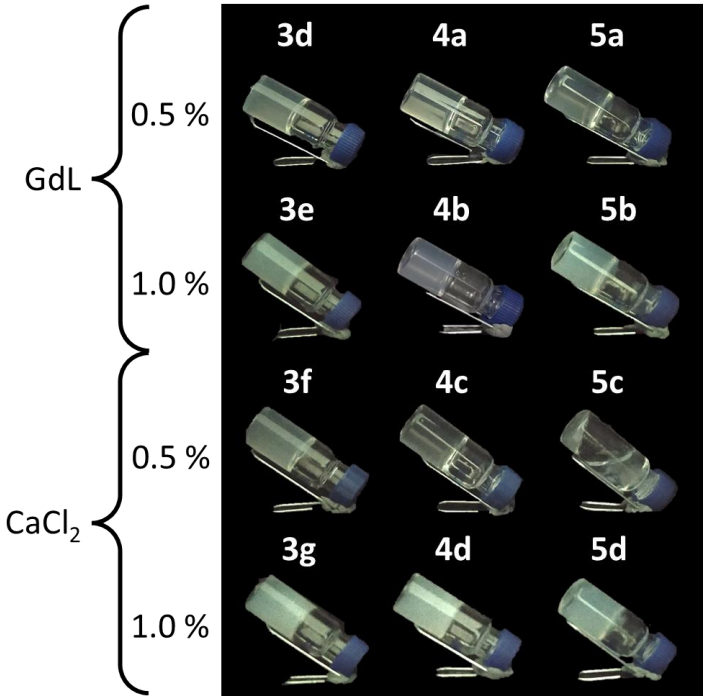


**Figure 2.13**. Photographs of the gels **3d-g**, **4a-d**, and **5a-d**, obtained from gelators **3**, **4**, and **5** respectively, with addition of GdL (**3d**, **3e**, **4a**, **4b**, **5a**, and **5b**) or calcium chloride (**3f**, **3g**, **4c**, **4d**, **5c**, and **5d**) in concentration of gelator either 0.5 % or 1.0 % w/V.

At a first sight, the presence of fluorine seems to favour the gelation, as all the trials formed a gel, apart from sample **5c** obtained from molecule **5** containing no fluorine atoms, which only partially gelled the solvent.

We further investigated the comparison of the gelation ability of these molecules with the solvent change method. The addition of a non-solubilising solvent results in a decrease in solubility and the gelator molecules start to aggregate, forming fibres. We first solubilised the gelators in an organic solvent, then added water, as non-solubilising solvent. None of the molecules was able to form a gel with a content of water lower than the 70% of the total volume, so we tested the formation of gels in the same concentrations as the previous experiments by dissolving the gelators in ethanol and adding water in a 3:7 ratio, to obtain materials **3h**, **3i**, **4e**, **4f**, **5e**, and **5f**. We repeated the experiment with isopropyl alcohol and water, to obtain materials **3j**, **3k**, **4g**, **4h**, **5g**, and **5h**. (Figure 2.14). Also in this case, the presence of fluorine seems to have a positive impact on the gelation ability of this scaffold,

as only sample **5g** containing gelator **5** did not form a gel. All the trials tested are summarised in Table 2.3.

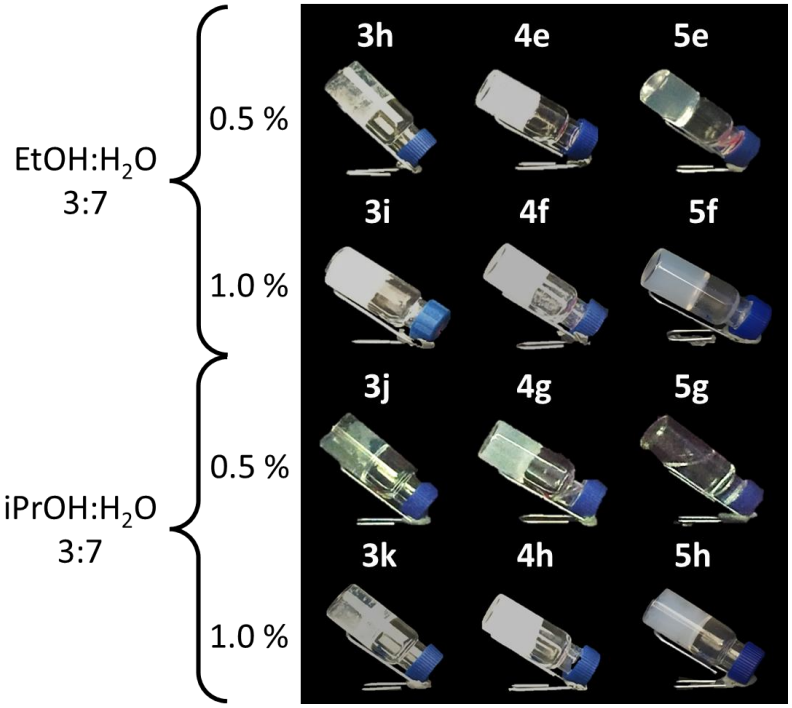


**Figure 2.14**. Photographs of the gels **3h-k**, **4e-f**, and **5e-f**, obtained from gelators **3**, **4**, and **5** respectively. Samples **3h**, **3i**, **4e**, **4f**, **5e**, and **5f** are obtained after dissolution in ethanol and addition of water, samples **3j**, **3k**, **4g**, **4h**, **5g**, and **5h** are obtained after dissolution in isopropyl alcohol and addition of water, in concentration of gelator either 0.5 % or 1.0 % w/V. In all cases, the ratio alcohol:water is 3:7.

We performed strain sweep experiments on the gels obtained to understand whether the presence of fluorine had an impact not only on the gelation ability but also on the stiffness of the materials and we observed that fluorine generally improves the stiffness of the materials obtained (Table 2.3), however increasing the number of fluorine atoms does not necessarily improve the stiffness, as shown by the behaviour of gels obtained from **3** against the ones obtained from **4**. In this case, other effects take place, i.e., different polarity and solubility.

**Table 2.3**. Summary of the gels of **3**, **4**, and **5**, with rheological properties and transparency.

| Gel | Conc. (%) | Solvent | Trigger | Result | G' (kPa) | G" (kPa) | Transp. |
|---|---|---|---|---|---|---|---|
| **3d** | 0.5 | PB | GdL | Gel | 23 ± 1.4 | 3.7 ± 0.6 | 46 |
| **3e** | 1.0 | PB | GdL | Gel | 96 ± 18 | 19 ± 5.1 | 4.7 |
| **3f** | 0.5 | PB | $CaCl_2$ | Gel | 23 ± 4.3 | 2.9 ± 0.9 | 22 |
| **3g** | 1.0 | PB | $CaCl_2$ | Gel | 87 ± 24 | 11 ± 4.4 | 1.0 |
| **4a** | 0.5 | PB | GdL | Gel | 25 ± 2.9 | 4.0 ± 0.4 | 64 |
| **4b** | 1.0 | PB | GdL | Gel | 160 ± 18 | 28 ± 2.0 | 49 |
| **4c** | 0.5 | PB | $CaCl_2$ | Gel | 6.2 ± 3.9 | 0.7 ± 0.3 | 75 |
| **4d** | 1.0 | PB | $CaCl_2$ | Gel | 52 ± 15 | 7.8 ± 2.5 | 12 |
| **5a** | 0.5 | PB | GdL | Gel | 3.3 ± 0.3 | 0.7 ± 0.1 | 57 |
| **5b** | 1.0 | PB | GdL | Gel | 109 ± 18 | 22 ± 10 | 15 |
| **5c** | 0.5 | PB | $CaCl_2$ | PG | N.D. | N.D. | N.D. |
| **5d** | 1.0 | PB | $CaCl_2$ | Gel | 110 ± 41 | 13 ± 4.3 | 1.4 |
| **3h** | 0.5 | EtOH | $H_2O$ | Gel | 28 ± 2.7 | 4.8 ± 0.4 | 55 |
| **3i** | 1.0 | EtOH | $H_2O$ | Gel | 140 ± 35 | 26 ± 7.8 | 0.9 |
| **3j** | 0.5 | iPrOH | $H_2O$ | Gel | 2.3 ± 0.6 | 0.5 ± 0.1 | 58 |
| **3k** | 1.0 | iPrOH | $H_2O$ | Gel | 11 ± 4.5 | 3.1 ± 1.2 | 77 |
| **4e** | 0.5 | EtOH | $H_2O$ | Gel | 49 ± 4.7 | 6.0 ± 1.9 | 1.1 |
| **4f** | 1.0 | EtOH | $H_2O$ | Gel | 120 ± 5.9 | 15 ± 1.4 | 0.1 |
| **4g** | 0.5 | iPrOH | $H_2O$ | Gel | 18 ± 5.8 | 4.5 ± 1.7 | 0.2 |
| **4h** | 1.0 | iPrOH | $H_2O$ | Gel | 46 ± 8.8 | 12 ± 1.7 | 0.1 |
| **5e** | 0.5 | EtOH | $H_2O$ | Gel | 9.0 ± 3.2 | 2.0 ± 0.8 | 67 |
| **5f** | 1.0 | EtOH | $H_2O$ | Gel | 93 ± 12 | 23 ± 2.7 | 5.4 |
| **5g** | 0.5 | iPrOH | $H_2O$ | Sol | N.D. | N.D. | N.D. |
| **5h** | 1.0 | iPrOH | $H_2O$ | Gel | 36 ± 4.6 | 9.8 ± 1.4 | 21 |

PG = partial gel; Sol = solution; N.D. = not determined; G' and G" are referred to $\gamma$ = 0.068 %; the transparency is measured as means of transmittance (%) at $\lambda$ = 630 nm.

All the gels were left to dry to obtain a xerogel, then a small portion of this was used to take images with optical microscope. This analysis revealed a fibrous matrix in all the samples. In particular, the samples triggered with calcium appeared branched with a fibrous structured more regular and ordered compared to the other samples (Figures 2.15 and 2.16).

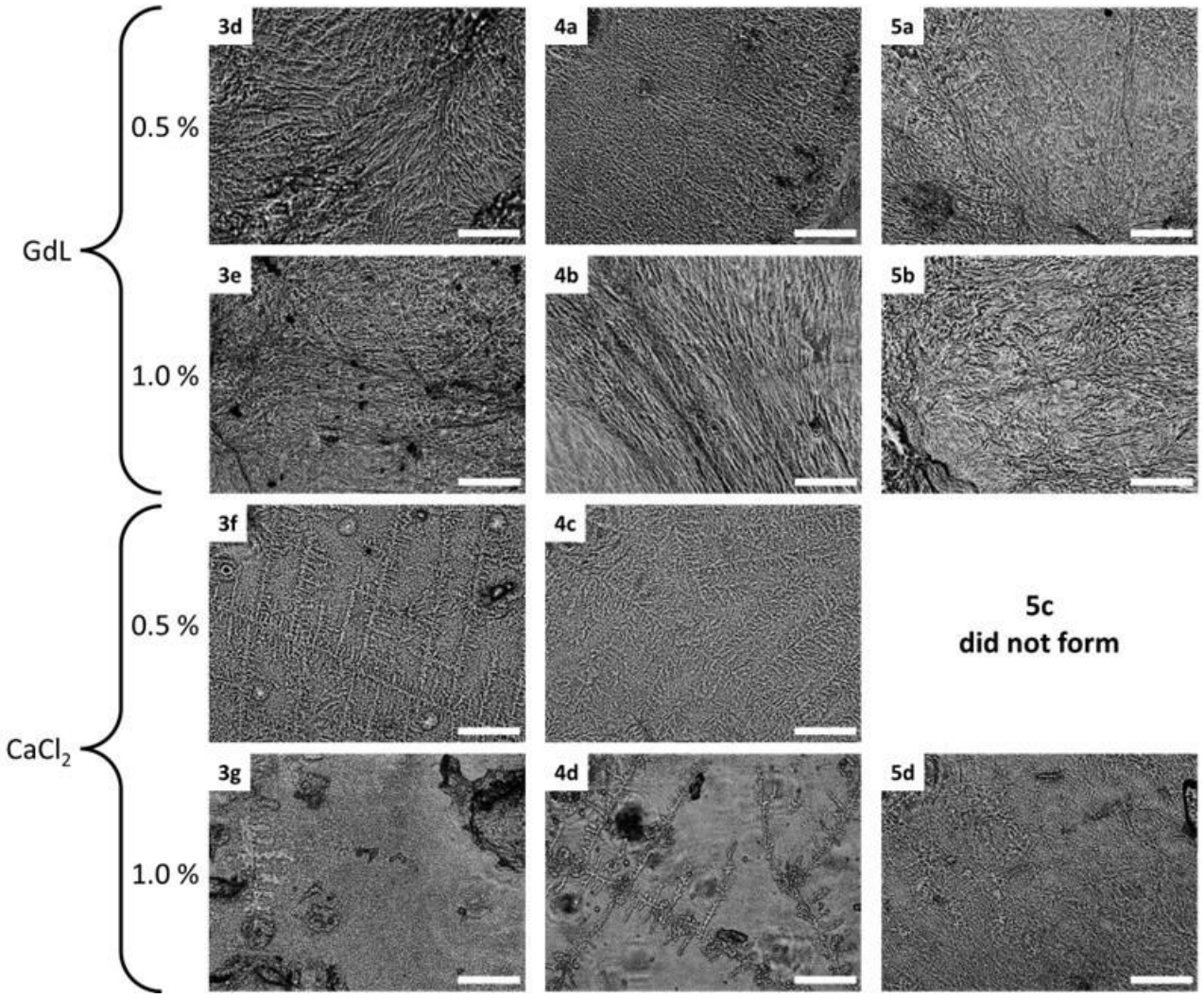


**Figure 2.15**. Optical microscope images of the xerogels of the materials **3d-g**, **4a-d**, and **5a-d**, obtained after dissolution in PB at pH 7.4 and addition of either GdL or $CaCl_2$. In all cases, the scalebar is 100 μm.

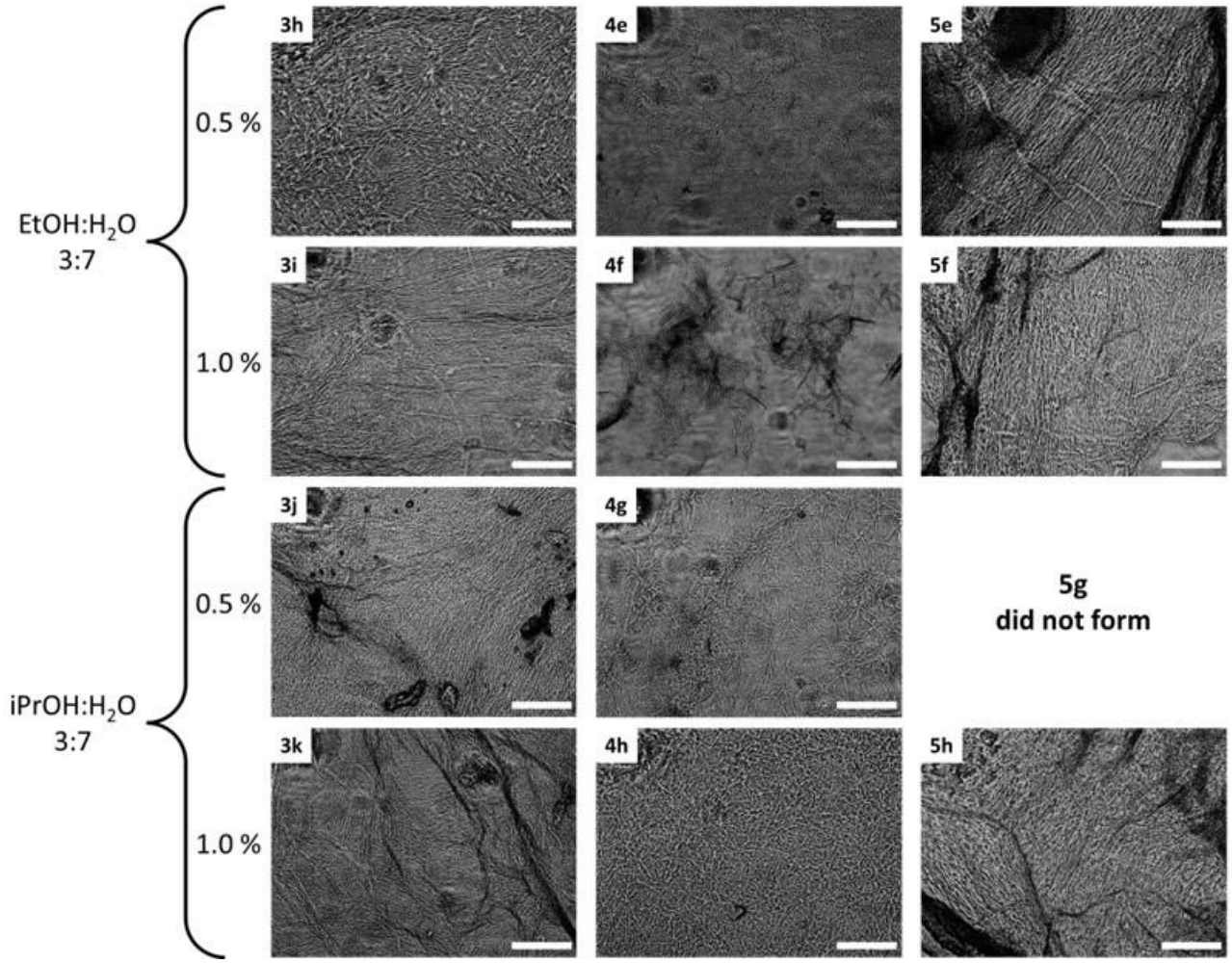


**Figure 2.16**. Optical microscope images of the xerogels of the materials **3h-k**, **4e-h**, and **5e-h**, obtained after dissolution in either ethanol or isopropyl alcohol and addition of water. In all cases, the scalebar is 100 μm.

The xerogels containing 1.0 % w/V of gelator were also characterised with SEM (Figure 2.17), as at this concentration all the trials formed a gel. Generally, the fibres of the gels of **5** appeared condensed and collapsed on each other, while the ones of the gels of Boc-$^{D}$Phe($F_2$)-$^{L}$Oxd-OH **3** and Boc-$^{D}$Phe($F_2$)-$^{L}$Oxd-OH **4**, appeared more separated and more visible. The SEM images also show an effect of the solvent on the organization of the molecules at the superstructure level. When xerogels are obtained from chemical systems containing GdL or calcium ions, the formation of the fibres is less evident with respect to xerogels from EtOH and iPrOH, although the greater aptitude of **3** and **4** to form fibres is confirmed. In ethanol and isopropyl alcohol, a similar behaviour is observed among the

different molecules. They all have the tendency to assemble in fibres. This effect is much more marked for the gels of **3** and **4**, while the xerogels of Boc-$^{D}$Phe-$^{L}$Oxd-OH **5** appears as amorphous aggregates in which some fibres are dispersed.

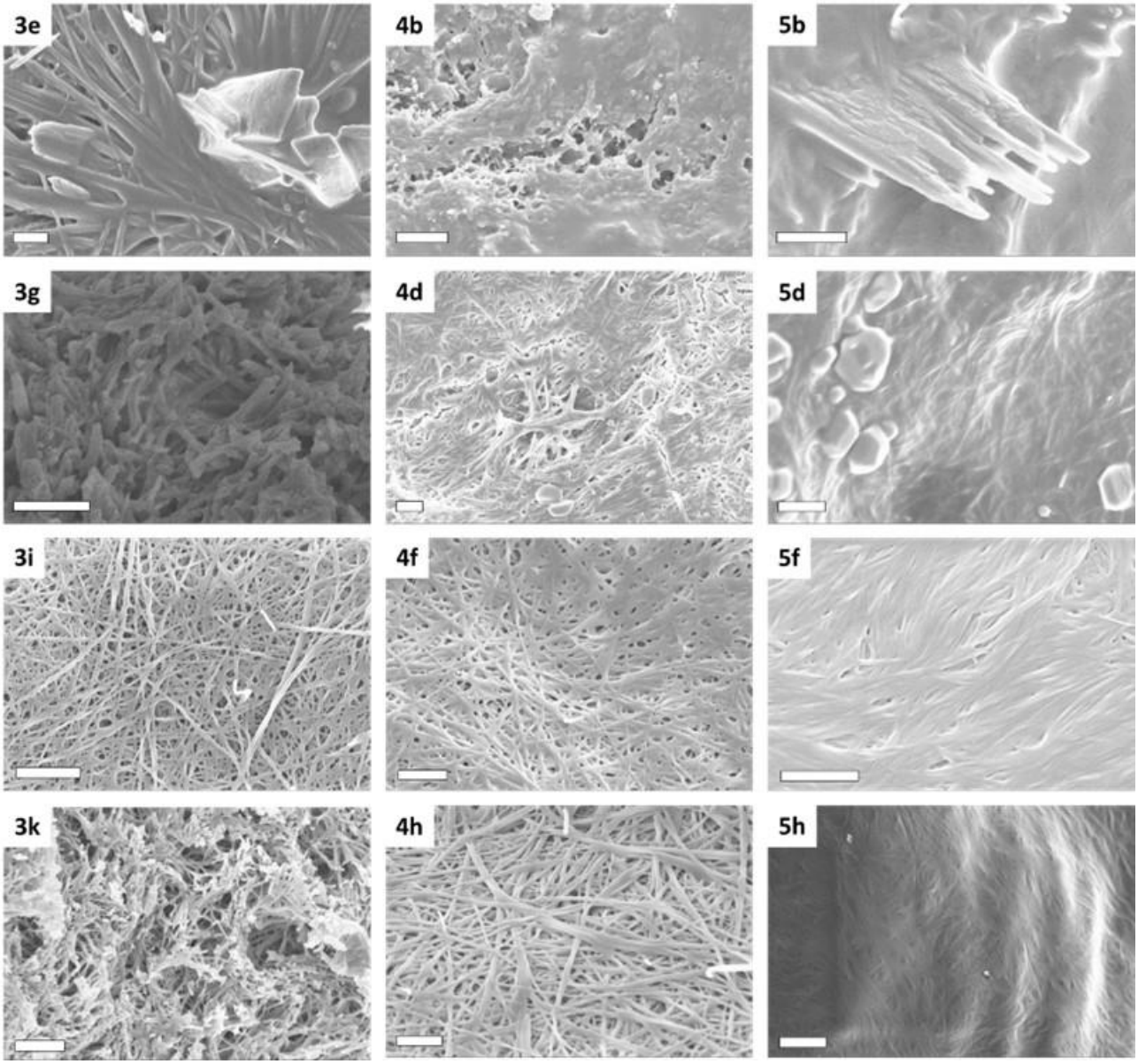


**Figure 2.17**. Scanning electron microscope (SEM) images of the xerogels of **3**, **4**, and **5**, obtained with all the methodologies studied. In all cases, a concentration of 1.0 % w/V of gelator was used. The scalebar is 2 μm.

Another interesting property showed by most of these materials is their self-healing ability. In fact, their network is spontaneously restored after vigorous shaking and an overnight

rest. All the gels obtained after dissolution in PB at pH 7.4 have this property apart from samples **3f** and **4c**, containing the 0.5 % w/V of gelator and triggered with $CaCl_2$ (Figure 2.18). Sample **3f** only partially recovered the gel network, while sample **4c** remained a viscous solution.

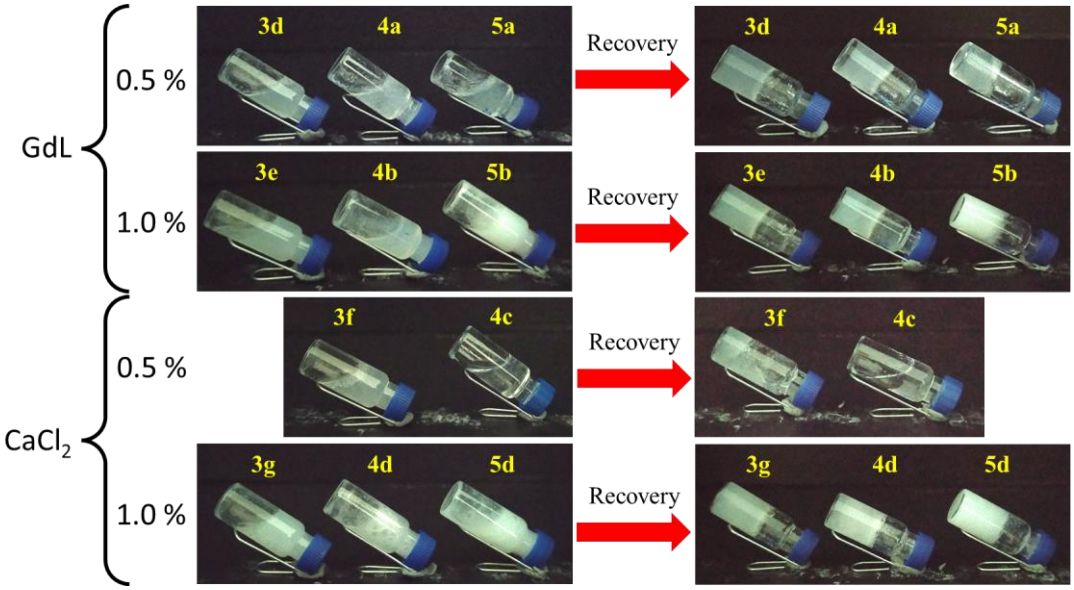


**Figure 2.18**. Recovery tests of the gels **3d-g**, **4a-d**, and **5a-d**, obtained after dissolution in PB at pH 7.4 and addition of either GdL or $CaCl_2$. The gels used for this experiment were left to form overnight, then shaken vigorously and left to recover overnight.

Also the gels triggered via the solvent switch method display this property, apart from samples **3j** and **4g**, obtained from iPrOH:$H_2O$ 3:7, at a concentration of 0.5 % w/V of gelator. In this case, both samples formed a viscous solution, translucent for sample **3j** and opaque for sample **4g** (Figure 2.19).

This behaviour was further investigated with thixotropy analysis with the rheometer. With this analysis, all the gels appeared thixotropic (data not shown). This indicates that although all the materials have a thixotropic behaviour, some of them are not able to self-heal after a more aggressive shaking.

Some of the gels prepared appeared also translucent, so we decided to probe their transparency by analysing their absorbance in the visible region. This is an appealing property for optical applications.[118] The transparency is expressed by means of

transmittance (%) at 630 nm (Table 2.3). The value at 630 nm was chosen as in the middle between 560 and 700 nm, where the molecules showed the highest transparency (a decrease in absorption). The gels of **3** appeared very transparent with the solvent switch methodology, the ones of **4** on the other hand gave the best results in terms of transparency when prepared with addition of either GdL or $CaCl_2$. Gels of **5** instead appeared transparent only at a concentration of 0.5% w/V.

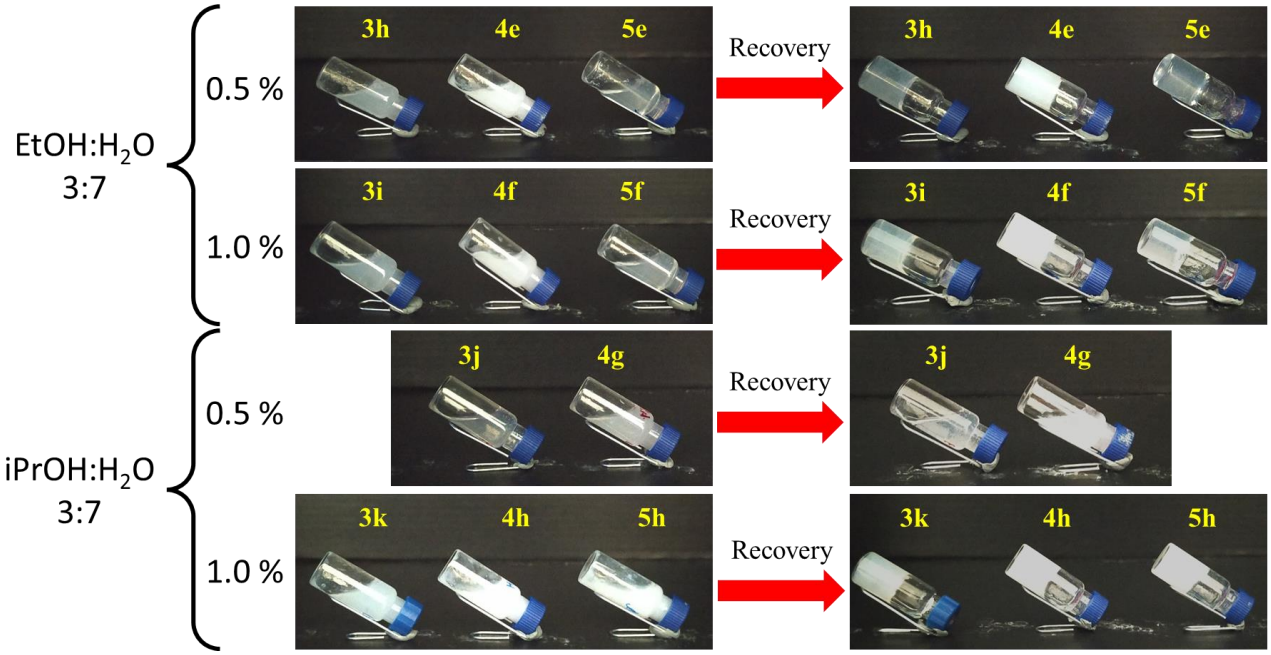


**Figure 2.19**. Recovery tests of the gels **3h-k**, **4e-h**, and **5e-h**, obtained after dissolution in either ethanol or isopropyl alcohol and addition of water. The gels used for this experiment were left to form overnight, then shaken vigorously and left to recover overnight.

Finally, we tested the biocompatibility of these molecules towards mouse embryonic fibroblasts NIH-3T3, with the MTT viability assay,[119,120] to probe the possibility of using these molecules as scaffold for the cellular growth (Table 2.4). This showed that all the gelators are biocompatible in low concentration (0.05 % w/V). At the concentration used for preparing gels (0.5 % w/V), the fluorine-free gelator **5** appeared toxic, while cells were more tolerant towards gelators **3** and **4**.

**Table 2.4**. Cell viability of NIH-3T3 cells after 24 h of treatment with 0.5 % and 0.05 % w/V of **3**, **4**, and **5**.

| Sample | Cell viability (%) control | Cell viability (%) 0.5 % w/V | Cell viability (%) 0.05 % w/V |
|---|---|---|---|
| **DPBS** | 100 ± 7 | - | - |
| **3** | - | 73 ± 9 | 99 ± 4 |
| **4** | - | 77 ± 7 | 90 ± 9 |
| **5** | - | 40 ± 5 | 89 ± 5 |

## *2.3. Applicability of the mild solubilisation conditions*

We slightly modified the molecule Boc-$^{D}$Phe-$^{L}$Oxd-OH **5** by adding a phenylalanine at the end of the chain and obtained the gelator Boc-$^{L}$Phe-$^{D}$Oxd-$^{L}$Phe-OH, **6** (Figure 2.21) to extend the applicability of the solubilisation methodology with PB at pH 7.4 to other gelators. Using this molecule, we prepared some gels with addition of either GdL or $CaCl_2$. In this case, we applied the previously reported methodology for the dissolution step, with PB solution at pH 7.4, and compared the results obtained with the methodology employing the dissolution step in water containing NaOH. This methodology allows the dissolution of the gelator in a mild aqueous environment, preventing the hydrolysis of sensitive groups.

Gels **6a-6i** were prepared with **6** at a concentration of 0.2 %, 0.5 %, and 1.0 % w/V. Gelator **6** underwent hydrolysis in presence of harsh basic conditions given by NaOH, to produce Boc-$^{L}$Phe-OH and the dipeptide H-$^{D}$Oxd-$^{L}$Phe-OH (figure 2.20). The hydrolysis takes place on the imidic bond, as reported in for gelator **3** even though in a lower degree compared to the previous study (see section 2.1). This may be due to the reduced amount of base used (1.2 eq. for **3** and 1.0 eq. for **6**).

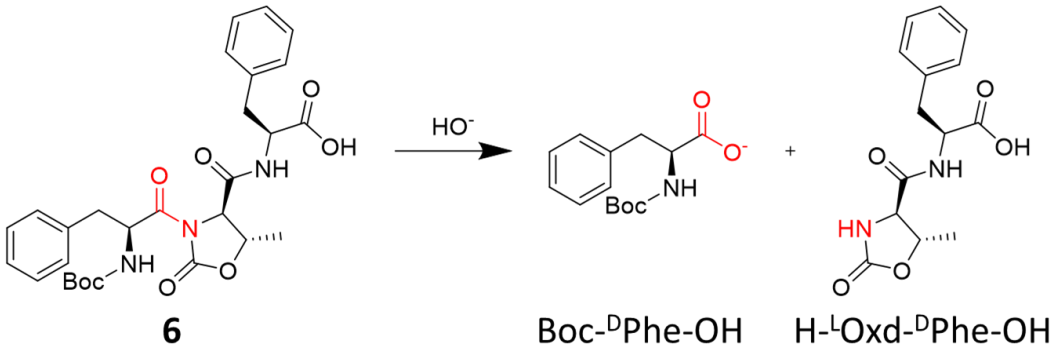


**Figure 2.20**. Hydrolysis reaction of gelator **6** in basic environment to produce Boc-$^{D}$Phe-OH and H-$^{L}$Oxd-$^{D}$Phe-OH.

In all the conditions tested, a gel was obtained (Figure 2.21). Table 2.5 reports the results for the formation of gels 6a-6i, including the concentrations and triggers tested for these

trials, the pH after the gelator dissolution and after the complete gel formation, and the corresponding degree of hydrolysis, detected through HPLC-MS.

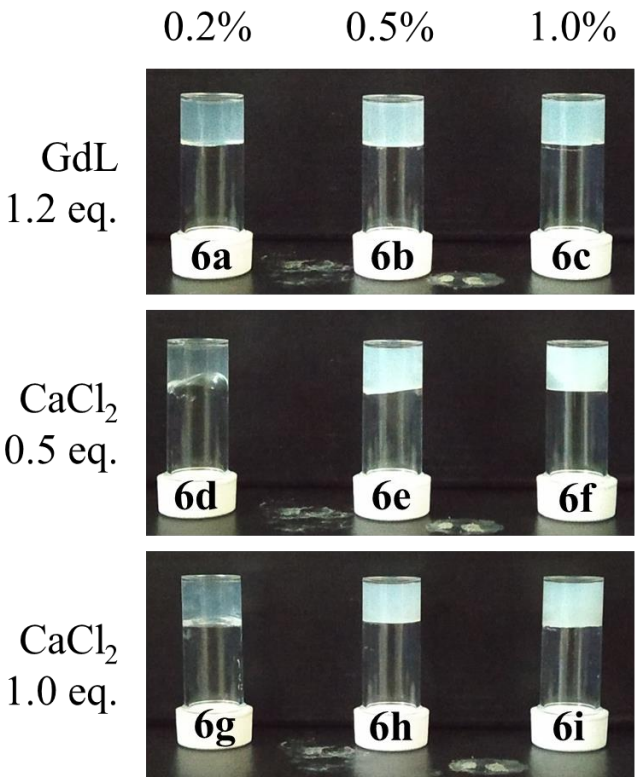


**Figure 2.21**. Photographs of the gels **6a-i**, obtained from gelators **6**, with addition of GdL (**6a-c**), 0.5 eq. (**6d-f**) or 1.0 eq. (**6g-i**) of calcium chloride, in concentration of gelator 0.2 %, 0.5 %, or 1.0 % w/V.

We repeated the gelation experiments dissolving the gelator in PB at pH 7.4 and following the same procedure reported in Table 2.6. In this case, the addition of the same amount of GdL used for the gels with NaOH allowed to reach a final pH of around 5.9, which was not sufficient to form a gel in some cases, therefore we increased the amount of GdL and obtained gels **6j-6l**. The addition of 0.5 eq. of $CaCl_2$ also resulted in the formation of incomplete gels in some cases, as calcium was partially sequestrated by the phosphate ions, so we obtained gels only with 1.0 eq. of $CaCl_2$. We obtained in this way gels **6j**-**6o** (Figure 2.22), whose properties are summarised in Table 2.6.

**Table 2.5**. Summary of the gels of **6** tested after dissolution in water containing 1.0 eq. of NaOH.

| Gel | Conc. (%) | $pH_0$ | Trigger | $pH_f$ | Hydrolysis (%) | Result |
|---|---|---|---|---|---|---|
| **6a** | 0.2 | 8.5 | GdL (1.2 eq.) | 4.1 | 3 | Gel |
| **6b** | 0.5 | 7.6 | GdL (1.2 eq.) | 4.1 | 5 | Gel |
| **6c** | 1.0 | 7.0 | GdL (1.2 eq.) | 3.8 | 14 | Gel |
| **6d** | 0.2 | 8.6 | $CaCl_2$ (0.5 eq.) | 6.0 | 8 | Gel |
| **6e** | 0.5 | 7.6 | $CaCl_2$ (0.5 eq.) | 6.0 | 13 | Gel |
| **6f** | 1.0 | 7.2 | $CaCl_2$ (0.5 eq.) | 5.6 | 20 | Gel |
| **6g** | 0.2 | 8.8 | $CaCl_2$ (1.0 eq.) | 7.1 | 3 | Gel |
| **6h** | 0.5 | 7.4 | $CaCl_2$ (1.0 eq.) | 5.9 | 19 | Gel |
| **6i** | 1.0 | 7.2 | $CaCl_2$ (1.0 eq.) | 5.3 | 22 | Gel |

$pH_0$ = starting pH (before trigger addition); $pH_f$ = final pH;

**Table 2.6**. Summary of the gels of Boc-$^{L}$Phe-$^{D}$Oxd-$^{L}$Phe-OH **6** tested after dissolution in PB at pH 7.4.

| Gel | Conc. (%) | PB conc. (%) | $pH_0$ | Trigger | $pH_f$ | Hydrolysis (%) | Result |
|---|---|---|---|---|---|---|---|
| **6j** | 0.2 | 9.6 mM | 6.9 | GdL | 4.8 | N.D. | Gel |
| **6k** | 0.5 | 24 mM | 6.9 | GdL | 4.8 | N.D. | Gel |
| **6l** | 1.0 | 48 mM | 6.8 | GdL | 4.7 | N.D. | Gel |
| **6m** | 0.2 | 9.6 mM | 6.9 | $CaCl_2$ | 6.4 | N.D. | Gel |
| **6n** | 0.5 | 24 mM | 6.9 | $CaCl_2$ | 6.6 | N.D. | Gel |
| **6o** | 1.0 | 48 mM | 6.8 | $CaCl_2$ | 6.3 | N.D. | Gel |

N.D. = not detected; $pH_0$ = starting pH (before trigger addition); $pH_f$ = final pH

In this way, the hydrolysis of the gelator, monitored through HPLC-MS, was neglected in every trial, so we envisage that this methodology for the dissolution step may be applied to all the gelators with an apparent p$K_a$ lower than 7.4.

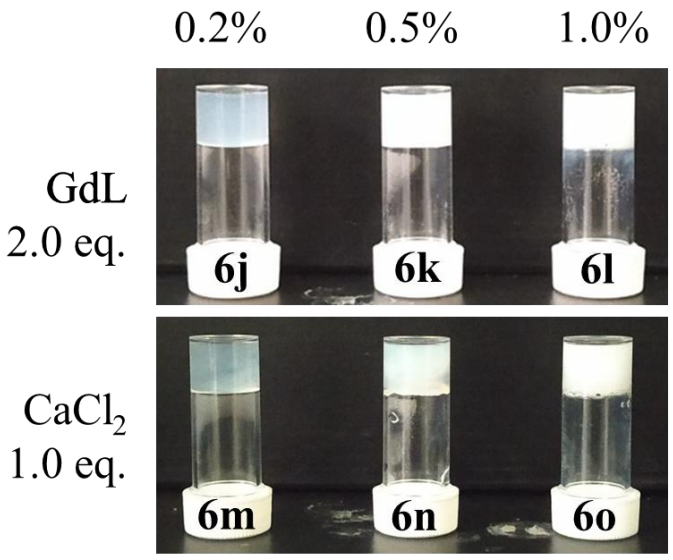


**Figure 2.22**. Photographs of the gels **6j-o**, obtained from Boc-$^{L}$Phe-$^{D}$Oxd-$^{L}$Phe-OH **6**, with addition of 2.0 eq. of GdL (**6j-l**), or 1.0 eq. of calcium chloride (**6m-o**), in concentration of gelator 0.2 %, 0.5 %, or 1.0 % w/V.

All the gels were characterised from a rheological and spectroscopical point of view, to outline the stiffness, elasticity, and transparency of the gels. These properties are reported in Table 2.7.

From these analyses, gels obtained from the dissolution in NaOH are 3-5 times weaker than the corresponding gels obtained from the dissolution with PB (**6a-c** vs. **6j-l**, and **6g-i** vs. **6m-o**). On the other hand, gels in NaOH resulted more transparent than the one in PB, so the two methodologies may be applied according to the final application of the gel, whether a stiffer or a more transparent gel is required.

We investigated the morphological aspect of the dried gels with optical microscopy, to outline possible differences in the fibrous matrices of the gels obtained with the two methodologies (Figure 2.23). Despite the macroscopic differences, the morphological structure is quite similar for the two methodologies adopted. The only differences arise varying the trigger i.e., switching from GdL to $CaCl_2$. In the case of the pH variation, long linear fibres are formed, while in the case of the addition of calcium, more branched fibres are obtained.

**Table 2.7**. Summary of the rheological and spectroscopical properties of the gels **6a-o**.

| Gel | G' (kPa) | G" (kPa) | LVER (%) | Crossover point (%) | Transp. (%) |
|---|---|---|---|---|---|
| **6a** | 1.6 ± 0.8 | 0.1 ± 0.05 | 1.0 | 100 | 70 |
| **6b** | 5.5 ± 1.1 | 0.6 ± 0.3 | 1.5 | 21 | 46 |
| **6c** | 25 ± 8.0 | 3.4 ± 1.0 | 1.5 | 55 | 26 |
| **6d** | 0.3 ± 0.1 | 0.04 ± 0.01 | 0.5 | N.D. | 78 |
| **6e** | 4.8 ± 0.9 | 0.6 ± 0.1 | 1.0 | N.D. | 18 |
| **6f** | 17 ± 10 | 2.3 ± 1.8 | 1.0 | 85 | 5 |
| **6g** | 0.4 ± 0.08 | 0.04 ± 0.02 | 2.2 | N.D. | 59 |
| **6h** | 6.1 ± 3.8 | 0.7 ± 0.2 | 0.5 | N.D. | 14 |
| **6i** | 22 ± 1.3 | 3.4 ± 0.3 | 2.2 | 60 | 1.9 |
| **6j** | 4.6 ± 2.9 | 0.4 ± 0.3 | 1.5 | 37 | 46 |
| **6k** | 28 ± 12 | 3.5 ± 1.3 | 2.2 | 19 | 0.7 |
| **6l** | 90 ± 34 | 6.9 ± 0.3 | 0.7 | N.D. | 0.6 |
| **6m** | 1.0 ± 0.3 | 0.2 ± 0.1 | 2.2 | N.D. | 31 |
| **6n** | 31 ± 14 | 6.9 ± 3.0 | 0.7 | 34 | 2.5 |
| **6o** | 76 ± 40 | 9.9 ± 4.1 | 0.5 | 15 | 1.2 |

N.D. = not detected; G' and G" are referred to a $\gamma = 0.046$ %; LVER and crossover point are expressed as means of $\gamma$; transparency is expressed as means of transmittance at 630 nm.

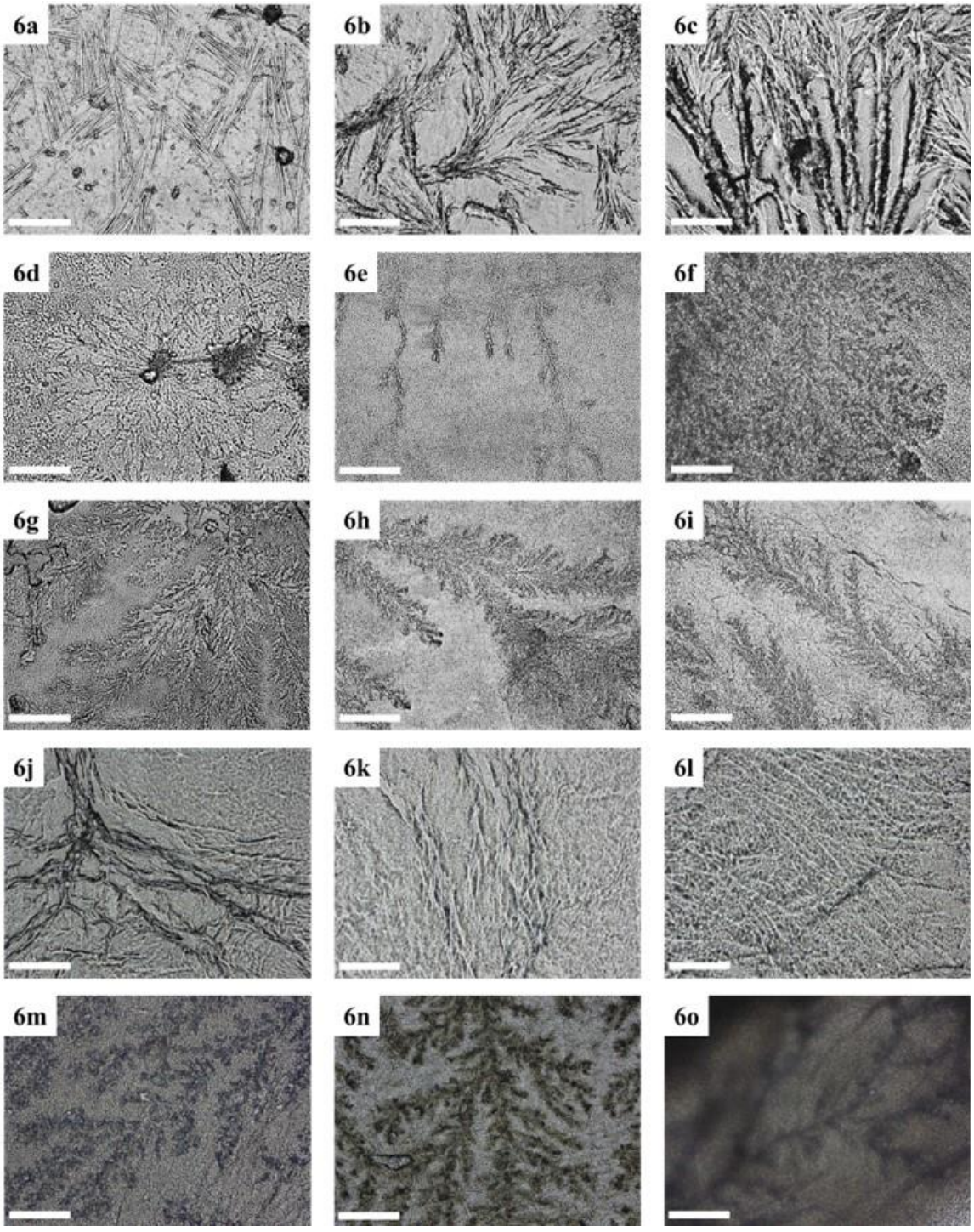


**Figure 2.23**. Optical microscope images of the dried gels **6a-o**. The scalebar is 50 μm.

## *2.4. Summary*

In this part of my work, I explored how to insert specific moieties or atoms to control the gelation ability of a scaffold. The presence of an oxazolidinone enhances the rigidity of the gelator improving or even neglecting the formation of a gel, depending on the chirality of the gelator. The insertion of one or two fluorine atoms usually has a positive impact on the gelation process, as it introduces new weak bonds and improves π-interactions, however, its presence is not always beneficial, as they alter the polarity of the gelator and therefore its solubility.

I also exploited different methodologies for the dissolution step to prevent inconveniences such as the hydrolysis of the gelator and finely tune the final properties of the material, according to the desired application.

# *Chapter 3. Gels programming*

Planning the formation of LMW gels over time is an evolving challenge that started few years ago, with the replacement of diluted solutions of HCl with the addition of solid GdL. This allowed a slow pH change from high to low thanks to the hydrolysis of GdL to produce gluconic acid.[41] Nowadays, the control over gel formation can be achieved in numerous ways and it is possible to create systems that evolve over time, creating for example, sol-gel-sol,[121,122] gel-sol-gel,[71] or even gel-gel-gel[123] transitions. These kinds of transitions are useful for creating self-erasing inks, or mimicking homeostasis. However, some of these systems change the morphology of the gel matrix, switching for example from spherulitic domains to worm-like fibres (Figure 3.1a). When applied to multicomponent gels, the transition can also cause a conversion from a co-assembled state to a self-sorted one. This means that if at the beginning the fibres are made of a co-assembly of the various gelators, at the end of the process each gelator builds its own network (Figure 3.1b).[86] This is usually carried out by annealing the gel (i.e., "rearranging" the fibres of the gel) in different ways. The thermal annealing surely is the most known method to carry out such transitions. We can consider as an example a bicomponent gel, whose single components can form a gel separately, in turn possessing different melting points ($T_{gel}$), namely $T_1$ and $T_2$. When mixed, however, the $T_{gel}$ of the bicomponent gel is different from the first two and usually between $T_1$ and $T_2$.[124,125] So, with the thermal annealing, a bicomponent gel should melt at a certain temperature, called $T_{1+2}$, then, when the temperature decreases again, the gelator with higher $T_{gel}$ (called $T_1$) should reassemble when $T = T_1$ and form its fibrous network, then when the temperature decreases again it reaches the $T_{gel}$ of the second gelator (called $T_2$) allowing this to form its own network when $T = T_2$. In this way, the thermal annealing allows to switch from a co-assembled network of fibres to a self-sorted one (Figure 3.1c). However, there are limitations in the use of this technique. For example, a temperature increase may lead to the degradation of one of the gelators. Therefore, other kinds of annealing have been explored, such as light[126] or pH[127].

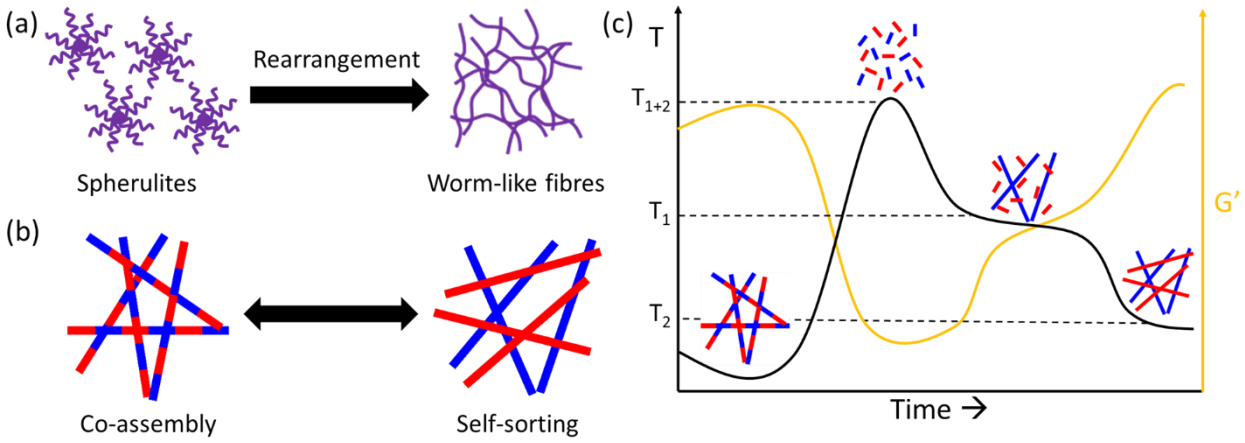


**Figure 3.1**. Cartoons representing (a) the rearrangement allowing to switch from a spherulitic network to a worm-like domain of fibres, (b) co-assembly versus self-sorting of fibres in the case of bicomponent gels, and (c) the variation of temperature and G' of a bicomponent gel over time as the temperature increases and decreases again.

Together with the temporal planning of LMW gels, it is possible to control the gel formation over space. LMW gels are very versatile, easy to break and reform by applying different stimuli. However, they are held by weak interactions so, they are usually quite weak and break at low strain. The spatiotemporal manipulation over the formation of such materials is therefore quite of a challenge. For example, photo-responsive gel formation can be controlled over space by applying a mask (to cover part of the medium to be gelled) or by using a punctual light source such as a confocal laser.[128–130] Such systems suffer from poor applicability, as they require a photo-responsive moiety in the gelator features that is able to trigger the gelation and/or its disruption. Moreover, photoirradiation may lead to degradation of the gelator itself.[131] Controlling the diffusion of reactants is another way to achieve spatial control in gelation. In this context, two reactants are confined in space at the beginning. After a while, the diffusion starts, and when the reactants meet, they form or trigger the gelator. This method is usually called reaction-diffusion. For example, the reactants may be separated in two non-miscible solvents[132] or physically separated, as in the case of nanoparticles containing one reactant, dispersed in a medium containing the other reactant.[45]

## *3.1. Programming of supramolecular gels through annealing*

We investigated the evolution of a bicomponent system with two gelators possessing an acidic moiety, namely 1ThNap-$^{L}$Phe-$^{L}$Phe-OH,[133] **7**, and Fmoc-$^{L}$Phe-$^{L}$Phe-OH,[134] **8** (Figure 3.2), undergoing a pH annealing.[135]

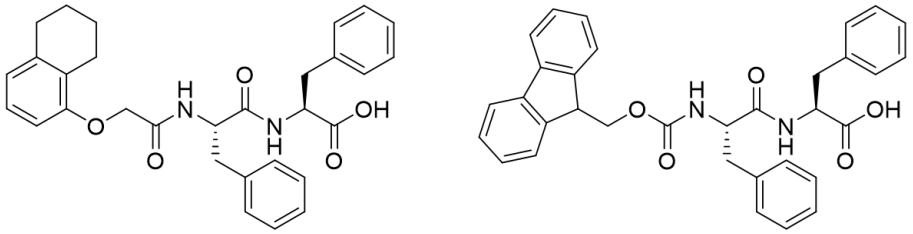


**Figure 3.2**. Molecular structures of 1ThNap-$^{L}$Phe-$^{L}$Phe-OH, **7**, and Fmoc-$^{L}$Phe-$^{L}$Phe-OH, **8**.

First, the gelation of the two molecules was tested in a DMSO:$H_2O$ (20:80 V/V) medium. Both were able to form a gel in a concentration of 0.2 % w/V, as well as when mixed, **(7+8)**, in the same concentration and the same medium. We obtained in this way gels **7a**, **8a**, and **(7+8)a** (Figure 3.3).

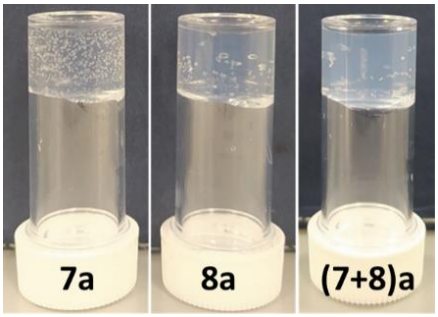


**Figure 3.3**. Photographs of the gels **7a**, **8a**, and **(7+8)a**, obtained from gelators **7**, **8**, and a mixture 1:1 (w/w) of gelators **7** and **8**, respectively.

Rheologically, gels **7a** and **8a** have comparable stiffness, while the stiffness of gel **(7+8)a** equals more or less the sum of the stiffnesses of gels **7a** and **8a** separately (Table 3.1) and

they all display a frequency-independent network, outlined through frequency sweep rheology (data not shown). This last analysis is useful to distinguish between gels, which have a frequency-independent behaviour, and viscous solutions, which are frequency-dependent, and despite having a G' > G" at low frequencies, the moduli may crossover at a certain point.[136]

**Table 3.1**. Summary of the gels of **7**, **8**, and **(7+8)** with rheological properties.

| Gel | 7 (%) | 8 (%) | Annealing | Result | G' (kPa) | G" (kPa) |
|---|---|---|---|---|---|---|
| **7a** | 0.2 | 0 | No | Gel | 3.2 ± 0.4 | 0.4 ± 0.03 |
| **8a** | 0 | 0.2 | No | Gel | 4.7 ± 0.3 | 0.6 ± 0.03 |
| **(7+8)a** | 0.2 | 0.2 | No | Gel | 9.9 ± 0.8 | 1.1 ± 0.1 |
| **7b** | 0.2 | 0 | Yes | Gel | 5.4 ± 0.4 | 0.8 ± 0.05 |
| **8b** | 0 | 0.2 | Yes | Gel | 4.8 ± 0.2 | 0.7 ± 0.03 |
| **(7+8)b** | 0.2 | 0.2 | Yes | Gel | 13 ± 1.7 | 1.8 ± 0.2 |

G' and G" are referred to $\gamma = 0.05$ %.

We investigated the morphology of the gels in the wet state through confocal microscopy. Each of the gels displayed a spherulitic network of fibres, small in the case of **7a**, big in the case of **8a**, and of an intermediate size in the case of **(7+8)a** (Figure 3.4). This usually indicates a co-assembly of the gelators when fibres are formed, as the spherulites are a result of a phase separation upon addition of water to the DMSO solutions containing the gelator.[137,138] However, other factors such as different rates of gelation and supersaturation effects may influence the spherulite size, so without other analyses this cannot be taken as a proof of co-assembly.[139,140]

To verify our hypothesis, we performed IR spectroscopy on the three gels and focussed our attention on the shifts of stretching and bending of the N-H bonds of the amides. Gel **7a** displays a band at 3286 $cm^{-1}$, attributable to the N-H stretching, and another band at 1720 $cm^{-1}$, attributable instead to the C=O stretching of the amide linking the protecting group to the phenylalalnine. Gel **8a** on the other hand displays the same bands at 3302

and 1691 $cm^{-1}$ respectively. In the case of the multicomponent gel **(7+8)a**, these peaks are merged. The N-H stretching appears a 3293 $cm^{-1}$, half-way between the corresponding peaks of gels **7a** and **8a**, the C=O stretching instead appears as a broad shoulder in the region between 1720 and 1691 $cm^{-1}$. This is strongly indicative of a co-assembly of the fibres (Figure 3.5).

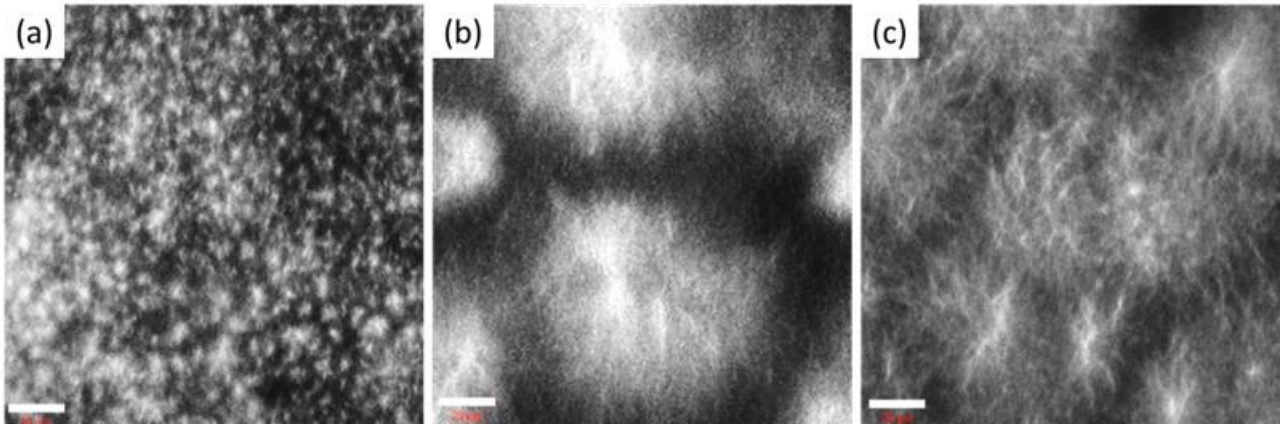


**Figure 3.4**. Confocal microscope images of the gels **7a**, **8a**, and **(7+8)a**. The scalebar is 20 μm.

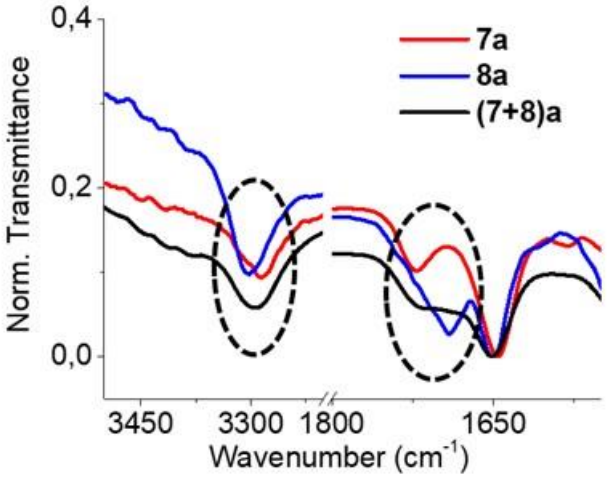


**Figure 3.5**. Zoom in the regions 3500-3200 $cm^{-1}$ and 1800-1500 $cm^{-1}$ of the IR spectra of gels **7a** (red), **8a** (blue), and **(7+8)a** (black). Peaks corresponding to the N-H stretching and bending are highlighted with a dotted circle.

At this point, we rearranged the gels fibres, changing their morphology and the assembly of the gelators by varying the pH. To carry out the pH-annealing of the gels, we formed these in presence of urea, urease and methyl formate and obtained the gels **7b**, **8b**, and **(7+8)b** (Table 3.1). The coupled reaction between urea, urease, and methyl formate can be regarded as a "fuel". At the beginning, urease rapidly hydrolyses urea to produce carbon dioxide and ammonia (fast activator) and increase the pH, reaching a maximum around 8.5. At high pH, the gels are disrupted and turned into a solution. Simultaneously, methyl formate gets slowly hydrolysed to produce methanol and formic acid (dormant activator), which in turn lowers the pH again (Figure 3.6).

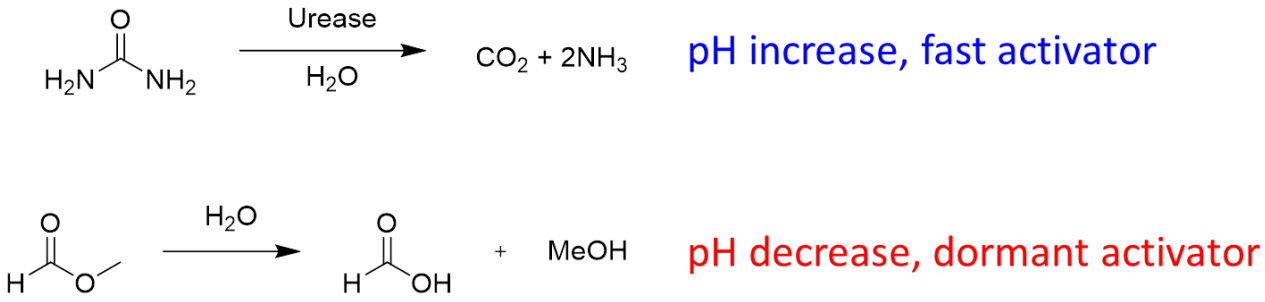


**Figure 3.6**. Reactions involved in the "fuel" composed of urea, urease, and methyl formate.

This means that upon addition of this fuel to the gel medium, we add energy that changes the microscopic and macroscopic behaviour of the medium. As the fuel runs out, the gel is restored. In the case of the gels **7b** and **8b**, the gels are restored when the pH meets the apparent p$K_a$ of the gelator, which is 6.3 in the case of 1ThNap-$^{L}$Phe-$^{L}$Phe-OH, **7**, and 7.4 in the case of Fmoc-$^{L}$Phe-$^{L}$Phe-OH, **8**. When annealing the multicomponent gel **(7+8)b**, regelation takes place in a multistep fashion. When the pH reaches the apparent p$K_a$ of **8** (7.4), this starts forming its own fibrous network, then, as the pH reaches the apparent p$K_a$ of gelator **7** (6.3), this forms in turn its network of fibres. This was clearly visible through time sweep rheology of **(7+8)b** (Figure 3.7).

Figure 3.7a reports pictures of the gel **(7+8)b** over time. At the beginning, a self-supporting material is formed. This rapidly disrupts completely within 10 minutes where

a clear solution is obtained and after 16 hours, the gel is restored. As shown in Figure 3.7b, at the beginning G' is higher than G", as a self-supporting network is formed. After ~5 min, the gel matrix starts disrupting, a solution is formed, and a crossover of the moduli is observed. As the pH decreases again, we observed another crossover of the moduli and the restorage of the gel matrix, in correspondence of the p$K_a$ of **8**. At this point, G' and G" reached a plateau, then stared increasing again in correspondence of the p$K_a$ of gelator **7**, until a second plateau was reached. This double step increase in the moduli is more visible in Figure 3.7c and clearly suggests that two kinds of aggregates are formed during the regelation process: the first step attributable to the formation of the network of **8** takes place within an hour when the pH reaches the value 7.0, below the apparent pKa of **8**. The step attributable to the gelation of **7** instead is at pH 6.3, in correspondence of its p$K_a$. This happens because the fibres are formed in a slower fashion when the pH is in correspondence of the apparent p$K_a$ of the gelator and becomes faster with the decrease in pH. So, at the early stages of the gelation, where methyl formate is hydrolysed faster, the fibres start to form in correspondence of the p$K_a$ of the gelator, but only after 1 h a remarkable difference in the moduli G' and G" is detected (G' is at least 5 times G"). The moduli keep increasing until they reach a plateau right before 4 h, indicating that the network of **8** is completely formed by that time. The pH keeps decreasing and reaches 6.3 after 7 hours. Here, the hydrolysis of methyl formate is rather slow and the network of gelator **7** starts forming in correspondence of that value.[141] Therefore, the annealing of gel **(7+8)b** apparently causes a change from a co-assembly of the fibres to a self-sorting of these, due to the different apparent p$K_a$s of the two gelators. Time sweep was done both with the cup and vane, to better outline the crossover point in the gel disruption, and the parallel plate geometry, to better outline the double step increase in the moduli.

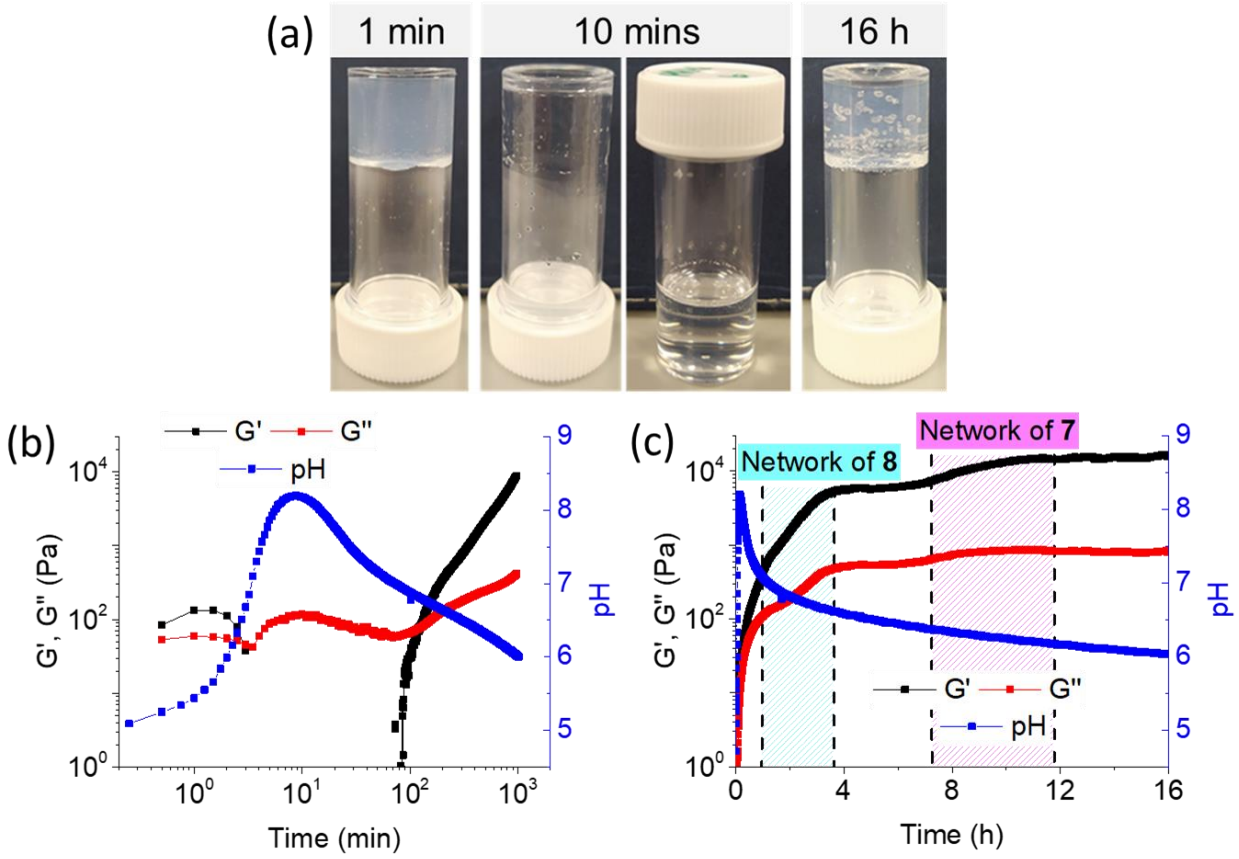


**Figure 3.7**. (a) Photographs of gel **(7+8)b** over time; (b, c) variation over time of G' (black), G" (red), and pH (blue) over time for the gel **(7+8)b**. For (b, c), experiments were done with (b) the cup and vane and (c) the parallel plate geometries. For (b) time is in a logarithmic scale, for (c) time is in a linear scale, to better see the double step increase in the rheological properties, highlighted in light blue (network of **8**) and magenta (network of **7**).

To prove our hypothesis, we performed IR spectroscopy on **(7+8)b**, however, the peaks were noninformative, as the peaks of methyl formate, formic acid and ammonia (present in the gel) covered the N-H stretching and bending of the gelators. For this reason, we used $^{1}$H-NMR to control the gel disruption e reformation over time. As free molecules and micelles are detectable through NMR, while fibres are not,[142–144] we could monitor the fibres formation through the integrals of the peaks corresponding to each gelator over time. As the fibres disrupt, the gelators peaks should start appearing, and as the first ones reassemble again the same peaks should disappear again. For this purpose, we chose the

aromatic region between 7.64 and 6.00 ppm as integral for the protons of both **7** and **8**, and the aliphatic region between 1.94 and 1.30 ppm for the protons of gelator **7** only. These integrals were then normalised. Unfortunately, the gel undergoes disruption so quickly that we could not monitor the early stages of the experiment, therefore we decided to study two gels over time. The first one prepared was gel **(7+8)n**, that contained **7**, **8**, and urea in the same concentration of **(7+8)b**, but no methyl formate and a reduced amount of urease to dramatically slow the hydrolysis of urea down. The second one was gel **(7+8)b** as previously prepared.

In gel **(7+8)n**, at the beginning no signal is detected, apart from the ones of urea and methyl formate. After a while, the gel is disrupted and the peaks of both gelator **7** and **8** are present. Their integrals keep increasing over a time of 6 hours. This is another proof of co-assembly at the beginning of the gelation, as the appearance of the peaks of both gelators is concomitant (Figure 3.8a).

In gel **(7+8)b**, as the gel starts reforming, the peaks intensities slowly decrease with the ones of **8** being decreased faster than the one of **7**. This indicates that **8** undergoes reassembly faster than **7**, therefore it can be taken as a proof of self-sorting (Figure 3.8b).

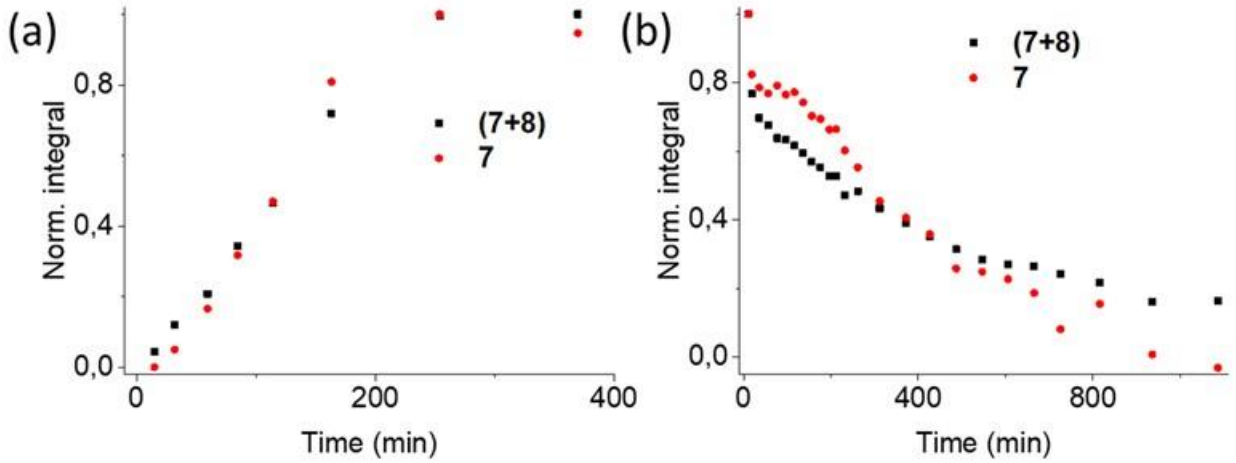


**Figure 3.8**. Plots of the normalised integrals of protons of **(7+8)** (black) and **7** (red) versus time (a) in gel **(7+8)n** and (b) in gel **(7+8)b**.

To further prove the self-sorting upon annealing, we decided to study the behaviour of each gel prepared before and after annealing with circular dichroism (CD) (Figure 3.9). Such spectra are complicated by potential linear dichroism (LD) and possibly circular intensity differential scattering, but nonetheless show that gels of 1ThNap-$^{L}$Phe-$^{L}$Phe-OH, **7**, display similar data before (**7a**) and after (**7b**) annealing; gels of Fmoc-$^{L}$Phe-$^{L}$Phe-OH, **8**, have some differences, as gel **8b**, obtained after annealing, shows an inversion in sign around 230 nm compared to gel **8a**, without annealing. The multicomponent systems show differences before (**(7+8)a**) and after (**(7+8)b**) annealing between 250 and 300 nm, as shown in Figure 3.9. Whilst difficult to interpret, these data imply that there is a difference in packing in the multicomponent systems before and after the pH increase and decrease, therefore it can be taken as an indirect proof of co-assembly before the annealing, whereas the fibres are self-sorted after annealing.

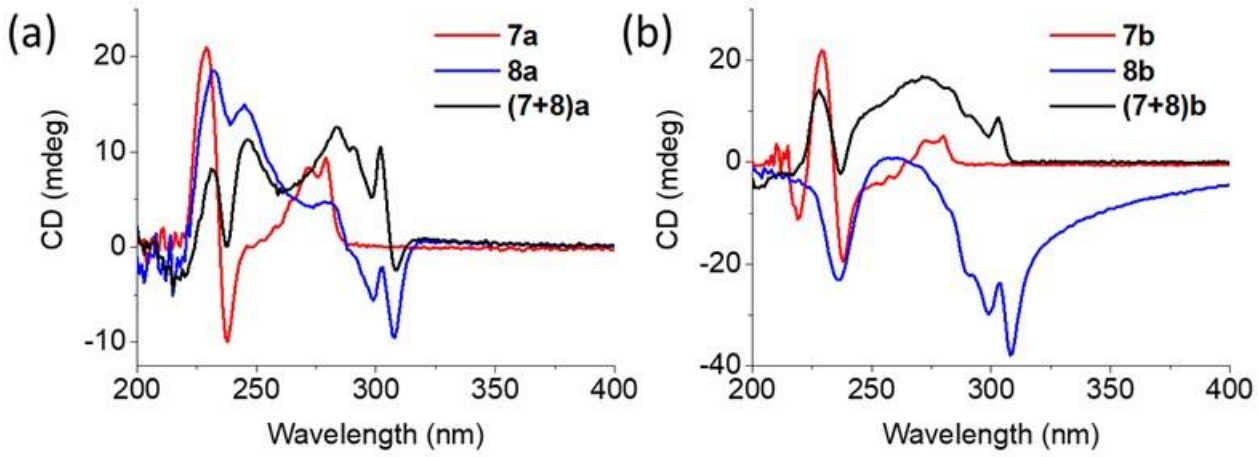


**Figure 3.9**. CD spectra of the gels (a) **7a** (red), **8a** (blue), and **(7+8)a** (black), obtained before annealing, and (b) **7b** (red), **8b** (blue), and **(7+8)b** (black), obtained after annealing.

This annealing approach can be used to finely tune the final properties of the resulting material by adjusting the amount of "fuel" inserted in the gel. We prepared three more samples, namely gels **(7+8)c**, **(7+8)d**, and **(7+8)e** and compared these with gel **(7+8)b**, to understand how the increase or decrease in urea, urease, or methyl formate would affect the gel properties, in terms of time required for the gel disruption and reformation, maximum and final pH reached, and stiffness of the gel after an overnight rest (Table 3.2).

**Table 3.2**. Summary of the gels **(7+8)b-e**, reporting the content of urease, urea and methyl formate with the associated properties.

| Gel | Urease (g/L) | Urea (mM) | MF (μL) | $t_d$ (min) | $t_r$ (min) | $pH_h$ | $pH_f$ | G' (kPa) | G" (kPa) |
|---|---|---|---|---|---|---|---|---|---|
| **(7+8)b** | 0.4 | 20 | 100 | 3 | 120 | 8.2 | 6.0 | 13 ± 1.7 | 1.8 ± 0.2 |
| **(7+8)c** | 0.4 | 20 | 150 | 2 | 160 | 7.8 | 5.6 | 26 ± 1.8 | 4.6 ± 0.3 |
| **(7+8)d** | 0.4 | 10 | 100 | 15 | 160 | 7.5 | 5.5 | 13 ± 1.1 | 2.1 ± 0.2 |
| **(7+8)e** | 0.2 | 20 | 100 | 6 | 250 | 7.7 | 5.9 | 5.4 ± 0.4 | 0.8 ± 0.05 |

MF = methyl formate; $t_d$ = time required for the gel disruption (1st crossover); $t_r$ = time required for the gel reformation (2nd crossover); $pH_h$ = maximum pH reached during annealing; $pH_f$ = final pH reached after annealing; G' is expressed as the value obtained through strain sweep experiment at $\gamma$ = 0.05 %.

We tuned the rate of pH change and hence the properties of the material by varying the amounts of methyl formate, urea, or urease used. A decrease in the concentration of either urea or urease resulted in decrease in the rate of the pH increase during annealing. The rate of pH change can further be controlled by increasing the concentration of methyl formate. Since **7** forms wormlike micelles at high pH[145] and there are indications that **8** does too,[11,146] the pH reached, and the length of time spent at high pH will likely affect the aggregates formed. Hence, even small changes in the rate of pH increase and decrease as well as differences in the time spent at the maximum pH will likely affect the mechanical properties of the gels formed on reacidification. Comparison of pH-time profiles with the rheological behaviour of the annealed gels shows that the mechanical properties of the final gels depend on the maximum pH during the pH cycles. A gradual decrease in maximum pH gives gels with a lower stiffness.

We then applied the annealing approach to single-components gel layers. In this case, two gels were prepared in a pre-cut and inverted syringe, by forming the first one at the bottom of the syringe and the second one on the top of this (Figure 3.10a).

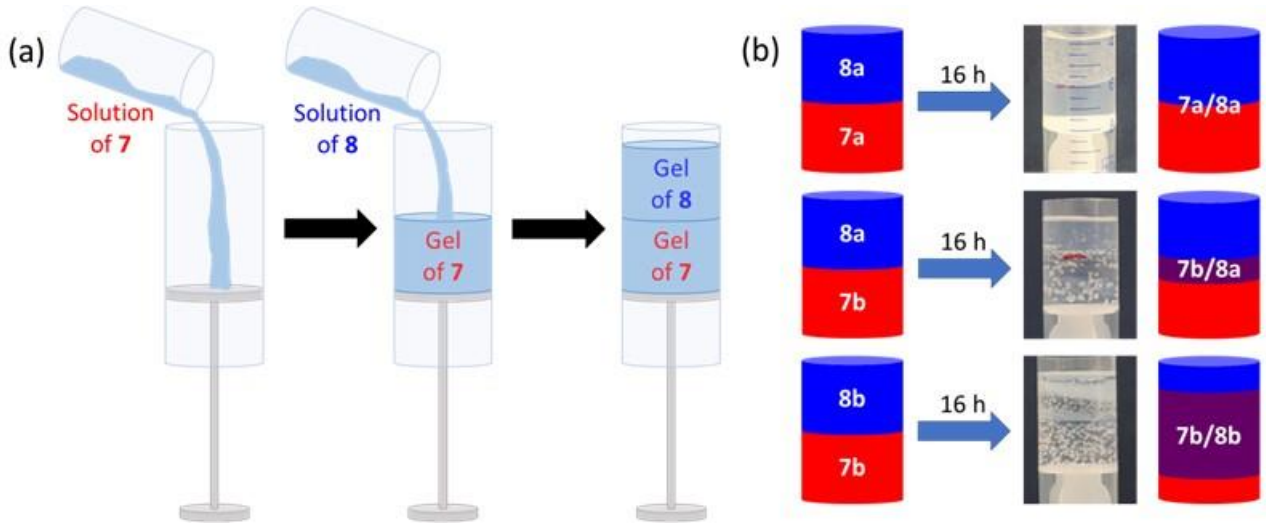


**Figure 3.10**. (a) Cartoon showing how gels **7a/8a**, **7b/8a**, and **7b/8b** were prepared; (b) cartoon and photographs showing how the gels **7a/8a**, **7b/8a**, and **7b/8b** appeared after an overnight rest.

We prepared in this way three gels to understand the effect of the annealing approach. First, we prepared the gel **7a/8a** by preparing the gel **7a** at the bottom, then, as soon as the gelation started (45 seconds), we poured the mixture for gel **8a** directly on top of the first gel, before gelation of this one occurred. The second layered gel prepared was **7b/8a**. Following the same procedure, we prepared at the bottom the gel **7b** and on top of this, after its gelation and before the gel disruption (45 seconds), we prepared gel **8a**, with no annealing. Finally, we prepared gel **7b/8b**, applying the annealing on both layers (Figure 3.10b). Each of the layered gels were then left to rest overnight, then cut into six sections (**L1-L6**, from top to bottom). Each one of these sections was analysed (i) with $^{1}$H-NMR (after freeze-drying and dissolution in $d_6$-DMSO) to understand if there was any mixing of the two gelators in any part of the gel, (ii) with rheology, to understand whether the stiffness of the gel sections was affected by the presence of the other gel layer, and (iii) with confocal microscopy to outline differences in the fibres in each layer.

**Table 3.3**. Summary of the composition (obtained from NMR) and stiffness of the layered gels, after slicing each gel in sections.

| Gel | Section | Composition (%) | | G' (kPa) |
|---|---|---|---|---|
| | | 7 | 8 | |
| 7a | / | / | / | 2.4 ± 1.1 |
| 7b | / | / | / | 2.7 ± 1.0 |
| 8a | / | / | / | 4.0 ± 0.7 |
| 8b | / | / | / | 7.2 ± 2.2 |
| 7a/8a | L1 | 100 | 0 | 3.9 |
| 7a/8a | L2 | 100 | 0 | 4.5 |
| 7a/8a | L3 | 100 | 0 | 3.1 |
| 7a/8a | L4 | 0 | 100 | 2.4 |
| 7a/8a | L5 | 0 | 100 | 3.7 |
| 7a/8a | L6 | 0 | 100 | 3.3 |
| 7b/8a | L1 | 96 | 4 | 5.4 |
| 7b/8a | L2 | 88 | 12 | 5.4 |
| 7b/8a | L3 | 75 | 25 | 5.6 |
| 7b/8a | L4 | 10 | 90 | 1.6 |
| 7b/8a | L5 | 6 | 94 | 1.8 |
| 7b/8a | L6 | 4 | 96 | 2.3 |
| 7b/8b | L1 | 100 | 0 | 8.8 |
| 7b/8b | L2 | 69 | 31 | 12 |
| 7b/8b | L3 | 68 | 32 | 14 |
| 7b/8b | L4 | 23 | 77 | 17 |
| 7b/8b | L5 | 15 | 85 | 9.8 |
| 7b/8b | L6 | 12 | 88 | 6.9 |

Gels **7a**, **7b**, **8a**, and **8b** for this study were prepared in syringe and sliced in three sections to obtain a mean value and standard deviation for their G'; composition was measured as means of $^{1}$H-NMR signals; G' was measured at $\gamma$ = 0.05 %. Red colour was used to indicate layers made of only **7** at the beginning, blue for the ones made of **8** only.

Before starting with the layered experiments, we prepared four single-layer and single-component gels, namely **7a**, **7b**, **8a**, and **8b** in the syringe. These gels were cut into three sections and each of these was analysed with the parallel plate. The average of the stiffness of these sections was then used as comparison for the rheological analysis of the layered gels (Table 3.3).

For the first gel **7a/8a**, from NMR we saw no mixing in any of the layers. Through rheology, each layer maintained a stiffness close to the single component gel, prepared and cut in the same way. These results indicate that both the layers maintained their identity. This was further proved by confocal microscopy, as only large spherulites (attributable to gelator **8**) were found in the top layer, while only small ones (attributable to gelator **7**) were found in the bottom layer (Figure 3.11).

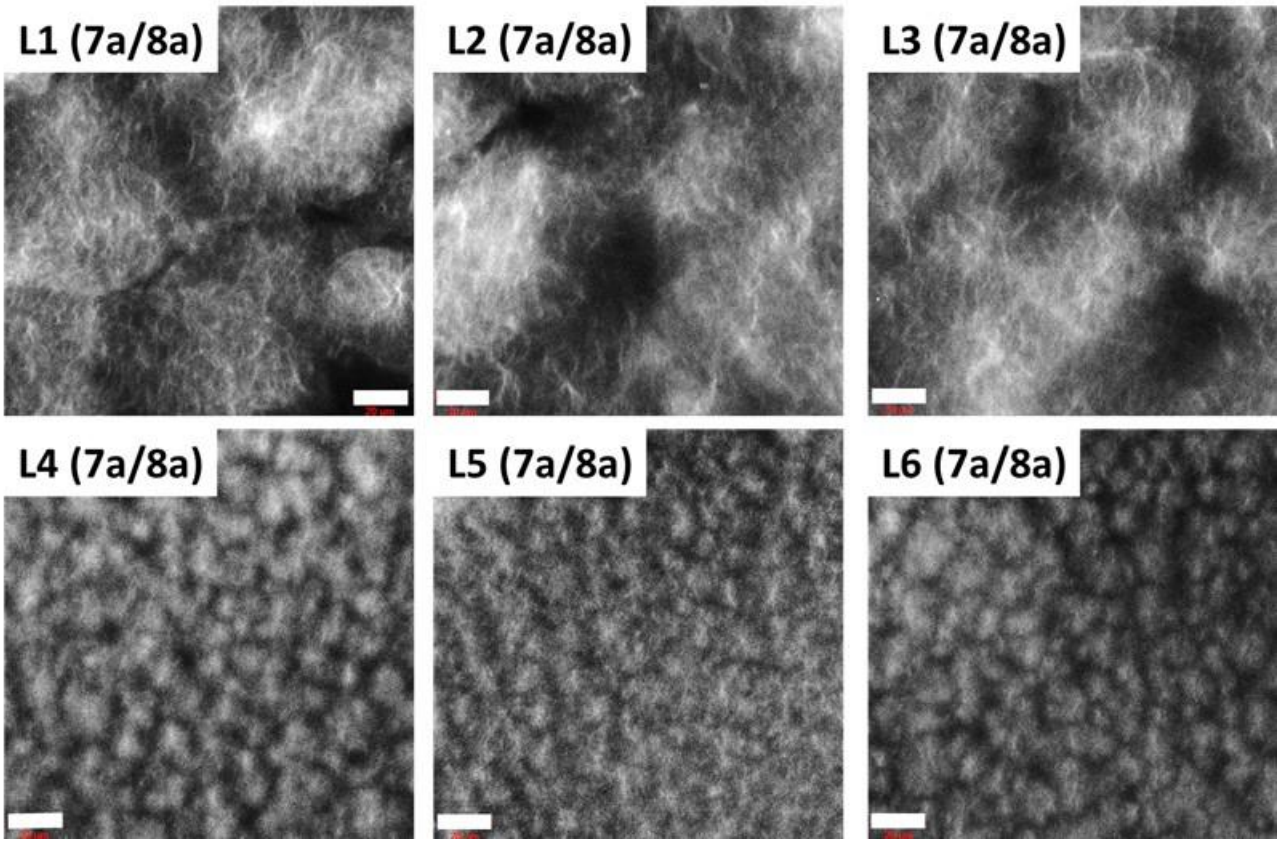


**Figure 3.11**. Confocal microscope images of sections **L1-L6** of the gel **7a/8a**.

NMR of the sections of the gel **7b/8a** showed a partial mixing throughout the whole length of the gel, and this phenomenon was more evident going from the edges to the interface between the two layers. Rheology showed that all the sections of the top layer **8a** (**L1-L3**) underwent a slight improvement in the stiffness, close to the one of gel **8b** alone, obtained after annealing, while the sections of layer **7b** (**L4-L6**) showed no significant changes in the stiffness. Confocal microscopy of these sections showed the presence of only spherulites in the first two sections (**L1**, **L2**) attributable to gel **8a**, a mixture of spherulites and worm-like fibres in section **L3**, and only thin fibres in the sections of layer **7b** (**L4-L6**). These results indicate that when one layer is annealed, both layers undergo a more prominent mixing approaching the junction between the layer, but overall, each layer maintains its own identity, rather than creating a composite material (Figure 3.12).

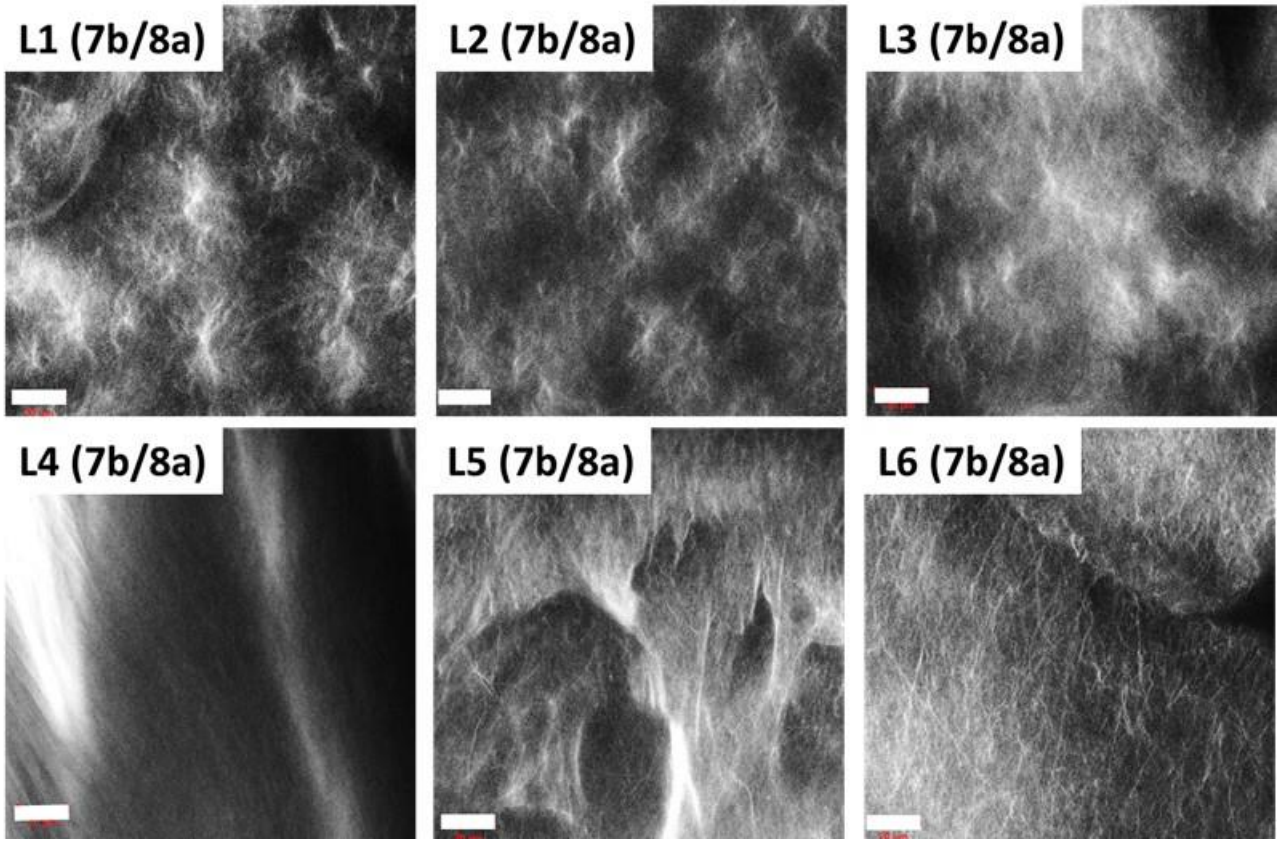


**Figure 3.12**. Confocal microscope images of sections **L1-L6** of the gel **7b/8a**.

Finally, in layered gel **7b/8b** the NMR analysis of the sections **L1-L6** showed again a mixing of the gelators that increased from the edges to the interface between the layers, with a higher degree compared to the previous case (apart from section **L1**). In this case, the stiffness of the various section displays a chiastic trend, as it increases going from the edges to the junction between the layers. Also, it is around an order of magnitude higher than the previous cases and closer to the stiffness of gel **(7+8)b**. From confocal microscopy, only worm-like fibres were visible, with variable size. At the top section L1, where NMR showed no mixing, fibres appear very thin and similar in size to the ones of gel **7b**, while the other sections, where mixing was more prominent, fibres are thicker, resembling the ones of gel **(7+8)b**. These results show that a composite material is formed when annealing is applied on both layers (Figure 3.13).

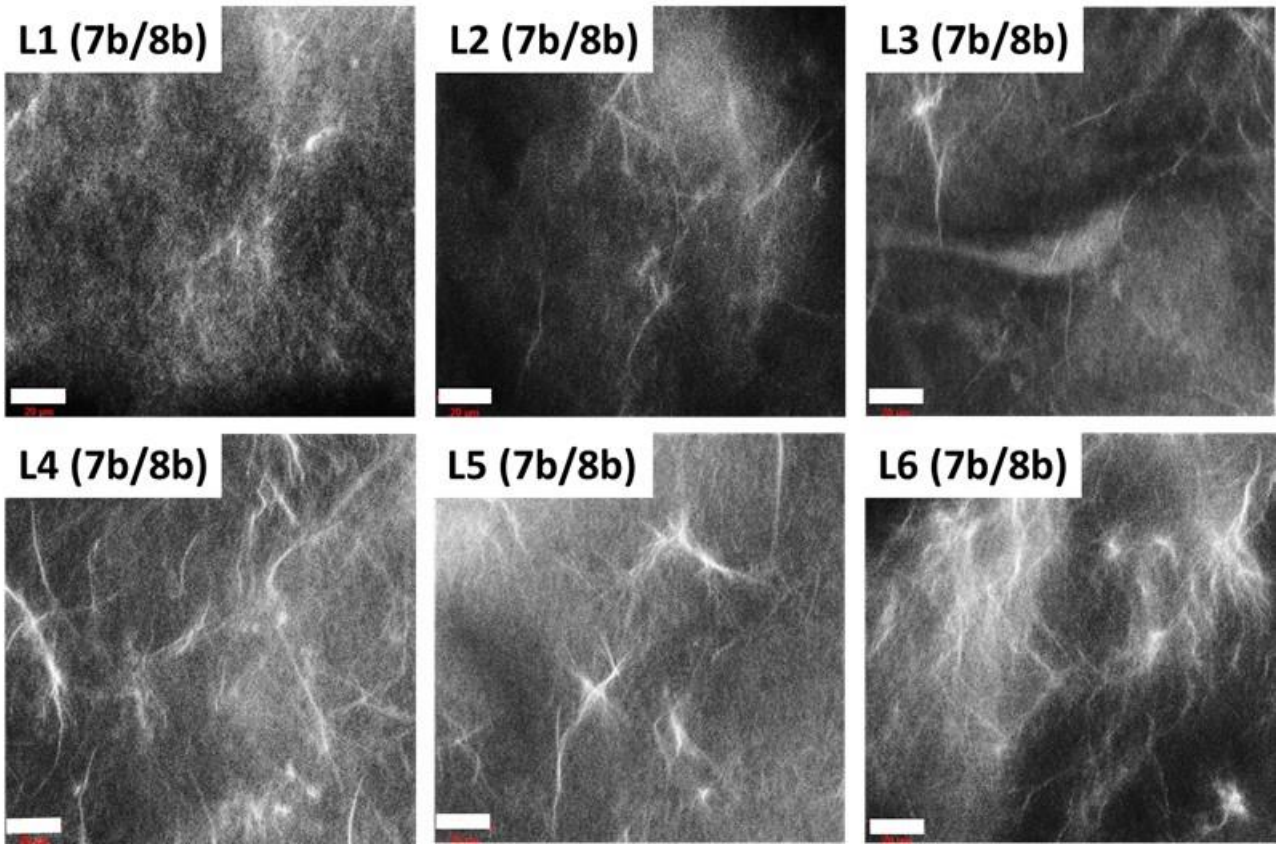


**Figure 3.13**. Confocal microscope images of sections **L1-L6** of the gel **7b/8b**. The scalebare is 20 μm.

## *3.2. Programming of physical gels with the reaction-diffusion method*

We studied the controlled formation of a hydrogel exploiting the reaction-diffusion methodology. For this study, we used the Fmoc-protected ethylendiamine (Fmoc-EDA) **9**, bearing an amine moiety and forming gels at basic pH (Figure 3.14).[147]

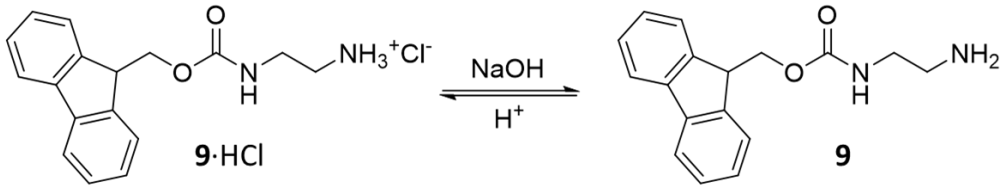


**Figure 3.14**. Molecular structure of gelator **9**.

We started by investigating the gel formation in concentration of 1.0 % w/V of gelator and in presence of a diluted solution of NaOH (in molar ratio 1:1 with the gelator) and obtained gel **9a**. The gelation in this case was very fast, difficult to control and hardly homogeneous (Figure 3.15).

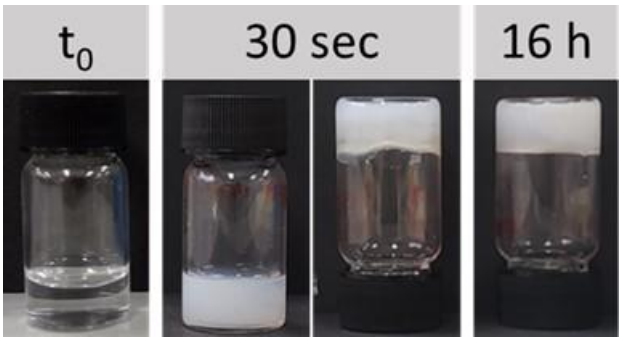


**Figure 3.15**. Photographs of the gelation steps of gel **9a**, obtained with addition of 1 eq. of NaOH.

We probed the fast gelation kinetics with time sweep rheology using a parallel plate geometry, relating this data with the pH variation. In fact, in the first point acquired by the instrument, the gel already displays a G' > G" and the moduli grow slowly to reach a plateau that is about the double of the ones at the beginning of the process, while the pH remains almost steady throughout the whole time of analysis (Figure 3.16), reaching 10.8

after 2 hours of analysis and 9.8 after an overnight rest. This difference in pH may be related to the slow incorporation of carbon dioxide in basic aqueous environment to produce carbonates, consuming hydroxide ions.

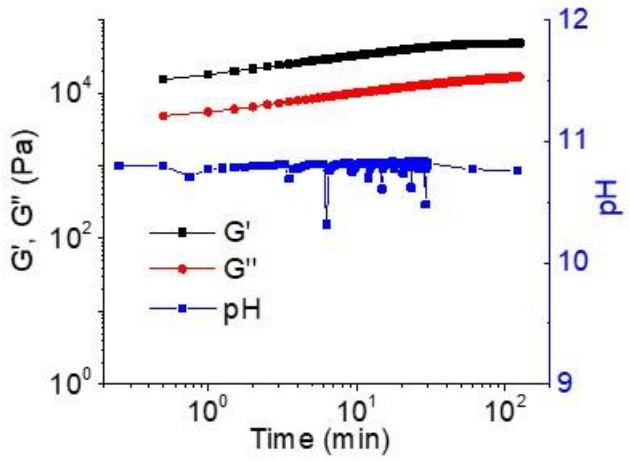


**Figure 3.16**. Variation of pH (blue), G' (black) and G" (red) of gel **9a** over 2 h.

To achieve spatial control over the gel formation, we devised a new methodology that exploits the reaction-diffusion method. We compartmentalised the reactants in two immiscible solvents: 2 mL of water at the bottom containing the gelator in concentration 1.0 % w/V, and 2 mL of a 0.075 M solution of N,N'-carbonyldiimidazole (CDI) in tertbutyl methyl ether (TBME) at the top. CDI slowly diffused into the aqueous layer and there got hydrolysed to produce carbon dioxide and imidazole. This resulted in an increase in pH and the formation of gel **9b**. In this case, the gel was spatially programmed, as it was formed from the interface between the layers to the bottom, following the diffusion and hydrolysis of CDI (Figure 3.17).

We probed the variation in pH during the reaction diffusion, relating this to the variation of storage and loss moduli as done before. Here, the pH follows a sigmoidal trend going from ~4.0 to ~7.7. To follow the spatial control, we recorded the time sweep with the parallel plate geometry, positioning the shaft at different heights, one in proximity of the interface between the solvents (6.0 mm from the bottom) and one closer to the bottom (4.0 mm from the bottom). In both cases, there is a crossover point that indicates the

beginning of the fibres formation, however at this point the moduli G' and G" are still very close to each other and the actual gel formation starts later at about 10 minutes (Figure 3.18).

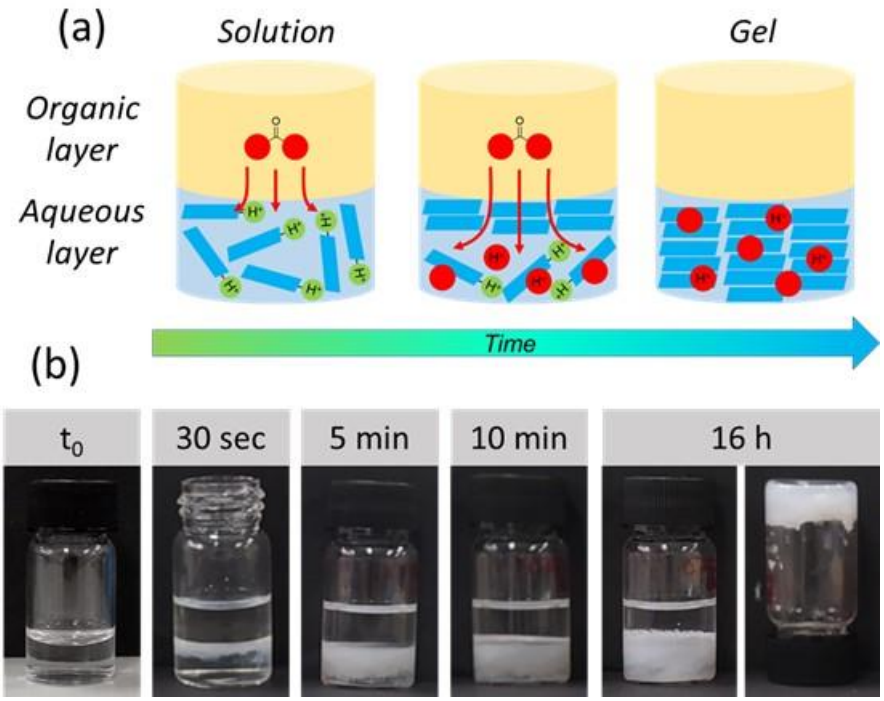


**Figure 3.17**. (a) Cartoon showing the reaction-diffusion of CDI of the method devised to form gradient gels; (b) photographs of the gel **9b** over time, obtained with reaction-diffusion of CDI from the TBME layer to the aqueous layer.

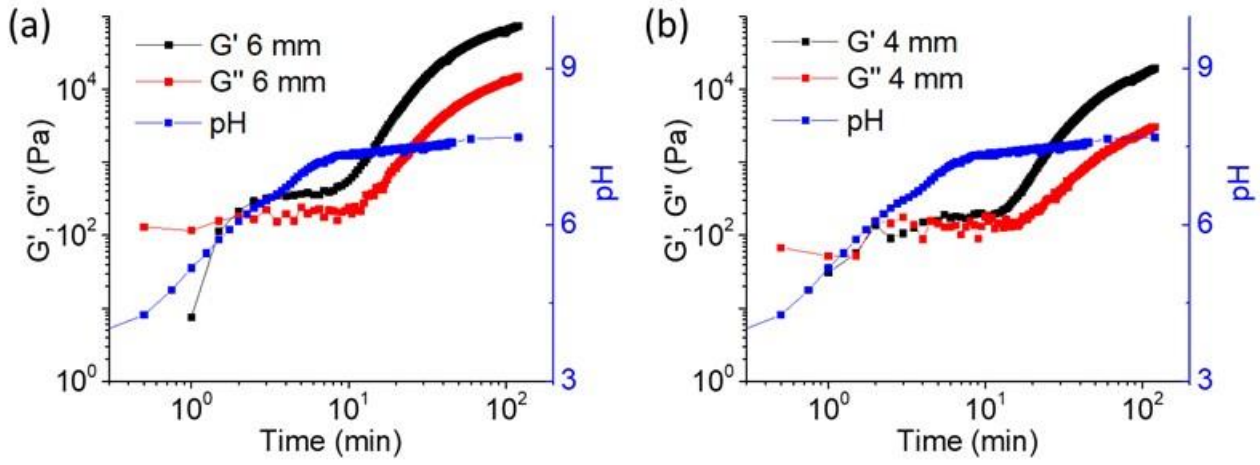


**Figure 3.18**. Variation of pH (blue), G' (black) and G" (red) of gel **9b** over 2 h, when the shaft is positioned at (a) 6 mm or (b) 4 mm from the bottom.

All the information obtained through time sweep rheology support the hypothesis of the formation of a gradient gel, meaning that this is formed following a direction, i.e., from top to bottom.

We performed strain sweep experiments on the gel formed after an overnight rest both with addition of NaOH (**9a**) and when in contact with the CDI solution (**9b**). Gel **9a** is more than twenty folds stiffer than gel **9b**. This is related to the different final pH of the gel, around 9.8 in the case of **9a** and around 7.7 in the case of **9b** (Table 3.4).

**Table 3.4**. Summary of the trials tested for the spatiotemporally programmed gels **9b-e**.

| Gel | NaOH (eq.) | [CDI] (M) | CDI sol. (mL) | CDI amount (mmol) | Result | G' (kPa) | G" (kPa) | pH |
|---|---|---|---|---|---|---|---|---|
| **9a** | 1.0 | None | None | None | Gel | 210 ± 17 | 39 ± 2.1 | 9.8 |
| **9b** | None | 0.075 | 2.0 | 0.150 | Gel | 8.9 ± 1.0 | 1.3 ± 0.4 | 7.7 |
| **9c** | None | 0.075 | 3.0 | 0.225 | Gel | 22 ± 1.2 | 3.7 ± 1.4 | 7.8 |
| **9d** | None | 0.050 | 2.0 | 0.100 | Gel | 3.4 ± 0.7 | 0.8 ± 0.1 | 7.4 |
| **9e** | None | 0.050 | 3.0 | 0.150 | Gel | 9.5 ± 4.2 | 1.9 ± 0.6 | 7.6 |

G' and G" values are referred to $\gamma$ = 0.05 %; the pH was measured after an overnight rest for the complete gel formation.

As the apparent p$K_a$ of gelator **9** is around 8.0, while gel **9b** has a final pH lower than this value, this gel should form either due to the high gelator concentration or because the gelator tends to form aggregates with the imidazolium ions. However, a lower extent of aggregation in the case of gel **9b** should be found. This was proven with fluorescence emission, UV-vis absorption and FTIR spectroscopy. For each of these experiments we compared the spectra of the aqueous solution of gelator **9**, gel **9a** and gel **9b** (Figure 3.19).

The solution of **9** exhibited strong emission at 322 nm and a relatively less intensified peak at 366 nm corresponding to the monomer and excimer emission of the Fmoc-group, respectively. The excimer emission appeared due to parallel overlapping of the fluorenyl

groups.[85] The monomer emission of **9** was almost fully quenched in the gel **9a** and the excimer emission was predominant at 490 nm, derived from the antiparallel overlapping of the fluorenyl groups.[86] In gel **9b**, the monomer emission is present and red-shifted to 338 nm along with a blue-shift to 460 nm of the antiparallel overlap of the fluorenyl groups (Figure 3.19a). These results indicate that the degree of deprotonation of **9** is higher with NaOH, enabling the amine to contribute more to self-assembly involving aromatic stacking. In contrast, the existence of the nongelling ammonium form of **9** in gel **9b** corroborates the lower stiffness of the material.

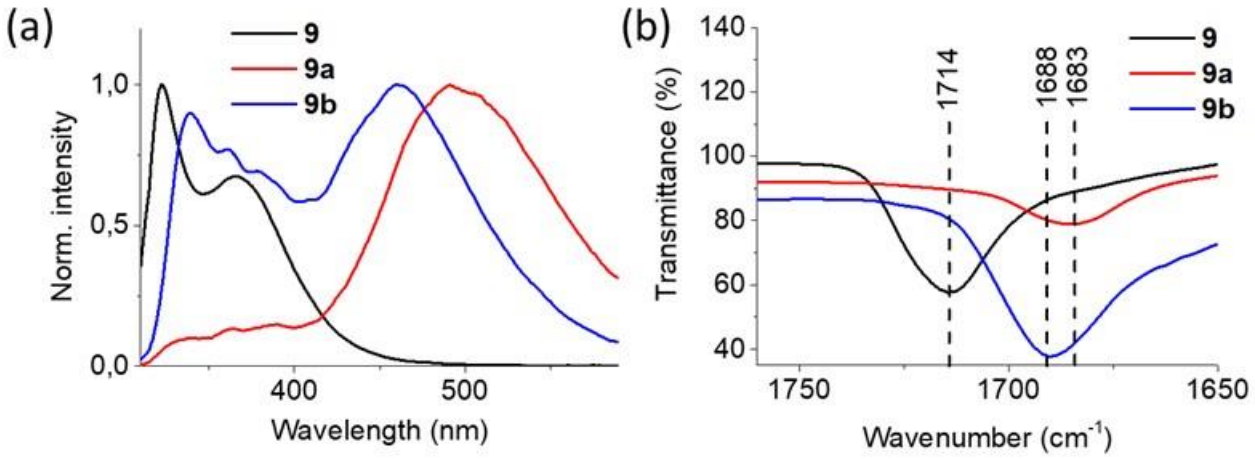


**Figure 3.19**. (a) Emission spectra and (b) zoom in the region 1650-1775 $cm^{-1}$ of the IR absorption spectra of the solution of **9** (black), the gel **9a** (red), and the gel **9b** (blue).

By FTIR spectroscopy on the freeze-dried gels, the carbamate carbonyl stretching of **9** at 1714 $cm^{-1}$ moved to the lower values of 1688 $cm^{-1}$ and 1683 $cm^{-1}$ in the gels **9b** and **9a**, respectively. The red-shifts of carbonyl groups are usually indicative of the involvement in H-bonds[148] and as they appear more prominent in the case of gel **9a**, these results suggest the formation of a stronger hydrogel network involving the amine, agreeing with the higher extent of deprotonation of **9** in presence of NaOH (Figure 3.19b).

Finally, we analysed the fibrous structure of the gels through confocal microscopy. Both gels **9a** and **9b** display a spherulitic network, with gel **9a** possessing fibres larger in size (Figure 3.20).

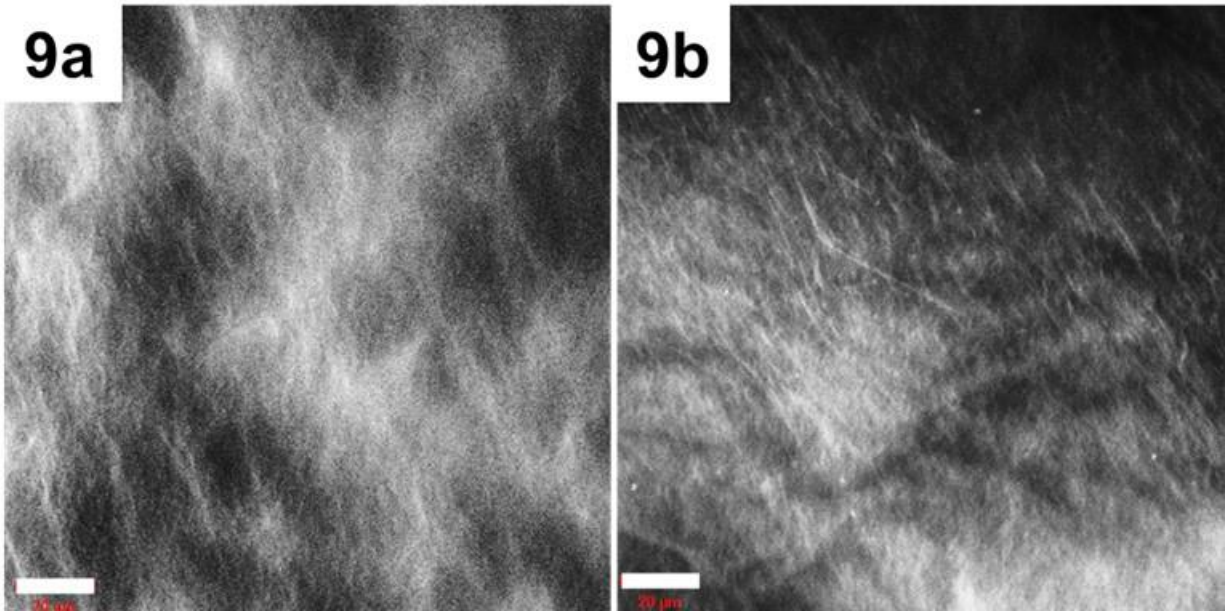


**Figure 3.20**. Confocal microscope images of gels **9a** and **9b**. The scalebar is 20 μm.

We then tried to manipulate the formation of the gel over time, by varying either the concentration or the total amount of CDI present in the TBME. To do so, we prepared three other gels with the same concentration of gelator in the aqueous layer (1.0 % w/V). Gel **9c** was prepared using 3 mL of a 0.075 M CDI solution in TBME, gel **9d** with 2 mL of a 0.050 M CDI solution in TBME, and gel **9e** with 3 mL of a 0.050 M CDI solution in TBME (Table 3.4).

Through time sweep rheology we outlined the kinetics of the gelation relating the data with the pH variation. Apparently, the rate of pH variation is highly affected by the total CDI amount diffused in the aqueous layer. Gel **9c**, sharing the same concentration of CDI with gel **9b** and having the highest total CDI amount, in fact has no longer a sigmoidal pH increase, but rather a linear one that reaches a plateau at pH 7.8. However, the gelation kinetics does not seem to be affected by the rapid increase in pH and follows a trend like the one of gel **9b**. Gel **9d**, having the lowest concentration and total amount of CDI, follows a sigmoidal pH increase to reach a final pH slightly above 7. The gelation kinetics in this case is slower compared to the previous cases and the gelation starts after 15 minutes. Finally, gel **9e**, having the lowest concentration and the same total CDI amount of gel **9b**, follows a sigmoidal pH increase too, reaching the same final pH value of gel **9b**,

but the gelation starts after 15 minutes, as for gel **9d** (Figure 3.21). Therefore, from this analysis we outlined that the gelation kinetics can be simply tuned by varying the concentration of CDI in TBME.

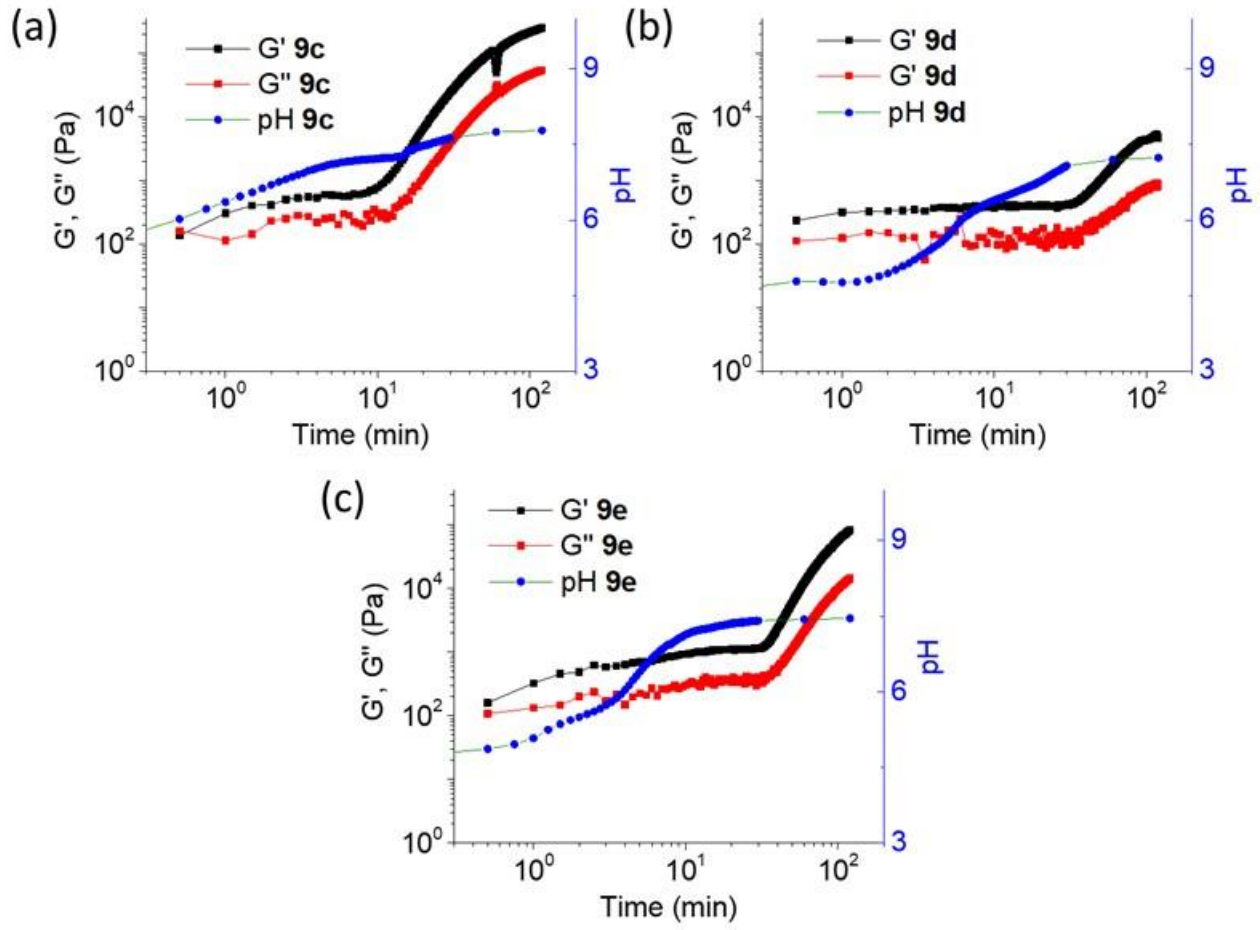


**Figure 3.21**. Variation of G' (black), G" (red), and pH (blue) of gels (a) **9c**, (b) **9d**, and (c) **9e** over 2 h, when the shaft is positioned at (a) 6 mm or (b) 4 mm (red) from the bottom.

We then studied the rheological properties of these gels through strain sweep rheology of the gels formed after an overnight rest. From this analysis, gels **9b** and **9e** display a similar stiffness, gel **9c** has the highest stiffness, and gel **9d** the lowest (Table 3.4). This trend is in line with the total CDI amount in TBME.

Finally, we applied the devised methodology to another hydrogelator to expand the applicability of the method. We then chose the Fmoc-protected diaminopropane (Fmoc-DAP) **10**, sharing the Fmoc-moiety with gelator **9** and possessing a primary amine. We

obtained gel **10a** spatiotemporally programming the gelation through the reaction-diffusion from 2 mL of a 0.075 M CDI solution in TBME to the aqueous layer containing 1.0 % w/V of gelator **10** (Figure 3.22).

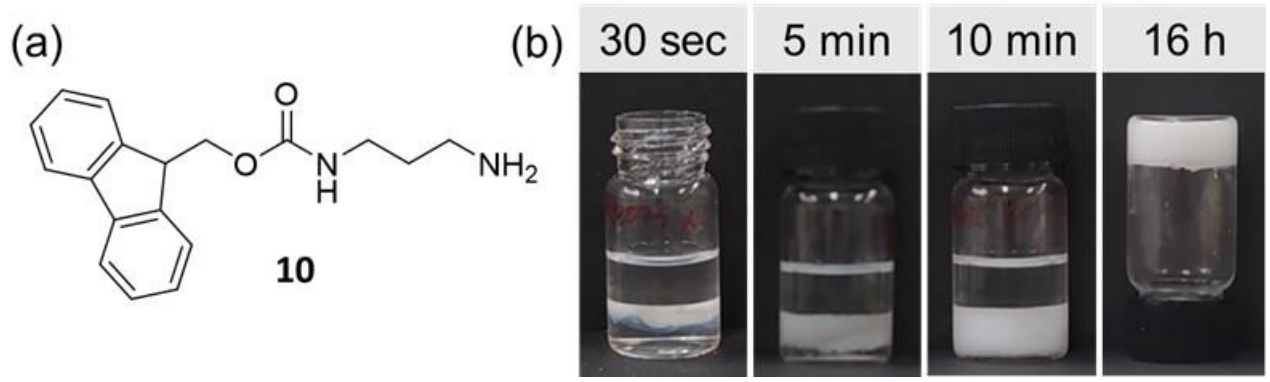


**Figure 3.22**. (a) Molecular structure of gelator **10**; (b) photographs over time of the formation of gel **10a**.

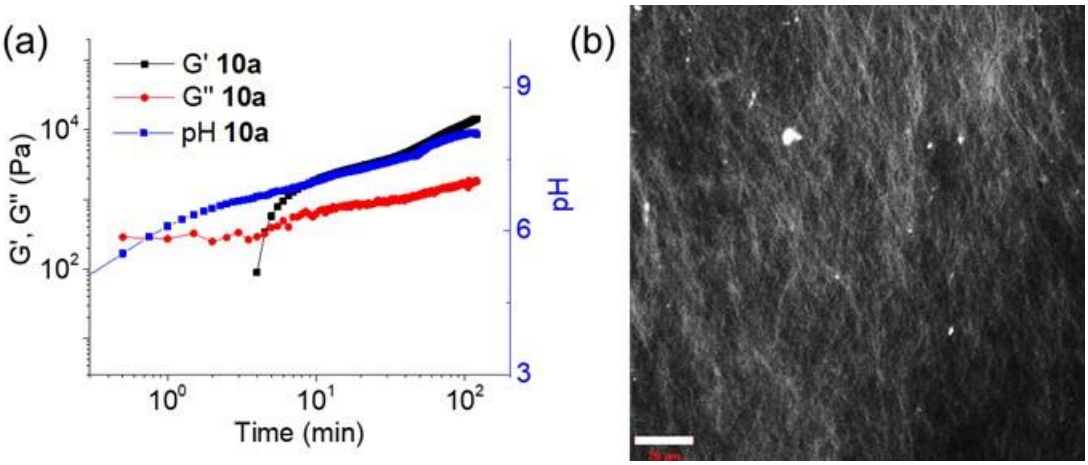


**Figure 3.23**. (a) Variation of G' (red), G" (black), and pH (blue) over time of gel **10a**; (b) confocal microscope image of gel **10a**. The scalebar is 20 μm.

Both the pH profile and time sweep rheology for gel **10a** showed significant differences compared to **10b**, with a decrease in the rate of pH change and a delay in the appearance of the gel respectively. At the end of the gelation, the gel appeared as made of long thin fibres, as revealed through the confocal microscope (Figure 3.23).

## *3.3. Summary*

We have shown how we the pH-annealing approach with the coupled reaction between urea urease and methyl formate can be used to control the formation of a gel over time and convert co-assembled systems to self-sorted ones. Initial addition of water to a solution of two gelators in DMSO favours co-assembly. Such a solvent-switch gelation is a phase separation process and there seems to be insufficient time or driving force for anything other than co-assembly to occur. Annealing by a pH increase and decrease results in self-sorted gels. Gelation on a slow pH decrease drives self-sorting on the basis of the apparent p$K_a$ of each gelator.

Annealing specific layers in two component gels allows complex hierarchical systems to be formed. It is possible to tune the annealing process on layers by varying the content of urea, urease, and methyl formate to change the composition and rates of pH change, thus allowing access to a far greater range of morphologies and complexity than can be achieved in single component systems.

We have devised a new reaction-diffusion methodology for programming the hydrogel formation over space and time using CDI and a bilayer system of two immiscible solvents. Tuning the reaction-diffusion is simple and the rate of gel formation can be controlled in many ways. Variation of the total CDI concentration in the organic phase modulates the rate of gel formation in the aqueous layer, whilst the final properties of the gels are dependent on the total amount of CDI and not related to the gelation rate. A large number of gelators contain pH-responsive amine-groups. However, there are limited methodologies available for increasing the pH and thereby synthesizing base-triggered gels.[141,149] In this context, CDI-triggered control over the pH increase is new. We envisage that our method can be extended to other hydrogelators with an amine functionality and could be useful in more complex systems such as multicomponent materials. We anticipate that our concept could be extended further to control diffusion gradients across gels for reaction-based systems, for example, reaction in localized sites followed by diffusion of the products across the gels controlled by the pH.

# *Chapter 4. Applications of gels*

LMW gels have numerous applications, spanning from their use as medium to grow crystals[150,151] to the removal of pollutant from water.[152,153] Hydrogels can incorporate significant amounts of liquids, such as water or biological fluids, as well as organic molecule dispersed in it. For this reason, LMW gels can work both for a controlled release of some substances and as a trap for some other, depending on the affinity of the gelator fibres with the specific compound.

This is one of the reasons why they are among the most used biomaterials in medical applications, not only to produce healthcare products but also for drug delivery systems, tissue engineering scaffolds, and wound dressings.[154,155] A recent possibility to form hydrogels for these applications is focused on the use of small molecules instead of polymers.[156,157] The use of small molecules able to gel water and organic solvents is an innovative process that is highly desirable for the formation of smart and sustainable materials. Hydrogels based on amino acids derivatives, peptides and pseudo-peptides present several advantages,[158,159] such as the easy and cost-effective synthesis and functionalization, low toxicity, high biocompatibility, and biodegradability. Different gelators can be also mixed to obtain a multicomponent gel, which may combine some of the properties of the two single components in the same material[160] or may be characterised by interesting new properties not accessible with a single component.[161] LMW gels can therefore be considered a valid alternative to polymers in many applications, especially in cosmetics, where these compounds can be used as rheological modifiers,[162] for skin care and topical therapies,[163,164] for perfume-controlled release[165] but have still received poor investigation.

## *4.1. Release of fragrances*

During my PhD, we used gels as catalytic site to control the hydrolysis of odorant molecules such as imines or Schiff bases (SB).[165] Such molecules are made of an aldehyde and a primary amine[166] and they slowly undergo hydrolysis in presence of water, releasing the two composing molecules. This strategy is often used in perfumery. Usually, the amine and the aldehyde have a high volatility and vapour over a short period. The imine resulted from the covalent binding between the two species, instead, has a lower vapour tension, resulting in a longer-lasting species that slowly releases the fragrances. Such molecules that release either fragrances or perfumes are called profragrances or properfumes, respectively.[167,168] The covalent bond can be then selectively cleaved by a specific stimulus, which in the case of imines is the presence of water.[169]

In this work, we prepared four SBs, namely **SB1**, **SB2**, **SB3**, and **SB4**. They were all obtained from methyl anthranilate (**MA**) as the primary amine and four aldehydes (**A**), namely **A1**, **A2**, **A3**, and **A4** (Figure 4.1). The compounds were obtained and used as racemate.

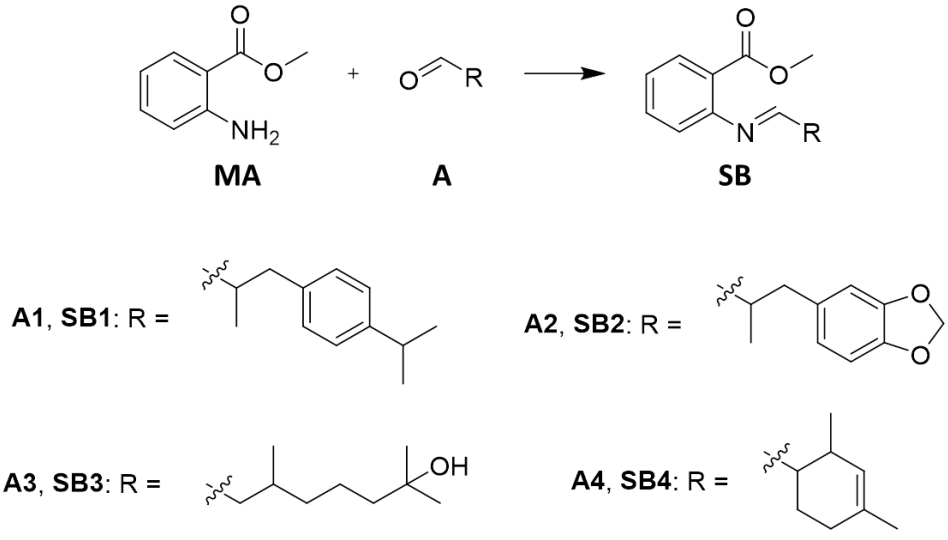


**Figure 4.1**. Scheme for the synthesis of the Schiff bases **SB1-4**, with structures of both aldehydes **A1-4** and imines **SB1-4**.

These reactions were carried out without any solvent and heating to 110 °C for different times and different ratios between the two reagents. The optimal conditions for each reaction were outlined by varying the relative ratio of the two reactants, testing 1:1, 2:1, and 1:2 molar ratio, and the time reaction time, testing 30, 60, and 120 minutes. These results together with the relative conversions are reported in Table 4.1. The conversions were calculated over the disappearance of the methyl anthranilate peak through HPLC-MS.

**Table 4.1**. Summary of the optimal conditions for obtaining imines **SB1-4**.

| Imine | Ratio A:MA | Time (min) | Conversion (%) |
|---|---|---|---|
| **SB1** | 2:1 | 30 | 93 |
| **SB2** | 2:1 | 30 | 98 |
| **SB3** | 1:2 | 120 | 82 |
| **SB4** | 2:1 | 60 | 82 |

A = aldehyde; MA = methyl anthranilate.

We were able to purify via crystallisation only **SB2** as the other three displayed a solubility similar to the starting materials. Some crystals were grown from methanol and analysed through single crystal X-ray diffraction (XRD). This Schiff base crystallised in the triclinic P-1 space group with one molecule in the asymmetric unit. The only intermolecular interaction found is a strong intramolecular hydrogen bond[170,171] involving the iminic nitrogen and carbonyl group ($N_{N\text{-}H}\cdots O_{C=O}$ = 2.657 Å). No other intermolecular interactions are detected, and crystal cohesion is mainly due to dispersion forces, with SB2 molecules stacking along the [100] crystallographic direction at about 4.9 Å (Figure 4.2).

Attempts through column chromatography to purify the imines failed as well, as each SB underwent hydrolysis over the acidic surface of silica gel. For this reason, we decided to use the imines synthesised without any further purification and the recrystallised imine **SB2** (from now on called **SB2c**) for our studies.

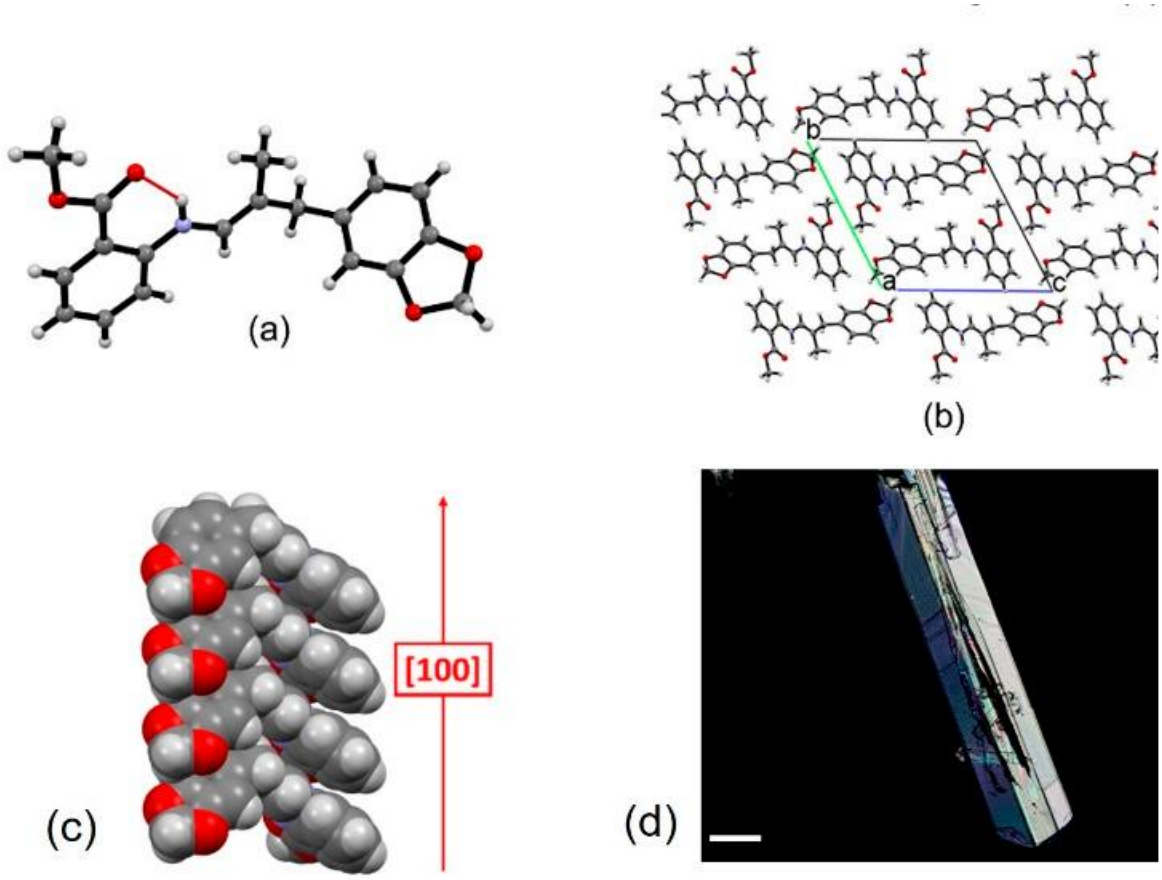


**Figure 4.2**. Structural features of crystalline **SB2**: (a) the asymmetric unit, showing the intramolecular $S_1^1(6)$ hydrogen bonding interaction between the iminic nitrogen and carbonyl group, (b) crystal packing viewed down the a-axis, and (c) detail of the columnar stacking extending along the [100] crystallographic direction; (d) optical microscope image (polarized light) of the crystals of **SB2**. The scalebar is 100 μm.

Through HPLC-MS, we studied the hydrolysis of these molecules in EtOH:$H_2O$ mixtures in ratio 85:15 and 70:30 at a concentration of 0.5 % w/V. The reaction over 24 hours in these mixtures is not very prominent apart from the cases of **SB2c** and **SB3**, so we included a small amount of acetic acid (20 mM) to each mixture to increase the rate of hydrolysis (Table 4.2).

As reported in the table, the hydrolysis is much more prominent in presence of acetic acid. Comparing the results of **SB2** against **SB2c**, the hydrolysis without acetic acid appears much faster in the case of **SB2c**. This may be due to the different pH. At the beginning,

the presence of methyl anthranilate in **SB2** slightly enhances the pH, reducing the rate of conversion of the imine. In presence of acetic acid, the recrystallised imine **SB2c** is instead more stable than **SB2**, probably because of the increased stability of the crystals compared to the mixture.

**Table 4.2**. Summary of the experiments of imines hydrolysis in solution with pH.

| Imine | EtOH:$H_2O$ | Acetic acid (mM) | $pH_0$ | Hydrolysis after 24 h (%) |
|---|---|---|---|---|
| **SB1** | 85:15 | none | 5.9 | 3.2 ± 1.9 |
| **SB1** | 70:30 | none | 5.0 | 3.2 ± 1.1 |
| **SB1** | 70:30 | 20 | 3.6 | 91 ± 4.3 |
| **SB2** | 85:15 | none | 5.7 | 2.6 ± 0.5 |
| **SB2** | 70:30 | none | 5.1 | 5.6 ± 3.8 |
| **SB2** | 70:30 | 20 | 3.6 | 75 ± 2.9 |
| **SB2c** | 85:15 | none | 4.8 | 23 ± 7.6 |
| **SB2c** | 70:30 | none | 4.8 | 28 ± 7.0 |
| **SB2c** | 70:30 | 20 | 3.6 | 43 ± 8.8 |
| **SB3** | 85:15 | none | 5.7 | 43 ± 0.6 |
| **SB3** | 70:30 | none | 5.3 | 40 ± 6.7 |
| **SB3** | 70:30 | 20 | 3.6 | 73 ± 4.4 |
| **SB4** | 85:15 | none | 5.9 | 12 ± 1.3 |
| **SB4** | 70:30 | none | 5.7 | 10 ± 6.5 |
| **SB4** | 70:30 | 20 | 3.7 | 92 ± 1.2 |

$pH_0$ = pH measured at the beginning of the hydrolysis reaction.

At this point, we repeated the hydrolysis in a gel matrix, to outline variations in the hydrolysis rate with the experiment in solution. For this purpose, we prepared gels with two derivatives of the amino acid 3,4-dihydroxyphenylalanine (Dopa). This amino acid, like Phe and Tyr, has an aromatic side chain, i.e., a catechol ring, which offers the possibility of creating stabilising intercations for the formation of hydrogels, such as π-

interactions and H-bonds. Furthermore, the –OH groups can be easily functionalised to insert other aromatic features. However, the catechol is a sensitive moiety, which can undergo oxidation to form the quinonic form with light or in basic aqueous environment. The catechol and the quinonic form of Dopa can also react and polymerise to form melanines.[172,173] For this reason, the side chain of Dopa is often protected. For our purposes, we synthesised Boc-$^{L}$Dopa(Bn)$_2$-OMe[174] (**11**) and Boc-$^{L}$Dopa(Bn)$_2$-OH[175] (**12**) (Figure 4.3). Gelator **11**, being an ester, should mimic the neutral conditions, while gelator **12**, being an acid, should mimic the acidic solution.

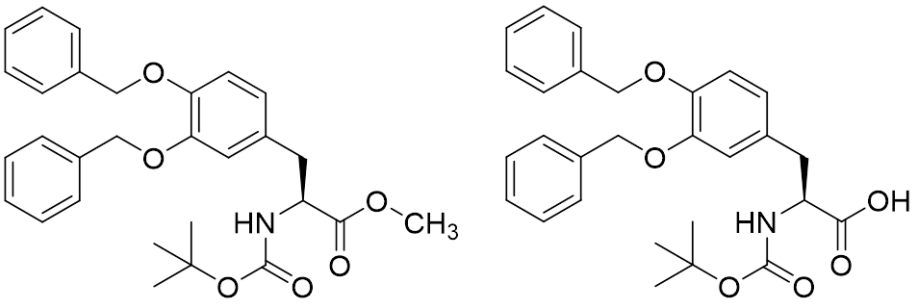


Boc-$^{L}$Dopa(Bn)$_2$-OMe, **11** Boc-$^{L}$Dopa(Bn)$_2$-OH, **12**

**Figure 4.3**. Molecular structure of gelators **11** and **12**.

The gel formation of these gelators was tested in the same conditions the hydrolysis experiment was carried out. The gelation ability of **11**, mimicking the neutral conditions, was studied in 85:15 and 70:30 solvent ratio, while gelator **12,** mimicking the condition obtained with the solvent mixture with the addition of acetic acid, was studied only in 70:30 solvent ratio.

Gels were prepared at a concentration of 1.0 % w/V using the solvent switch method. In this case, the gelators were dissolved in ethanol in the required amount, then water was added. The addition of water caused an unbalance in the gelator solubility, resulting in the gel formation. We obtained in this way gels **11a**, **11b**, and **12a** (Figure 4.4).

Each of these gels was study through strain sweep rheology, to outline the stiffness of the material. These data are reported in Table 4.3, together with the pH at the end of the gelation process.

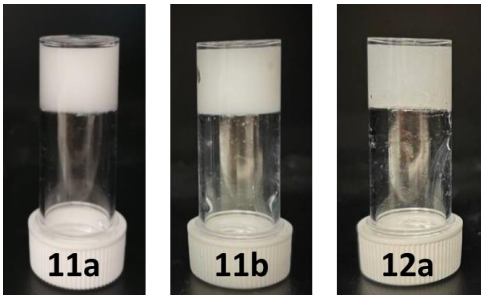


**Figure 4.4**. Photographs of the gels **11a**, **11b**, and **12a**.

**Table 4.3**. Summary of the gels **11a**, **11b**, and **12a** with rheological properties and pH.

| Gel | EtOH:$H_2O$ | G' (kPa) | G" (kPa) | $pH_f$ |
|---|---|---|---|---|
| **11a** | 85:15 | 130 ± 23 | 41 ± 3.9 | 6.4 ± 0.2 |
| **11b** | 70:30 | 88 ± 22 | 16 ± 3.2 | 6.0 ± 0.2 |
| **12a** | 70:30 | 43 ± 11 | 12 ± 3.1 | 3.8 ± 0.03 |

G' and G" values are reported at $\gamma$ = 0.03 %; $pH_f$ = pH at the end of the gelation process.

We then incorporated the imines previously synthetised in the gels, studied their hydrolysis over time, and compared the results obtained with the data in solution (Figure 4.5). For such study we used only gel **11b** as neutral medium, to make a direct comparison with the results obtained for gel **12a**.

The comparison between the results in solution and in gel indicates that the acidic catalysis is always crucial for the hydrolysis reaction. The gel **11b** with a pH around 6 is not able to significatively enhance the hydrolysis rate in any condition, as only **SB3** reaches 63% hydrolysis after 96 h. This medium is preferred for a very slow odour release, lasting weeks, but with reduced intensity.

On the other hand, gel **12a** has a final pH lower than 4 due to the acidic moiety contained in the chemical structure that catalyses the hydrolysis. However, in any case the hydrolysis

in solution is faster than in gel, although the pH is very similar. This medium should be preferred if the odour release is required within few days.

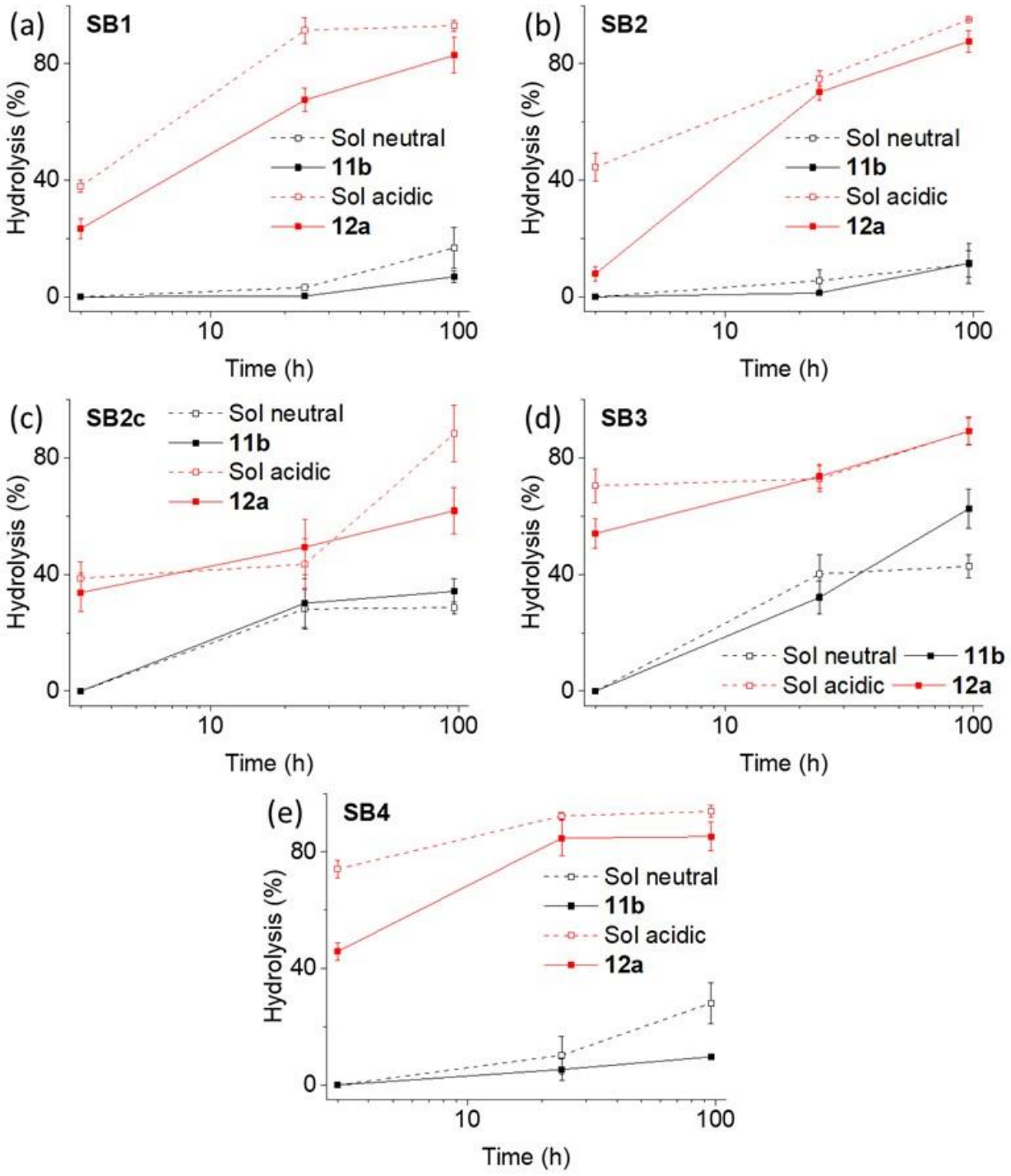


**Figure 4.5**. Hydrolysis of the imines (a) **SB1**, (b) **SB2**, (c) **SB2c**, (d) **SB3**, and (e) **SB4** over time in neutral solution (black open symbols), neutral gel **11b** (black solid symbols), acidic solution (red open symbols), and acidic gel **12a** (red solid symbols).

## *4.2. Release of bioactive compounds*

We formed a new multicomponent gel using one of the two gelators also as trigger for the gel formation. The two peptide components used for this study were Boc-$^{L}$Dopa(OBn)$_2$OH, **12** and Boc-$^{L}$Ala-Aib-$^{L}$Val-OH, **13** (Figure 4.6). The gelling ability of **12** was already investigated under several conditions,[150,176] however, none of the gels obtained displayed a pH suitable for biological applications. In fact, **12** forms strong white hydrogels with GdL, reaching a pH around 4-5, and $CaCl_2$, reaching a pH around 8. On the other hand, **13** was not able to form gels in the same conditions, but only in either ethanol or isopropyl alcohol and water mixtures.[177]

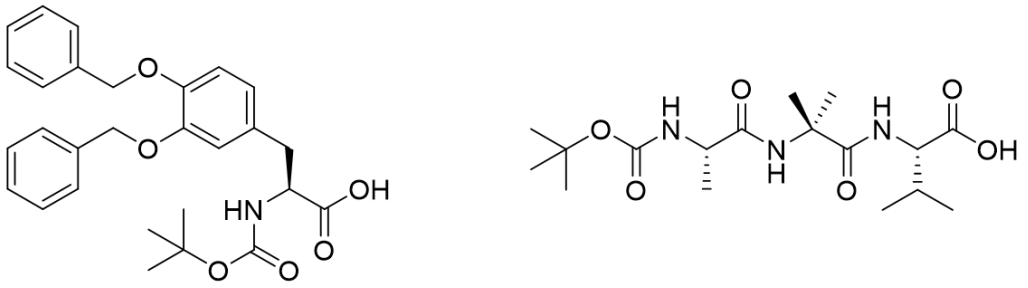


Boc-$^{L}$Dopa(Bn)$_2$-OH, **12** Boc-$^{L}$Ala-Aib-$^{L}$Val-OH, **13**

**Figure 4.6**. Molecular structure of the gelators Boc-$^{L}$Dopa(OBn)$_2$OH, **12** and Boc-$^{L}$Ala-Aib-$^{L}$Val-OH, **13**.

By mixing the two gelators in different ratios, we were able to finely tune both the mechanical properties and the pH of the final materials. The pH can be further modified with the addition of citric acid, currently used in many products applied on the skin.[178,179]

As **12** is not soluble in PB at pH 7.4, we dissolved it in water containing NaOH, reaching a pH around 10, while **13** was dissolved in a 30 mM PB at pH 7.4, reaching a pH of about 6. The solution of **13** was added to the first one and used as a trigger. Different mixtures of **12** and **13** were combined to find gels with pH ranging between 5.5 and 7.4 (Table 4.4). All the hydrogels have an overall concentration of about 1.0 % w/V of the two

components **12** and **13**. The role of **13** is to contribute to the gel formation and to reduce the overall pH, as it contains an acidic moiety.

**Table 4.4**. Summary of the multicomponent gels of **(12+13)** prepared.

| Gel | 12 (%) | 13 (%) | Citric acid (%) | 14 (%) | 15 (%) | T (°C) | pH | Result |
|---|---|---|---|---|---|---|---|---|
| **(12+13)a** | 0.65 | 0.35 | None | None | None | 23 | 7.6 | Gel |
| **(12+13)b** | 0.65 | 0.50 | None | None | None | 23 | 7.3 | Gel |
| **(12+13)c** | 0.35 | 0.65 | None | None | None | 23 | 6.8 | Gel |
| **(12+13)d** | 0.35 | 0.65 | 0.38 | None | None | 23 | 5.8 | ppt |
| **(12+13)e** | 0.35 | 0.65 | 0.38 | None | None | 60 | 5.6 | Gel |
| **(12+13)f** | 0.35 | 0.65 | None | 0.10 | None | 40 | 6.7 | Gel |
| **(12+13)g** | 0.35 | 0.65 | None | None | 0.10 | 40 | 6.7 | Gel |

The pH was measured at the end of the gelation process.

Hydrogels **(12+13)a** and **(12+13)b** have a pH higher than 7, as they contain more **12**, dissolved in NaOH at pH around 10, than **13**, dissolved in PB at pH around 7. We prepared gel **(12+13)d** by adding a biocompatible acid, i.e., citric acid to further reduce the pH to a value lower than 6, suitable for skin applications. However, the gel did not form as some precipitate formed right after the addition of citric acid. Therefore, a different method for the gel preparation was developed. We heated separately the vials containing **12** and **13**, the last one containing citric acid, up to 60 °C and mixed them while hot. Under these conditions, we obtained gel **(12+13)e** right after the mixing of the two solutions.

Hydrogels **(12+13)c** and **(12+13)e** were chosen for further characterizations as their pH is suitable for topical applications. The mechanical properties of hydrogels **(12+13)c** and **(12+13)e** were tested first by shaking the samples then with the rheometer. Both samples showed excellent thixotropic properties in any case, highlighted by their behaviour against the reiterated process of disruption by vigorous shaking and restoration after 16 hours

(Figure 4.7). The gels broken and restored once will be called **(12+13)c-r** and **(12+13)e-r**, the ones broken and restored twice will be called **(12+13)c-r2** and **(12+13)e-r2**.

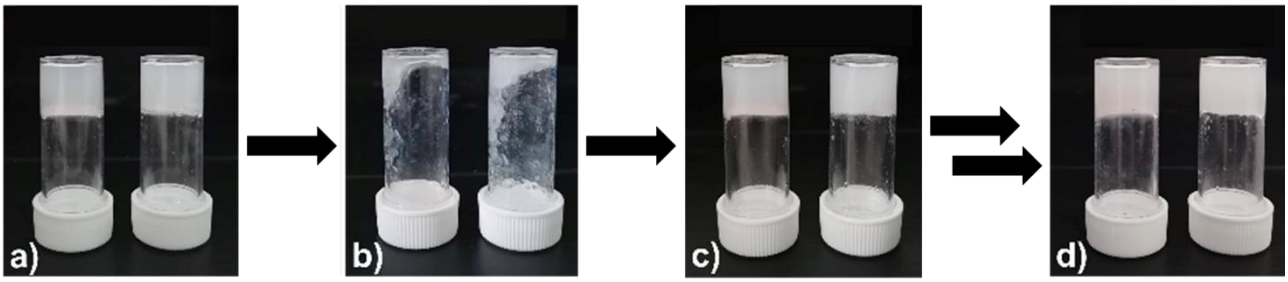


**Figure 4.7**. Photographs of gels **(12+13)c** (left of each photograph) and **(12+13)e** (right of each photograph) (a) after formation, (b) after disruption by vigorous shaking, (c) restoration after 16 hours, **(12+13)c-r** and **(12+13)e-r**, and (d) after a second disruption-and-restoration process, **(12+13)c-r2** and **(12+13)e-r2**.

We investigated the hydrogels rheological properties by measuring the amplitude sweep before, i.e., **(12+13)c** and **(12+13)e** and after breaking, i.e., **(12+13)c-r** and **(12+13)e-r** the gels. Gels **(12+13)c** and **(12+13)e** show a moderate strength of about 6 kPa and a long linear viscoelastic range (LVER). In particular, the first one shows a great elasticity and the absence of a proper breaking point. This behaviour is also confirmed by the step-strain experiment performed after breaking and reforming the samples two times, i.e., **(12+13)c-r2** (Figure 4.8).

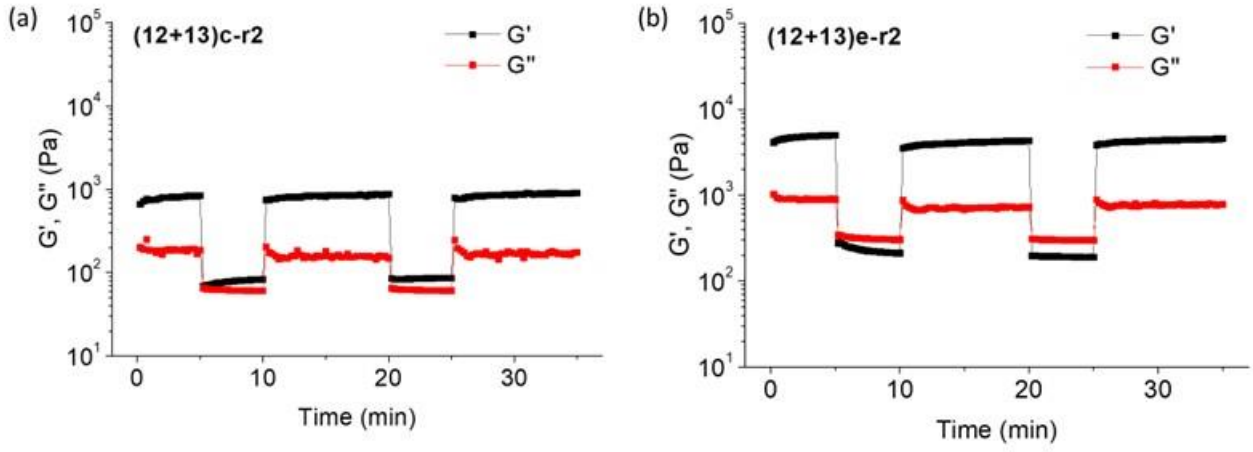


**Figure 4.8**. Step-strain experiments on gels (a) **(12+13)c-r2** and (b) **(12+13)e-r2**.

**Table 4.5**. Summary of the rheological properties of the gels after formation, **(12+13)c** and **(12+13)e**, and after disruption and restoration, **(12+13)c-r** and **(12+13)e-r**.

| Gel | G' (kPa) | G" (kPa) | LVER (%) | Break point (%) |
|---|---|---|---|---|
| **(12+13)c** | 5.9 ± 0.9 | 1.4 ± 0.2 | 0.46 | N.D. |
| **(12+13)e** | 6.7 ± 2.2 | 1.5 ± 0.2 | 0.46 | 74 |
| **(12+13)c-r** | 1.5 ± 0.1 | 0.4 ± 0.04 | 0.67 | N.D. |
| **(12+13)e-r** | 5.8 ± 2.3 | 1.2 ± 0.5 | 0.31 | N.D. |
| **(12+13)f** | 4.2 ± 1.1 | 1.0 ± 0.4 | 1.0 | N.D. |
| **(12+13)g** | 24 ± 2.8 | 4.3 ± 0.6 | 0.31 | 22 |
| **(12+13)f-r** | 2.0 ± 0.9 | 0.5 ± 0.3 | 1.0 | N.D. |
| **(12+13)g-r** | 7.5 ± 1.9 | 1.4 ± 0.2 | 0.69 | 40 |

G' and G" are measured at $\gamma$ = 0.046 %; N.D. = not detected.

Gel **(12+13)c-r** has a slightly lower G', while sample **(12+13)e-r** completely recovers the previous stiffness (Table 4.5). The step-strain experiments show that both samples completely recover their G' after repeated disruption of the network. The difference between the G' moduli registered with the step-strain experiment and the amplitude sweep after restoration lies in the different stress applied to the material: harsh in the case of the vigorous shaking, and moderate in the case of the step-strain experiment. For this reason, gel **(12+13)c-r** displays a lower G' than **(12+13)c**.

The hydrogels **(12+13)c** and **(12+13)e** prepared display both the right pH and rheological behaviour for transdermal applications purposes, therefore we decided to test the release of two tripeptides, namely molecules TFA-$^{L}$Val-$^{L}$Tyr-$^{L}$Val-OH, **14**, and Pal-$^{L}$Lys-$^{L}$Val-$^{L}$Lys-OH, **15** (Figure 4.9). We chose these two tripeptides as they have a strong cosmetic activity, acting as anti-aging agents. TFA-$^{L}$Val-$^{L}$Tyr-$^{L}$Val-OH, **14** (trade name: Trifluoroacetyl tripeptide-2) is used in the commercial formulation Progeline™ by Lucas Meyer Cosmetics for its unique mechanism of action on progerin synthesis

modulation.[180,181] Pal-$^{L}$Lys-$^{L}$Val-$^{L}$Lys **15** (trade name: Palmitoyl tripeptide-5, also known as SYN®-COLL) has been widely used for its activity of collagen stimulation.[180,182]

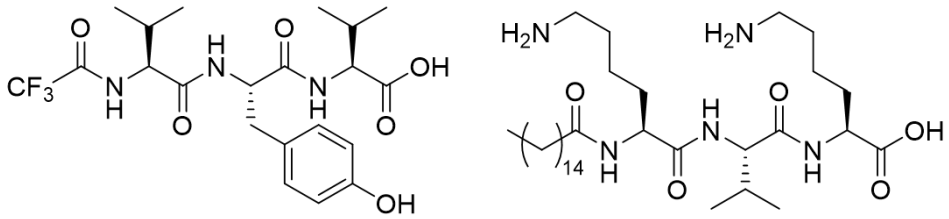


**Figure 4.9**. Molecular structure of the tripeptides TFA-$^{L}$Val-$^{L}$Tyr-$^{L}$Val-OH, **14**, and Pal-$^{L}$Lys-$^{L}$Val-$^{L}$Lys-OH, **15**.

Following the same technique reported for the preparation of hydrogel **(12+13)e**, we prepared the two hydrogels **(12+13)f** and **(12+13)g**, replacing the citric acid with the two active peptides **14** and **15** and mixing the two solutions at 40 °C for 2 minutes, since the active ingredients can undergo degradation at high temperature. The two bioactive peptides were added to the formulation in a quantity 0.10 % w/V, obtaining hydrogels **(12+13)f** and **(12+13)g** (Figure 4.10), both having a pH of 6.7 (Table 4.4).

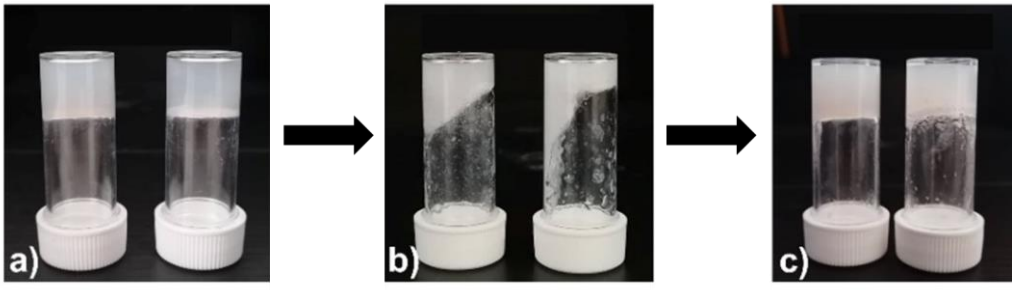


**Figure 4.10**. Photographs of gels **(12+13)f** (left of each photograph) and **(12+13)g** (right of each photograph) (a) after formation, (b) after disruption by vigorous shaking, and (c) restoration after 16 hours, **(12+13)f-r** and **(12+13)g-r**.

The mechanical properties of hydrogels **(12+13)f** and **(12+13)g** were measured with thixotropy test and rheological analyses, as done for the gels **(12+13)c** and **(12+13)e** (Table 4.5 and Figure 4.11).

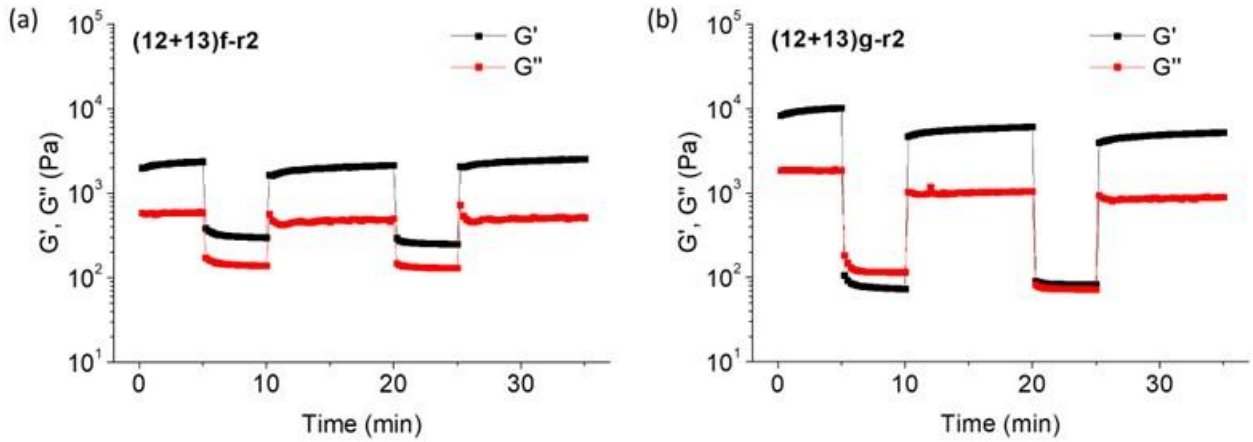


**Figure 4.11**. Step-strain experiments on gels (a) **(12+13)f-r2** and (b) **(12+13)g-r2**.

These samples behave as the previously reported ones, as they both recover their solid structure after disruption on shaking the samples multiple times (Figures 4.10 and 4.11). Sample **(12+13)f** has a lower G' and a higher elasticity compared to gel **(12+13)g**. Even after the strong shaking, **(12+13)f** does not convert to solution, but remains a viscous slurry (Figure 4.10b). This is also confirmed by the step strain experiment, where G' remains higher than G" in every point of the measurement (Figure 4.11a). This rheological behaviour means that the presence of **14** and **15** does not prevent gel formation, but the two active tripeptides slightly influence the rheological properties of the resulting gels. In particular, tripeptide **15** seems to positively interact with the gel network, as we can see from the increased G'.

The controlled release of the cosmetic active peptides **14** and **15** from hydrogels **(12+13)f** and **(12+13)g** was assessed with the help of diffusion in Franz cells, a widely used methodology to evaluate *in vitro* drug permeation.[183] These cells present some advantages such as few handlings of tissues, no continuous sample collection, and a small amount of drug required for analysis. A membrane, synthetic or natural, separates the two compartments of Franz cells.[184] Synthetic membranes (polysulfone, cellulose or

polydimethylsiloxane) must be inert, provide high permeability and not occlude the drug penetration.[185,186] Structural and biochemical characteristics of pig ear skin have shown to provide comparable results to human skin,[187] which is considered the best model in transdermal delivery systems. Therefore, we used pig ears as membrane in Franz cells and phosphate buffer at pH 7.4 as receiving solution.

The analytes released from the gel were analysed through HPLC-MS. After 24 hours, the tripeptide **14** was released in 39 %, while almost no release of peptide **15** was observed. On the other hand, both gelators were released after 24 hours. Boc-$^{L}$Dopa(Bn)$_2$-OH, **12**, was released from hydrogels **(12+13)f** and **(12+13)g** in 8 % and 6 % respectively. Boc-$^{L}$Ala-Aib-$^{L}$Val-OH, **13**, was released from hydrogels **(12+13)f** and **(12+13)g** in 46 % and 49 % respectively (Figure 4.12).

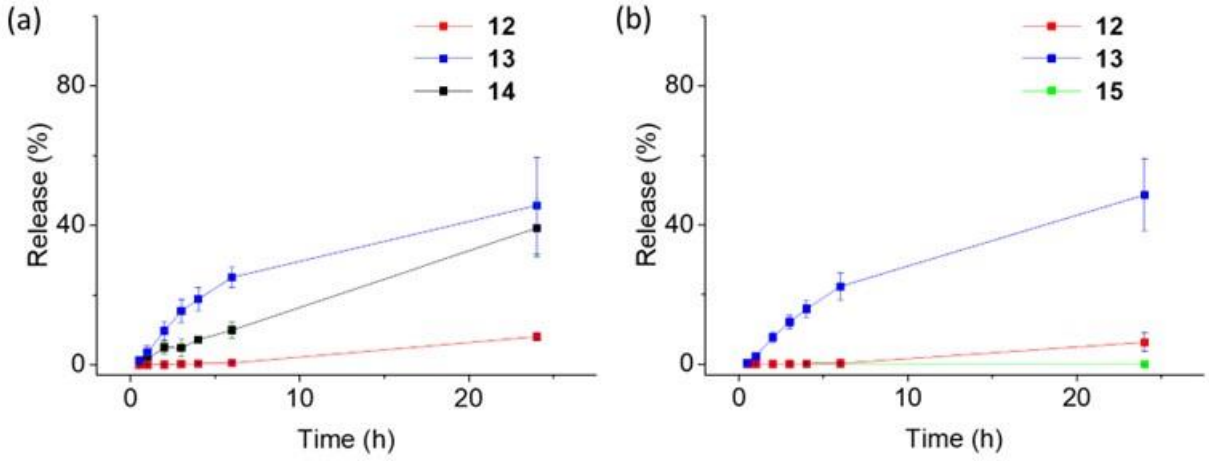


**Figure 4.12**. Release studies of molecules **12** (red), **13** (blue), **14** (black), and **15** (green) from the gels (a) **(12+13)f** and (b) **(12+13)g**.

The viability/cytotoxicity of the individual components (**12**, **13**, **14**, and **15**) of the gels was tested in vitro, using a secondary human keratinocyte line. A quantity of 1 mg of each individual component was incubated with the cells for 24 and 48 hours. The individual components are non-toxic and the cells continue to proliferate after 48 hours (data not shown).

The hydrogels prepared are thixotropic, show a moderate stiffness and an excellent linear viscoelastic range with the absence of a proper breaking point in the studied range of strain, confirmed by thixotropy experiments.

## *4.3. Removal of pollutants*

The increased level of water consumption and correspondingly high levels of pollution have generated a prominent need for managing the water quality by maintaining safe levels for the water to be used in specific applications. In this respect, water remediation methods have taken a forward thrust[188–191] to increase the water quality of potable water as well as that of industrial grade water in to prevent contamination of natural water resources due to the discharge of industrial effluents. LMW hydrogels find application also in this field[152], acting as a trap for pollutants.

When forming a LMW gel, aromatic moieties play a pivotal role as they allow the formation of key weak interactions such as cation-π and π-π stacking that drive the self-assembly.[192,193] However, the presence of aromatic rings in the feature of a gelator is usually accompanied with a low biodegradability of the molecule itself, so the use of aromatic-free gelators for the formation of supramolecular materials is highly desirable.

We synthesised two aromatic-free peptide-based gelators, namely Boc-$^{L}$Ala-Aib-$^{L}$Val-OH, **13**, previously discussed, and Boc-$^{L}$Val-Aib-$^{L}$Val-OH, **16** (Figure 4.13) and compared their behaviour against the gelation of mixtures of methanol, ethanol, or isopropyl alcohol and water (Table 4.6).[177] In any case, we dissolved the gelator in the organic solvent and after complete dissolution we added water to trigger the gelation and obtain a concentration of gelator of 1.0 % w/V.

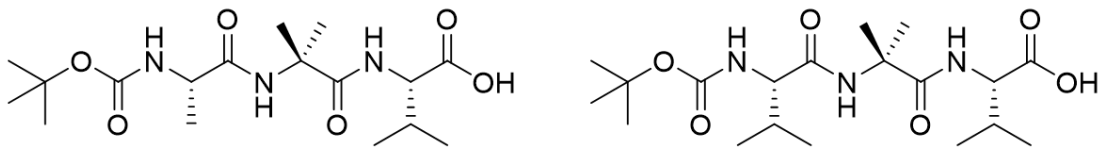

Boc-$^{L}$Ala-Aib-$^{L}$Val-OH, **13**  Boc-$^{L}$Val-Aib-$^{L}$Val-OH, **16**

**Figure 4.13**. Molecular structure of the gelators Boc-$^{L}$Ala-Aib-$^{L}$Val-OH, **13**, and Boc-$^{L}$Val-Aib-$^{L}$Val-OH, **16**.

Gelator **13** was able to gel mixtures of both ethanol/water and isopropyl alcohol/water in 3:7 ratio and was able to form a partial gel with the mixture of methanol/water in the same volumetric ratio (Figure 4.14). On the other hand, gelator **16** did not form a gel in any of the tested conditions but rather tended to crystallise.

**Table 4.6**. Summary of the gels prepared with **13** and **16**.

| Gel | Gelator | Solvent (%) | Water (%) | Result |
|---|---|---|---|---|
| **13a** | **13** | MeOH, 30 | 70 | Partial gel |
| **13b** | **13** | MeOH, 50 | 50 | Solution |
| **13c** | **13** | MeOH, 70 | 30 | Solution |
| **13d** | **13** | EtOH, 30 | 70 | Gel |
| **13e** | **13** | EtOH, 50 | 50 | Solution |
| **13f** | **13** | EtOH, 70 | 30 | Solution |
| **13g** | **13** | iPrOH, 30 | 70 | Gel |
| **13h** | **13** | iPrOH, 50 | 50 | Solution |
| **13i** | **13** | iPrOH, 70 | 30 | Solution |
| **16a** | **16** | MeOH, 30 | 70 | Precipitate |
| **16b** | **16** | MeOH, 50 | 50 | Solution |
| **16c** | **16** | MeOH, 70 | 30 | Solution |
| **16d** | **16** | EtOH, 30 | 70 | Solution |
| **16e** | **16** | EtOH, 50 | 50 | Solution |
| **16f** | **16** | EtOH, 70 | 30 | Solution |
| **16g** | **16** | iPrOH, 30 | 70 | Solution |
| **16h** | **16** | iPrOH, 50 | 50 | Solution |
| **16i** | **16** | iPrOH, 70 | 30 | Solution |

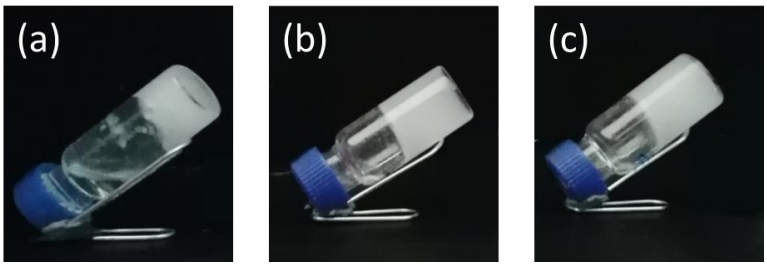


**Figure 4.14**. Photographs of the gels (a) **13a**, (b) **13d**, and (c) **13g**.

To better understand the different propensity to form gels, we investigated the the packing of the two gelators by performing X-ray diffraction (XRD) analyses. Structural XRD analysis revealed that **13** and **16** crystallise in the chiral space groups triclinic-P1 and orthorhombic-$P2_12_12_1$ respectively. In the case of **13**, we could not fully model the structure because of the severe crystallographic disorder affecting one out of the two Boc-$^{L}$Ala-Aib-$^{L}$Val-OH molecules comprising the asymmetric unit; on the other hand, **16** was easily located and successfully refined. In each case, the packing includes a crystallization solvent molecule, water for **13** and ethanol for **16**. As the result of the weak and distorted intramolecular hydrogen bond between the Boc-carbonyl and the NH from the Val-residue of the O-terminus (Figure 4.15), and analogously to other reported Boc-protected tripeptides,[194,195] both compounds adopt a similar folded conformation, corresponding to a distorted β-turn structure.[196,197]

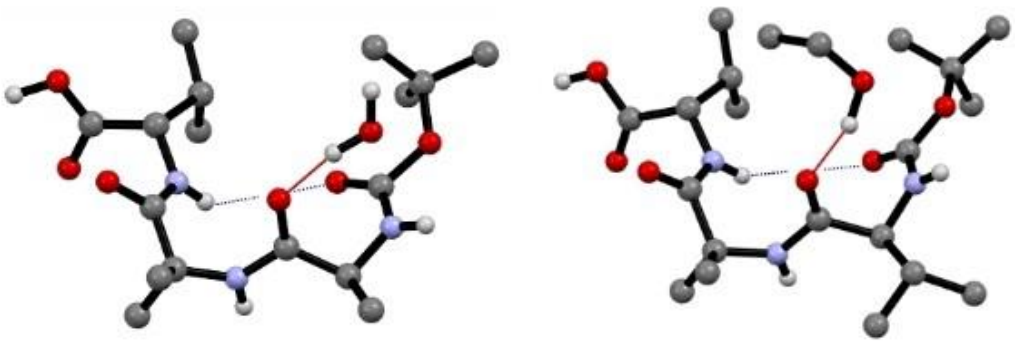

**Figure 4.15**. Molecular structure of crystalline **13** (left) and **16** (right) showing the intramolecular hydrogen bond (blue dots) responsible for the folded conformations, and the intermolecular hydrogen bond with the respective crystallization solvents (red line). $H_{CH}$ atoms omitted for clarity.

Despite the very similar molecular conformations, **13** and **16** show quite different crystal packings. This could directly consequence the different N-terminus residue and crystallization solvents, which play an active role in determining the solid-state arrangements. In crystalline **13**, water molecules bridge the adjacent peptide molecules through hydrogen bonds with the Val- and Ala-residues to form chains which are further stabilized by additional interactions between the N-H and carbonyl belonging to the same residues. Water molecules also link adjacent chains via interactions with the C=O from another Val-residue, whereas the Aib-residues form hydrogen bonds among them, the overall result is the formation of a complex 2D net (data not shown). In crystalline **16**, EtOH engages intermolecular hydrogen bonding interactions with the Val-residues from the N- and O-termini and belonging to adjacent Boc-Val-Aib-Val-OH molecules. The two Val-residues also form direct hydrogen bonds, leading to a 1D chain running along the a-axis. Other hydrogen bonding interactions are detected among the Aib-residues and are responsible for forming 1D chains that run along the b-axis (data not shown).

At this point, we studied the gelled samples, **13d** and **13g**, from a rheological point of view. We assessed the behaviour of these gels against a heat-cool cycle (thermal annealing) and labelled these new gels **13d-h** and **13g-h**, by heating the gels at 60 °C to completely dissolve the gel and leave it to reform a 25 °C for 4 hours. After this process, both gels reformed undergoing syneresis (i.e., the gel reforms using only part of the solvent and leaving some non-gelled solvent), with gel **13g-h** gelling more solvent than **13d-h** (Figure 4.16).

We then formed a new gel, namely **13j**, from gelator **13**, by using the same conditions used for gel **13g** and increasing the gelator concentration to 2.0 %. On this gel, we repeated the same experiments done for gels **13d** and **13g**, i.e., assessing its behaviour against shaking and a heat-cool cycle. In this case, the gel was able to recover after vigorous shaking (gel **13j-s**) and was able to gel all the solvent after a heat-cool cycle (gel **13j-h**) (Figure 4.16).

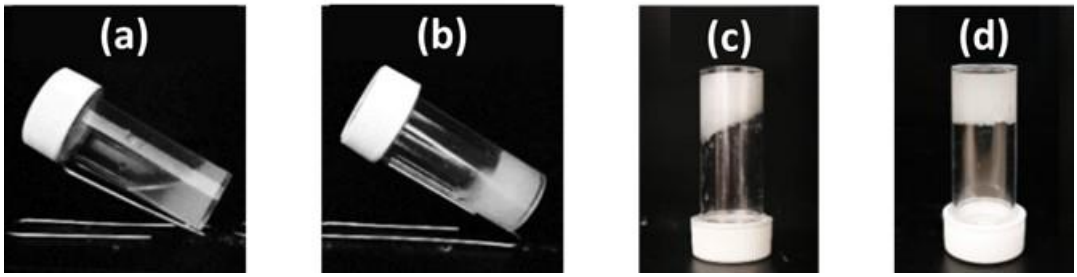


**Figure 4.16**. Photographs of the gels (a) **13d-h**, (b) **13g-h**, (c) **13j-s**, and (d) **13j-h**.

**Table 4.7**. Summary of the gels of **13** before and after undergoing a thermal annealing at 60 °C (heat-cool cycle), with rheological properties.

| Gel | Conc. (%) | Syneresis | G' (kPa) | G" (kPa) | LVER (%) | Breaking point (%) |
|---|---|---|---|---|---|---|
| **13d** | 1.0 | No | 41 ± 9.7 | 9.6 ± 1.7 | 0.02 | 22 |
| **13d-h** | 1.0 | Yes | 25 | 7.0 | 0.02 | 2.7 |
| **13g** | 1.0 | No | 32 ± 3.5 | 8.5 ± 0.7 | 0.02 | 7.4 |
| **13g-h** | 1.0 | Yes | 66 | 16 | 0.02 | 18 |
| **13j** | 2.0 | No | 250 ± 19 | 48 ± 5.2 | 0.03 | 10 |
| **13j-h** | 2.0 | No | 180 | 35 | 0.02 | 6.8 |

We measured the stiffness and the thixotropy of these gels by performing amplitude sweep (Table 4.7) and step-strain (Figure 4.17) analyses respectively. Gels **13d** and **13g** display comparable stiffness in the order of $10^2$ kPa, while gel **13j** has the highest stiffness being an order of magnitude higher than the previous ones. Although **13d** and **13g** behave similarly, the thixotropy test provides a better outcome with gel **13g**, as disclosed in the shaking and melting experiments. Consistently, gel **13j** showed excellent thixotropy properties with complete recovery of the mechanical properties (Figure 4.17). The mechanical properties of the three samples **13d-h**, **13g-h** and **13j-h** were analysed again with the rheometer after the heating and cooling process. The new amplitude sweeps show similar behaviour to those before the heating and cooling process, although for gels **13d-**

**h** and **13g-h** some solvent outside the gel was observed and may partially alter the outcome (Table 4.7).

We studied the morphology of gels **13d** and **13g** (assuming that an increase in concentration would not affect the fibres aspect) on both wet samples, using an optical microscope, and dry samples, using Scanning Electron Microscopy (SEM). Wet samples show similar structures, with long thin and flexible fibres randomly aligned (Figure 4.18).

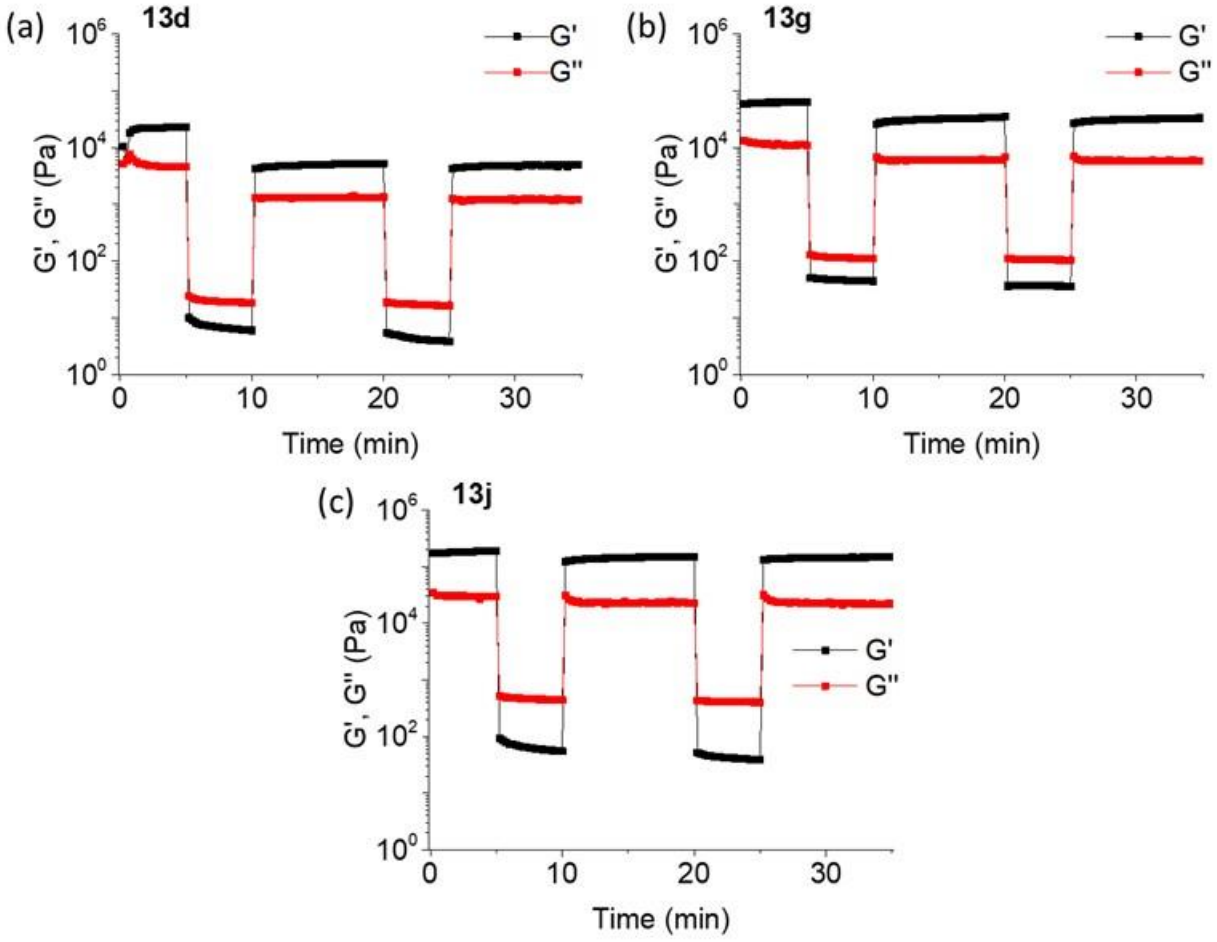


**Figure 4.17**. Step-strain experiments of gels **13d**, **13g**, and **13j**.

SEM analysis, instead, highlights differences in aspect ratio and texture in the fibres making the xerogels from sample **13d** and sample **13g** (Figure 4.19). The fibres of the gels have a maximum width of about 10 μm and about 5 μm for sample **13d** and **13g**, respectively. Sample **13d** shows a laminar structure and well-defined crystalline faces. In this sample bundles of fibres are observed, but the fibres are not branched (Figure 4.19a

and c). Differently, sample **13g** shows a poor crystalline aspect having fibres with rounded edges and highly branched and interconnected (Figure 4.19b and d).

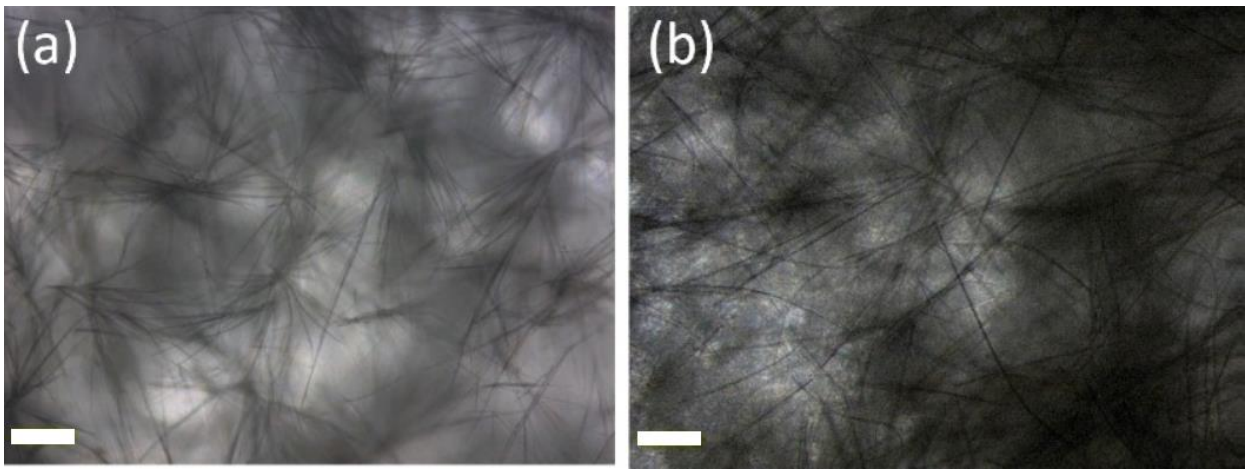


**Figure 4.18**. Optical microscope images of gels (a) **13d** and (b) **13g**. Scalebar is 100 μm.

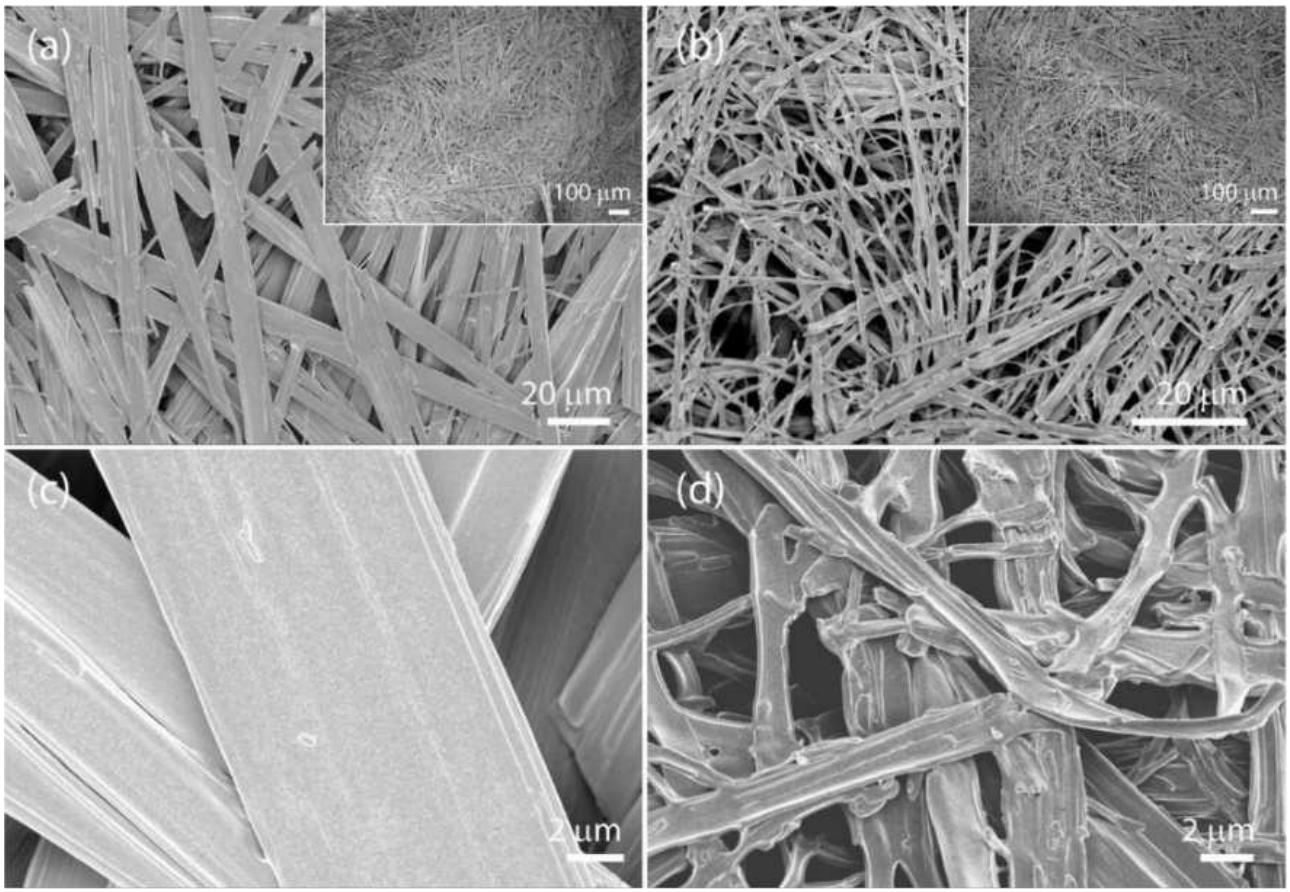


**Figure 4.19**. Scanning electron microscope (SEM) images of dried gels (a, c) **13d** and (b, d) **13g**. For (a, b), scalebar is 20 μm (100 μm for the small pictures) and 2 μm for (c,d).

As the possibility of trapping pollutants in water has already been studied with aromatic-containing gelators,[150,198] we studied the ability of this non-aromatic gel to remove pollutant from water. In particular, we used gels **13g** and **13j** to relate their trapping ability to the stiffness of the material. Eosine Y (EY, 0.016 mg/mL) was chosen as model dye pollutant,[198] while Diclofenac sodium (DIC, 0.02 mg/mL) was chosen as drug, since it belongs to the therapeutic group most found in water.[199–203] The pollutant solutions were eluted through a 2 mL gel column, that was prepared directly into a 10 mL syringe (Figure 4.20).

For both pollutants, a calibration curve was built (data not shown). Eosin Y may be easily quantified using a UV-vis spectrophotometer, through the comparison of the results with the calibration curve.

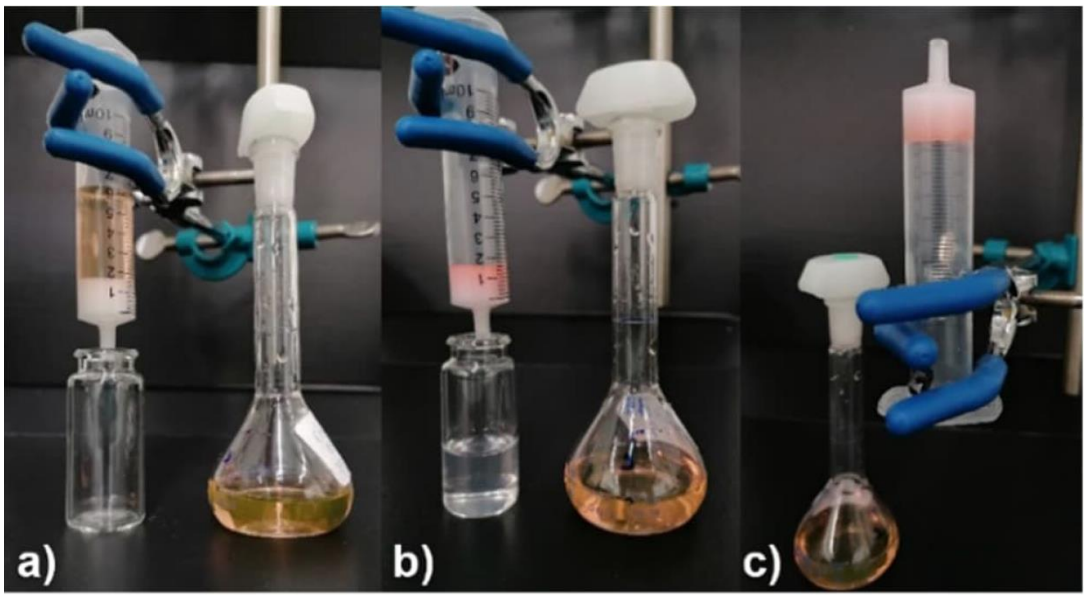


**Figure 4.20**. Absorption test of 5 mL of an EY solution on gel **13j** (a) at the beginning of the process, (b) at the end of the elution, and (c) after the inversion test.

In Table 4.8 (entries I-IV) the results are reported for both gels **13g** and **13j**. The increased strength of **13j** increases the pollutant absorption, under the same conditions, blocking more than the 90 % of EY. At the end of the absorption experiment, all gels were stable enough to be inverted without flowing.

**Table 4.8**. Summary of pollutant removal tests using gels **13g** and **13j**.

| Entry | Gel | Gelator conc. (%) | Pollutant (μmol) | Solution eluted (mL) | Detained pollutant (%) |
|---|---|---|---|---|---|
| **I** | **13g** | 1.0 | EY, 0.12 | 5.0 | 81 ± 0.5 |
| **II** | **13g** | 1.0 | EY, 0.24 | 10 | 65 ± 6.0 |
| **III** | **13j** | 2.0 | EY, 0.12 | 5.0 | 98 ± 0.9 |
| **IV** | **13j** | 2.0 | EY, 0.24 | 10 | 91 ± 3.2 |
| **V** | **13g** | 1.0 | DIC, 0.32 | 5.0 | 45 ± 3.2 |
| **VI** | **13g** | 1.0 | DIC, 0.65 | 10 | 26 ± 3.3 |
| **VII** | **13j** | 2.0 | DIC, 0.32 | 5.0 | 84 ± 0.4 |
| **VIII** | **13j** | 2.0 | DIC, 0.65 | 10 | 51 ± 4.7 |
| **IX** | **13j** | 2.0 | DIC, 0.62 | 5.0 | 92 ± 3.0 |

The absorption ability of hydrogels **13g** and **13j** was also tested for DIC (Table 4.8, entries V-IX). In these cases, the absorption ability of both hydrogels **13g** and **13j** is lower than for EY, although in gel **13j** we afforded better results. When the volume of polluted solution is increased (from 5 to 10 mL), we can observe a decreased ability of pollutant absorption. However, when the same pollutant amount is dissolved in a reduced volume (increasing its concentration), the absorption capability of the gel is improved.

## *4.4. Summary*

LMW gels find application in numerous field, due to their ability of entrapping the solvent and the molecules there dispersed. This may present many advantages, depending on the interactions between the fibres and the molecule dispersed in the solvent.

The release of odorant molecules from the gel matrix is controlled, compared to the solution and the gel fibres may also act as catalytic site for the hydrolysis of profragrances to release fragrances. In the same medium, it is also possible to choose the rate of the degradation desired, as in the acidic gel of **12** the hydrolysis rate is much higher compared to neutral conditions of the gel **11**.

The addition of two cosmetic active peptides (**14** and **15**) in the hydrogels of **(12+13)** was successful, without modifying their final pH and rheological properties. Their controlled release was analysed with the help of Franz diffusion cells and porcine ear skin as the membrane. The HPLC-MS analyses of the withdrawn samples from the receiving solutions showed that peptide **14** was released in considerable amount while almost no release of peptide **15** was observed, demonstrating that these hydrogels are tuneable and biocompatible media, suitable for the transdermal delivery of organic molecules.

It is possible to use the aromatic-free short peptides **13** to prepare gels able to trap polluting molecules. The study of the most suitable tripeptide was crucial to obtain an efficient soft material for water remediation. As a consequence of our careful screening combining all these techniques, we envisaged a self-supporting hydrogel containing only 2.0 % w/V of tripeptide **13** that is able to trap up to 97.8% of the Eosin Y and up to 92.0% of Diclofenac sodium. This remediation method is low impact, very fast and cheap, as the trapping system may be easily prepared in any condition with readily available reagents. The gelator degradation has no drawbacks, as the tripeptides are fully biocompatible.

# *Chapter 5. Optical properties in gels*

As reported in the previous chapters, the gels fibres interact with several molecules, acting either as a trap for polluting substances or as media to control the release of odorant molecules or drugs. However, gels basically act as media with physical properties dramatically different from the solvent alone, for example changing the conductivity[204,205] of the solvent. This change in properties is usually detectable through numerous techniques, such as IR, UV-vis and fluorescence spectroscopy. In this context, solvatochromic species like azobenzenes,[206,207] stilbens,[208,209] and fulgides[206,210] should undergo a shift in the absorbance or emission, according to the different medium in which they are dispersed. Such species are well known to undergo photoisomerisation. The different specimens that can be obtained display different optical properties, as they absorb and emit light in different regions, and solubility, as the isomers may have different polarity. In fact, by irradiating the compound with a certain wavelength of light some covalent bonds can be either cleaved or formed and the starting isomer can be obtained by irradiating the compound with another wavelength of light or, in some cases, after a prolonged rest in the dark.

## *5.1. Photocromic species in gel*

In this topic, during my PhD I worked with organogels, i.e., gels made by organic solvents only, and studied their behaviour when hosting a light-sensitive spyropyran[211–213] **SP**. This molecule is able to reversibly interconvert to merocyanine **MC** by using different wavelengths of light (Figure 5.1). The *cis*-merocyanine **c-MC** is a transient intermediate that isomerises to produce **MC** when irradiated with UV light or closes to generate **SP** when irradiated with visible light.

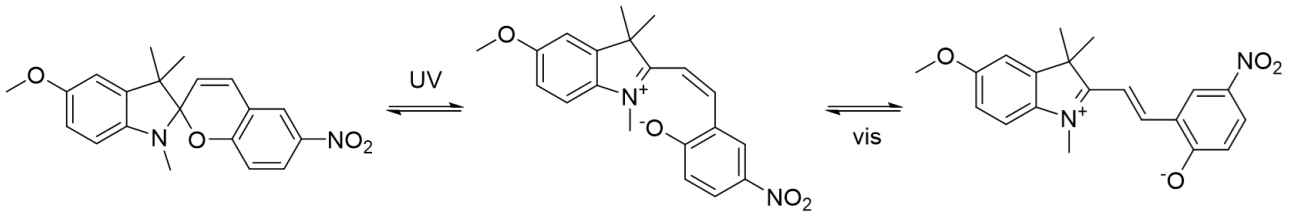


**Figure 5.1**. Molecular structure and interconversion reaction of spiropyran **SP** and merocyanine **MC**.

The protected tripeptide Boc-$^{L}$Phe-$^{D}$Oxd-$^{L}$Phe-OBn, **17** (Figure 5.2), was already known for its ability to gel some organic solvents, such as toluene, *tert*-butyl methyl ether (TBME), and ethanol.[39] All these gels appeared transparent, property required for the study of light-sensitive molecules, however no proper study of the rheological or morphological properties was done.

We prepared the organogels at a concentration of 1.0 % w/V through sonication at room temperature for 5 minutes and left to rest overnight for the complete gel formation. As previously observed, the gels obtained from toluene (**17a**) and ethanol (**17c**) appeared translucent, while the one from TBME (**17b**) is opaquer, but still disclosing a good transparency (Table 5.1, Figure 5.3a-c). We investigated the morphology of these gels through confocal microscopy on the gel in the wet state to avoid artifacts due to drying. The fibrous matrix appeared clear in all the samples, with thin long fibres formed in each

one of those. However, while the fibres in gels **17a** and **17b** appeared in bundles, in gel **17c** they appeared more isolated (Figure 5.3d-f).

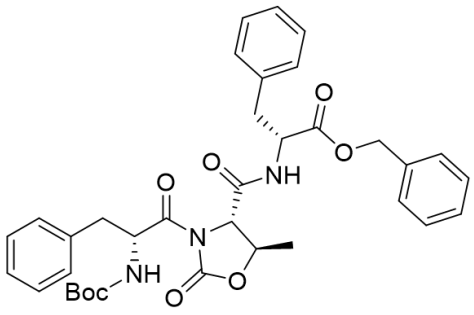


Boc-$^{L}$Phe-$^{D}$Oxd-$^{L}$Phe-OBn, **17**

**Figure 5.2**. Molecular structure of the organogelator Boc-$^{L}$Phe-$^{D}$Oxd-$^{L}$Phe-OBn, **17**.

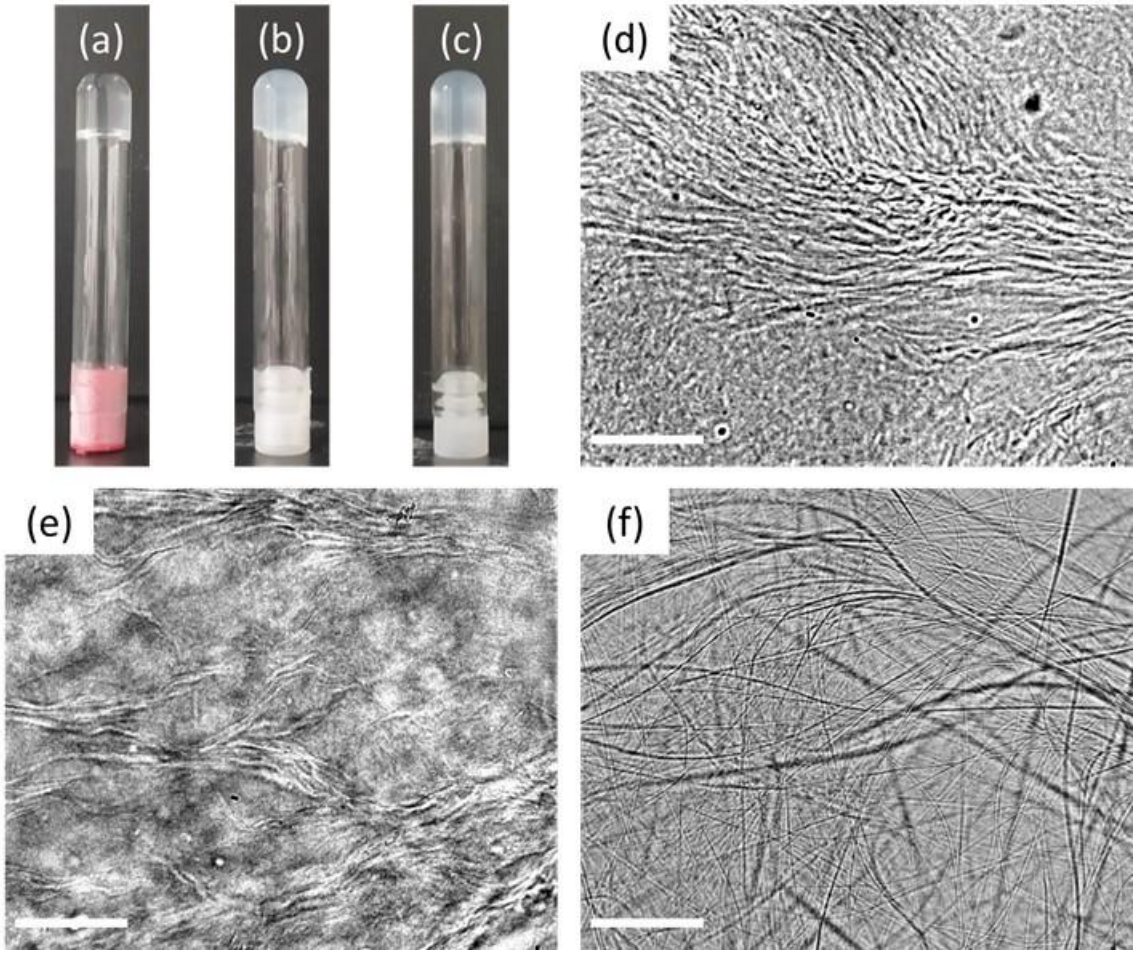


**Figure 5.3**. Photographs of the organogels (a) **17a**, (b) **17b**, and (c) **17c**; confocal microscope images of the organogels (d) **17a**, (e) **17b**, and (f) **17c**. The scalebar is 50 μm.

We investigated the transparency of the obtained materials by analysing their absorbance in the UV-vis range between 250 and 750 nm. The spectra showed a broad range of transparency in the visible region (Table 5.1).

**Table 5.1**. Summary of the solvents used and transparency of gels **17a-c**.

| Gel | Solvent | Result | Transparency (%) |
|---|---|---|---|
| **17a** | Toluene | Gel | 98 |
| **17b** | TBME | Gel | 42 |
| **17c** | Ethanol | Gel | 61 |

The transparency is reported as means of transmittance at 630 nm.

We then studied the rheological properties of these gels through amplitude sweep. All the gels displayed a stiffness around 10 kPa, with **17b** being the stiffest. The gels **17a** and **17b** also displayed a long linear viscoelastic range (LVER) and the moduli G' and G" do not crossover, meaning that the gels do not break in the studied strain range (Table 5.2).

Once we ascertained that these materials were suitable for the isomerization studies, we repeated the experiment including a sample of freshly prepared either spiropyran or merocyanine in the gels to understand whether the molecules could interfere with the organogels formation. For this purpose, we prepared six gels, namely **17d-i**, all containing the gelator in the concentration of 1.0 % w/V and either spiropyran **SP** or merocyanine **MC** in the three solvents in the concentration of 0.5 % w/V (Table 5.2).

The properties of these gels were studied by strain sweep analysis, under the above reported conditions. Gels of toluene and TBME containing **SP** or **MC** tend to be slightly less stiff compared to the gel containing only the gelator, while the opposite phenomenon occurs in the case of ethanol. However, the presence of either **SP** or **MC** has almost no impact on the rheological properties.

At this point, the effect of the three solvents and of the three organogels on the equilibrium among the forms **SP** and **MC** was studied. First, we prepared three solutions of the product in the three solvents in 0.5 % w/V concentration, dissolving in any case a

sample of **SP**. Initially the solutions in toluene and TBME were yellow, indicating that the equilibrium in these solvents privileged the **SP** form. On the other hand, the ethanol solution was red, suggesting that in this case the **MC** form was preferred.[214] These results agreed with the different polarity of the solvents: apolar solvents stabilise the apolar **SP** structure, while the polar solvent stabilises the polar **MC** form.

**Table 5.2**. Summary of the gels **17a-o** with or without additives (**SP** or **MC**) with corresponding rheological properties. Gels **17j-o** were not studied from this point of view, assuming that the presence of a very small amount of either of the additives would not affect the rheological properties of the gel.

| Gel | Solvent | Additive (%) | G' (kPa) | G" (kPa) | LVER (%) | Breaking point (%) |
|---|---|---|---|---|---|---|
| **17a** | Toluene | None | 9.3 ± 1.1 | 2.2 ± 0.4 | 0.47 | N.D. |
| **17b** | TBME | None | 12 ± 1.7 | 3.5 ± 0.5 | 0.47 | N.D. |
| **17c** | Ethanol | None | 8.2 ± 0.8 | 2.3 ± 0.2 | 0.15 | 10.0 |
| **17d** | Toluene | **SP**, 0.5 | 3.5 ± 0.9 | 0.7 ± 0.1 | 0.68 | N.D. |
| **17e** | Toluene | **MC**, 0.5 | 4.3 ± 0.9 | 1.0 ± 0.8 | 0.32 | N.D. |
| **17f** | TBME | **SP**, 0.5 | 6.0 ± 1.7 | 1.2 ± 0.5 | 0.32 | N.D. |
| **17g** | TBME | **MC**, 0.5 | 9.9 ± 1.4 | 2.6 ± 0.2 | 0.68 | N.D. |
| **17h** | Ethanol | **SP**, 0.5 | 11 ± 2.2 | 2.7 ± 0.9 | 0.067 | 30.5 |
| **17i** | Ethanol | **MC**, 0.5 | 14 ± 3.5 | 3.9 ± 1.3 | 0.15 | 5.85 |
| **17j** | Toluene | **SP**, 0.005 | - | - | - | - |
| **17k** | Toluene | **MC**, 0.005 | - | - | - | - |
| **17l** | TBME | **SP**, 0.005 | - | - | - | - |
| **17m** | TBME | **MC**, 0.005 | - | - | - | - |
| **17n** | Ethanol | **SP**, 0.005 | - | - | - | - |
| **17o** | Ethanol | **MC**, 0.005 | - | - | - | - |

G' and G" were measured at $\gamma$ = 0.05 %; N.D. = not detected.

To verify that the interconversion would happen in any solvent, the solutions in toluene and TBME were irradiated with UV (365 nm) light to allow the complete conversion to **MC**, with the formation of a blue solution. We repeated the same process for the ethanol solution containing **MC**, so we irradiated it with white light to induce the formation of **SP**.

After irradiation, each solution was wrapped in aluminium foil to mimic a completely dark environment and left to rest 5 minutes. After this time, each solution reconverted to the starting point (Figure 5.4), thus confirming that the polarity of the solvent strongly affects the equilibrium among the two species.

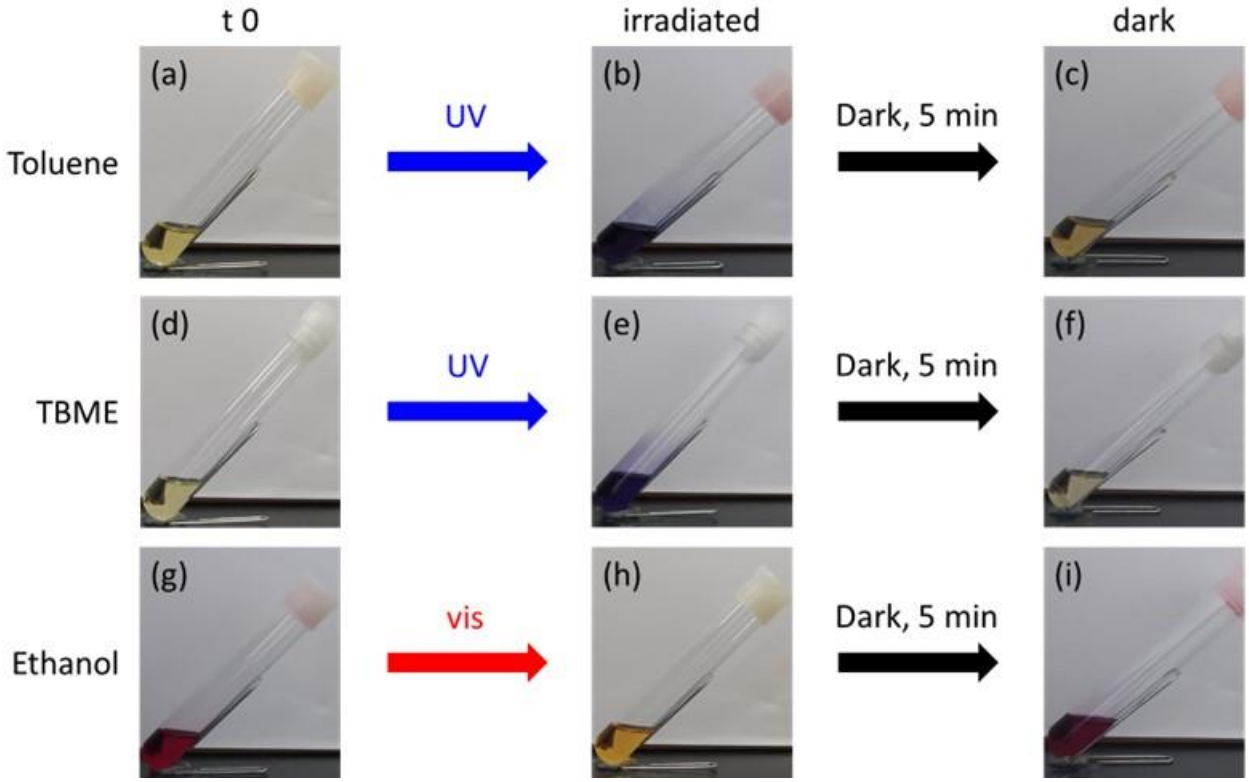


**Figure 5.4**. Photographs of the **SP** solutions in (a-c) toluene, (d-f) TBME, and (g-i) ethanol, after (a, d, g) dissolution of **SP**, (b, e, h) irradiation, and (c, f, i) a rest of 5 minutes wrapped in aluminium foil. For (b, e) UV light (365 nm) was used, while for (h) white light was implied. In all cases, the concentration of **SP** is 0.5 % w/V.

The experiment was repeated by including **SP** in the gels in the same concentrations to understand whether the gel could modify the equilibria, stabilising the **SP** or **MC** form. For this purpose, the gelator in concentration 1.0 % w/V was sonicated in a 0.5 % w/V **SP** solution and left to rest overnight. To do so, each solution containing the gelator was irradiated either with UV or white light prior to and during sonication to obtain respectively the **MC** or the **SP** form in the gels. Immediately after sonication, the gels were always wrapped in aluminium foil to mimic dark conditions.

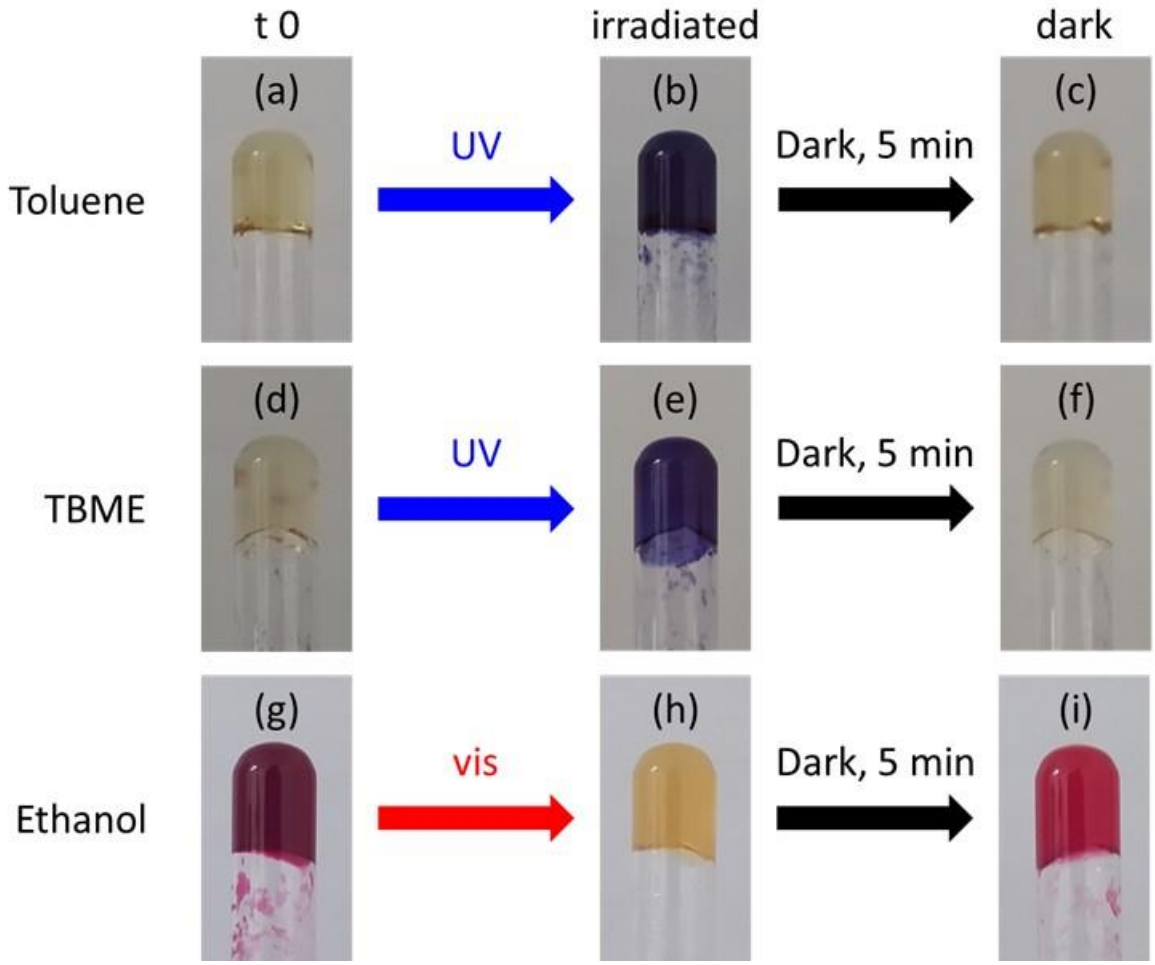


**Figure 5.5**. Photographs of the gels (a-c) **17e**, (d-f) **17g**, and (g-i) **17h**, after (a, d, g) an overnight rest in the dark, (b, e, h) irradiation with (b, e) UV (365 nm) or (h) white light, and (c, f, i) after 5 minutes in the dark.

The gels were first formed in presence of **MC** and left to form overnight wrapped in aluminium foil. After this time, the gels in toluene (**17e**) and in TBME (**17g**) turned yellow

again, indicating the reconversion to **SP**. These gels were irradiated again with UV light after its complete formation, wrapped in aluminium foil and checked after 5 minutes. After this time, the conversion to **SP** was completed (Figure 5.5a-f). The gel in ethanol (**17i**) instead remained red, suggesting that the **MC** was stabilised in this case.

Then the gels were formed in the presence of **SP** and left to form overnight wrapped in aluminium foil. The gels in toluene (**17d**) and TBME (**17f**) containing the **SP** form appeared yellow and were stable throughout the night. On the other hand, the gel in ethanol (**17h**) containing **SP** turned red overnight, indicating the conversion to **MC**. This gel was irradiated with visible light again after its complete formation, wrapped in aluminium foil and checked after 5 minutes. Within this time the reconversion to MC was started, although appearing less coloured than it was at the beginning (Figure 5.5g-i).

To confirm if the gelator network may affect the equilibrium among the two species, a spectrophotometric study was carried out. A quantification of the conversion of **SP** to **MC** and vice versa was made by preparing solutions and gels containing 0.005 % w/V of **SP**, as at higher concentrations (0.5 % w/V) the signal was too intense and could not be recorded with the spectrophotometer.

We prepared six solutions, three of which containing **SP** in the three solvents and the other three containing instead **MC**. The first three were irradiated with visible light for 1 minute to allow complete formation of **SP**. The last three were instead irradiated with UV light for 1 minute to allow complete formation of **MC**. We first recorded the UV-vis spectra of these solutions to identify the wavelength of the maximum corresponding to the **MC** signal in the visible region.

Then, we prepared the gels containing 1.0 % w/V of **17** and the same solutions containing 0.005 % w/V of either **SP** or **MC**, to obtain gels **17j-o** (Table 5.2) and recorded the UV-vis spectra. In this case, we did not measure the rheological properties of these gels, assuming that such a small amount of additive would not impact their properties. In each gel, a blue-shift of 3-5 nm is identified in the maximum of the **MC** peak compared to solution. Unfortunately, we could not compare the UV-vis absorption spectra of the **SP** form in gel and solution because the signal of **17** covered the one of **SP** (Figure 5.6).

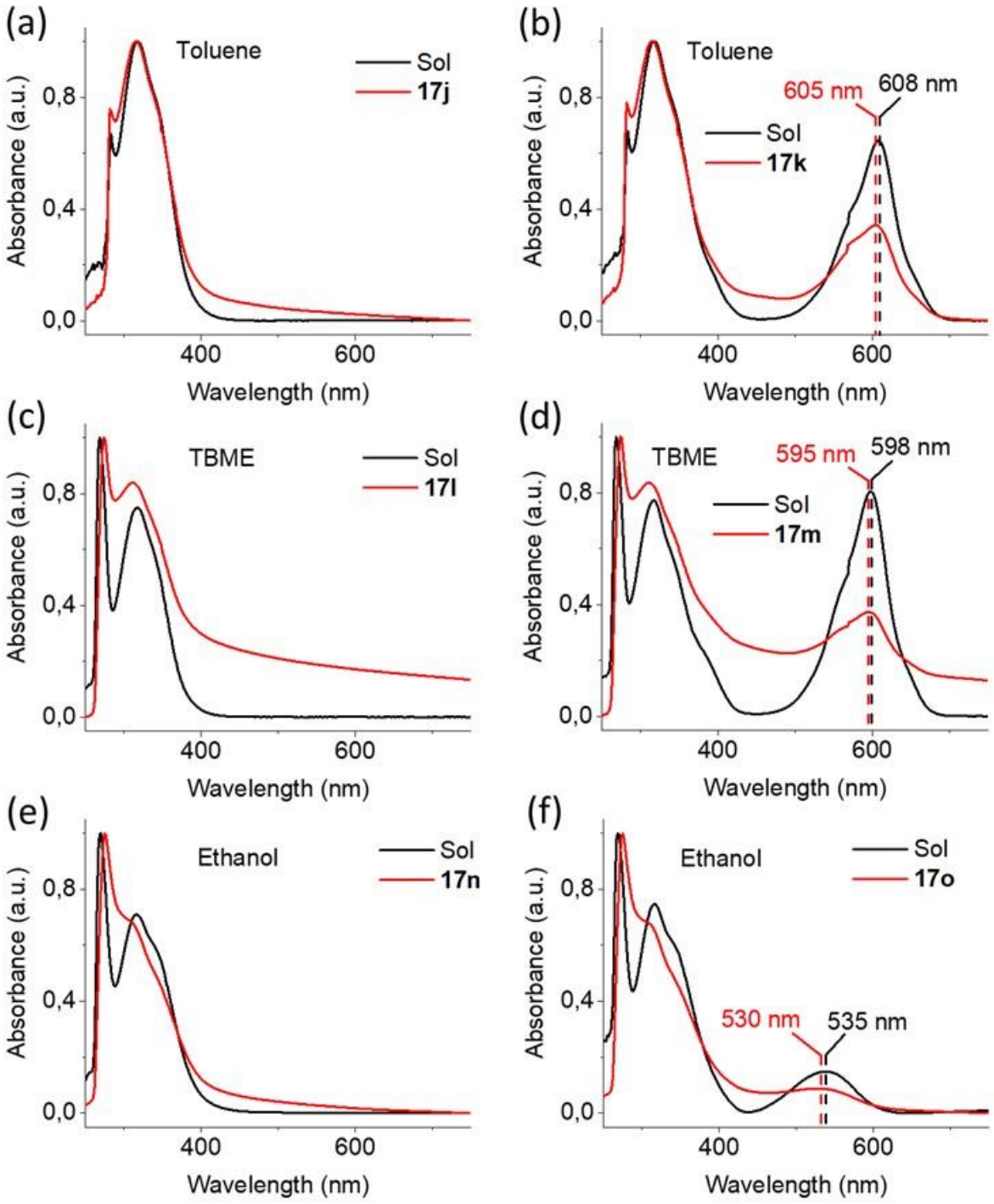


**Figure 5.6**. UV-vis absorption spectra of solutions (black) and gels (red) containing 0.005 % w/V of **SP** (a, c, e) or **MC** (b, d, f) in toluene (a, b), TBME (c, d), and ethanol (e, f).

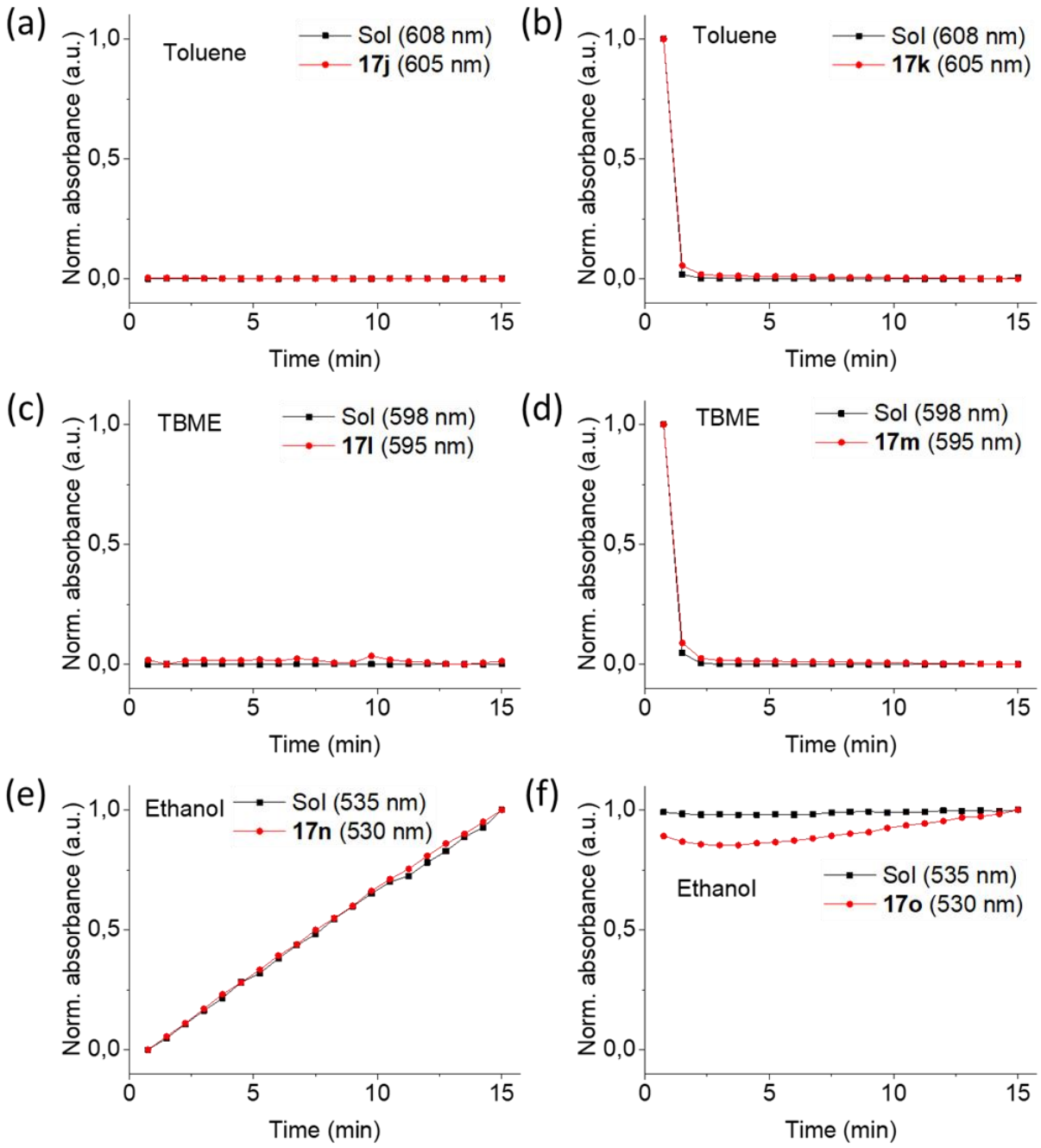


**Figure 5.7**. Trend of the normalised absorbance versus time of the solution (black) and gel (red) at the maximum corresponding to the **MC** signal (legend, in brackets). Media contain either (a-c) **MC** or (d-f) **SP**. The solvents are (a, d) toluene, (b, e) TBME, and (c, f) ethanol. In each case, the concentration of **SP** or **MC** is 0.005 % w/V.

Then the UV-vis absorption of the twelve samples was also recorded in 20 cycles over a short period of 15 minutes. For each cycle, the absorbance at the maximum corresponding to the **MC** signal was measured. Gels of toluene and TBME stabilise the **SP** form, while

gels of ethanol stabilise the **MC** form. To better show these results, the trends obtained are reported in Figure 5.7, taking into consideration the wavelength corresponding to the **MC** maximum as a function of time over 15 minutes. In each case, the conversion or stabilisation of the species in gel follows the same trend of the solution. Unlike one would expect, the gel matrix does not affect the kinetics of the conversion, but it leaves it unaltered, suggesting that there is no stabilising interaction between the gel fibres and either **SP** or **MC**.

## *5.2. Summary*

We have shown how the presence of a light-sensitive species like a non-gelling spiropyran has almost no impact in the final rheological properties of the material, leaving mostly unaltered the stiffness, breaking point, and linear viscoelastic range of these. When this specimen is immersed in the gel matrix, it behaves as in solution, interconverting to the most stable form, dictated by the polarity of the solvent, following the same kinetics of conversion both in gel and in solution. The use of a transparent gel also allows an effective irradiation of the medium both with UV and visible light.

On the other hand, the gel fibres affect the properties of the medium, not only from the rheological point of view, but also changing how the photochromic spiropyran interacts with light. In particular, the absorbance in the UV-vis region are blue-shifted of 3 nm in the case of toluene and TBME, from 608 nm to 605 nm and from 598 nm to 595 nm respectively, and of 5 nm in the case of ethanol, from 535 nm to 530 nm.

# *Chapter 6. Experimental section*

All the compounds synthesised were analysed using one or more of the following methodologies and instruments, unless specified otherwise. Solvents were dried by distillation before use. All reactions were carried out in dried glassware. All compounds were dried in vacuo and all the sample preparations were performed in a nitrogen atmosphere. All compounds were dried in vacuo and all the sample preparations were performed in a nitrogen atmosphere. Deionised water was used in all the purification processes and experiments. The melting points of the compounds were determined in open capillaries and are uncorrected. High-quality infrared spectra (64 scans) were obtained at 2 $cm^{-1}$ resolution with an ATR-IR Agilent Cary 630 FTIR spectrometer. NMR spectra were recorded with a Varian Inova 400 spectrometer at 400 MHz ($^{1}$H-NMR), at 100 MHz ($^{13}$C-NMR), and at 376.5 MHz ($^{19}$F-NMR). Chemical shifts are reported in δ values relative to the solvent peak. A Jasco P-2000 Polarimeter was used to check the optical rotatory power of the compounds. HPLC-MS analyses were carried out with an Agilent 1260 Infinity II liquid chromatograph coupled to an electrospray ionization mass spectrometer (LC-ESI-MS), using a Phenomenex Gemini C18-3μ-110 Å column, and $H_2O/CH_3CN$ with 0.2 % formic acid as acid solvent at 40 °C.

## *6.1. Synthesis and characterisation of gelators 1-3 and analysis of their gels*

### 6.1.1 General remarks for the synthetic procedure of **1**, **2**, and **3**

The gelator Boc-$^{D}$Phe($F_2$)-OH, **1**, was used as purchased. The 0.1 M phosphate buffer (PB) solution was prepared by dissolving $KH_2PO_4$ in water, then adding NaOH to adjust the pH to 7.4 and adding other fresh water to reach a final concentration of 0.1 M. This solution was diluted to the concentration required for the experiment prior to use.

### 6.1.2 Synthesis of compounds **1**, **2**, and **3**

Boc-$^{D}$Phe($F_2$)-$^{D}$Oxd-OH, **2**, and Boc-$^{D}$Phe($F_2$)-$^{L}$Oxd-OH, **3** (Figure 6.1)

The compound H-$^{D}$Oxd-OBn was synthesised following the procedure reported in reference[105]. Boc-$^{D}$Phe($F_2$)-OH, **1** (500 mg, 1.66 mmol) was dissolved in 20 mL of acetonitrile (ACN) and then hexafluorophosphate benzotriazole tetramethyl uronium (HBTU, 693 mg, 1.83 mmol) was added. The mixture was stirred at room temperature for 10 min. A solution containing H-$^{D}$Oxd-OBn (390 mg, 1.66 mmol) and N,N'-diisopropylethylamine (DIEA, 0.9 mL, 5.31 mmol) in ACN (10 mL) was then added dropwise to the first one. The mixture was stirred for 6 h, then the solvent was removed under reduced pressure and replaced with ethyl acetate (40 mL). The organic mixture was washed with $H_2O$ (10 mL), 1 M aqueous HCl (10 mL), and brine (10 mL), then it was dried over $Na_2SO_4$ and the solvent evaporated under vacuum. The solid obtained was finally purified through flash chromatography (dichloromethane:ethyl acetate 95:5). Boc-$^{D}$Phe($F_2$)-$^{D}$Oxd-OBn was obtained as a white solid and directly hydrogenolysed.

In a flask containing Boc-$^{D}$Phe($F_2$)-$^{D}$Oxd-OBn (700 mg, 1.49 mmol) and methanol (MeOH, 50 mL), Pd/C 10 % w/w (70 mg) was added to the solution. The air left in the flask was removed through a water pump, then the mixture was posed under hydrogen atmosphere and stirred for 2 h until the reaction was complete, then it was filtered on a

celite pad. The solution was evaporated under reduced pressure and the product was obtained as a white solid in 89% overall yield. Melting point (M.p.) = 112 °C (dec.); $[\alpha]^{25}_{D}$ +3.0° (c = 0.5 in EtOAc); IR (ATR-IR): ν 3276, 2978, 2935, 1785, 1716, 1644, 1610, 1518 $cm^{-1}$; $^{1}$H-NMR ($CD_3OD$, 400 MHz): δ 1.33 (9H, s, $CH_3$ t-Bu), 1.55 (3H, d, J = 6.4 Hz, $CH_3$ Oxd), 2.63 (1H, dd, J = 11.2, 13.6 Hz, CH benzyl), 3.26 (1H, m, CH benzyl), 4.58 (1H, d, J = 4.0 Hz, CαH Oxd), 4.74 (1H, m, CβH Oxd), 5.46 (1H, d, J = 8.8 Hz, CαH Phe($F_2$)), 5.57 (1H, d, J = 9.2 Hz, NH-Boc), 7.20 (3H, m, CH aromatic); $^{13}$C ($CD_3OD$, 100 MHz): δ 19.79, 27.15, 36.16, 54.72, 61.66, 74.74, 79.31, 116.44, 117.89, 125.58, 134.79, 148.25, 150.69, 152.53, 156.51, 170.04, 172.26; $^{19}$F ($CD_3OD$, 376.5 MHz): δ −143.97, −141.23.

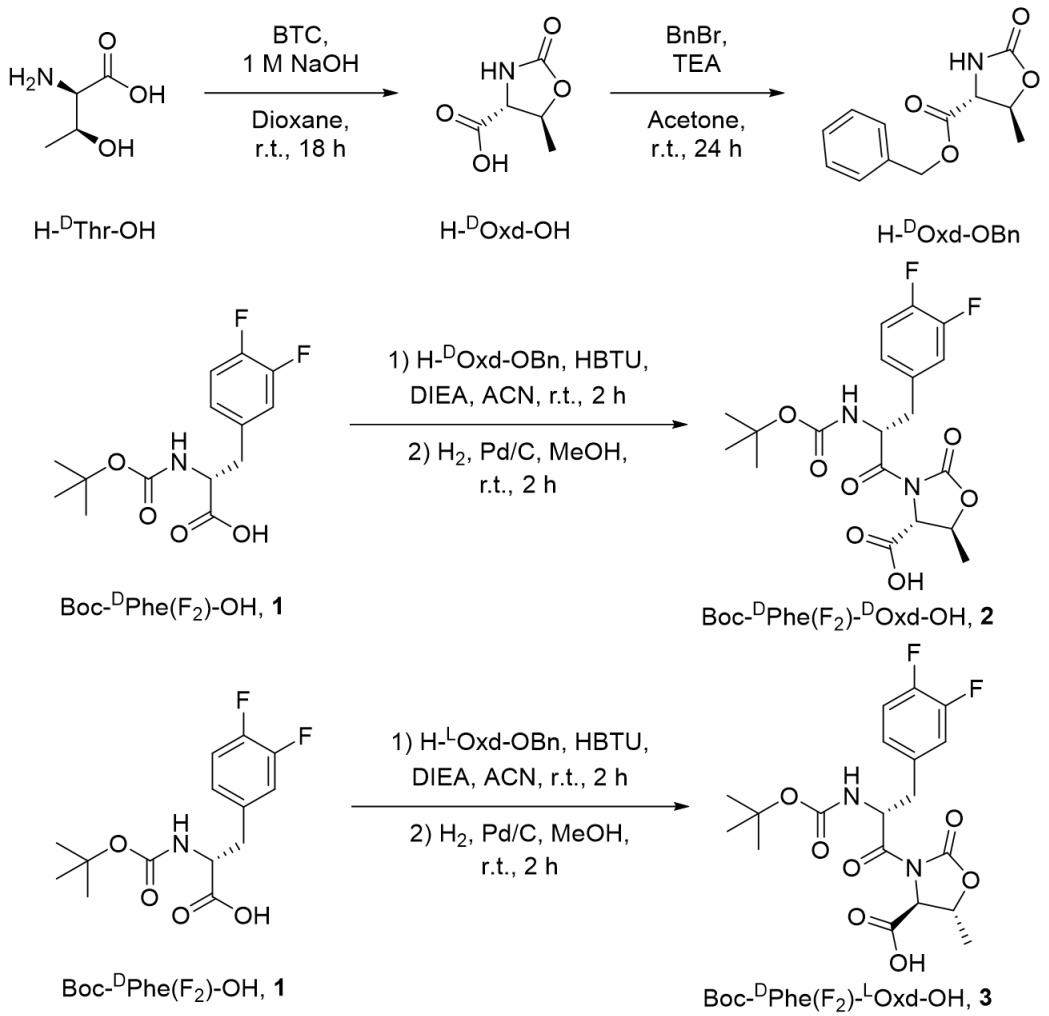


**Figure 6.1**. Multistep synthetic path to obtain gelators **2** and **3**.

The product Boc-$^{D}$Phe($F_2$)-$^{L}$Oxd-OH, **3** was prepared following the synthetic procedure described for the preparation of **2** and replacing H-$^{D}$Oxd-OBn with H-$^{L}$Oxd-OBn,[105] overall yield 88%. M.p. = 142 °C (dec.); $[\alpha]^{25}_{D}$ −38.0 ° (c = 0.5 in EtOAc); IR (ATR-IR): ν 3358, 2982, 2933, 1779, 1722, 1683, 1610, 1518 $cm^{-1}$; $^{1}$H-NMR ($CD_3OD$, 400 MHz): δ 1.31 (9H, s, $CH_3$ t-Bu), 1.50 (3H, d, J = 6.4Hz, $CH_3$ Oxd), 2.66 (1H, dd, J = 15.6, 10.4 Hz, CH benzyl), 3.13 (1H, m, CH benzyl), 4.43 (1H, d, J = 4.0 Hz, CαH Oxd), 4.73 (2H, dq, J = 6.4, 4.0 Hz, CβH Oxd), 5.58 (1H, dd, J = 10.0, 3.6 Hz, CαH Phe($F_2$)), 7.16 (3H, m, CH aromatic); $^{13}$C ($CD_3OD$, 100 MHz): δ 19.75, 27.14, 37.12, 54.39, 62.10, 74.76, 79.08, 116.45, 117.95, 125.58, 134.79, 148.25, 150.69, 152.53, 156.51, 170.04, 172.26; $^{19}$F ($CD_3OD$, 376.5 MHz): δ -143.98, -141.26.

## 6.1.3. Preparation of gels **1a-c**, **2a-c**, and **3a-d**

The gels were prepared and tested directly in the 7 mL Thermo Fisher Scientific Sterilin cup, which fits in the rheometer. Gels **1a-c**, **2a-c**, and **3a-c** were prepared by dissolving the correct amount of gelator (0.5 % w/V for **1a**, **2a**, and **3a**, 1.0 % w/V for **1b**, **2b**, and **3b**, and 2.0 % w/V for **1c**, **2c**, and **3c**) in water containing 1.2 eq. of NaOH, then 1.4 eq. of GdL were added. The gels were left to rest overnight for their complete formation.

Gel **3d** was prepared by dissolving the gelator (0.5 % w/V) in 30 mM phosphate buffer (PB) at pH 7.4, then 1.4 eq. of GdL were added. The gel was left to rest overnight for its complete formation. The PB solution was prepared dissolving $KH_2PO_4$ in water and adjusting the pH to a final value of 7.4 by adding NaOH 1 M to reach a final concentration of 100 mM. This solution was then diluted to obtain the concentration required.

## 6.1.4. Rheological analysis of gels **1a-c**, **2a-c**, and **3a-d**

All rheological measurements were performed using an Anton Paar MCR102 rheometer. A vane and cup measuring system was used, setting a gap of 2.1 mm. Time sweep experiments were performed at 23 °C (controlled by an integrated Peltier system)

using a constant shear strain (γ) of 0.5 % and a constant angular frequency (ω) of 10 rad/s, collecting 1 point every 20 s. Oscillatory amplitude sweep experiments (γ: 0.01 – 100 %) were also performed at 23 °C using a constant angular frequency of 10 rad/s. Step strain experiments were performed on hydrogels, subjecting the sample to consecutive deformation and recovery steps. The recovery step was performed by keeping the sample at a constant strain γ = 0.03 %, i.e., within the linear viscolastic range (LVER), for a period of 400 s. The deformation step was performed by applying to the gel a constant strain of γ = 100 %, i.e., above the LVER of the sample, for a period of 300 s. The cycles were performed at a fixed frequency of ω = 10 rad $s^{-1}$ and repeated three times.

### 6.1.5. Optical microscope images of gels **1a-c**, **2a-c**, and **3a-d**

The optical microscope images were recorded using a Nikon 13 ECLIPSE Ti2 Inverted Research Microscope with a 10× or 40× magnifier. A piece of the gel sample prepared in the Sterilin cups was cut using a bistoury and analysed both while wet and after complete drying.

### 6.1.6. Scanning electron microscopy of gels **1a-c**, **2a-c**, and **3a-d**

Scanning electron micrographs of the samples were recorded using a Hitachi 6400 field emission gun scanning electron microscope operating at 15 kV. A piece of the gel sample prepared in the Sterilin Cups was cut using a bistoury and analyzed after complete drying.

## *6.2. Synthesis and characterisation of gelators **3-5** and analysis of their gels*

### 6.2.1 General remarks for the synthetic procedure of **3**, **4**, and **5**

The phosphate buffer (PB) solution was prepared as described in section 6.1.1. This solution was diluted to the concentration required for the experiment prior to use.

### 6.2.2. Synthesis of compounds **3**, **4**, and **5**

The synthesis of gelator Boc-$^{D}$Phe($F_2$)-$^{L}$Oxd-OH **3** is reported in the section 6.1.3.

Boc-$^{D}$Phe(F)-$^{L}$Oxd-OH **4**, and Boc-$^{D}$Phe-$^{L}$Oxd-OH **5** (Figure 6.2).

H-$^{L}$Oxd-OBn was prepared according to the procedure reported in reference[105]. Synthesis of compounds **4** and **5** was carried out following the same procedure as the one reported for the synthesis of **3**. Boc-$^{D}$Phe($F_n$)-OH (with n = 1 or 0) (2.00 mmol) was dissolved in 20 mL of acetonitrile (10 mL) and HBTU (2.20 mmol) was added. The mixture was stirred at room temperature for 10 min. A solution containing H-$^{L}$Oxd-OBn (2.00 mmol) and DIEA (4.40 mmol) in ACN (10 mL) was then added dropwise to the first one. The mixture was stirred for 2 h, then the solvent was removed under reduced pressure and replaced with ethyl acetate (40 mL). The organic mixture was washed with $H_2O$ (10 mL), 1 M aqueous HCl (10 mL) and brine (10 mL), then it was dried over $Na_2SO_4$ and the solvent evaporated under vacuum. The solid obtained was finally purified through flash chromatography (dichloromethane:ethyl acetate 95:5).

All the Boc-$^{D}$Phe($F_n$)-$^{L}$Oxd-OBn samples were obtained as white solids and directly hydrogenolysed. They were dissolved in MeOH to obtain a concentration of 10 mg/mL, then the 10% w/w of Pd/C was added. The reaction mixture was vigorously stirred under hydrogen atmosphere for 2 h at room temperature, then it was filtered over a celite pad. The solvent was removed under reduced pressure and the product was used without further purification. Characterization of **4** is reported as follows. The product **4** is obtained

as a white solid with an 87% yield. M.p. = 172-178°C; $[\alpha]^{D}_{25}$ -32.2 ° (c = 0.5 in MeOH); IR (ATR-IR): ν 3370, 3364, 2984, 2937, 1778, 1720, 1687, 1603, 1510 $cm^{-1}$; $^{1}$H-NMR ($CD_3OD$, 400 MHz): δ 1.31 (9H, s, $CH_3$ t-Bu), 1.47 (3H, d, J = 6.4 Hz, $CH_3$ Oxd), 2.71 (1H, dd, J = 10.0, 13.2 Hz, CH benzyl), 3.10 (1H, m, CH benzyl), 4.41 (1H, d, J = 3.6 Hz, CαH Oxd), 4.69 (1H, m, CβH Oxd), 5.63 (1H, dd, J = 4.0, 9.6 Hz, CαH Phe(F)), 6.97 (2H, m, CH Ar), 7.30 (2H, m, CH Ar); $^{13}$C ($CD_3OD$, 100 MHz): δ 19.77, 27.18, 37.19, 54.37, 61.92, 74.57, 79.04, 114.32, 114.53, 130.85, 130.93, 132.88, 152.28, 155.89, 163.07, 170.04, 172.44; $^{19}$F ($CD_3OD$, 376.5 MHz): δ -118.46.

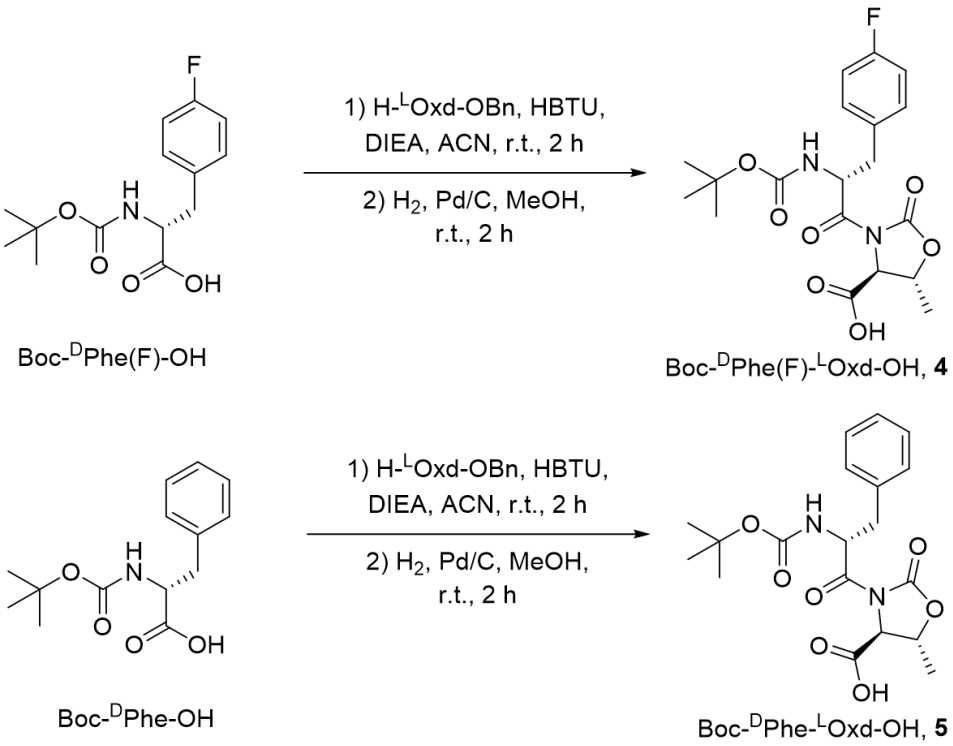


**Figure 6.2**. Synthetic paths to obtain gelators **4** and **5**.

Characterization of **5** matched the literature values reference[108].

## 6.2.3. Preparation of gels **3d-k**, **4a-h**, and **5a-h**

The gels used for absorbance measurements were directly prepared in plastic cuvettes, the gels used for pictures were prepared in a 1.5 mL glass vial and the gels used for the

rheological analysis were prepared in 7 mL Sterilin Cups. All the gels were left to rest overnight at room temperature before their use.

Gel **3d** was prepared as indicated in section 6.1.4. The gels **3f**, **4a**, **4c**, **5a**, and **5c** were all dissolved using a phosphate buffer (PB) solution whose final concentration is 30 mM, prepared as indicated in section 6.1.4. For the gels **4a** and **5a** the gelators were dissolved in a 30 mM PB solution at pH 7.4, then 1.4 eq of GdL was added. Samples **3f**, **4a**, and **5a** were prepared by dissolving the gelators in a 40 mM PB solution at pH 7.4, then 1.0 eq of 60 mM $CaCl_2$ aqueous solution was added. Samples **3e**, **4b**, and **5b** were prepared following the same procedure used for samples **4a** and **5a**, using a 60 mM PB solution. Samples **3g**, **4d**, and **5d** were prepared following the same procedure used for samples **3f**, **4a**, and **5a**, using an 80 mM PB solution.

The gels **3h-k**, **4e-h**, and **5e-h** were prepared by dissolving the gelators in the organic solvent (ethanol or isopropyl alcohol) by alternating manual shaking and ultrasound sonication, then water was added during sonication.

## 6.2.4. Rheological Analysis of gels **3d-k**, **4a-h**, and **5a-h**

Gel **3d** was analysed as described in section 6.1.4.

All rheological measurements were performed using an Anton Paar MCR102 rheometer. A vane and cup measuring system was used, setting a gap of 2.1 mm. The gels were prepared as described and tested directly in the Sterilin Cup which fits in the rheometer. Time sweep experiments were performed at 23 °C (controlled by an integrated Peltier system) using a constant shear strain ($\gamma$) of 0.5 % and a constant angular frequency ($\omega$) of 10 rad/s, collecting one point every 20 s. Oscillatory amplitude sweep experiments ($\gamma$: 0.01–100 %) were also performed at 23 °C using a constant angular frequency of 10 rad/s. Step strain experiments were performed on hydrogels, subjecting the sample to consecutive deformation and recovery steps. The recovery step was performed by keeping the sample at a constant strain $\gamma$ = 0.03 %, i.e., within the LVER, for a period of 400 s. The deformation step was performed by applying to the gel a constant strain of $\gamma$ = 100

%, i.e., above the LVER of the sample, for a period of 300 s. The cycles were performed at a fixed frequency of $\omega = 10$ rad $s^{-1}$ and repeated three times.

## 6.2.5. Optical microscope images of gels **3d-k**, **4a-h**, and **5a-h**

Gel **3d** was analysed as described in section 6.1.5.

The optical microscope images were recorded using an ECLIPSE Ti2 Inverted Research Microscope with a 10× or 20× magnifier. A piece of the gel sample prepared in the Sterilin Cups was cut using a bistoury and analyzed after complete drying.

## 6.2.6. Scanning electron microscope images of gels **3d-k**, **4a-h**, and **5a-h**

Gel **3d** was analysed as described in section 6.1.6.

Scanning electron micrographs were recorded on carbon-coated samples using a Zeiss LEO 1530. A piece of the gel sample prepared in the Sterilin Cups was cut using a bistoury and analyzed after complete drying.

## 6.2.7. X-ray Powder Diffraction Analysis of gels **3d-k**, **4a-h**, and **5a-h**

X-ray powder diffraction (XRPD) measurements were performed with a PanAnalytical X'Pert Pro diffractometer equipped with X'Celerator detector with Cu Kα radiation. The samples were ground before the measurements. A piece of the gel sample prepared in the Sterilin Cups was cut using a bistoury and analyzed after complete drying.

## 6.2.8. Cell Viability Measurement of gelators **3**, **4**, and **5**

Mouse embryonic fibroblast (NIH-3T3) cells were cultured under standard conditions in the minimum essential medium (MEM), supplemented with 10 % (V/V) fetal bovine

serum (FBS), 2 mM $^{L}$Gln, 0.1 mM MEM Non-Essential Amino Acids (NEAA), 100 units/mL penicillin and 100 units/mL streptomycin. Cells were seeded in 96-well plates at a density $10^5$ cells per $cm^2$ and grown for 24 h before exposure to **3**, **4** and **5**. Cells were incubated for 24 h in a humidified incubator set at 37 °C. Cellular viability was assessed by 3-(4,5-dimethylthiazol-2-yl)-2,5-diphenyltetrazolium bromide (MTT) assay, measuring intracellular reduction of tetrazolium salts into purple formazan by viable cells. Cells were incubated with MTT solution (5 mg/mL MTT) for 2 h at 37 °C, 5 % $CO_2$. Subsequently, the MTT solution was discarded and dimethyl sulfoxide (DMSO) was added to each well. Optical density (OD) was read on a microplate reader at 550 nm (Thermo Scientific Varioskan Flash Multimode Reader). Cell viability for each treatment was calculated as the ratio of the mean OD of replicated wells relative to that of the control. All data represented the mean ± standard deviation.

### 6.2.9. Spectrophotometric analysis of gels **3d-k**, **4a-h**, and **5a-h**

The gel samples were directly prepared into disposable cuvettes with 10 mm optical path. The spectrophotometric analyses were performed using a Cary 300 UV-vis double beam spectrophotometer, using a cuvette with the solvent as reference.

## *6.3. Synthesis and characterisation of gelator **6** and analysis of its gels*

### 6.3.1 General remarks for the synthetic procedure of **6**

The phosphate buffer (PB) solution was prepared as described in section 6.1.1. This solution was diluted to the concentration required for the experiment prior to use.

### 6.3.2. Synthesis of gelator **6**

Gelator Boc-$^{L}$Phe-$^{D}$Oxd-$^{L}$Phe-OH **6** was prepared with liquid phase synthesis, following a procedure already reported in literature.[39] All the characterisation data matched the literature values.

### 6.3.3. Preparation of gels **6a-o**

Gels **6a-i** were prepared dissolving gelator **6** in the required concentration (see Table 2.5) in $H_2O$ containing 1.0 eq. of NaOH, by alternating ultrasound sonication and vigorous shaking over a short period of 2 minutes. After complete dissolution, the trigger was added. Gels with GdL (**6a-c**) were formed by adding 1.2 eq. of GdL in the solution, swirling the resulting solution for a few seconds until complete dissolution of GdL and leaving the gel to form overnight. Gels with $CaCl_2$ (**6d-i**) were formed by adding 100 mM $CaCl_2$ aqueous solution (either 0.5 for gels **6d-f** or 1.0 eq. for gels **6g-i**) to the gelator solution, then leaving the gel to form overnight.

Gels **6j-o** were prepared dissolving **6** in the required concentration (see Table 2.6) in phosphate buffer (PB) at pH 7.4 at different concentrations depending on the gelator concentration, by alternating ultrasound sonication and vigorous shaking over a short period of 2 minutes. For the gels at 0.2 % w/V of gelator concentration, the final concentration of PB was 9.6 mM, for the ones at 0.5 % w/V it was 24 mM, for the ones at 1.0 % w/V it was 48 mM. After complete dissolution, the trigger was added. Gels with GdL (gels **6j-l**) were formed by adding 2.0 eq. of GdL in the solution, swirling the resulting

solution for a few seconds until complete dissolution of GdL and leaving the gel to form overnight. Gels with $CaCl_2$ (gels **6m-o**) were formed by adding 100 mM $CaCl_2$ aqueous solution (1.0 eq.) to the gelator solution, then leaving the gel to form overnight.

Gels used for photographs and rheology were prepared on a total volume of 2 mL in a Sterilin cup.

### 6.3.4. Rheological analysis of gels **6a-o**

The rheological measurements were performed using an Anton Paar rheometer, with a vane and cup measuring system, setting a gap of 2.1 mm. The gels were prepared as described and tested directly in the 7 mL Sterilin cup which fits in the rheometer. Oscillatory amplitude sweep experiments ($\gamma$: 0.01 – 100 %) were performed at 23 °C using a constant angular frequency of 10 rad/s.

### 6.3.5. Spectrophotometric analysis of gels **6a-o**

Gels used for spectrophotometric analysis were prepared on a total volume of 1 mL into disposable cuvettes with 10 mm optical path. The spectrophotometric analyses were performed using a Cary 300 UV-vis double beam spectrophotometer, in the range between 250 and 750 nm, using a cuvette with water as reference.

### 6.3.6. HPLC-MS analysis of gelator **6** hydrolysis in gels **6a-o**

Gels used for HPLC-MS analysis were prepared on a total volume of 1 mL in glass vials for HPLC. The gels were then transferred in a larger vial and dissolved with 3 mL of fresh ACN, then 0.1 mL of the resulting solution were diluted with 0.9 mL of fresh ACN. These samples were injected. HPLC-MS analyses were carried out with an Agilent 1260 Infinity II liquid chromatography coupled to an electrospray ionization mass spectrometer (LC-

ESI-MS), using a Phenomenex Gemini C18 - 3µ - 110 Å column, $H_2O/CH_3CN$ with 0.2% formic acid as acid solvent at 40 °C (positive ion mode, mz = 50-2000, fragmentor 70 V).

### 6.3.7. Optical microscopy on dried gels **6a-o**

Xerogels used for microscopy were prepared by transferring a small amount of the gel prepared in Sterilin cups onto a microscope glass slide. The samples were left to dry over a period of 16 h at r.t. in a box to avoid deposition of dust. The images of the xerogels deposited on glass slides were recorded using a Nikon 13 ECLIPSE Ti2 Inverted Research Microscope with a 40x magnifier.

## *6.4. Synthesis and characterisation of gelators **7** and **8** and analysis of their gels*

### 6.4.1. General remarks for the synthetic procedure of **7** and **8**

In the following experiments, we used urease U4002-100KU from Jack Beans, 100000 units/g solid.

### 6.4.2. Synthesis of gelators **7** and **8**

Gelator 1ThNap-$^{L}$Phe-$^{L}$Phe-OH **7** was synthesised following the procedure reported in reference[133]. The characterisation data matched the literature values.

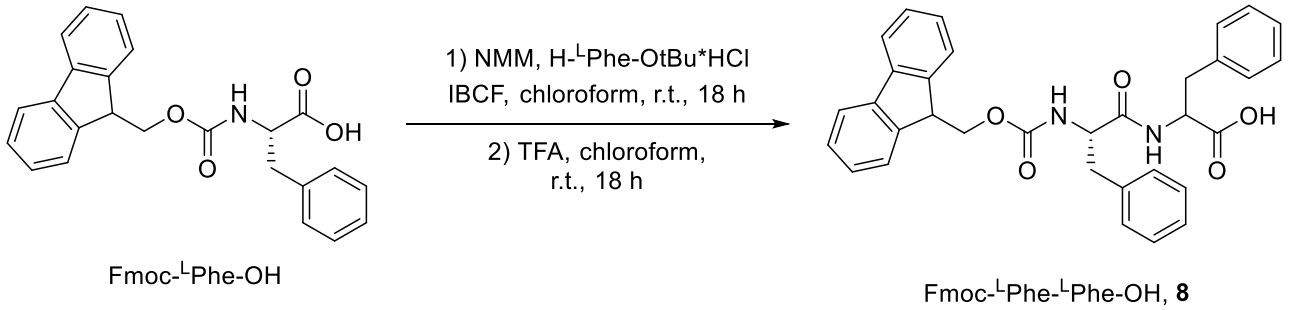


**Figure 6.3**. Synthetic path to obtain gelator **8**.

Fmoc-$^{L}$Phe-$^{L}$Phe-OH **8** (Figure 6.3).

To a solution of Fmoc-$^{L}$Phe-OH (5.62 g, 14.5 mmol) in chloroform (70 mL) was added *N*-methylmorpholine (NMM, 1 eq., 1.59 mL) followed by *iso*-butyl chloroformate (IBCF, 1 eq., 1.89 mL). After stirring for 5 minutes, $H_2$-$^{L}$Phe-OtBu·HCl (1.05 eq., 3.92 g) and another portion of NMM (1 eq., 1.59 mL) were added and the reaction mixture was stirred overnight. It was then diluted with chloroform, washed in turn with 1 M HCl, water, and brine, dried over $MgSO_4$, and evaporated under reduced pressure. The crude title compound Fmoc-$^{L}$Phe-$^{L}$Phe-OtBu was used as such in the next step.

To a solution of crude Fmoc-$^{L}$Phe-$^{L}$Phe-OtBu (8.27 g, 14.0 mmol) in chloroform (40 mL) was added trifluoroacetic acid (TFA, 18 eq., 20 mL) and the solution was stirred overnight. After this time, diethyl ether (200 mL) was added to the reaction mixture resulting in a white precipitate. This was stirred for 20 minutes, filtered, and washed with diethyl ether in the filter. The solid was transferred into a conical flask, then slurried in diethyl ether and decanted twice. Residual solvents were removed from the solid on a rotary evaporator, then by storing in an oven at 80 °C overnight. The title compound was thus obtained as a white solid in 77 % yield. The presence of rotamers (in a ca. 1:9 ratio) complicates the proton and carbon NMR spectra causing peak splitting. $^{1}$H-NMR (DMSO-$d_6$, 400 MHz) 2.72 (1H, dd, *J* = 13.63, 11.07, $PhCH_2$), 2.91-2.98 (2H, m, $PhCH_2$), 3.08 (1H, dd, *J* = 13.89, 5.19, $PhCH_2$), 3.97-4.18 (3 H, m, $OCH_2CH$), 4.24-4.30 (0.88 H, m, CαH), 4.32-4.36 (0.12 H, m, CαH), 4.44-4.50 (0.88 H, m, CαH), 4.52-4.55 (0.12 H, m, CαH), 7.09-7.64 (17 H, m, NH and HAr), 7.87 (2H, d, *J* = 7.59, HAr), 8.28 (0.88 H, d, *J* = 7.8, NH), 8.42 (0.12 H, d, *J* = 7.6, NH), 12.79 (1H, br s, COOH). $^{13}$C (DMSO-$d_6$, 100 MHz) 36.74, 37.44, 46.58, 53.50, 55.70, 65.70, 120.08, 125.28, 125.37, 126.25, 126.48, 127.08, 127.65, 128.04, 128.21, 129.18, 129.27, 137.37, 138.14, 140.68, 143.73, 143.80, 155.73, 171.65, 172.79. HRMS (ESI) m/z: $[M+Na]^+$ calculated for $C_{33}H_{30}N_2NaO_5$ 557.2047; found 557.2045

## 6.4.3. Preparation of solutions of **7**, **8**, urea, and urease

Stock solutions of **7** and **8** were prepared in DMSO at a concentration of 2.0 % w/V by stirring. The stock solutions of urease were prepared at the concentrations of 0.253 mg/mL and 0.506 mg/mL in $H_2O$. The enzyme concentration in the stock solution was determined from the mass (in mg) dissolved in known volume of $H_2O$. Stock solution of the urea was prepared in $H_2O$ in the concentration of 2 M. The enzyme and urea are highly soluble in water at room temperature, and therefore did not require stirring. Solutions of gelator, urease and urea were prepared freshly before each experiment. Stock solution of NaOH was prepared in water at a concentration of 0.1 M.

### 6.4.4. Preparation of gels of **7a**, **7b**, **8a**, **8b**, and **(7+8)a-e**

All these samples were prepared in 7 mL Sterilin cups and were left to rest overnight prior to any measurement. In all cases, the final volumetric ratio DMSO:$H_2O$ is 20:80. For the single component gels of **7** and **8**, we firstly prepared the hydrogels **7a** and **8a**. In this case, 1.6 mL of $H_2O$ were added to the mixture of 0.2 mL of DMSO and 0.2 mL of respective solution of the gelator (final concentration 0.2 % w/V). In the same way, to prepare the multicomponent gel **(7+8)a**, 1.6 mL of $H_2O$ were transferred to the vial containing a mixture of the stock solutions of **7** and **8**, present in a volume of 0.2 mL each, to obtain a final concentration of 0.2 % w/V of each gelator.

To anneal the gels involving the enzymatic reaction, a common procedure was followed. The single component gels **7b** and **8b** were prepared by mixing the 0.2 mL of the stock solution of the respective gelator with 0.2 mL of fresh DMSO, then adding 10 μL of 2 M urea solution and 100 μL of methyl formate. After this, 1.58 mL of the 0.253 mg/mL urease solution were mixed with 10 μL of fresh $H_2O$ and the resulting mixture was added to the DMSO mixture. The bicomponent gels **(7+8)b-e** were prepared in a similar way. First, 0.2 mL of the stock solutions of the two gelators were mixed, then either 10 or 20 μL of 2 M urea and either 100 or 150 μL of methyl formate were added. After this, 1.58 mL of either the 0.253 or the 0.506 mg/mL urease solution were added to the DMSO mixture (Table 3.2).

### 6.4.5. Preparation of layered gels **7a/8a**, **7b/8a**, and **7b/8b**

For the preparation of these gels the tip of a 12 mL polypropylene syringe was cut off. The plunger of the syringe was then adjusted to leave about 5 mL of volume and secured on the bench using some blue tack. First, the single layer gels **7a**, **7b**, **8a**, and **8b** were prepared in the syringe as described in section 6.4.4 and covered with some parafilm. After an overnight rest, these were extruded from the syringe, cut into three sections and analysed with rheology as described in section 6.4.7 to define a reference for the bilayer gels.

Next, we prepared bilayer gels as follows. Either the gel **7a** or **7b** was prepared directly at the bottom of the syringe and rested for about 45 seconds for the early formation of the gel, before gel disruption could occur (in the case of gel **7b**). After this time, the mixture of gel either **8a** or **8b** (i.e., the mixture containing all the components of the gel before gelation occurred) was poured onto the gel of **7**. Each of these gels was covered with some parafilm and left to rest overnight, then they were extruded with the plunger and cut into equal parts to obtain six sections (**L1-L6**). These were then analysed through rheology, $^{1}$H-NMR, and confocal microscopy as described in the following sections 6.4.7, 6.4.9, and 6.4.10, respectively.

## 6.4.6. pH measurements of gels **7a**, **7b**, **8a**, **8b**, and **(7+8)a-e**

A FC200 pH probe from HANNA instruments with a 6 mm x 10 mm conical tip was used for pH measurements. For the urea-urease reaction involving the gelator, the reaction mixtures were prepared as described above at a 2 mL volume in a 7 mL Sterilin vial and the pH change was monitored over time. The temperature was maintained at 25 °C during the measurement by using a circulating water bath.

## 6.4.7. Rheological analysis of gels **7a**, **7b**, **8a**, **8b**, and **(7+8)a-e** and layered gels **7a/8a**, **7b/8a**, and **7b/8b**

All rheological measurements were undertaken on an Anton Paar Physica MCR 101 rheometer at 25 °C. For gels prepared in sterilin cups, strain, frequency, and time sweeps were performed using a vane and cup geometry. Strain sweeps were performed at 10 rad/s from 0.01 % to 1000 % strain. Frequency sweeps were carried out from 1 rad/s to 100 rad/s at 0.5 % strain. Time sweeps were performed at an angular frequency of 50 rad/s and with a strain of 0.5%. For these experiments, gels were prepared as mentioned earlier in 2 mL volume in a 7 mL Sterilin vials. Long-term time sweeps were performed on an Anton Paar Physica MCR 301 rheometer at 25 °C. The time sweeps were collected using

an angular frequency of 50 rad/s and strain of 0.5%. For these measurements, the samples were prepared immediately before positioning the vial in the rheometer cup system. The data was collected over a period of 64 hours. To prevent evaporation of the gel over time, aluminium foil was placed around the measuring system.

For gels sections of single- and double layer systems measurements a parallal plate (PP) geometry (d = 12.5 mm) was used for strain sweep experiments. The gel disks were transferred onto a piece of sandpaper secured on the rheometer plate with some tape. Additional strain sweep experiments were carried out on gels sections of single-layer gels of the single components (**7a**, **7b**, **8a**, **8b**) to compare the results obtained for the bilayer system with the same geometry. Strain sweeps were performed at 10 rad/s from 0.01 % to 1000 % strain. For these experiments, gels were prepared as mentioned earlier in a 12 mL cut syringe. All gels were left ~16 hours before being measured.

### 6.4.8. Circular dichroism of gels **7a**, **7b**, **8a**, **8b**, **(7+8)a**, and **(7+8)b**

Data were collected using a Chirascan VX spectrometer (applied photophysics) using a 0.01 mm path length quartz cuvette. All spectra were aquired at 25 °C with a scanning step size of 1.0 nm, scanning rate of 0.25 s, in the range 180-400 nm. All gel samples were prepared in 2 mL volume in Sterilin vials using the same methodology as described earlier and were left to rest overnight.

### 6.4.9 NMR spectroscopy experiments of gelator **8**, multicomponent gels **(7+8)b**, **(7+8)n** and layered gels **7a/8a**, **7b/8a**, and **7b/8b**

$^{1}$H-NMR spectrum of gelator **8** was recorded on a Bruker Avance III 400 MHz instrument.

$^{1}$H-NMR spectra to follow the annealing process (gels **(7+8)n** and **(7+8)b**) were recorded at 298 K on a Bruker 500 MHz Avance III spectrometer with 16 scans and two dummy

scans, a 30° pulse, relaxation delay of 1 s and signal acquisition time of 3.2 s. Spectra were referenced to the residual $^1$H signal from the $d_6$-DMSO at 2.60 ppm.

The samples undergoing annealing (gels **(7+8)b** and **(7+8)n**) were prepared directlty in a 5 mm diameter NMR tube following the section 6.4.4 but replacing DMSO and $H_2O$ with $d_6$-DMSO and $D_2O$ respectively and with the volumes adjusted to achieve a total volume of 550 μL. Immediately upon addition of the $D_2O$ solution, the sample was shaken vigorously while still turbid and the tube immediately centrifuged (< 1000 rpm) for 5 s on a Hettich H1011 hand centrifuge to drive away the air bubbles. This shaking and centrifugation step was found to be necessary to achieve the homogenous mixing in the 5 mm tube required to obtain good quality NMR spectra. The gel **(7+8)n**, involving urea, urease, but no methyl formate was prepared as for sample **(7+8)b**, but with only 10 μg/mL of urease and 10 mM ammonium formate to act as a reference for $^1$H integration.

The layered gels **7a/8a**, **7b/8a**, and **7b/8b** were prepared following the methodology described in the section 6.4.5, dividing each section and freeze-drying them separately to remove the solvent. To prepare the samples for NMR spectroscopy, the freeze-dried samples were then dissolved in 0.5 mL of $d_6$-DMSO.

## 6.4.10. Confocal microscopy of gels **7a**, **8a**, **(7+8)a**, and **(7+8)b** and layered gels **7a/8a**, **7b/8a**, and **7b/8b**

A Zeiss LSM710 confocal microscope with an LDEC Epiplan NEUFLUAR 50X, 0.55 DIC objective was used for imaging. All gel samples were prepared in presence of Nile blue (2 μL/mL of a 0.1 wt % solution in water). The gels described in the section 6.4.4 which did not involve the use of methyl formate, urea and urease (gels **7a**, **8a**, and **(7+8)a**) were prepared directly in CELLview culture dishes by depositing 40 μL of the gelator solution in DMSO. For **7a** and **8a** 20 μL of the corresponding peptide were mixed with 20 μL of DMSO, for **(7+8)a** 20 μL of each solution were mixed, then 160 μL of $H_2O$ were added onto the DMSO solutions. The culture dishes were covered with their own lid and the samples were left to rest for 16 hours in a closed box with a wet piece of blue

roll to prevent drying of the samples. The gels which instead involved the use of urea, urease and methyl formate (gels **7b**, **8b**, and **(7+8)b**) were prepared as described in section 6.4.4 in a volume of about 2 mL of solvent in 7 mL Sterilin cups. Then a small amount of each section was deposited onto glass microscope slides. A cover slip was gently placed on the gel. The gels sections of layered gels **7a/8a**, **7b/8a**, and **7b/8b** were prepared as described in section 6.4.5 in 12 mL cut syringes and cut after 16 hours. Then a small amount of each section was deposited onto glass microscope slides. A cover slip was gently placed on the gel.

All the samples were excited at 633 nm using a He-Ne laser. Images were captured using Carl Zeiss ZEN 2011 v7.0.3.286 software.

## *6.5. Characterisation of gels of **9** and **10***

### 6.5.1. General remarks for the gels of **9** and **10**

Compounds Fmoc-EDA **9**, Fmoc-DAP **10**, and N,N'-carbonyl diimidazole (CDI) were used as purchased. Deionised water was used throughout all experiments.

### 6.5.2. Preparation of solutions of **9**, **10**, and CDI

Stock solutions of **9** and **10** were prepared in $H_2O$ at a concentration of either 1.33 % or 1.0 % w/V by stirring. The solutions of CDI were prepared in TBME at a concentration of either 75 mM or 50 mM through ultrasound sonication for about 20 minutes. These were used within 30 mins from their complete dissolution. Solutions of gelators and CDI were prepared freshly before each experiment. Stock solution of NaOH was prepared in water at a concentration of 1 M.

### 6.5.3. Preparation of gels **9a-e** and **10a**

For gel **9a** with NaOH, 1.5 mL of the 1.33 % w/V aqueous solution of **9** were poured into a glass vial, then 500 μL of $H_2O$ containing 1.0 eq. of NaOH were added to the previous solution, to obtain a final concentration of 1.0 % w/V of the gelator. For the gels **9b-e** and **10a** involving the bilayer system with CDI solution, 2 mL of the 10 mg/mL aqueous solution of the peptide were poured into a 7 mL squat glass vial. Then either 2 mL or 3 mL of either 75 mM or 50 mM CDI solution in TBME was gently transferred on the aqueous layer and the vial was immediately closed with a screw cap. Gels used for pH measurements were prepared in a 7 mL aluminium vial. Gels used for all the other purposes were prepared in 7 mL squat glass vials.

## 6.5.4. pH measurements of gels **9a-e** and **10a**

A FC200 pH probe from HANNA instruments with a 6 mm x 10 mm conical tip was used for pH measurements. The gels were prepared as described above at a 2 mL volume of the aqueous phase in a 7 mL aluminium vial and the pH change was monitored with time.

## 6.5.5. Rheological analysis of gels **9a-e** and **10a**

All rheological measurements were undertaken on an Anton Paar Physica MCR 101 rheometer at 25 °C. For the NaOH triggered gel of **9** (gel **9a**), the time sweep was performed using a vane and cup geometry. For all the other samples (gels **9b-e** and **10a**), the parallel plate (d = 12.50 mm) geometry was used. Strain sweeps were performed at 10 rad/s from 0.01 % to 1000 % strain. Frequency sweeps were carried out from 1 rad/s to 100 rad/s at 0.1 % strain. For strain and frequency sweeps the shaft was adjusted at a position where it could touch the surface of the gel without compressing it. Time sweeps were performed at an angular frequency of 50 rad/s and with a strain of 0.1%. For the geometry, the shaft was adjusted at a height of either 6.0 mm or 4.0 mm from the bottom of the vial. For these experiments, gels were prepared as mentioned earlier in 2 mL volume of aqueous phase in a 7 mL squat glass vials. All gels were left to rest overnight before being measured.

## 6.5.6. Fluorescence spectroscopy of solution of **9** and gels **9a** and **9b**

Emission spectra were collected on an Agilent Technologies Cary Eclipse fluorescence spectrometer. Samples were prepared in polymethylmetacrylate (PMMA) cuvettes with a path length of 10 mm by following the same procedure as mentioned earlier. All gels were left to rest overnight before measurements were carried out. Solvent evaporation was prevented by sealing the cuvette with tape. In all cases, the excitation wavelength was 300 nm. The excitation slit width was 10 nm, while the emission slit width was 5 nm.

### 6.5.7. FTIR spectroscopy of solution of **9** and gels **9a** and **9b**

Data were recorded using an Agilent Cary 630 ATR-FTIR spectrometer. All gels were prepared following the methodology described in section 6.5.3, then the solvent was removed by freezedrying. For the solid samples, the background of the empty ATR crystal was taken. Then small amounts of the freeze-dried samples were deposited on the ATR crystal before recording the spectra.

### 6.5.8. Confocal microscopy of gels **9a**, **9b**, and **10a**

A Zeiss LSM710 confocal microscope with an LDEC Epiplan NEUFLUAR 50X, 0.55 DIC objective was used for imaging. All gel samples were prepared in presence of Nile blue (5 μL/mL of a 0.1 wt % solution in water). Gel **9a** was prepared directly in CELLview culture dishes. For gels **9b** and **10a**, gels were prepared following the same procedure described earlier. Then a small amount of the gel was deposited onto glass microscope slides. A cover slip was gently placed on the gel. All the samples were excited at 633 nm using a He-Ne laser. Images were captured using Carl Zeiss ZEN 2011 v7.0.3.286 software.

## *6.6. Synthesis and characterisation of gelators **11** and **12** and their gels*

### 6.6.1. General remarks for the synthesis of **SB1-4** and gelators **11** and **12**

The aldehydes **A1**-**4** and the corresponding Schiff's bases **SB1**-**4** obtained were used as racemate.

### 6.6.2. Synthesis of **SB1-4** and gelators **11** and **12**

**SB1** (Figure 6.4).

Cyclamal aldehyde (126 mg, 0.662 mmol) and methyl anthranilate (50 mg, 0.331 mmol) were mixed in 2:1 ratio in a vial and placed in an oil bath preheated at 110 °C. The reaction mixture was stirred for 30 min. Then the crude was dissolved in EtOH and the conversion was quantified using an HPLC-MS. HPLC-MS (API-ES): 17.87 min, $[M+H]^+$=324.

**SB2** (Figure 6.4).

Helional aldehyde (127 mg, 0.662 mmol) and methyl anthranilate (50 mg, 0.331 mmol) were mixed in 2:1 ratio in a vial and placed in an oil bath preheated at 110 °C. The reaction mixture was stirred for 30 min. Then the crude (**SB2**) was dissolved in EtOH and the conversion was quantified using an HPLC-MS. The reaction was also repeated on 2.60 mmol of aldehyde (1.30 mmol of MA) and the crude was dissolved in methanol (10 mL), heated until completely solubilization and left to crystallise overnight. The crystals (**SB2c**) were then filtered and washed several times with cold methanol (yield: 22.4%).

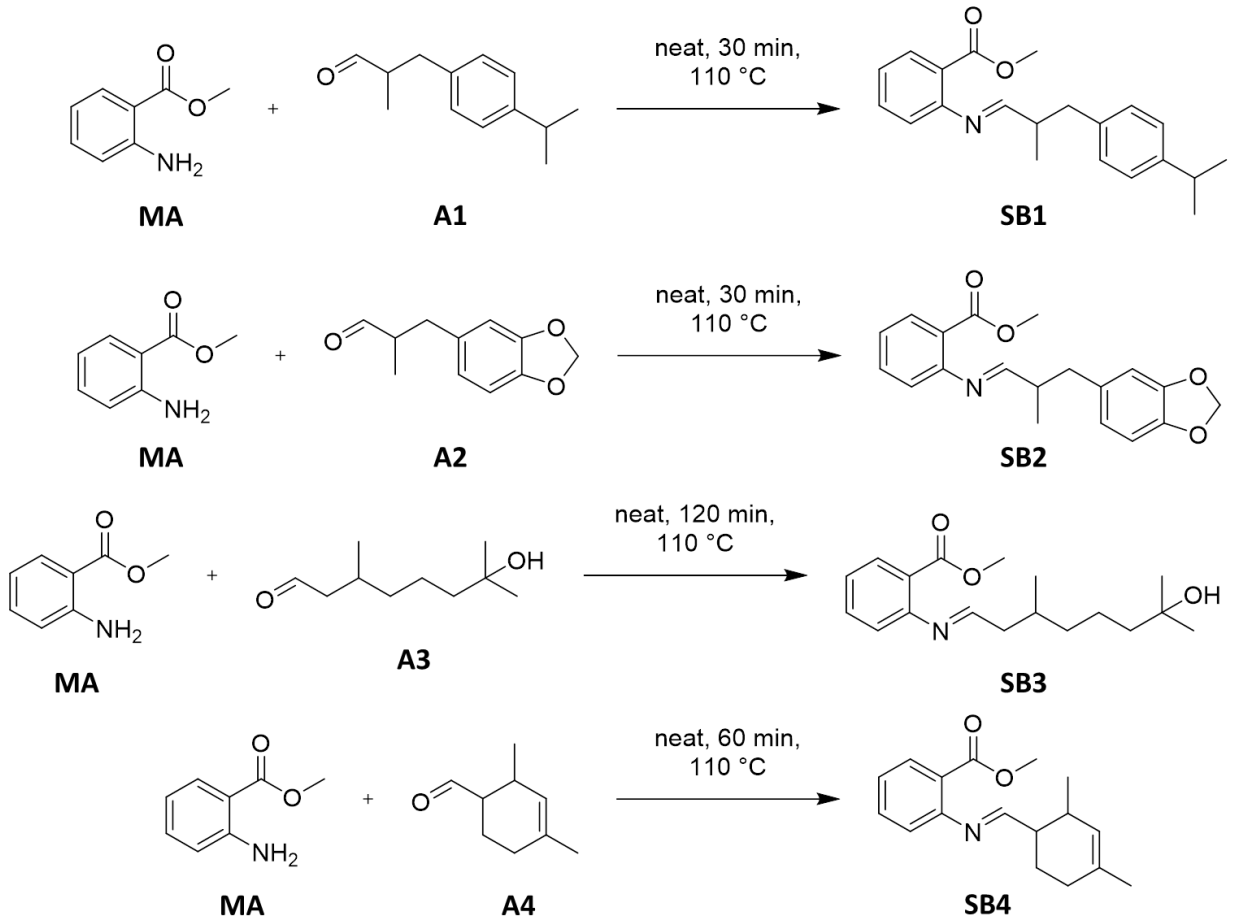


**Figure 6.4**. Synthetic paths to obtain Schiff bases **SB1-4**.

**SB2c**.

HPLC-MS (API-ES): 11.68 min, $[M+H]^+$=326. M.p. = 82-84 °C; FTIR: ν = 3302, 3261, 1658, 1606, 1584, 1520, 1483, 1435 $cm^{-1}$; $^1$H-NMR ($CDCl_3$, 400MHz) δ: 1.67 (3H, d, *J* = 1.6 Hz, C-$CH_3$), 3.28 (2H, bs, Ar-$CH_2$), 3.87 (3H, s, O-$CH_3$), 5,91 (2H, s, O-$CH_2$-O), 6.38 (2H, dd, *J* = 1.2, 10.4 Hz, Ar-CH), 6.69 (4H, m, Ar-CH), 6,91 (1H, dd, *J* = 1.2, 8.8 Hz, Ar-CH), 7.36 (1H, m, Ar-CH), 7.91 (1H, dd, *J* = 1.6, 8.0 Hz, Ar-CH), 9.51 (1H, *J* = 10.4 Hz, CH=N); $^{13}$C-NMR ($CDCl_3$) δ: 14.50, 42.80, 51.68, 100.75, 107.98, 109.08, 110.23, 111.66, 115.42, 116.08, 121.14, 121.53, 131.66, 134.20, 134.63, 145.81, 146.75, 147.58, 169.05.

**SB3** (Figure 6.4).

Hydroxy citronellal aldehyde (57 mg, 0.331 mmol) and methyl anthranilate (100 mg, 0.662 mmol) were mixed in 1:2 ratio in a vial and placed in an oil bath preheated at 110 °C. The reaction mixture was stirred for 120 min. Then the crude was dissolved in EtOH and the conversion was quantified using an HPLC-MS. HPLC-MS (API-ES): 10.43 min, $[M+H]^+$=306.

**SB4** (Figure 6.4).

Triplal aldehyde (91.5 mg, 0.662 mmol) and methyl anthranilate (50 mg, 0.331 mmol) were mixed in 2:1 ratio in a vial and placed in an oil bath preheated at 110 °C. The reaction mixture was stirred for 60 min. Then the crude was dissolved in EtOH and the conversion was quantified using an HPLC-MS. HPLC-MS (API-ES): 14.65 min, $[M+H]^+$=272

Gelators Boc-$^L$Dopa(Bn)$_2$-OMe[174] **11** and Boc-$^L$Dopa(Bn)$_2$-OH[175] **12** were synthesised following the procedure reported in literature. Characterisation matched literature data.

## 6.6.3. Hydrolysis study in solution of **SB1-4**

After the reaction has undergone the optimum time for the specific Schiff base synthesis, the product was dissolved in 8.5 mL of ethanol and 1.5 mL of water in a 10 mL volumetric flask. HPLC-MS analysis was carried out at the desired time intervals to analyze the hydrolysis of the Schiff base, by taking a withdrawal of 100 μL of the **SB** solution and adding 900 μL of ACN. The same procedure was followed for the hydrolysis in the 70:30 EtOH/$H_2O$ solution, but the product was dissolved in 7.0 mL of ethanol and 3.0 mL of water in a 10 mL volumetric flask (Table 4.2).

For the solutions including acetic acid, each Schiff base was dissolved in EtOH, then this solution was diluted in an EtOH:$H_2O$ solution (in 70:30 volumetric ratio) so that the concentration of Schiff base in this final solution resulted 0.5 % w/V. Then, the mmol of gelator were replaced with mmol of glacial acetic acid to obtain a similar pH and added to the solution. To take the hydrolysis value at different times, different vials were prepared, all containing the same SB/acetic acid ratio.

### 6.6.4. Preparation of gels **11a**, **11b** and **12a**

After the synthesis, each SB was dissolved in EtOH, then this solution was poured onto 10 mg of gelator (either **11** or **12**) and diluted in more ethanol to reach a volume of either 0.70 mL. The resulting solution was sonicated until the dissolution of the two compounds was achieved. Then, to trigger the formation of the gel, 0.30 mL of $H_2O$ were added to the vial and gently swirled to achieve a homogeneous gel. In all the cases, the final concentration of gelator in the gel was 1.0 % w/V, while the one of Schiff base was 0.5 % w/V. To take the hydrolysis value at different times, it was necessary to prepare the same gel in several vials, as to improve the homogenization of the sample tested with the HPLC, the whole gel had to be dissolved in acetonitrile.

### 6.6.5. Optical microscope images of gels **11a**, **11b** and **12a**

The optical microscope images were recorded using a Nikon 13 ECLIPSE Ti2 Inverted Research Microscope with a 10× magnifier. The images of the crystals were taken using polarized light. The images of the gels were instead taken in epifluorescence mode, using a fluorescent filter cube V-2A and an excitation LED ($\lambda$ = 395 nm). The gel samples were analyzed while wet.

### 6.6.6. Single-crystal X-ray diffraction of **SB2c**

Single-crystal data for compound **SB2c** were collected at RT on an Oxford XCalibur S CCD diffractometer equipped with a graphite monochromator (Mo-$K_\alpha$ radiation, $\lambda$ = 0.71073 Å). The structure was solved by the intrinsic phasing method with SHELXT[215] and refined on $F^2$ by full-matrix least squares refinement with SHELXL[216] implemented in the Olex2 software[217]. All non-hydrogen atoms were refined anisotropically applying the rigid-body RIGU restraint[218]. $H_{CH}$ atoms for all compounds were added in calculated

positions and refined riding on their respective carbon atoms. The Mercury[219] program was used to calculate intermolecular interactions and for molecular graphics.

### 6.6.7. Rheological analysis of gels **11a**, **11b** and **12a**

The rheological measurements were performed using an Anton Paar MCR102 rheometer. The gels were directly prepared in the 7 mL Thermo Fisher Scientific Sterilin cup, which fits in the rheometer. A vane and cup measuring system was used, setting a gap of 2.1 mm. Oscillatory amplitude sweep experiments (γ: 0.01 – 100 %) were performed in triplicate at 23 °C using a constant angular frequency of 10 rad/s, 16 h after the addition of water, to allow a complete gel formation.

## *6.7. Synthesis and characterisation of peptides **12**, **13**, **14**, and **15** and their gels*

### 6.7.1. General remarks for the synthesis of peptides **12**, **13**, **14**, and **15** and preparation of their gels

The 0.1 M phospate buffer (PB) solution was prepared following the procedure in section 6.1.1. This solution was diluted to the concentration required for the experiment prior to use.

### 6.7.2. Synthesis of peptides **12**, **13**, **14**, and **15**

Gelator Boc-$^{L}$Dopa(Bn)$_2$-OH, **12** was synthesised as described in reference[175]. Characterisation matched the literature values.

Gelator Boc-$^{L}$Ala-Aib-$^{L}$Val-OH **13** was synthesised after a multistep synthesis as follows (Figure 6.5).

Boc-Aib-$^{L}$Val-OMe. 900 mg of Boc-Aib-OH, (4.43 mmol) are dissolved in 60 mL of anhydrous ACN and 2 g of HBTU (5.21 mmol) are added under inert atmosphere at r.t.. A solution containing 782 mg of H-$^{L}$Val-OMe·HCl (4.43 mmol), 20 mL of anhydrous ACN and 2.34 mL of DIEA (13.73 mmol) is added dropwise to the first one. The reaction is left under stirring for 3 h, then the solvent is removed under vacuum, the residue suspended in 20 mL of $H_2O$, extracted with ethyl acetate (x3) and washed with 1 M HCl (x2), saturated solution of $NaHCO_3$ (x2) and brine (x2). The organic layer is dried over $Na_2SO_4$ and the solvent evaporated under vacuum. The product, Boc-Aib-$^{L}$Val-OMe was obtained as a white solid with 95% yield.

Boc-$^{L}$Ala-Aib-$^{L}$Val-OMe. Boc-Aib-$^{L}$Val-OMe (4.22 mmol, 1.34 g) is dissolved in 40 mL of anhydrous DCM, then 5.9 mL of TFA (75.96 mmol) are added under inert atmosphere. The reaction is left under vigorous stirring for 2 h at room temperature, then the solvent is removed under reduced pressure. The whole residue, made of the remaining TFA and

the desired intermediate H-Aib-$^{L}$Val-OMe, is used for the next step of the reaction, considering a quantitative yield for this one.

799 mg of Boc-L-Ala-OH (4.22 mmol) are dissolved in 60 mL of anhydrous ACN and 1.76 g of HBTU (4.64 mmol) are added under $N_2$ atmosphere at room temperature. A solution containing the residue of the former step, 20 mL of anhydrous ACN and 3.7 mL of DIEA (22.0 mmol) is added dropwise to the first one. The reaction is left under stirring for 3 h, then the solvent is removed under vacuum, the residue suspended in 10 mL of $H_2O$, extracted with ethyl acetate (x3) and washed with 1 M HCl, brine, saturated solution of $NaHCO_3$ and brine once again. The organic layer is dried over $Na_2SO_4$ and the solvent evaporated under vacuum. The product is eventually purified through a flash chromatography (DCM 100%, DCM:EtOAc 80:20, DCM:EtOAc 70:30). Boc-$^{L}$Ala-Aib-$^{L}$Val-OMe is obtained as a white solid with a yield of 84% (3.54 mmol, 1.37 g).

Boc-$^{L}$Ala-Aib-$^{L}$Val-OH **13**.

A solution containing 1.37 g of Boc-$^{L}$Ala-Aib-$^{L}$Val-OMe in 6 mL of MeOH and 12 mL of THF was cooled to 0 °C and treated with 4.4 mL of 1 M NaOH. As the ice bath was removed, the mixture was left to warm up and stir overnight. A solution of 5.3 ml of 1 M HCl was added to the reaction mixture, then it was concentrated in vacuo to remove the volatiles. The reduced volume was then extracted with DCM (x3). The combined organic phase was washed with water, dried over $Na_2SO_4$, filtered and evaporated in vacuo, to afford pure Boc-$^{L}$Ala-Aib-$^{L}$Val-OH (95%) as a white solid. M.p.: 175-182 °C; $[\alpha]^{D}_{25}$ -20 (c = 5 mg/mL in MeOH); ATR-FTIR: ν 3507, 3412, 3395, 3330, 3294, 3279, 3072, 2978, 2932, 1701, 1685, 1670, 1645, 1558, 1524. $^{1}$H-NMR ($CD_3OD$, 400 MHz): δ 0.93 (6H, dd, *J* = 9.2 Hz, $CH_3$ Val), 1.27 (3H, d, *J* = 7.1 Hz, $CH_3$ Ala), 1.42 (9H, s, tBu), 1.44 (3H, s, $CH_3$ Aib), 1.46 (3H, s, $CH_3$ Aib), 2.23 – 2.04 (1H, m, CH Val), 4.00 (1H, q, *J* = 7.1 Hz), 4.23 (1H, d, *J* = 5.6 Hz), 6,72 (1H, d, NHBoc, *J* = 5.6 Hz), 7.38 (1H, d, NH Val, *J* = 8.3 Hz), 8.04 (1H, s, NH Aib). $^{13}$C-NMR ($CD_3OD$, 100 MHz): δ 16.62, 17.27, 18.18, 23.27, 24.76, 27.31, 30.43, 50.25, 56.53, 57.77, 79.17, 156.24, 173.17, 173.87, 175.24.

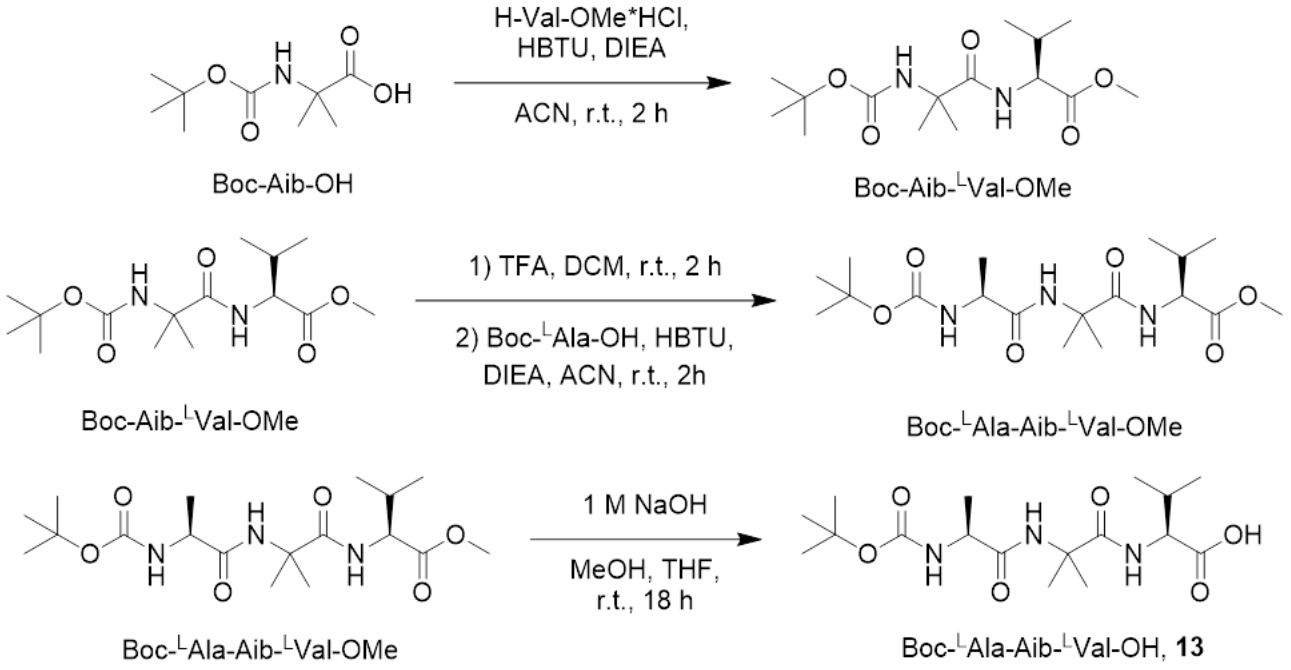


**Figure 6.5**. Synthetic path to obtain gelator **13**.

Tripeptide TFA-$^{L}$Val-$^{L}$Tyr-$^{L}$Val-OH **14** was synthesised after a convergent multistep synthesis, as follows (Figure 6.6).

Boc-$^{L}$Tyr(Bn)-$^{L}$Val-OMe.

Boc-$^{L}$Tyr(Bn)-OH (500 mg, 1.346 mmol) and HBTU (561 mg, 1.481 mmol) were dissolved in 15 mL of dry ACN. H-$^{L}$Val-OMe·HCl (226 mg, 1.346 mmol), DIEA (0.733 ml, 4.307 mmol) and 10 mL of dry ACN were added dropwise to the mixture. The reaction solution was stirred at room temperature for 2 h under a $N_2$ atmosphere. The solvent was evaporated and the residue was dissolved in EtOAc. The residue was washed with 1 M HCl (x2), $NaHCO_3$ (x2) and Brine (x1). The organic phase was dried over $Na_2SO_4$. The solvent was evaporated and Boc-$^{L}$Tyr(Bn)-$^{L}$Val-OMe was obtained in 95% yield (620 mg, 1.279 mmol). HPLC-MS (ESI): 9.64 min, $[(M\text{-}Boc)+H]^+ = 385$, $[M+Na]^+ = 507$.

TFA-$^{L}$Val-OH.

Parallely, this intermediate was obtained as previously reported.[220] Trifluoroacetic anhydride (0.840 mL, 6.074 mmol) was added to a solution of H-$^{L}$Val-OH (593 mg, 5.062 mmol) in trifluoroacetic acid (2.5 mL) and the resulting mixture was stirred for 1.5 h. TFA

was then evaporated under reduced pressure. Water was added and the residue was extracted with EtOAc (3x). The organic layer was then dried over $Na_2SO_4$ and the solvent was evaporated. The product was washed with n-hexane and obtained in 96% yield (1.035 g, 4.860 mmol). The characterization matched the values reported in reference[220].

TFA-$^{L}$Val-$^{L}$Tyr(Bn)-$^{L}$Val-OMe.

Boc-$^{L}$Tyr(Bn)-$^{L}$Val-OMe (500 mg, 1.032 mmol) and TFA (1.43 mL, 18.57 mmol) were added to dry DCM (6 mL). The reaction was stirred at room temperature for 2 h under a $N_2$ atmosphere, then the solvent was removed under reduced pressure. The product H-$^{L}$Tyr(Bn)-$^{L}$Val-OMe·TFA was obtained in quantitative yield and used for the following reaction without any further purification.

TFA-$^{L}$Val-OH (220 mg, 1.032 mmol) and HBTU (430 mg, 1.135 mmol) were dissolved in 10 ml of dry ACN. H-$^{L}$Tyr(Bn)-$^{L}$Val-OMe·TFA (398 mg, 1.032 mmol) and DIEA (1.36 mL, 8.0 mmol) were dissolved in dry ACN (5 mL) and added dropwise to the mixture. The reaction solution was stirred at room temperature for 3 h under $N_2$ atmosphere. The solvent was removed and the residue was dissolved in EtOAc and was washed with 1 M HCl (x2), $NaHCO_3$ (x2) and Brine (x1). The organic layer was then dried over $Na_2SO_4$. The solvent was evaporated under reduced pressure. The residue was washed with n-hexane (2x) and the product TFA-$^{L}$Val-$^{L}$Tyr(Bn)-$^{L}$Val-OMe obtained in an 82% yield (504 mg, 0.846 mmol). HPLC-MS (ESI): 9.09 min, $[M+H]^+ = 580$, $[M+Na]^+ = 602$.

TFA-$^{L}$Val-$^{L}$Tyr-$^{L}$Val-OH **14**.

TFA-$^{L}$Val-$^{L}$Tyr(Bn)-$^{L}$Val-OMe (246 mg, 0.414 mmol) was dissolved in 0.66 ml of MeOH and 1.32 ml of THF. The reaction mixture was placed in an ice bath before the addition of 1 M NaOH (0.518 mL, 0.518 mmol). The mixture was left under stirring overnight. After 18 h, 1 M HCl (0.580 ml, 0.580 mmol) was added. The solvents were removed under reduced pressure and the residue was dissolved in DCM and washed with water. The organic layer was dried over $Na_2SO_4$ and the solvent evaporated. The product TFA-$^{L}$Val-$^{L}$Tyr(Bn)-$^{L}$Val-OH was obtained in 95% yield (229 mg, 0.393 mmol).

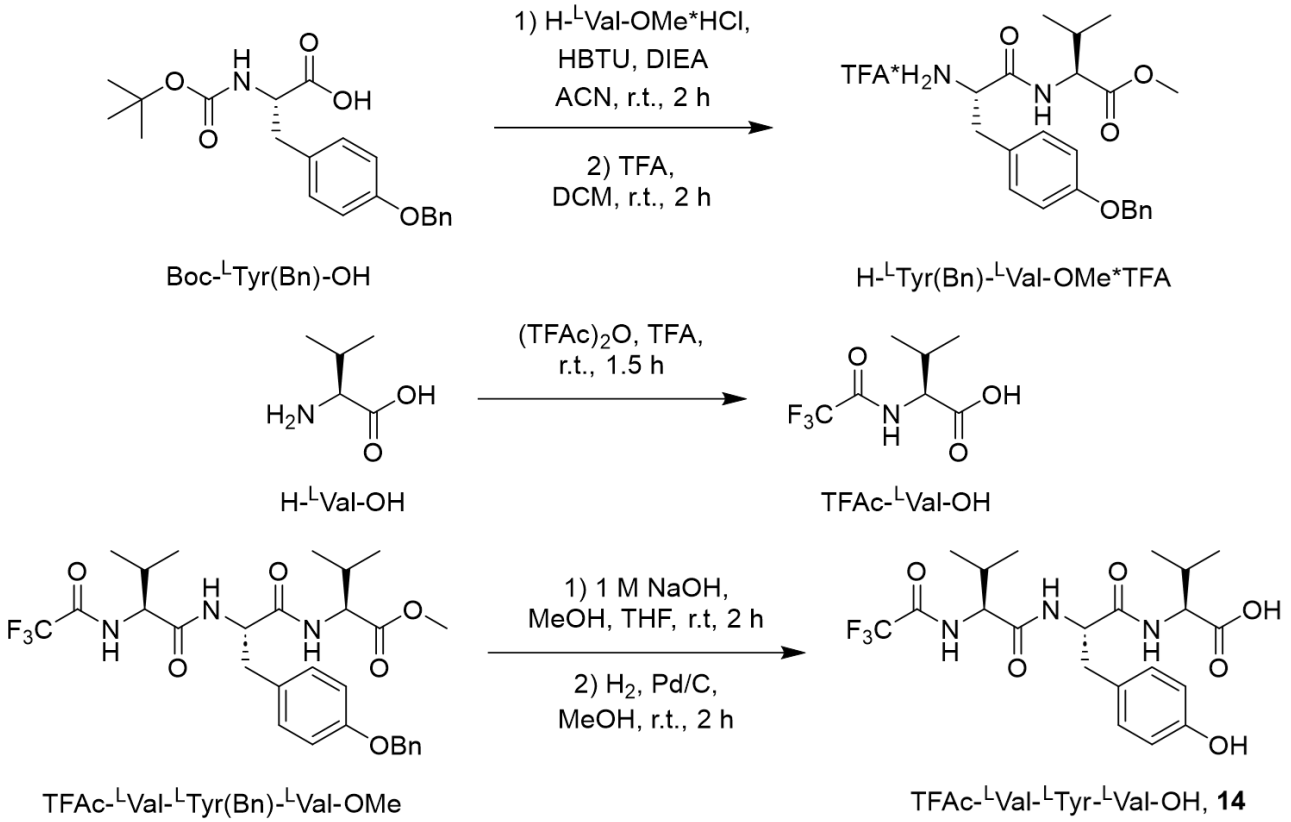


**Figure 6.6**. Synthetic path to obtain the tripeptide **14**.

TFA-$^{L}$Val-$^{L}$Tyr(Bn)-$^{L}$Val-OH (230 mg, 0.396 mmol) was dissolved in 23 mL of methanol in presence of Pd/C (10 % w/w) and a $H_2$ atmosphere. The reaction was left under stirring for 24 h then the solution was filtered through a celite pad and the solvent removed under reduced pressure. The product TFA-$^{L}$Val-$^{L}$Tyr-$^{L}$Val-OH was obtained as a white solid in 99% yield (193 mg, 0.392 mmol). $[\alpha]_D^{20}$ = -14.6 (*c* = 5 mg/mL, MeOH). M.p.: 150 - 152 °C. HPLC-MS (ESI): 4.29 min, $[M+H]^+$ = 476, $[M+Na]^+$ = 498. $^1$H-NMR ($CD_3OD$, 400 MHz, mixture of conformers): δ 0.61 – 0.91 (m, 12H, 2 $(CH_3)_2$ Val), 1.89 – 2.12 (m, 2H, 2 $CH(CH_3)_2$ Val), 2.76 - 3.07 (2H, m, $CH_2Ar$), 4.14 (m, 1H, $C_\alpha H$ Val), 4.23 – 4.33 (m, 1H, $C_\alpha H$ TFA-Val), 4.73 (m, 1H, $C_\alpha H$ Tyr), 6.65 (m, 2H, Ar Tyr), 7.00 (m, 2H, Ar Tyr), 7.97-8.10 (m, 1H, NH TFA-Val), 8.40 (m, 1H, NH Tyr), 8.90 (m, 1H, NH Val). $^{13}$C-NMR ($CD_3OD$, 100 MHz): δ 18.21, 18.33, 18.60, 18.86, 19.38, 19.51, 31.72, 31.90, 37.48, 38.27, 55.96, 58.89, 60.72, 116.10, 128.76, 129.13, 131.30, 157.09, 157.19, 171.84, 173.38, 174.40. ATR-FTIR: ν 3277, 2963, 2412, 2163, 2011, 1973, 1702, 1643, 1549, 1514 cm$^{-1}$.

Tripeptide Pal-$^{L}$Lys-$^{L}$Val-$^{L}$Lys-OH **15** was synthesised after a convergent multistep synthesis, as follows (Figure 6.7).

Boc-$^{L}$Lys(2Cl-Z)-$^{L}$Val-OH.

Boc-$^{L}$Lys(2Cl-Z)-OH (400 mg, 0.964 mmol) and HBTU (379 mg, 1.05 mmol) were dissolved in dry ACN (10 mL). H-$^{L}$Val-OMe·HCl (161 mg, 0.964 mmol), DIEA (0.525 mL, 3.085 mmol) and dry ACN (5 mL) were added dropwise to the mixture. The reaction solution was stirred at room temperature for 2 h under a $N_2$ atmosphere. The solvent was evaporated and the residue was dissolved in EtOAc. The residue was washed with 1 M HCl (x2), $NaHCO_3$ (x2) and Brine (x1). The organic phase was dried over $Na_2SO_4$. The solvent was evaporated and Boc-$^{L}$Lys(2Cl-Z)-$^{L}$Val-OMe was obtained in 99% yield (471 mg, 0.954 mmol). HPLC-MS (ESI): 8.66 min, $[(M\text{-}Boc)+H]^+ = 428$, $[M+Na]^+ = 550$.

Boc-$^{L}$Lys(2Cl-Z)-$^{L}$Val-OMe (471 mg, 0.954 mmol) was dissolved in 1.88 ml of MeOH and 3.76 ml of THF. The reaction mixture was placed in an ice bath and 1 M NaOH (1.2 mL, 1.20 mmol) was added. The mixture was left under stirring at r.t. overnight. After 18 h, 1 M HCl (1.4 ml, 1.40 mmol) was added and after 10 min, the solvent was removed under reduced pressure. The residue was dissolved in DCM, washed with water (x2) and dried over $Na_2SO_4$. The solvent was evaporated and the product Boc-$^{L}$Lys(2Cl-Z)-$^{L}$Val-OH was obtained in 98% yield (480 mg, 0.935 mmol). HPLC-MS (ESI): 7.31 min, $[(M\text{-}Boc)+H]^+ = 414$, $[M+Na]^+ = 536$.

H-$^{L}$Lys(2Cl-Z)-OBn·TFA.

Boc-$^{L}$Lys(2Cl-Z)-OH (500 mg, 1.205 mmol), anhydrous $K_2CO_3$ (250 mg, 1.807 mmol) and benzyl bromide (0.157 mL, 1.326 mmol) were dissolved in anhydrous ACN (10 mL). The reaction was left under stirring at r.t. overnight in an $N_2$ atmosphere. The solvent was then removed under reduced pressure. The residue was extracted with EtOAc (x3) and dried over $Na_2SO_4$. The solvent was removed and the crude was purified with silica gel chromatography (4:1 to 3:1 cHex:EtOAc). The product Boc-$^{L}$Lys(2Cl-Z)-OBn was obtained in 90% yield (547 mg, 1.084 mmol). HPLC-MS (ESI): 10.14 min, $[(M\text{-}Boc)+H]^+ = 405$, $[M+Na]^+ = 527$.

Boc-$^{L}$Lys(2Cl-Z)-OBn (547 mg, 1.084 mmol) was dissolved in 8 ml of anhydrous DCM. TFA (1.4 ml, 17.82 mmol) was added to the flask. The reaction was left under stirring in an $N_2$ atmosphere for 2 h. The solvent was removed and the residue of H-$^{L}$Lys(2Cl-Z)-OBn·TFA was used in the next step without any further purification.

H-$^{L}$Lys(2Cl-Z)-$^{L}$Val-$^{L}$Lys(2Cl-Z)-OBn·TFA.

Boc-$^{L}$Lys(2Cl-Z)-$^{L}$Val-OH (480 mg, 0.935 mmol) and HBTU (390 mg, 1.028 mmol) were dissolved in dry ACN (8 mL). H-$^{L}$Lys(2Cl-Z)-OBn·TFA (379 mg, 0.935 mmol) and DIEA (0.850 mL, 5.0 mmol) were dissolved in dry ACN (5 mL) and added dropwise to the mixture. The reaction solution was stirred at room temperature for 3 h under $N_2$ atmosphere. The solvent was removed and the residue was dissolved in $CH_2Cl_2$ and was washed with 1 M HCl (x2), $NaHCO_3$ (x2) and Brine (x1). The organic layer was then dried over $Na_2SO_4$. The solvent was evaporated under reduced pressure. The residue was purified with silica chromatography (4:1 to 3:1 cHex:EtOAc) and the product Boc-$^{L}$Lys(2Cl-Z)-$^{L}$Val-$^{L}$Lys(2Cl-Z)-OBn was obtained in a 70% yield (504 mg, 0.846 mmol). HPLC-MS (ESI): 11.10 min, $[(M\text{-}Boc)+H]^+ = 802$, $[M+H_3O]^+ = 920$.

Boc-$^{L}$Lys(2Cl-Z)-$^{L}$Val-$^{L}$Lys(2Cl-Z)-OBn (504 mg, 0.846 mmol) was dissolved in 7 ml of anhydrous DCM. TFA (1.2 ml, 15.55 mmol) was added to the flask. The reaction was left under stirring in an $N_2$ atmosphere for 4 h. The solvent was removed and H-$^{L}$Lys(2Cl-Z)-$^{L}$Val-$^{L}$Lys(2Cl-Z)-OBn·TFA was obtained in quantitative yield and used in the next step without further purification.

Pal-$^{L}$Lys-$^{L}$Val-$^{L}$Lys-OH.

Palmitic acid ($CH_3(CH_2)_{14}CO_2H$, Pal-OH, 128 mg, 0.500 mmol) and HBTU (209 mg, 0.55 mmol) were dissolved in anhydrous ACN (8 mL). H-$^{L}$Lys(2Cl-Z)-$^{L}$Val-$^{L}$Lys(2Cl-Z)-OBn·TFA (457 mg, 0.500 mmol) and DIEA (0.340 mL, 2.00 mmol) were dissolved in anhydrous ACN (5 mL) and added dropwise to the mixture. The reaction solution was stirred at room temperature for 4 h under $N_2$ atmosphere. The solvent was removed and $H_2O$ was added. The residue was extracted with DCM (x3) and washed with 1 M HCl (x2), $NaHCO_3$ (x2) and Brine (x1). The organic layer was then dried over $Na_2SO_4$. The solvent

was evaporated under reduced pressure. The product Pal-$^{L}$Lys(2Cl-Z)-$^{L}$Val-$^{L}$Lys(2Cl-Z)-OBn was then washed with n-hexane (2x) and obtained in 85% yield (441 mg, 0.425 mmol).

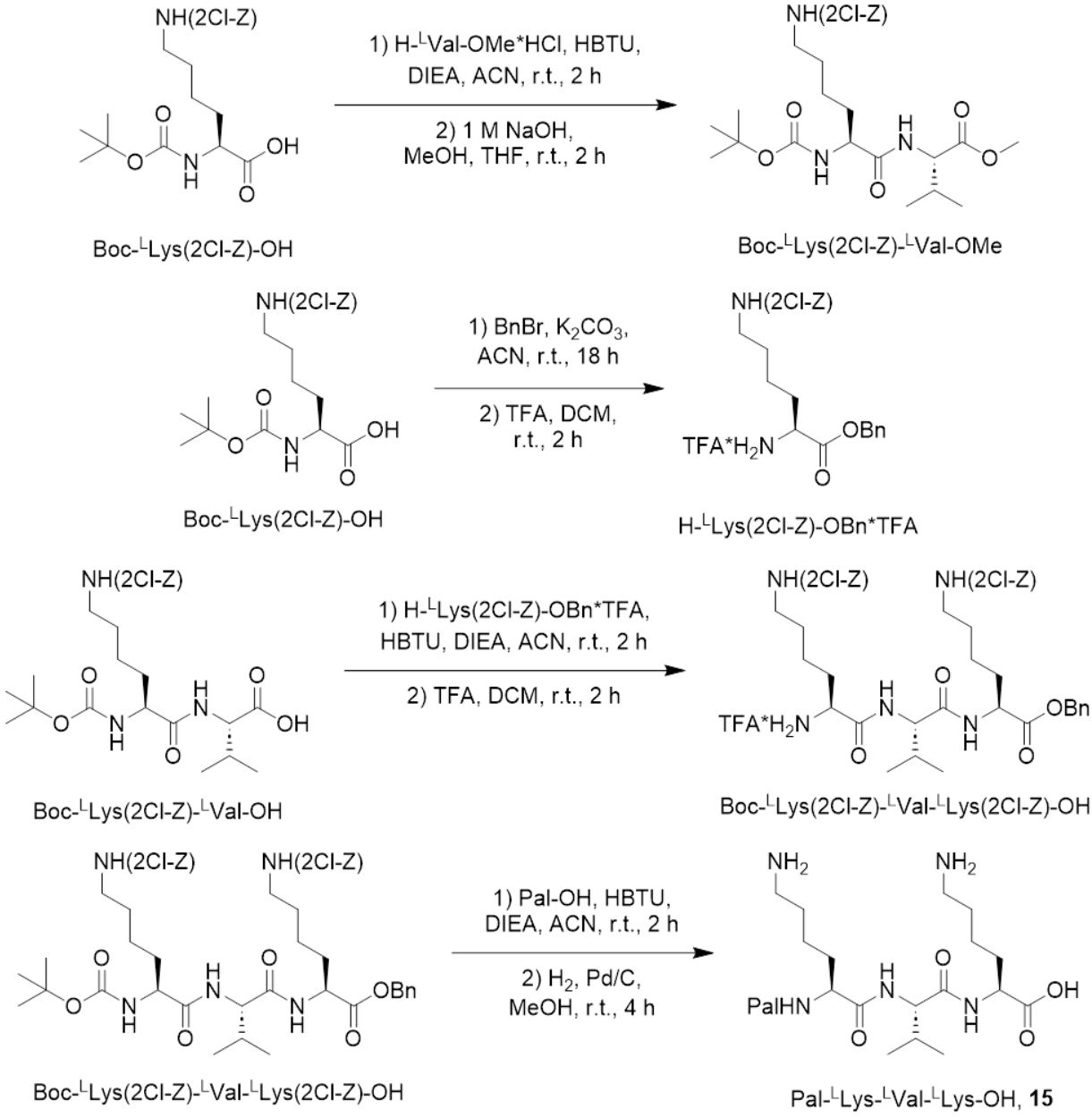


**Figure 6.7**. Synthetic path to obtain tripeptide **15**.

Pal-$^{L}$Lys-$^{L}$Val-$^{L}$Lys-OH **15**.

Pal-$^{L}$Lys(2Cl-Z)-$^{L}$Val-$^{L}$Lys(2Cl-Z)-OBn (441 mg, 0.425 mmol) was dissolved in MeOH (40 mL) (10% V/w) in presence of Pd/C (10% w/w) and a $H_2$ atmosphere. The reaction

was left under stirring for 24 h, then the solution was filtered through a paper pad and the solvent removed under reduced pressure. The product Pal-$^{L}$Lys-$^{L}$Val-$^{L}$Lys-OH was obtained as a waxy solid in 84% yield (218 mg, 0.357 mmol). $[\alpha]_D^{20}$ = - 41.7 ($c$ = 2.5 mg/mL, $H_2O$). HPLC-MS (ESI): 5.56 min, $[M-H]^-$ = 610. $^1$H-NMR (400 MHz, $D_2O$): δ 0.74 – 0.90 (m, 9H, $(CH_3)_2$ Val, $CH_3$ Pal), 1.14 – 1.50 (m, 28H, $(CH_2)_{12}$ Pal, 2 $CH_2$ Lys), 1.60 – 1.85 (m, 8H, 4 $CH_2$ Lys), 1.96 – 2.34 (m, 5H, $CH(CH_3)_2$ Val, 2 $CH_2$ Lys), 2.94 (m, 4H, 2 $CH_2$ Lys), 4.08 – 4.31 (m, 3H, $C_\alpha$H Lys, $C_\alpha$H Val, $C_\alpha$H Lys). $^{13}$C-NMR (100 MHz, $D_2O$): δ 12.16, 13.88, 16.33, 17.79, 18.46, 20.80, 22.62, 25.46, 25.85, 26.40, 27.62, 29.46, 29.97, 31.95, 35.61, 39.27, 42.59, 44.39, 50.61, 53.04, 54.41, 173.36, 174.31, 174.95, 175.41. ATR-FTIR: ν 3291, 3059, 2917, 2851, 1626, 1533 cm$^{-1}$.

## 6.7.3. Preparation of gels **(12+13)a-g**

For gels **(12+13)a-c**, the required amount of gelator **12** (see Table 4.4) was dissolved in a first Sterilin cup with $H_2O$ and 1.0 eq. of 1 M NaOH and left under stirring for 2 h. Gelator **13** (Table 4.4) was dissolved in a second vial using 0.670 mL of a 0.1 M PB solution at pH 7.4. After the complete dissolution, the solution of the second vial was added inside the first vial. The final solution was gently swirled and then left to rest overnight.

For gel **(12+13)d**, gelator **12** (7 mg) was dissolved in a first Sterilin vial by adding $H_2O$ (1.275 mL) and 1.0 eq. of 1 M NaOH (0.015 mL) and left under stirring for 2 h. Gelator **13** (13 mg) was dissolved in a second vial using 0.670 mL of the 0.1 M PB solution at pH 7.4. After the complete dissolution of **13**, 0.040 mL of 1 M citric acid aqueous solution were added, and the formation of some precipitate was observed. The resulting solution was added to the first one, gently swirling for few seconds, and left to rest overnight. After this time, a viscous solution was obtained.

For gel **(12+13)e**, the two vials were prepared with the same quantities and methods of gel **(12+13)c** and then heated separately by placing them in a water bath (60 °C) for 5 min. This led to a complete dissolution of the precipitate in the vial containing gelator **13**. At this point, the content of this vial was added in the first one and left in the hot bath for

few seconds while gently swirling, then it was removed from the hot bath and left to cool down and rest overnight.

For gels **(12+13)f** and **(12+13)g**, gelator **12** (7 mg) was dissolved in a first Sterilin vial by adding $H_2O$ (1.315 mL) and 1.0 eq. of 1 M NaOH (0.015 mL) and leaving under stirring for 2 h. Gelator **13** and 2 mg of either of the bioactive tripeptides **14** or **15** were dissolved in a second vial in 0.670 mL of the 0.1 M PB solution at pH 7.4. After the complete dissolution, the two vials were heated separately by placing them in a water bath at 40 °C for 5 min. At this point, the content of the second vial was added in the first one and left in the warm bath for few seconds while gently swirling, then the vial was removed from the warm bath and left to cool down and rest overnight.

### 6.7.4. Rheological analysis of gels **(12+13)a-g**, **(12+13)c-r**, **(12+13)e-r**, **(12+13)f-r**, and **(12+13)g-r**

All rheological analyses were performed using an Anton Paar MCR102 Rheometer. A vane and cup measuring system was used, setting a gap of 2.1 mm. The gels were prepared as described and tested directly in the 7 mL Sterilin Cup. All analyses were performed at a fixed temperature of 23 °C controlled by an integrated Peltier system. Oscillatory amplitude sweep experiments ($\gamma$: 0.01 – 100 %) were performed using a constant angular frequency of 10 rad/s. Step-strain experiments were performed on gel samples that were already broken and reformed twice. The samples were subjected to consecutive deformation and recovery steps. The first step was performed by keeping the sample at a constant strain $\gamma$ = 0.05 %, i.e., within the LVER, and at a fixed frequency of = 10 rad/s for a period of 300 s, simulating the conditions of the gel at rest. The deformation step was performed by applying to the gel a constant strain of $\gamma$ = 100 %, i.e., above the LVER of the sample, for a period of 300 s. The recovery step was then performed at a constant strain $\gamma$ = 0.05 %, i.e., within the LVER, and at a fixed frequency of = 10 rad/s for a period of 600 s. The deformation/recovery cycles were performed and repeated two times.

## 6.7.5. *In vitro* membrane permeation test from gels **(12+13)f** and **(12+13)g**

The membrane permeation test was conducted on a Copley Scientific Vertical Diffusion Cell HDT 1000 equipped with Copley Scientific Vertical Diffusion Cell (15 mm x 11 mL) Type "C" receptor. A 0.1 M phosphate buffer saline solution (PBS) at pH 7.4 was added to each receptor compartment, maintaining a temperature of 37 °C. The model membrane (pork ear skin, thickness: 1.2 ± 0.3 mm) was rinsed with physiological saline solution and then washed with the PBS solution at pH 7.4. The membrane was clamped between the two compartments (receptor and donor). When the system was stable, 0.5 mL of gel formulation (either gel **(12+13)f** or gel **(12+13)g**) was applied on the skin membrane, for each different diffusion cell. Samples (1 mL) were withdrawn from the sampling port of the receptor compartment at a regular time interval (0.5, 1, 1.5, 2, 4, 6 and 24 h) and analyzed by the HPLC-MS method described in section 6.7.6. After each sample withdrawal, the receptor was refilled by an equal volume of PBS solution at pH 7.4 to maintain sink condition. For these studies, triplicate experiments have been performed.

## 6.7.6. Standard solutions and sample preparation for HPLC-MS analysis of permeation test from gels **(12+13)f** and **(12+13)g**

Stock standard solutions of Boc-$^{L}$Dopa(OBn)$_2$-OH **12**, Boc-$^{L}$Ala-Aib-$^{L}$Val-OH **13**, TFAc-$^{L}$Val-$^{L}$Tyr-$^{L}$Val-OH **14** and Pal-$^{L}$Lys-$^{L}$Val-$^{L}$Lys-OH **15** were prepared by dissolving each compound at a concentration of 1.0 mg/mL in a mixture 30:70 (V/V) of 0.2 % (V/V) formic acid in ACN/ 0.2 % (V/V) formic acid in $H_2O$. Stock solutions were stored at 4 °C. Serial dilutions of stock solutions in the same mixture were prepared and calibration curves were plotted for all analytes. The linearity range was found to be between 0.01 and 20 μg/mL. All the analyses were performed in triplicate.

Sample preparation was performed by diluting the aliquots withdrawn from the sampling port of the receptor compartment of Franz cells, so that the analyte concentration would fall within the linearity range.

### 6.7.7. HPLC-MS analyses of permeation test from gels **(12+13)f** and **(12+13)g**

HPLC-MS analyses were carried out on an Agilent 1260 Infinity II Chromatograph coupled with Mass Spectrometer MSD/XT equipped with electrospray ionization Source and operating with a single quadrupole mass analyzer.

ESI system employed a 5.0 V (positive polarity) spray voltage and a gas temperature 350 °C. The nebulizer gas and drying gas flows were 50 % and 12 L/min, respectively. The mass chromatograms were acquired in total ion current (TIC) modality from 50 to 3000 m/z, and in single ion monitoring (SIM) mode on the ESI generated most abundant ion for each analyte; 396 m/z for Boc-$^{L}$Dopa(OBn)$_2$-OH **12**, 306 m/z for Pal-$^{L}$Lys-$^{L}$Val-$^{L}$Lys-OH **15**, 378 m/z for Boc-$^{L}$Ala-Aib-$^{L}$Val-OH **13**, 498 m/z for TFAc-$^{L}$Val-$^{L}$Tyr-$^{L}$Val-OH **14**. The chromatographic analyses were conducted on a Poroshell 120 EC-C18 (Agilent Technologies, USA) column (100 mm, 3.0 mm, 5 μm particle size). The mobile phase was composed by: phase A (0.2 % formic acid in acetonitrile) and phase B (0.2 % formic acid in water). The linear gradient elution was: A:B 30:70 (v/v) to A:B 90:10 (v/v) in 15 min at a flow rate of 0.4 mL/min. The re-equilibrium time was 3 min. The injection volume was 5 μL.

### 6.7.8. Cell viability test on molecules **12**, **13**, **14**, and **15**

Molecules **13**, **14** and **15** were dissolved in DPBS 1x (purchased from Merck), while **12** was dissolved in $H_2O$ with 1.0 eq. of NaOH because of its insolubility in the above-mentioned buffer, all at a concentration of 2 mg/mL. 0.5 mL of each solution were deposited on the

multiwell. The solutions of the individual components of the gels were added after reaching a confluence of 60 % within the well.

Human immortalized keratinocytes (HaCaT) cells were cultured under standard conditions in the MEM medium, supplemented with 10 % (V/V) FBS, 2 mM $^{L}$Gln, 100 units/mL penicillin and 100 units/mL streptomycin. Cells were seeded on samples at a density of $10^5$ cells per $cm^2$. Cells were incubated for 24 h and 28 h in a humidified incubator set at 37 °C.

Cell viability was determined by resazurin reduction assay; the reagent is an oxidized form of the redox indicator that is blue in color and non-fluorescent. When incubated with viable cells, the reagent is reduced, and it changes its color from blue to red becoming fluorescent. Briefly, cells were seeded on samples with complete medium. After incubation times, the resazurin reagent was added directly to the culture medium with 10 % volume of medium contained in each sample and incubated for 4 h at 37 °C with 5 % $CO_2$. Subsequently, aliquots from each sample were transferred to a 96 multiwell plate for fluorescence measurement at $\lambda_{exc}$ 560 nm and $\lambda_{em}$ 590 nm (Thermo Scientific Varioskan Flash Multimode Reader). We included a negative control of only medium without cells to determine the background signal and a positive control of 100 % reduced resazurin reagent without cells.

## *6.8. Synthesis and characterisation of gelators 13 and 16 and their gels*

### 6.8.1. Synthesis of gelators **13** and **16**

Gelator **13** was synthesised as described in section 6.7.1.

Gelator **16** was synthesised after a convergent multistep synthesis as follows (Figure 6.8).

H-Aib-$^{L}$Val-OMe·TFA was synthesised as described in section 6.7.2, then it was coupled with Boc-$^{L}$Val-OH instead of Boc-$^{L}$Ala-OH to afford Boc-$^{L}$Val-Aib-$^{L}$Val-OMe. To do so, 917 mg of Boc-L-Val-OH (4,22 mmol) were dissolved in 60 mL of anhydrous ACN and 1,76 g of HBTU (4,64 mmol) were added under $N_2$ atmosphere. A solution containing H-Aib-$^{L}$Val-OMe·TFA, 20 mL of anhydrous ACN and 3,7 mL of DIEA (22,0 mmol) was added dropwise to the first one. The reaction was left under stirring for 3 h at r.t., then the solvent was removed under vacuum, the residue suspended in $H_2O$, extracted with ethyl acetate (x3) and washed with 1 M HCl, brine, saturated solution of $NaHCO_3$, and brine once again. The organic layer was dried over $Na_2SO_4$ and the solvent evaporated under vacuum. The product is eventually purified through a flash chromatography (cHex:ethyl acetate 80:20, cHex:ethyl acetate 70:30). Boc-$^{L}$Val-Aib-$^{L}$Val-OMe was obtained as a white solid with a yield of 80%.

A solution containing 1.47 g of Boc-$^{L}$Val-Aib-$^{L}$Val-OMe in 6 mL of MeOH and 12 mL of THF was cooled to 0 °C and treated with 4.4 mL of 1 M NaOH. As the ice bath was removed, the mixture was left to warm up and stir overnight. A solution of 5.3 ml of 1 M HCl was added to the reaction mixture, then it was concentrated in vacuo to remove the volatiles. The reduced volume was then extracted with DCM (x3). The combined organic phase was washed with water, dried over $Na_2SO_4$, filtered and evaporated in vacuo, to afford pure Boc-$^{L}$Val-Aib-$^{L}$Val-OH (95%) as a white solid. M.p.: 97-103 °C; $[\alpha]_D^{25}$ -10 (c = 5 mg/mL in MeOH); ATR-FTIR: ν 3447, 3347, 3259, 3220, 3065, 2970, 2928, 2877, 2853, 1721, 1702, 1666, 1547, 1519 $cm^{-1}$. $^{1}$H-NMR ($CD^3OD$, 400 MHz): δ 0.92 (12H, 2d, *J* = 6.8 Hz, $CH_3$ Val), 1.42 (9H, s, tBu), 1.48 (6H, s, $CH_3$ Aib), 1.96 (1H, dq, *J* = 6.8, 6.8 Hz, CH Val), 2.14 (1H, dq, *J* = 5.6, 6.8 Hz, CH Val), 3.80 (1H, d, *J* = 7.2 Hz, CαH), 4.26 (1H, m, CαH), 7.35 (1H, s, NHBoc), 8.17 (1H, d, *J* = 8 Hz, NH Aib). $^{13}$C-NMR ($CD_3OD$,

100 MHz): δ 17.21, 17.26, 18.20, 18.32, 22.86, 25.10, 27.32, 30.43, 30.58, 56.67, 57.74, 60.06, 79.13, 156.60, 172.54, 173.18, 175.13.

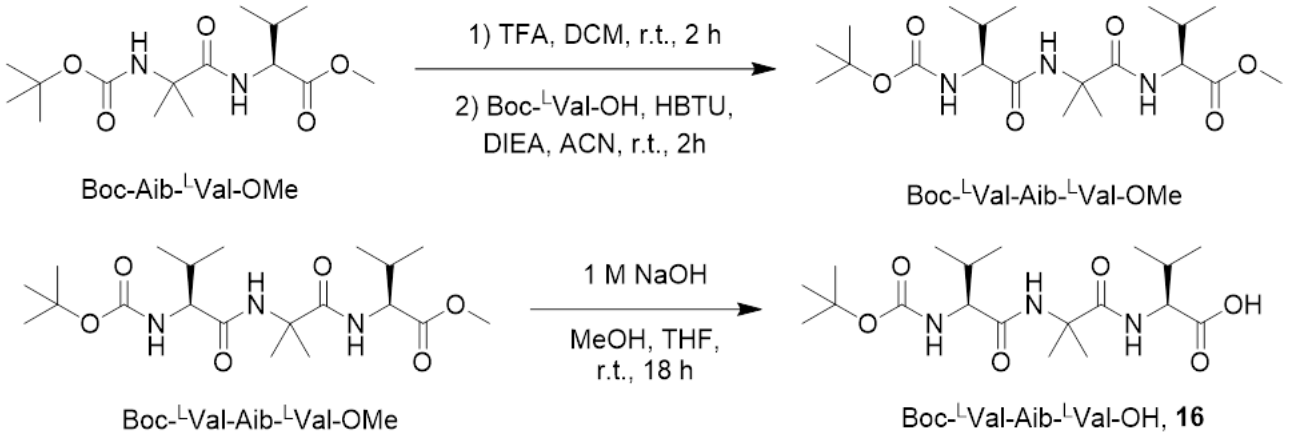


**Figure 6.8**. Synthetic path to obtain gelator **16**.

## 6.8.2. Preparation of gels **13a-j**, **13d-h**, **13g-h**, **13j-h**, and **16a-i**

To prepare the 1.0 % w/V gels (**13a-i**, and **16a-i**) 10 mg of either gelator **13** or **16** were weighted in a 2 mL vial. Then the organic solvent (ethanol, methanol or isopropyl alcohol, Table 4.6) was added, and the mixture was sonicated for 10 minutes to achieve complete dissolution of the gelator. The required amount of $H_2O$ to reach the final volume of 1 mL was then added to the solution. All samples were left to stand quiescently overnight before the analyses. The same procedure was followed to prepare the 2.0 % w/V gel **13j**, using 20 mg of compound **13** instead of 10 mg.

To prepare the gel undergoing a heat-cool cycle (Table 4.7, gels **13d-h**, **13g-h**, and **13j-h**), we first prepared gels **13d**, **13g**, and **13j**, following the procedure reported above, then the gel was placed inside a water bath and the temperature increased up to 60°C. This process resulted in the dissolution of the gel with the formation of a clear solution, that was left to rest afterwards at 25°C for 4 hours.

The gel **13j-s** resulted from the recovery of 4 h after vigorous shaking of gel **13j**.

For the preparation of the gels at 1.0 % w/w concentration (gels **13d**, and **13g**) in syringe to study the water remediation, 2 mL of gel column were prepared into a 10 mL syringe,

sealed at the bottom with parafilm. The gelator powder (20 mg) was weighted into a vial and sonicated with the correct volume of organic solvent. When a clear solution was obtained, it was transferred into the syringe, and water was added directly into the syringe to form the gel. The ratio between organic solvent and water were the same reported in Table 4.6. For the preparation of the gels at 2.0 % w/V concentration (gel **13j**) in syringe, 2 mL of gel column were prepared into a 10 mL syringe, sealed at the bottom with parafilm. The gelator powder (40 mg) was weighted into a vial and dissolved with the correct volume of organic solvent by simple manual agitation, until a clear solution is formed. The sonication in this case should be avoided because it causes the formation of a gel even before the addition of water, due to the high concentration of gelator. When the gelator is dissolved, water was added directly inside the vial and then the solution was immediately transferred into the syringe.

### 6.8.3. Crystal structure determination of gelators **13** and **16**

Single-crystal data for the gelators Boc-$^{L}$Ala-Aib-$^{L}$Val-OH **13** and Boc-$^{L}$Val-Aib-$^{L}$Val-OH **16** were collected at r.t. on an Oxford XCalibur S CCD diffractometer equipped with a graphite monochromator (Mo-Kα radiation, λ=0.71073 Å). All samples were of poor quality, invariably obtained as small needles and weakly diffracting. Additionally, crystals of **13** suffered heavily from twinning, for the best sample found and analyzed, two twin unit cells were indexed, and the reflection data were integrated with the default configuration for twinned crystals of the *CrysAlisPro* software.

Subsequent structure solution and refinement were performed using the HKLF4 file containing nonoverlapped reflections. The structures were solved by intrinsic phasing with SHELXT[215] and refined on F2 by full-matrix least squares refinement with SHELXL[216] implemented in the Olex2 software.[217] All non-hydrogen atoms were refined anisotropically and applying the rigid-body RIGU restraint.[218] H atoms for all compounds were directly located or added in calculated positions and refined riding on their respective atoms. In crystalline **13**, one molecule could not be unambiguously determined because of

severe disorder; therefore, its contribution to the calculated structure factors was removed by using the Solvent Mask function implemented in the Olex2 software.[217] The Mercury[219] program was used to calculate intermolecular interactions and for molecular graphics.

### 6.8.4. Powder diffraction measurements of gelators **13** and **16**

For phase identification X-ray Powder diffraction experiments, diffractograms were recorded on a PANalytical X'Pert Pro automated diffractometer equipped with an X'Celerator detector in Bragg-Brentano geometry, using Cu-Kα radiation (λ=1.5418 Å) without monochromator in the 2θ range between 5 ° and 40 ° (continuous scan mode, step size 0.0167 °, counting time 19.685 s, Soller slit 0.04 rad, antiscatter slit 1/2, divergence slit 1/4, 40 mA, 40 kV). The program Mercury[219] was used for the calculation of the X-ray powder patterns on the basis of single-crystal data collected in this work. The identity between the polycrystalline materials samples and the structures obtained by single crystals was always verified by comparing calculated and experimental powder diffraction patterns.

### 6.8.5. Rheological analysis of gels **13d**, **13g**, **13j**, **13d-h**, **13g-h**, and **13j-h**

All rheological measurements were performed using an Anton Paar MCR102 rheometer. The gels were prepared as described and tested directly in the 7 mL Thermo Fisher Scientific Sterilin cup. A vane and cup measuring system was used, setting a gap of 2.1 mm. Oscillatory amplitude sweep experiments (γ: 0.01 – 100 %) were performed at 23 °C using a constant angular frequency of 10 rad/s, after 16 h from the addition of water, to allow a complete gel formation. Also step strain experiments were performed on hydrogels after 16 h, subjecting the sample to consecutive deformation and recovery steps. The first step (rest conditions) was performed at a constant strain γ = 0.05 % (within the LVER)

and at a fixed frequency of $\omega = 10$ rad/s for a period of 300 s. The deformation step was performed applying a constant strain of $\gamma = 100$ %, (above the LVER) for a period of 300 s. The recovery cycle was performed with the same conditions of the first step for a period of 400 s. Deformation and recovery steps were repeated two times.

### 6.8.6. Optical microscope images of gels **13d** and **13g**

The optical microscope images were recorded using a Nikon 13 ECLIPSE Ti2 Inverted Research Microscope with a 10× magnifier. A piece of the gel sample prepared in the Sterilin cups was analysed while wet and after complete drying. The images after dye absorption were taken in epifluorescence mode, using a fluorescent filter cube V-2 A and an excitation LED ($\lambda = 395$ nm).

### 6.8.7. Scanning electron microscopy on gels **13d** and **13g**

Scanning electron micrographs were recorded on carbon coated samples of the dried gels using a Zeiss LEO 1530.

## *6.9. Synthesis and characterisation of gelator **17** and spiropyran **SP** and analysis of their gels*

### 6.9.1. Synthesis of gelator **17** and spiropyran **SP**

Gelator **17** was synthesised following the procedure reported in reference[39] and characterisation matched literature values.

The photosensitive spiropyran **SP** was synthesised following a multistep procedure, as described below (Figure 6.9).

The indole intermediate **SP-i** was synthesised following the procedure reported in reference[221] and the characterisation matched literature values, 2-hydroxy-5-nitrobenzaldehyde was used as purchased from TCI.

5-methoxy-1,2,3,3-tetramethyl-3H-indol-1-ium **SP-ii**.

500 mg of indole **SP-i** (2.45 mmol) were dissolved in 10 mL of 1:1 toluene:ACN, 305 μL of $CH_3I$ (4.90 mmol) are added and the mixture is heated to reflux for 8 h. The solid precipitate is filtered on filter paper and washed with diethyl ether. The product 5-methoxy-1,2,3,3-tetramethyl-3H-indol-1-ium **SP-ii** is obtained as a dark pink solid with a 94% yield.

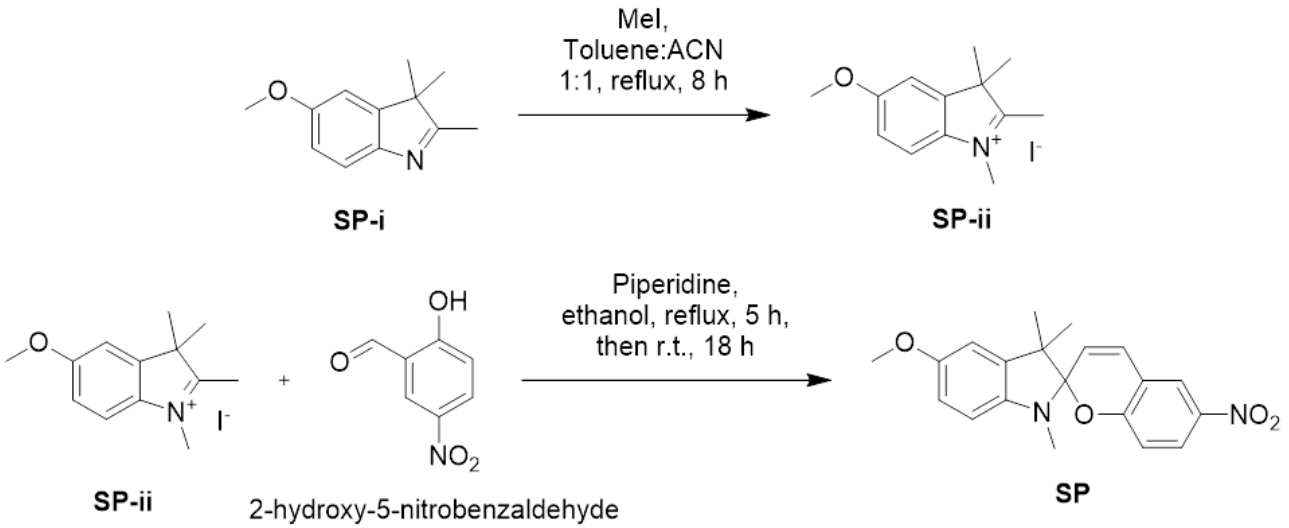


**Figure 6.9**. Synthetic path to obtain the spiropyran **SP**.

5'-methoxy-1',3',3'-trimethyl-6-nitrospiro[chromene-2,2'-indoline] **SP**.

500 mg of indolium salt **SP-ii** (1.51 mmol), 250 mg of 2-hydroxy-5-nitrobenzaldehyde (1.51 mmol), and 300 μL of piperidine (3.02 mmol) were dissolved in 5 mL of absolute ethanol. The mixture was stirred and heated to reflux in a hot silicon oil bath for 5 h, then left cooling slowly overnight in the oil bath. The solvent was then removed under reduced pressure and the crude was purified through flash chromatography on silica gel with eluent cyclohexane:ethyl acetate 4:1. The pure product was obtained as a dark yellow powder in 88% yield. M.p. = 70 - 78 °C (dec.); $[\alpha]_D^{25}$ - 4.27 ° (c = 0.5 in MeOH); ATR-FTIR: ν 2922, 2860, 1734, 1644, 1595 $cm^{-1}$; $^1$H-NMR ($CDCl_3$, 400 MHz): δ 1.13 (3H, s, $CH_3$), 1.26 (3H, s, $CH_3$), 2.68 (3H, s, $NCH_3$), 3.78 (3H, s, $OCH_3$), 5.84 (1H, d, *J* = 10.4 Hz, CH=CH), 6.45 (1H, m, CH=CH), 6.71 (2H, m, CH Ar), 6.75 (1H, m, CH Ar), 6.90 (1H, d, *J* = 10.2 Hz, CH Ar), 7.99 (2H, m, CH Ar); $^{13}$C-NMR ($CDCl_3$, 100 MHz): δ 19.84, 25.78, 29.18, 52.37, 55.89, 106.82, 107.18, 109.51, 111.42, 115.41, 118.67, 121.56, 122.64, 125.80, 128.16, 137.69, 140.85, 141.87, 154.15, 159.86.

## 6.9.2. Preparation of gels **17a-o**

**SP** solutions were prepared freshly at a concentration of 5 mg/mL in toluene, TBME or ethanol by swirling. Solutions with 0.05 mg/mL of **SP** were prepared by dilution of the solution 5 mg/mL with fresh solvent.

Gels **17a-o** were prepared at a concentration of 1.0 % w/V of gelator in a 12 mL glass test tube with either fresh solvent (gels **17a-c**) or **SP** solutions (5 mg/mL for gels **17d-i** or 0.05 mg/mL for gels **17j-o**) in a total volume of 2.5 mL. The mixture was sonicated and swirled until a homogeneous phase was obtained.

Gels used for rheology, photographs, and confocal microscopy (gels **17a-i**) were left to sonicate for additional 5 minutes, then left to rest overnight to allow complete gel formation.

Gels used for UV-vis spectroscopy (gels **17j-o**) instead, were prepared by using 1.5 mL of the homogeneous phase containing 1.0 % w/V of **17** and 0.05 mg/mL of either **SP** or

**MC**. This amount was transferred in a quartz cuvette (path length 5.0 mm) during sonication before gelation occurred and left to rest overnight to allow complete gel formation.

Gels containing **SP** (**17d**, **17f**, **17h**, **17j**, **17l**, **17n**) were prepared by pouring the solution of **SP** irradiated with white light (300 W) to ensure complete conversion, on the solid gelator. Then, the solutions were sonicated maintaining the irradiation and as they were removed from the sonicating bath, they were wrapped in aluminium foil to mimic dark conditions and left to rest overnight.

Gels containing **MC** (**17e**, **17g**, **17i**, **17k**, **17m**, **17o**) were prepared in the same way, replacing the use of white light with the use of UV light (365 nm, 0.2 W).

### 6.9.3. Rheological analysis of gels **13a-i**

All rheological measurements were performed using an Anton Paar MCR102 rheometer. The gels were prepared as described and tested directly in 12 mL glass test tube (diameter = 16 mm, fitting the rheometer). A vane and cup measuring system was used, setting a gap of 2.1 mm. Oscillatory amplitude sweep experiments ($\gamma$: 0.01 – 100 %) were performed at 23 °C using a constant angular frequency of 10 rad/s, after 16 h from the removal of the gel solution from the sonication bath, to allow a complete gel formation.

### 6.9.4. Confocal microscopy on gels **17a-c**

The confocal microscope images were recorded using a Nikon A1R and a 40× magnifier. Gels **17a-c** used for confocal microscopy were prepared as described in section 6.9.2, then a small piece of the gel was transferred onto a glass microscope slide and gently covered with a cover slip.

### 6.9.5. UV-vis spectroscopy of solutions of **SP** and **MC** and gels **17a-c** and **17j-o**

Gels used for probing the transparency of these media (**17a-c**) were prepared as described in section 6.9.2, by using 1.5 mL of the homogeneous phase containing 1.0 % w/V of **17** in the solvent chosen. Then, this amount was transferred in a quartz cuvette (path length 5.0 mm) during sonication before gelation occurred and left to rest overnight to allow complete gel formation.

Solutions of **SP** and **MC** were prepared by dissolving 0.05 mg/mL of **SP** in the required solvent and irradiating it with either white (300 W) or UV (365 nm, 0.2 W) light respectively for 1 minute to ensure complete conversion to the needed specimen.

Gels used for studying the conversion from **SP** to **MC** and vice versa (gels **17j-o**), were prepared in the same way, replacing the fresh solvent with a 0.05 mg/mL solution of either **SP** or **MC** in the required solvent. The **SP** solution was obtained after irradiation with white light (300 W), the **MC** solution was obtained after irradiation with UV light (365 nm, W).

# *References*


[1] U.-J. Kim, J. Park, C. Li, H.-J. Jin, R. Valluzzi, D. L. Kaplan, *Biomacromolecules* **2004**, *5*, 786–792.

[2] C. Vepari, D. L. Kaplan, *Prog. Polym. Sci.* **2007**, *32*, 991–1007.

[3] J. E. Key, *Eye Contact Lens* **2007**, *33*.

[4] A. Martinsen, G. Skjåk-Bræk, O. Smidsrød, *Biotechnol. Bioeng.* **1989**, *33*, 79–89.

[5] R. Yang, S. Peng, T. C. Hughes, *Soft Matter* **2014**, *10*, 2188–2196.

[6] C.-W. Hsu, C. Sauvée, H. Sundén, J. Andréasson, *Chem. Sci.* **2018**, *9*, 8019–8023.

[7] J. H. Jung, G. John, M. Masuda, K. Yoshida, S. Shinkai, T. Shimizu, *Langmuir* **2001**, *17*, 7229–7232.

[8] H. Kobayashi, A. Friggeri, K. Koumoto, M. Amaike, S. Shinkai, D. N. Reinhoudt, *Org. Lett.* **2002**, *4*, 1423–1426.

[9] K. J. C. van Bommel, C. van der Pol, I. Muizebelt, A. Friggeri, A. Heeres, A. Meetsma, B. L. Feringa, J. van Esch, *Angew. Chemie Int. Ed.* **2004**, *43*, 1663–1667.

[10] Z. Yang, G. Liang, M. Ma, Y. Gao, B. Xu, *J. Mater. Chem.* **2007**, *17*, 850–854.

[11] L. Chen, G. Pont, K. Morris, G. Lotze, A. Squires, L. C. Serpell, D. J. Adams, *Chem. Commun.* **2011**, *47*, 12071–12073.

[12] M. Wallace, D. J. Adams, J. A. Iggo, *Soft Matter* **2013**, *9*, 5483–5491.

[13] A. Z. Cardoso, L. L. E. Mears, B. N. Cattoz, P. C. Griffiths, R. Schweins, D. J. Adams, *Soft Matter* **2016**, *12*, 3612–3621.

[14] V. J. Nebot, D. K. Smith, in *Funct. Mol. Gels*, The Royal Society Of Chemistry, **2014**, pp. 30–66.

[15] E. R. Draper, D. J. Adams, *Langmuir* **2019**, *35*, 6506–6521.

[16] E. R. Draper, H. Su, C. Brasnett, R. J. Poole, S. Rogers, H. Cui, A. Seddon, D. J. Adams, *Angew. Chemie Int. Ed.* **2017**, *56*, 10467–10470.

[17] N. Singh, A. Lopez-Acosta, G. J. M. Formon, T. M. Hermans, *J. Am. Chem. Soc.* **2022**, *144*, 410–415.

[18] K. Nakamura, W. Tanaka, K. Sada, R. Kubota, T. Aoyama, K. Urayama, I. Hamachi, *J. Am. Chem. Soc.* **2021**, *143*, 19532–19541.

[19] L. E. Buerkle, S. J. Rowan, *Chem. Soc. Rev.* **2012**, *41*, 6089–6102.

[20] J. Raeburn, D. J. Adams, *Chem. Commun.* **2015**, *51*, 5170–5180.

[21] K. J. Skilling, F. Citossi, T. D. Bradshaw, M. Ashford, B. Kellam, M. Marlow, *Soft Matter* **2014**, *10*, 237–256.

[22] B. O. Okesola, D. K. Smith, *Chem. Soc. Rev.* **2016**, *45*, 4226–4251.

[23] A. Wicklein, S. Ghosh, M. Sommer, F. Würthner, M. Thelakkat, *ACS Nano* **2009**, *3*, 1107–1114.

[24] S. S. Babu, S. Prasanthkumar, A. Ajayaghosh, *Angew. Chemie Int. Ed.* **2012**, *51*, 1766–1776.

[25] Y. Huang, Z. Qiu, Y. Xu, J. Shi, H. Lin, Y. Zhang, *Org. Biomol. Chem.* **2011**, *9*, 2149–2155.

[26] D. Limón, E. Amirthalingam, M. Rodrigues, L. Halbaut, B. Andrade, M. L. Garduño-Ramírez, D. B. Amabilino, L. Pérez-García, A. C. Calpena, *Eur. J. Pharm. Biopharm.* **2015**, *96*, 421–436.

[27] F. Gelain, A. Horii, S. Zhang, *Macromol. Biosci.* **2007**, *7*, 544–551.

[28] H. Storrie, M. O. Guler, S. N. Abu-Amara, T. Volberg, M. Rao, B. Geiger, S. I. Stupp, *Biomaterials* **2007**, *28*, 4608–4618.

[29] S. Ray, A. K. Das, A. Banerjee, *Chem. Mater.* **2007**, *19*, 1633–1639.

[30] A. Patwa, J. Labille, J.-Y. Bottero, A. Thiéry, P. Barthélémy, *Chem. Commun.* **2015**, *51*, 2547–2550.

[31] P. Terech, R. G. Weiss, *Chem. Rev.* **1997**, *97*, 3133–3160.

[32] L. A. Estroff, A. D. Hamilton, *Chem. Rev.* **2004**, *104*, 1201–1218.

[33] J. Cui, Z. Shen, X. Wan, *Langmuir* **2010**, *26*, 97–103.

[34] Y. Wang, L. Tang, J. Yu, *Cryst. Growth Des.* **2008**, *8*, 884–889.

[35] M. S. Kurbasic Sabrina; Garcia, Ana M.; Kralj, Slavko; Parisi, Evelina; Deganutti, Caterina; De Zorzi, Rita; Marchesan, Silvia, *Synthesis (Stuttg).* **2019**, *51*, 2829–2838.

[36] S. Kralj, O. Bellotto, E. Parisi, A. M. Garcia, D. Iglesias, S. Semeraro, C. Deganutti, P. D'Andrea, A. V. Vargiu, S. Geremia, R. De Zorzi, S. Marchesan, *ACS Nano* **2020**, *14*, 16951–16961.

[37] A. Mahler, M. Reches, M. Rechter, S. Cohen, E. Gazit, *Adv. Mater.* **2006**, *18*, 1365–1370.

[38] N. A. Dudukovic, C. F. Zukoski, *Langmuir* **2014**, *30*, 4493–4500.

[39] L. Milli, N. Castellucci, C. Tomasini, *European J. Org. Chem.* **2014**, *2014*, 5954–5961.

[40] L. Chen, T. O. McDonald, D. J. Adams, *RSC Adv.* **2013**, *3*, 8714–8720.

[41] D. J. Adams, M. F. Butler, W. J. Frith, M. Kirkland, L. Mullen, P. Sanderson, *Soft Matter* **2009**, *5*, 1856–1862.

[42] G. Panzarasa, T. Sai, A. L. Torzynski, K. Smith-Mannschott, E. R. Dufresne, *Mol. Syst. Des. Eng.* **2020**, *5*, 445–448.

[43] A. Mori, M. Nagayama, H. Mandai, *Bull. Chem. Soc. Jpn.* **1971**, *44*, 1669–1672.

[44] X. Fan, A. Walther, *Angew. Chemie Int. Ed.* **2021**, *60*, 3619–3624.

[45] A. Q. Mai, T. Bánsági, A. F. Taylor, J. A. Pojman, *Commun. Chem.* **2021**, *4*, 101.

[46] A. Mata, L. Hsu, R. Capito, C. Aparicio, K. Henrikson, S. I. Stupp, *Soft Matter* **2009**, *5*, 1228–1236.

[47] H. S. Cooke, L. Schlichter, C. C. Piras, D. K. Smith, *Chem. Sci.* **2021**, *12*, 12156–12164.

[48] D. Chang, W. Yan, Y. Yang, Q. Wang, L. Zou, *Dye. Pigment.* **2016**, *134*, 186–189.

[49] S. Riedel, T. Schweizer, K. Smith-Mannschott, E. R. Dufresne, G. Panzarasa, *Soft Matter* **2021**, *17*, 1189–1193.

[50] S. Riedel, G. Panzarasa, *Mol. Syst. Des. Eng.* **2021**, *6*, 883–887.

[51] A. Fortunato, A. Sanzone, S. Mattiello, L. Beverina, M. Mba, *New J. Chem.* **2021**, *45*, 13389–13398.

[52] A. Fortunato, M. Mba, *Gels* **2022**, *8*, DOI 10.3390/gels8100672.

[53] S. Wu, Q. Zhang, Y. Deng, X. Li, Z. Luo, B. Zheng, S. Dong, *J. Am. Chem. Soc.* **2020**, *142*, 448–455.

[54] J. Cui, A. Liu, Y. Guan, J. Zheng, Z. Shen, X. Wan, *Langmuir* **2010**, *26*, 3615–3622.

[55] X. Huang, P. Terech, S. R. Raghavan, R. G. Weiss, *J. Am. Chem. Soc.* **2005**, *127*, 4336–4344.

[56] J. Vandaele, B. Louis, K. Liu, R. Camacho, P. H. J. Kouwer, S. Rocha, *Soft Matter* **2020**, *16*, 4210–4219.

[57] M. P. Conte, N. Singh, I. R. Sasselli, B. Escuder, R. V Ulijn, *Chem. Commun.* **2016**, *52*, 13889–13892.

[58] R. Afrasiabi, H.-B. Kraatz, *Chem. – A Eur. J.* **2013**, *19*, 1769–1777.

[59] D. R. Trivedi, P. Dastidar, *Chem. Mater.* **2006**, *18*, 1470–1478.

[60] W. Zhao, L. Feng, L. Xu, W. Xu, X. Sun, J. Hao, *Langmuir* **2015**, *31*, 5748–5757.

[61] M. de Loos, J. van Esch, R. M. Kellogg, B. L. Feringa, *Angew. Chemie Int. Ed.* **2001**, *40*, 613–616.

[62] S. Miljanić, L. Frkanec, Z. Meić, M. Žinić, *European J. Org. Chem.* **2006**, *2006*, 1323–1334.

[63] E. R. Draper, E. G. B. Eden, T. O. McDonald, D. J. Adams, *Nat. Chem.* **2015**, *7*, 848–852.

[64] J. Wang, K. Liu, R. Xing, X. Yan, *Chem. Soc. Rev.* **2016**, *45*, 5589–5604.

[65] W. Miao, S. Wang, M. Liu, *Adv. Funct. Mater.* **2017**, *27*, 1–9.

[66] J. J. D. de Jong, T. D. Tiemersma-Wegman, J. H. van Esch, B. L. Feringa, *J. Am. Chem. Soc.* **2005**, *127*, 13804–13805.

[67] S. Pu, C. Zhang, C. Fan, G. Liu, *Dye. Pigment.* **2016**, *129*, 24–33.

[68] F. Zhao, Y. Gao, J. Shi, H. M. Browdy, B. Xu, *Langmuir* **2011**, *27*, 1510–1512.

[69] S. Panja, D. J. Adams, *Chem. Commun.* **2022**, *58*, 5622–5625.

[70] Z. Qiu, H. Yu, J. Li, Y. Wang, Y. Zhang, *Chem. Commun.* **2009**, *7345*, 3342–3344.

[71] S. Panja, D. J. Adams, *Chem. Commun.* **2019**, *55*, 10154–10157.

[72] C. Liu, D. Yang, Q. Jin, L. Zhang, M. Liu, *Adv. Mater.* **2016**, *28*, 1644–1649.

[73] M. Wallace, J. A. Iggo, D. J. Adams, *Soft Matter* **2015**, *11*, 7739–7747.

[74] M. Wallace, J. A. Iggo, D. J. Adams, *Soft Matter* **2017**, *13*, 1716–1727.

[75] B. Reif, S. E. Ashbrook, L. Emsley, M. Hong, *Nat. Rev. Methods Prim.* **2021**, *1*, 2.

[76] M. A. Farrukh, Ed. , *Advanced Aspects of Spectroscopy*, IntechOpen, Rijeka, **2012**.

[77] S. Iqbal, F. Rodríguez-LLansola, B. Escuder, J. F. Miravet, I. Verbruggen, R. Willem, *Soft Matter* **2010**, *6*, 1875–1878.

[78] M. Yang, Z. Zhang, F. Yuan, W. Wang, S. Hess, K. Lienkamp, I. Lieberwirth, G. Wegner, *Chem. – A Eur. J.* **2008**, *14*, 3330–3337.

[79] M. Suzuki, M. Yumoto, H. Shirai, K. Hanabusa, *Chem. – A Eur. J.* **2008**, *14*, 2133–2144.

[80] E. K. Johnson, D. J. Adams, P. J. Cameron, *J. Mater. Chem.* **2011**, *21*, 2024–2027.

[81] E. R. Draper, T. O. McDonald, D. J. Adams, *Chem. Commun.* **2015**, *51*, 12827–12830.

[82] Y. M. Abul-Haija, S. Roy, P. W. J. M. Frederix, N. Javid, V. Jayawarna, R. V Ulijn, *Small* **2014**, *10*, 973–979.

[83] P. Xing, X. Chu, S. Li, F. Xin, M. Ma, A. Hao, *New J. Chem.* **2013**, *37*, 3949–3955.

[84] G. Yu, X. Yan, C. Han, F. Huang, *Chem. Soc. Rev.* **2013**, *42*, 6697–6722.

[85] J. W. Sadownik, J. Leckie, R. V Ulijn, *Chem. Commun.* **2011**, *47*, 728–730.

[86] S. Panja, B. Dietrich, A. J. Smith, A. Seddon, D. J. Adams, *ChemSystemsChem* **2022**, *4*, e202200008.

[87] C. Colquhoun, E. R. Draper, E. G. B. Eden, B. N. Cattoz, K. L. Morris, L. Chen, T. O. McDonald, A. E. Terry, P. C. Griffiths, L. C. Serpell, D. J. Adams, *Nanoscale* **2014**, *6*, 13719–13725.

[88] K. Sugiyasu, S. Kawano, N. Fujita, S. Shinkai, *Chem. Mater.* **2008**, *20*, 2863–2865.

[89] C. Felip-León, S. Díaz-Oltra, F. Galindo, J. F. Miravet, *Chem. Mater.* **2016**, *28*, 7964–7972.

[90] B. Huang, A. R. Hirst, D. K. Smith, V. Castelletto, I. W. Hamley, *J. Am. Chem. Soc.* **2005**, *127*, 7130–7139.

[91] J.-B. Guilbaud, A. Saiani, *Chem. Soc. Rev.* **2011**, *40*, 1200–1210.

[92] E. R. Draper, D. J. Adams, *Chem. Soc. Rev.* **2018**, *47*, 3395–3405.

[93] C. A. Lagadec, D. K. Smith, *Chem. Commun.* **2012**, *48*, 7817–7819.

[94] N. Singh, K. Zhang, C. A. Angulo-Pachón, E. Mendes, J. H. van Esch, B. Escuder, *Chem. Sci.* **2016**, *7*, 5568–5572.

[95] E. R. Draper, L. L. E. Mears, A. M. Castilla, S. M. King, T. O. McDonald, R. Akhtar, D. J. Adams, *RSC Adv.* **2015**, *5*, 95369–95378.

[96] T. Shimada, N. Sakamoto, R. Motokawa, S. Koizumi, M. Tirrell, *J. Phys. Chem. B* **2012**, *116*, 240–243.

[97] Nonappa, U. Maitra, *Soft Matter* **2007**, *3*, 1428–1433.

[98] Nonappa, M. Lahtinen, B. Behera, E. Kolehmainen, U. Maitra, *Soft Matter* **2010**, *6*, 1748–1757.

[99] L. Thomson, D. McDowall, L. Marshall, O. Marshall, H. Ng, W. J. A. Homer, D. Ghosh, W. Liu, A. M. Squires, E. Theodosiou, P. D. Topham, L. C. Serpell, R. J. Poole, A. Seddon, D. J. Adams, *ACS Nano* **2022**, *16*, 20497–20509.

[100] A. M. Smith, R. J. Williams, C. Tang, P. Coppo, R. F. Collins, M. L. Turner, A. Saiani, R. V. Ulijn, *Adv. Mater.* **2008**, *20*, 37–41.

[101] A. Dutta, D. Chattopadhyay, A. Pramanik, *Supramol. Chem.* **2010**, *22*, 95–102.

[102] R. V Ulijn, A. M. Smith, *Chem. Soc. Rev.* **2008**, *37*, 664–675.

[103] H.-F. Chow, J. Zhang, C.-M. Lo, S.-Y. Cheung, K.-W. Wong, *Tetrahedron* **2007**, *63*, 363–373.

[104] A. Banerjee, G. Palui, A. Banerjee, *Soft Matter* **2008**, *4*, 1430–1437.

[105] E. Falb, A. Nudelman, A. Hassner, *Synth. Commun.* **1993**, *23*, 2839–2844.

[106] N. Castellucci, G. Angelici, G. Falini, M. Monari, C. Tomasini, *European J. Org. Chem.* **2011**, 3082–3088.

[107] C. Tomasini, N. Zanna, *Biopolymers* **2017**, *108*, 1–14.

[108] G. Angelici, G. Falini, H.-J. Hofmann, D. Huster, M. Monari, C. Tomasini, *Chem. - A Eur. J.* **2009**, *15*, DOI 10.1002/chem.200900185.

[109] J. S. Mason, I. Morize, P. R. Menard, D. L. Cheney, C. Hulme, R. F. Labaudiniere, *J. Med. Chem.* **1999**, *42*, 3251–3264.

[110] K. C. Nicolaou, J. A. Pfefferkorn, A. J. Roecker, G.-Q. Cao, S. Barluenga, H. J. Mitchell, *J. Am. Chem. Soc.* **2000**, *122*, 9939–9953.

[111] P. Ravarino, D. Giuri, D. Faccio, C. Tomasini, *Gels* **2021**, *7*, DOI 10.3390/gels7020043.

[112] P. Metrangolo, G. (Eds. . Resnati, *Halogen Bonding*, Springer, Berlin, Heidelberg, **2008**.

[113] Q. Li, R. Li, H. Lan, Y. Lu, Y. Li, S. Xiao, T. Yi, *ChemistrySelect* **2017**, *2*, 5421–5426.

[114] S. M. Ramalhete, J. S. Foster, H. R. Green, K. P. Nartowski, M. Heinrich, P. C. Martin, Y. Z. Khimyak, G. O. Lloyd, *Faraday Discuss.* **2017**, *203*, 423–439.

[115] D. M. Ryan, S. B. Anderson, B. L. Nilsson, *Soft Matter* **2010**, *6*, 3220–3231.

[116] A. Pizzi, L. Lascialfari, N. Demitri, A. Bertolani, D. Maiolo, E. Carretti, P. Metrangolo, *CrystEngComm* **2017**, *19*, 1870–1874.

[117] P. Ravarino, N. Di Domenico, M. Barbalinardo, D. Faccio, G. Falini, D. Giuri, C. Tomasini, *Gels* **2022**, *8*, DOI 10.3390/gels8020098.

[118] D. Eyrich, F. Brandl, B. Appel, H. Wiese, G. Maier, M. Wenzel, R. Staudenmaier, A. Goepferich, T. Blunk, *Biomaterials* **2007**, *28*, 55–65.

[119] P. R. Twentyman, M. Luscombe, *Br. J. Cancer* **1987**, *56*, 279–285.

[120] M. Barbalinardo, D. Gentili, F. Lazzarotto, F. Valle, M. Brucale, M. Melucci, L. Favaretto, M. Zambianchi, A. I. Borrachero-Conejo, E. Saracino, V. Benfenati, D. Natalini, P. Greco, M. G. Di Carlo, G. Foschi, M. Cavallini, *Small Methods* **2018**, *2*, 1700377.

[121] M. Tena-Solsona, B. Rieß, R. K. Grötsch, F. C. Löhrer, C. Wanzke, B. Käsdorf, A. R. Bausch, P. Müller-Buschbaum, O. Lieleg, J. Boekhoven, *Nat. Commun.* **2017**, *8*, 15895.

[122] H. Lu, J. Hao, X. Wang, *ChemSystemsChem* **2022**, *4*, e202100050.

[123] S. Panja, D. J. Adams, *Giant* **2021**, *5*, 100041.

[124] A. M. Fuentes-Caparrós, F. de Paula Gómez-Franco, B. Dietrich, C. Wilson, C. Brasnett, A. Seddon, D. J. Adams, *Nanoscale* **2019**, *11*, 3275–3280.

[125] J. R. Moffat, D. K. Smith, *Chem. Commun.* **2009**, 316–318.

[126] R. D. Mukhopadhyay, V. K. Praveen, A. Hazra, T. K. Maji, A. Ajayaghosh, *Chem. Sci.* **2015**, *6*, 6583–6591.

[127] S. Panja, A. M. Fuentes-Caparrós, E. R. Cross, L. Cavalcanti, D. J. Adams, *Chem. Mater.* **2020**, *32*, 5264–5271.

[128] J. Eastoe, M. Sánchez-Dominguez, P. Wyatt, R. K. Heenan, *Chem. Commun.* **2004**, 2608–2609.

[129] D. J. Cornwell, O. J. Daubney, D. K. Smith, *J. Am. Chem. Soc.* **2015**, *137*, 15486–15492.

[130] A. Legrand, L.-H. Liu, P. Royla, T. Aoyama, G. A. Craig, A. Carné-Sánchez, K. Urayama, J. J. Weigand, C.-H. Lin, S. Furukawa, *J. Am. Chem. Soc.* **2021**, *143*, 3562–3570.

[131] L. Thomson, R. Schweins, E. R. Draper, D. J. Adams, *Macromol. Rapid Commun.* **2020**, *41*, 2000093.

[132] Y. Nishida, A. Tanaka, S. Yamamoto, Y. Tominaga, N. Kunikata, M. Mizuhata, T. Maruyama, *Angew. Chemie Int. Ed.* **2017**, *56*, 9410–9414.

[133] S. Panja, B. Dietrich, A. Trabold, A. Zydel, A. Qadir, D. J. Adams, *Chem. Commun.* **2021**, *57*, 7898–7901.

[134] J. Raeburn, G. Pont, L. Chen, Y. Cesbron, R. Lévy, D. J. Adams, *Soft Matter* **2012**, *8*, 1168–1174.

[135] P. Ravarino, S. Panja, S. Bianco, T. Koev, M. Wallace, D. J. Adams, *Angew. Chemie - Int. Ed.* **2022**, DOI 10.1002/anie.202215813.

[136] D. J. Adams, *J. Am. Chem. Soc.* **2022**, *144*, 11047–11053.

[137] L. Chen, J. Raeburn, S. Sutton, D. G. Spiller, J. Williams, J. S. Sharp, P. C. Griffiths, R. K. Heenan, S. M. King, A. Paul, S. Furzeland, D. Atkins, D. J. Adams, *Soft Matter* **2011**, *7*, 9721–9727.

[138] N. A. Dudukovic, C. F. Zukoski, *Soft Matter* **2015**, *11*, 7663–7673.

[139] R. Wang, X.-Y. Liu, J. Xiong, J. Li, *J. Phys. Chem. B* **2006**, *110*, 7275–7280.

[140] J.-L. Li, X.-Y. Liu, *Adv. Funct. Mater.* **2010**, *20*, 3196–3216.

[141] S. Panja, D. J. Adams, *Chem. – A Eur. J.* **2021**, *27*, 8928–8939.

[142] D. C. Duncan, D. G. Whitten, *Langmuir* **2000**, *16*, 6445–6452.

[143] B. Escuder, M. LLusar, J. F. Miravet, *J. Org. Chem.* **2006**, *71*, 7747–7752.

[144] K. L. Morris, L. Chen, J. Raeburn, O. R. Sellick, P. Cotanda, A. Paul, P. C. Griffiths, S. M. King, R. K. O'Reilly, L. C. Serpell, D. J. Adams, *Nat. Commun.* **2013**, *4*, 1480.

[145] D. McDowall, M. Walker, M. Vassalli, M. Cantini, N. Khunti, C. J. C. Edwards-Gayle, N. Cowieson, D. J. Adams, *Chem. Commun.* **2021**, *57*, 8782–8785.

[146] C. Tang, A. M. Smith, R. F. Collins, R. V. Ulijn, A. Saiani, *Langmuir* **2009**, *25*, 9447–9453.

[147] P. Ravarino, S. Panja, D. J. Adams, *Macromol. Rapid Commun.* **2022**, *n/a*, 2200606.

[148] M. De Loos, B. L. Feringa, J. H. Van Esch, *European J. Org. Chem.* **2005**, 3615–3631.

[149] D. Del Giudice, F. Frateloreto, C. Sappino, S. Di Stefano, *European J. Org. Chem.* **2022**, *2022*, e202200407.

[150] D. Giuri, L. Jurković, S. Fermani, D. Kralj, G. Falini, C. Tomasini, *ACS Appl. Bio Mater.* **2019**, *2*, 5819–5828.

[151] D. Giuri, L. J. Marshall, C. Wilson, A. Seddon, D. J. Adams, *Soft Matter* **2021**, *17*, 7221–7226.

[152] G. Guidetti, D. Giuri, N. Zanna, M. Calvaresi, M. Montalti, C. Tomasini, *ACS Omega* **2018**, *3*, 8122–8128.

[153] D. Giuri, N. Zanna, C. Tomasini, *Gels* **2019**, *5*, 27.

[154] C. Ning, Z. Zhou, G. Tan, Y. Zhu, C. Mao, *Prog. Polym. Sci.* **2018**, *81*, 144–162.

[155] J. Jacob, J. T. Haponiuk, S. Thomas, S. Gopi, *Mater. Today Chem.* **2018**, *9*, 43–55.

[156] J. Mayr, C. Saldías, D. Díaz Díaz, *Release of Small Bioactive Molecules from Physical Gels*, **2018**.

[157] S. Mondal, S. Das, A. K. Nandi, *Soft Matter* **2020**, *16*, 1404–1454.

[158] C. Tomasini, N. Castellucci, *Chem. Soc. Rev.* **2013**, *42*, 156–172.

[159] A. Valls, M. Isabel Burguete, L. Kuret, B. Altava, S. V Luis, *J. Mol. Liq.* **2022**, *348*, 118051.

[160] D. Giuri, L. J. Marshall, B. Dietrich, D. McDowall, L. Thomson, J. Y. Newton, C. Wilson, R. Schweins, D. J. Adams, *Chem. Sci.* **2021**, *12*, 9720–9725.

[161] B. O. Okesola, A. Mata, *Chem. Soc. Rev.* **2018**, *47*, 3721–3736.

[162] F. A. F. Genio, M. C. Paderes, *ChemistrySelect* **2021**, *6*, 7906–7911.

[163] S. Uzan, D. Barış, M. Çolak, H. Aydın, H. Hoşgören, *Tetrahedron* **2016**, *72*, 7517–7525.

[164] M. Carrancá Palomo, V. Martín Prieto, P. Kirilov, *Gels* **2017**, *3*, DOI 10.3390/gels3030033.

[165] G. Nicastro, L. M. Black, P. Ravarino, S. d'Agostino, D. Faccio, C. Tomasini, D. Giuri, *Int. J. Mol. Sci.* **2022**, *23*, DOI 10.3390/ijms23063105.

[166] H. Schiff, *Justus Liebigs Ann. Chem.* **1864**, *131*, 118–119.

[167] M. Liu, C. Yan, J. Han, Z. Guo, W.-H. Zhu, Z. Xiao, Y. Wu, J. Huang, *AIChE J.* **2021**, *67*, e17265.

[168] J. Lopez-Sanchez, M. Alajarin, A. Pastor, J. Berna, *J. Org. Chem.* **2021**, *86*, 15045–15054.

[169] V. Tchakalova, E. Lutz, S. Lamboley, E. Moulin, D. Benczédi, N. Giuseppone, A. Herrmann, *Chem. – A Eur. J.* **2021**, *27*, 13468–13476.

[170] D. Braga, S. d'Agostino, F. Grepioni, *Organometallics* **2012**, *31*, 1688–1695.

[171] M. Jabłoński, *Molecules* **2021**, *26*, DOI 10.3390/molecules26206319.

[172] Y. Z. Zhou, R. G. Alany, V. Chuang, J. Wen, *Chromatographia* **2012**, *75*, 597–606.

[173] E. S. Bronze-Uhle, J. V. Paulin, M. Piacenti-Silva, C. Battocchio, M. L. M. Rocco, C. F. de O. Graeff, *Polym. Int.* **2016**, *65*, 1339–1346.

[174] D. Giuri, K. A. Jacob, P. Ravarino, C. Tomasini, *European J. Org. Chem.* **2020**, *2020*, 7144–7150.

[175] N. Zanna, D. Iaculli, C. Tomasini, *Org. Biomol. Chem.* **2017**, *15*, 5797–5804.

[176] M. F. Di Filippo, D. Giuri, G. Marchiori, M. Maglio, S. Pagani, M. Fini, C. Tomasini, S. Panzavolta, *Mater. Today Chem.* **2022**, *24*, 100991.

[177] D. Giuri, S. D'Agostino, P. Ravarino, D. Faccio, G. Falini, C. Tomasini, *ChemNanoMat* **2022**, *8*, e202200093.

[178] E. F. BERNSTEIN, C. B. UNDERBILL, J. LAKKAKORPI, C. M. DITRE, J. UITTO, R. J. YU, E. VAN SCOTT, *Dermatologic Surg.* **1997**, *23*.

[179] A. Kornhauser, S. G. Coelho, V. J. Hearing, *Dermatol. Res. Pract.* **2012**, *2012*, 710893.

[180] S. K. Schagen, *Cosmetics* **2017**, *4*, DOI 10.3390/cosmetics4020016.

[181] V. Rizzi, J. Gubitosa, P. Fini, P. Cosma, *Cosmetics* **2021**, *8*, DOI 10.3390/cosmetics8030066.

[182] F. Han, D. Luo, W. Qu, D. Chen, Y. Hong, J. Sheng, X. Yang, W. Liu, *J. Drug Deliv. Sci. Technol.* **2020**, *57*, 101693.

[183] C. H. Salamanca, A. Barrera-Ocampo, J. C. Lasso, N. Camacho, C. J. Yarce, *Pharmaceutics* **2018**, *10*, DOI 10.3390/pharmaceutics10030148.

[184] E. Limpongsa, K. Umprayn, *AAPS PharmSciTech* **2008**, *9*, 464–470.

[185] P. Clément, C. Laugel, J. P. Marty, *J. Control. Release* **2000**, *66*, 243–254.

[186] T. Uchida, W. R. Kadhum, S. Kanai, H. Todo, T. Oshizaka, K. Sugibayashi, *Eur. J. Pharm. Sci.* **2015**, *67*, 113–118.

[187] A. M. Barbero, H. F. Frasch, *Toxicol. Vitr.* **2009**, *23*, 1–13.

[188] Y. Luo, W. Guo, H. H. Ngo, L. D. Nghiem, F. I. Hai, J. Zhang, S. Liang, X. C. Wang, *Sci. Total Environ.* **2014**, *473–474*, 619–641.

[189] S. Homaeigohar, *Nanomaterials* **2020**, *10*, DOI 10.3390/nano10020295.

[190] A. M. Awad, R. Jalab, A. Benamor, M. S. Nasser, M. M. Ba-Abbad, M. El-Naas, A. W. Mohammad, *J. Mol. Liq.* **2020**, *301*, 112335.

[191] F. Lu, D. Astruc, *Coord. Chem. Rev.* **2020**, *408*, 213180.

[192] N. M. Sangeetha, U. Maitra, *Chem. Soc. Rev.* **2005**, *34*, 821.

[193] S. Awhida, E. R. Draper, T. O. McDonald, D. J. Adams, *J. Colloid Interface Sci.* **2015**, *455*, 24–31.

[194] Y. Inai, T. Oshikawa, M. Yamashita, T. Hirabayashi, T. Hirako, *Biopolymers* **2001**, *58*, 9–19.

[195] S. K. Maji, D. Haldar, M. G. B. Drew, A. Banerjee, A. K. Das, A. Banerjee, *Tetrahedron* **2004**, *60*, 3251–3259.

[196] B. V. V. Prasad, H. Balaram, P. Balaram, *Biopolymers* **1982**, *21*, 1261–1273.

[197] G. D. Rose, L. M. Glerasch, J. A. Smith, in (Eds.: C.B. Anfinsen, J.T. Edsall, F.M.B.T.-A. in P.C. Richards), Academic Press, **1985**, pp. 1–109.

[198] L. Milli, N. Zanna, A. Merlettini, M. Di Giosia, M. Calvaresi, M. L. Focarete, C. Tomasini, *Chem. – A Eur. J.* **2016**, *22*, 12106–12112.

[199] T. Heberer, *Toxicol. Lett.* **2002**, *131*, 5–17.

[200] Q. Sun, H. Zheng, X. Hu, M. Salam, M. Sun, C. Zhao, B. Bao, *Sep. Purif. Technol.* **2021**, *274*, 118694.

[201] J. Rivera-Utrilla, M. Sánchez-Polo, M. Á. Ferro-García, G. Prados-Joya, R. Ocampo-Pérez, *Chemosphere* **2013**, *93*, 1268–1287.

[202] H. Guo, Z. Xu, D. Wang, S. Chen, D. Qiao, D. Wan, H. Xu, W. Yan, X. Jin, *Chemosphere* **2022**, *286*, 131580.

[203] E. Brillas, *Chemosphere* **2022**, *286*, 131849.

[204] M. Bielejewski, A. Rachocki, J. Kaszyńska, J. Tritt-Goc, *Phys. Chem. Chem. Phys.* **2018**, *20*, 5803–5817.

[205] M. Lakdusinghe, M. Abbaszadeh, S. Mishra, D. Sengottuvelu, R. Wijayapala, S. Zhang, A. R. Benasco, X. Gu, S. E. Morgan, D. O. Wipf, S. Kundu, *ACS Appl. Nano Mater.* **2021**, *4*, 8003–8014.

[206] J. Henzl, M. Mehlhorn, H. Gawronski, K.-H. Rieder, K. Morgenstern, *Angew. Chemie Int. Ed.* **2006**, *45*, 603–606.

[207] H. M. D. Bandara, S. C. Burdette, *Chem. Soc. Rev.* **2012**, *41*, 1809–1825.

[208] J. Zhang, J. K. Whitesell, M. A. Fox, *Chem. Mater.* **2001**, *13*, 2323–2331.

[209] W. Fuß, C. Kosmidis, W. E. Schmid, S. A. Trushin, *Angew. Chemie Int. Ed.* **2004**, *43*, 4178–4182.

[210] Y. Chen, C. Wang, M. Fan, B. Yao, N. Menke, *Opt. Mater. (Amst).* **2004**, *26*, 75–77.

[211] G. Berkovic, V. Krongauz, V. Weiss, *Chem. Rev.* **2000**, *100*, 1741–1754.

[212] V. I. Minkin, *Chem. Rev.* **2004**, *104*, 2751–2776.

[213] R. Klajn, *Chem. Soc. Rev.* **2014**, *43*, 148–184.

[214] L. Poisson, K. D. Raffael, B. Soep, J.-M. Mestdagh, G. Buntinx, *J. Am. Chem. Soc.* **2006**, *128*, 3169–3178.

[215] G. M. Sheldrick, *Acta Crystallogr. Sect. A Found. Crystallogr.* **2015**, *71*, 3–8.

[216] G. M. Sheldrick, *Acta Crystallogr. Sect. C Struct. Chem.* **2015**, *71*, 3–8.

[217] O. V. Dolomanov, L. J. Bourhis, R. J. Gildea, J. A. K. Howard, H. Puschmann, *J. Appl. Crystallogr.* **2009**, *42*, 339–341.

[218] A. Thorn, B. Dittrich, G. M. Sheldrick, *Acta Crystallogr. Sect. A Found. Crystallogr.* **2012**, *68*, 448–451.

[219] C. F. Macrae, I. J. Bruno, J. A. Chisholm, P. R. Edgington, P. McCabe, E. Pidcock, L. Rodriguez-Monge, R. Taylor, J. Van De Streek, P. A. Wood, *J. Appl. Crystallogr.* **2008**, *41*, 466–470.

[220] I. M. Pastor, P. Västilä, H. Adolfsson, *Chem. - A Eur. J.* **2003**, *9*, 4031–4045.

[221] E. I. Balmond, B. K. Tautges, A. L. Faulkner, V. W. Or, B. M. Hodur, J. T. Shaw, A. Y. Louie, *J. Org. Chem.* **2016**, *81*, 8744–8758.